Mechanisms and Salt Effects in Photoredox and Quenching Processes
Involving Cobalt(III) Complexes

by

Lezhen Cai
B.Sc., XiaMen University, P.R. China, 1983
M.Sc., ZheJiang University, P.R. China, 1989

A Dissertation Submitted in Partial Fulfillment of the
Requirements for the Degree of

DOCTOR OF PHILOSOPHY

in the Department of Chemistry

We accept this dissertation as conforming
to the required standard

Dr. Alexander D. Kirk, Supervisor (Department of Chemistry)

Dr. Alexander McAuley, Department Member (Department of Chemistry)

Dr. Cornelia Bohne, Department Member (Department of Chemistry)

Dr. Arthur Watton, Outside Member (Department of Physics)

Dr. Cooper H. Langford, External Examiner (Department of Chemistry, University of Calgary)

Supervisor: Dr. Alexander D. Kirk

Abstract

The novel complexes *trans-/cis*-$[Co(NCS)_2(NH_3)_4]^+$ and *trans-/cis*-$[Co(NCS)_2(en)_2]^+$ were prepared and characterized. Photoredox quantum yields for the formation of Co^{2+} ($\emptyset_{Co^{2+}}$) from the above compounds were measured on irradiation at 360 nm to be 0.065, 0.082, 0.0088 and 0.0040 respectively. With added thiocyanate a significant increase in $\emptyset_{Co^{2+}}$ occurred. This can be modeled in two ways; (i) scavenging of thiocyanate radical from an initial caged radical pair giving 6-25 ps estimates for the lifetime of the latter species; (ii) photolysis of a thiocyanate/complex ion pair, giving formation constants of 0.19, 0.09, 0.08 and 0.05 for the complexes *trans-/cis*-$[Co(NCS)_2(NH_3)_4]^+$ and *trans-/cis*-$[Co(NCS)_2(en)_2]^+$ respectively. Sub-nanosecond laser flash photolysis studies showed evidence for the formation of $(NCS)_2^{-\cdot}$. The effects of added electrolytes and of viscosity on the formation and decay of $(NCS)_2^{-\cdot}$ were also investigated.

To help to distinguish between the above two mechanisms, the zero-charged novel complex Co(tacn)$(NCS)_3$ (tacn = 1,4,7-triazacyclononane) was synthesized and characterized. It is thermally stable in aqueous/DMSO solution, but on irradiation at 360 nm undergoes parallel photosubstitution to form DMSO and aqua-substituted products with an overall quantum yield of 0.012. The product yields increase linearly with added thiocyanate. For a 1 M thiocyanate solution, the quantum yield for disappearance of the starting complex rose to 0.022 and a small redox yield of 0.0008 was found. Under these same conditions, ns laser flash photolysis at 355 nm revealed a transient absorption owing to $(NCS)_2^{-\cdot}$, which was produced with a quantum yield of 0.036. These results are interpreted in terms of scavenging of radical pair species by thiocyanate ion followed by back electron transfer to give a photosubstituted product, and a radical pair quantum yield of 0.29 and lifetime of 12 ps was derived.

The emission of $*[Pt_2(pop)_4]^{4-}$ (where pop = μ-pyrophosphite-P,P') can be quenched by the complexes $[Co(CN)_5X]^{3-}$ (where X = N_3^-, I^-, Br^-, Cl^-, but not CN^-) only in the presence of electrolytes. The salt effects have been studied using the salts MCl, $M'Cl_2$, or $R_nNH_{4-n}Cl$ (where M, M' and R represent alkali, alkaline earth metals, and alkyl respectively, with n = 0-3), and K_nX (X = Cl^-, Br^-, NO_3^-, SO_4^{2-}, $[Co(CN)_6]^{3-}$, n = 1-3). For 0.5 M cation concentration, second-order quenching rate constants k_q lie in the range 10^7 to 10^9 M^{-1} s^{-1}. For the different quencher complexes used, k_q decreases in the order $[Co(CN)_5I]^{3-} > [Co(CN)_5N_3]^{3-} > [Co(CN)_5Br]^{3-} > [Co(CN)_5Cl]^{3-}$. The oxidative quenching products $[Pt_2^{III}(pop)_4X_2]^{4-}$ (X = I, Br, or Cl) are observed, and their quantum yields are 0.083 and 0.027 respectively for the reaction of $*[Pt_2(pop)_4]^{4-}$ with $[Co(CN)_5I]^{3-}$ and $[Co(CN)_5Br]^{3-}$ in 0.5 M KCl / pH2 solution. The quenching occurred by atom transfer (dominant) and electron transfer (minor) for quencher $[Co(CN)_5I]^{3-}$ or $[Co(CN)_5N_3]^{3-}$, while only electron transfer was observed for $[Co(CN)_5Br]^{3-}$ and $[Co(CN)_5Cl]^{3-}$ quenchers. The quenching efficiency of the cobalt complexes increases with electrolyte concentration and specific cation effects are observed in the k_q with the following trends $Li^+ < Na^+ < K^+ < Cs^+$; $Mg^{2+} < Ca^{2+} < Sr^{2+} < Ba^{2+}$; $NH_4^+ < MeNH_3^+ < Me_2NH_2^+ < Me_3NH^+$; $Et_3NH^+ < Et_2NH_2^+ < EtNH_3^+$; $n\text{-}PrNH_3^+ < EtNH_3^+ < MeNH_3^+$.

Examiners:

Dr. Alexander D. Kirk, Supervisor (Department of Chemistry)

Dr. Alexander McAuley, Department Member (Department of Chemistry)

Dr. Cornelia Bohne, Department Member (Department of Chemistry)

Dr. Arthur Watton, Outside Member (Department of Physics)

Dr. Cooper H. Langford, External Examiner (Department of Chemistry, University of Calgary)

Table of Contents

CHAPTER TWO

CHAPTER THREE

PHOTOREDOX BEHAVIOUR OF *TRANS-* AND *CIS-* DIISOTHIOCYANATOTETRAAM(M)INECOBALTATE(III) COMPLEXES **74**

List of Tables

List of Figures

List of Abbreviations

Ac	acetate
am(m)ine	amine and/or ammine
[13]-aneN_4	1,4,7,11-tetraazacyclotridecane
n-amyl	normal-pentyl
Ar	aryl
bpy	2,2'-bipyridine
n-Bu	normal-butyl
t-Bu	tert-butyl
dan	1,4,7-triazaheptane
DMF	dimethylformamide
DMSO	dimethylsulphoxide
EDTA	ethylenediaminetetraacetate
en	ethylenediamine
Et	ethyl
EtOH	ethanol
ferrioxalate	trisoxalatoferrate(III), $[Fe(C_2O_4)_3]^{3-}$
Me	methyl
Me_3tacn	N, N', N''-trimethyltriazacyclonane
NMF	N-methylformamide
ox	oxalate anion
n-Pr	normal-propyl
$[Pt_2(pop)_4]^{4-}$	tetrakis(μ-pyrophosphite-P,P')diplatinate(II) anion, $[Pt_2(\mu\text{-}P_2O_5H_2)_4]^{4-}$
phen	1,10-phenanthroline
pop	pyrophosphite^{2-}
PVS	N,N-diisopropylviologensulfonate

py	pyridine
R	alkyl
tacn	1,4,7-triazacyclononane
THF	tetrahydrofuran
TMS	tetramethylsilane
tn	1,3-propanediamine

AT	atom transfer
C_p	heat capacity
CT	charge transfer
CTTS	charge transfer to solvent
D	dielectric constant
D^0_{298}	bond strength (or bond dissociation energy) at 298 K
DE	Debye-Eigen equation
DHB	Debye-Hückel Brønsted equation
$E^{0\text{-}0}$ (or E_υ)	zero-zero spectroscopic energy level (or excited state energy)
ET	electron transfer
EN-T	energy transfer
Flu	fluorescence
FT-IR	Fourier transform infra red
ΔH	enthalpy change
HPLC	high pressure liquid chromatography
IP	ion pair
IPCT	ion pair charge transfer
LC	ligand centered transition
LF	ligand field

LFP	laser flash photolysis
LMCT	ligand to metal charge transfer
MC	metal centered transition
MLCT	metal to ligand charge transfer
NMR	nuclear magnetic resonance
Phos	phosphorescence
RP	radical pair
ΔS	entropy change
SCE	saturated calomel electrode
SHE (NHE)	standard hydrogen electrode (normal hydrogen electrode)
SMDE	static mercury dropping electrode
SV	Stern-Volmer
t_R	retention time
UV/Vis	ultra violet and visible

α	transfer coefficient, or polarizability
δ	NMR chemical shift
Δ	crystal field splitting
ε^0	vacuum permittivity
ε_{max}	molar absorptivity at λ_{max}
$\emptyset$	quantum yield
η	viscosity of a solvent
η_{ce}	cage escape efficiency
η_{isc}	efficiency of inter system crossing
λ	wavelength
μ	ionic strength

ρ	density of a solvent
σ	collision diameter
τ	lifetime

Acknowledgments

I wish to express my sincere thanks to my supervisor Dr. A.D. Kirk for his guidance and assistance throughout this research project.

I am very grateful to Dr. D.A. House for his assistance and suggestions in the synthesis of several cobalt(III) compounds. I am also in debt to C. Greenwood for running the NMR spectra, K. Beveridge and Dr. G. Bushnell for solving the X-ray crystal structure, I. Mackay for providing the tacn·3HCl sample, Dr. D.M. Kneeland for allowing the use of some of her picosecond data, and L. Netter for solving problems related to computer software and maintenance.

I appreciate the cooperation from the technical staff in the instrumental, mechanical and glass shops, useful discussion with fellow graduate students, and the wonderful working environment of this department.

This dissertation is dedicated to

my mother XiuBao Lü,

father LingDe Cai,

and

uncle GuangShun Lü

in recognition of their love, support, and encouragement.

And God said, "let there be light!",
and there was light.
God saw that the light was good, ...

Genesis 1:3-4

神說，要有光，就有了光。
神看光是好的.....

《聖經》創世記 1:3-4

CHAPTER ONE

INTRODUCTION

1.1 General

Photochemistry is a branch of modern science which studies the interaction of light and chemical substances. Natural phemomena such as the fading of dyes, the necessity of sunlight for the growth of plants, and the darkening of certain silver salts due to exposure to light are examples of photochemical processes. Photochemistry is involved in areas of chemistry, physics, and biology, and is likely the key for the origin of the life on earth.[1]

Photochemistry of coordination compounds has been drawing intense attention due to its potential industrial application. Examples include: the conversion and storage of solar energy (one of the primary interests in this field is the generation of chemical fuels using sunlight as driving force, especially the photochemical production of hydrogen from water), creation and protection of the enviroment (e.g. photosmog problems, photo-induced decomposition of polymer wastes, and maintenance of ozone layer), photocatalysis, photosynthesis of some compounds which are difficult to prepare thermally, the conversion of chemical energy into light, the analytical application of luminescence methods to quantitatively determine traces of various species in solution, unconventional photographic processes (image recording), and experimental cancer phototherapy.[2-12]

Unfortunately, there are still many problems in the field of photochemistry connected with the simulation and/or the industrial application of some natural processes. Mechanistic studies on photochemical reactions will contribute to better understanding of the photochemical processes involved and provide knowledge to be used as a guide for further application.

Some background knowledge will be provided in this Chapter, followed by the experimental section in Chapter 2. The mechanistic studies on the photoredox and photosubstitution reactions of cobalt(III)-am(m)ine-isothiocyanato complexes will be presented in Chapter 3 and 4. Chapter 5 includes kinetic salt effects and the quenching

mechanism in quenching process involving acidopentacyanocobaltate(III) complexes as quenchers.

1.1.1 Electronic States in Coordination Complexes

Photochemistry studies the causes and courses of chemical deactivation processes of molecules from their electronically excited states produced by absorption of light (usually visible or ultraviolet). The nature of any photochemical and photophysical process which results from the absorption of light by molecules (eq.1.1) is strongly determined by the type of electronic transition involved.

$$D + hv \longrightarrow D^* \qquad (1.1)$$

Figure 1.1 shows a molecular orbital diagram and various kinds of electronic transitions for an octahedral coordination complex. Transition types include:

(i) metal centered (MC) or ligand field (LF) bands, the transitions between levels arising from energy of the metal d-orbitals in the field generated by coordination of ligands to the metal;

(ii) ligand to metal charge transfer (LMCT) bands, the transitions in which electronic charge is essentially transferred from the ligands toward the metal;

(iii) metal to ligand charge transfer (MLCT) bands, the transitions in which electronic charge is essentially transferred from the coordinating metal to the ligands;

(iv) ligand centered (LC) bands, the transitions between energy levels of the ligands;

(v) ion pair charge transfer (IPCT), the transitions in which electronic charge is transferred from the polarizable anion to the antibonding d orbitals of the central metal atom in the ion pairs, or *vice versa*;

(vi) charge transfer to solvent (CTTS) transitions, in which electronic charge moves to the solvent.

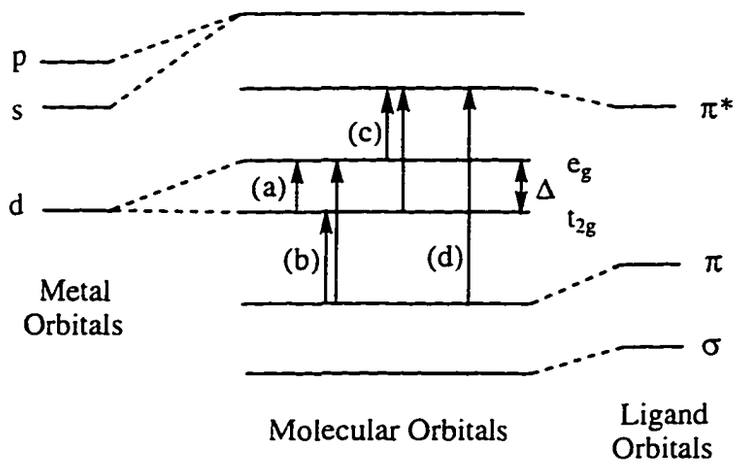

Figure 1.1 Schematic molecular orbital diagram for an octahedral coordination complex and some possible electronic transitions.
Transition types: (a) MC, metal centered; (b) LMCT, ligand to metal charge transfer; (c) MLCT, metal to ligand charge transfer; (d) LC, ligand centered. Δ, the crystal field splitting, is the energy difference between the e_g and t_{2g} orbitals.

The crystal field splitting Δ, Figure 1.1, is determined by several factors: the radius of the metal ion, the charge on the central ion, and the chemical nature of the ligands. For a given central metal ion with a specified ionic charge, the magnitude of Δ can range widely. The common ligands have been arranged in order of their ligand field strengths, that is, their effect on Δ. This is known as the spectrochemical series; a typical series is:[13]

$$CN^- > NO_2^- > \text{phen} > \text{bpy} > SO_3^{2-} \approx \text{en} > NH_3 \approx \text{py} > NCS^- > H_2O \approx \text{ox}^{2-} > ONO^- \approx OH^- > F^- > SCN^- > Cl^- > Br^- > I^-.$$

1.1.2 Intensities of Electronic Transitions

In solution, the intensity of the light transmitted (I_t) through a sample of pathlength l, (cm) and molar concentration c, (mol L^{-1}) at a particular wavelength λ, (nm) can be represented by the Beer-Lambert Law:

$$I_t = I_0\ 10^{-\varepsilon c l} \qquad (1.2)$$

or $$A = \varepsilon c l \qquad (1.3)$$

where I_0 is the incident light intensity, ε the molar absorptivity (L mol^{-1} cm^{-1}), and A the absorbance which is defined as:

$$A = -\log\left[\frac{I_t}{I_0}\right] \qquad (1.4)$$

The intensity is influenced by the following electric dipole selection rules:[13-15]

(i) transitions between states of different multiplicity ($\Delta S \neq 0$) are forbidden (spin forbidden transition). Therefore, S ⟷ T is forbidden, but S ⟷ S, T ⟷ T are allowed transitions (S and T represent the singlet and triplet electronic states respectively);

(ii) for molecules having a center of symmetry (which is quite common in coordination compounds), electric dipole transitions between states of equal parity are forbidden (parity forbidden or Laporte forbidden transition). Therefore, g ⟷ g, u ⟷ u are forbidden, but g ⟷ u is allowed transition (g and u represent those states which are , respectively, symmetric and antisymmetric with respect to inversion);

(iii) transitions involving the simultaneous excitation of two or more electrons are forbidden.

As a consequence, allowed transitions have large molar absorptivity (ε: 10^4-10^5 M^{-1} cm^{-1}), and forbidden transitions have low values (ε: 0.1-10^2 M^{-1} cm^{-1}).

1.1.2 Deactivation Pathways of Excited States

The absorption of light results in the excitation of an electron from a lower to a higher molecular energy level. The electronically excited molecule is obviously energetically unstable with respect to the ground state, and will lose its excitation energy to return to the ground state via physical processes, for which only the quantum state of the molecule changed, or undergo chemical reaction to form new species (Figure 1.2).

The physical processes include radiative decay (phosphorescence, $\Delta S \neq 0$, and fluorescence, $\Delta S = 0$), non-radiative transitions (internal conversion, IC, if the spin states are identical; intersystem crossing, ISC, for different spin states) and vibrational relaxation (VR). These unimolecular deactivation pathways can be illustrated by means of a Jablonski diagram.

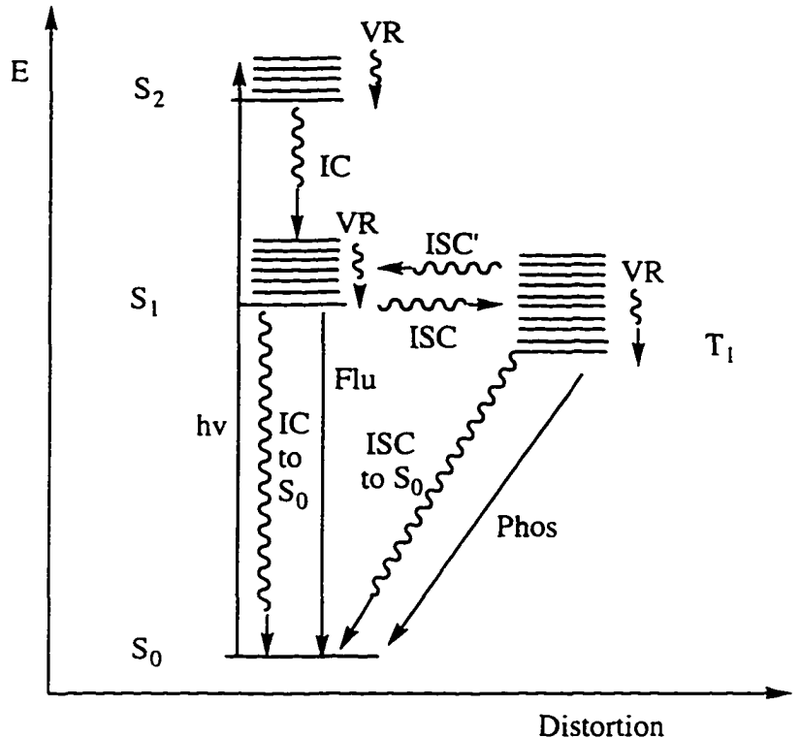

Figure 1.2 A Jablonski diagram showing decay pathways available to an excited complex.
Radiative transitions are shown as straight lines, non-radiative, as wavy lines. S_0, ground state; S_1 and S_2, excited states with same multiplicity as S_0; T_1, excited state with different multiplicity; hv, absorption; VR, vibrational relaxation; IC, internal conversion; ISC, intersystem crossing; ISC', back intersystem crossing; Flu, fluorescence; Phos, phosphorescence.

The excited state molecules can also be deactivated (quenched) by other species in a bimolecular interaction, as shown in the scheme of Figure 1.3. Here k_d is the diffusion-controlled rate constant for the formation of an encounter pair; k_{-d} is the encounter pair dissociation rate constant; $k_{EN\text{-}T}$, k_{chem}, k_{rad}, and $k_{non\text{-}rad}$ represent the rate constants of the energy transfer, chemical reaction, radiative, and non-radiativ quenching processes in the

encounter respectively. The values of k_d and k_{-d} can be calculated theoretically (see section 1.4.1).

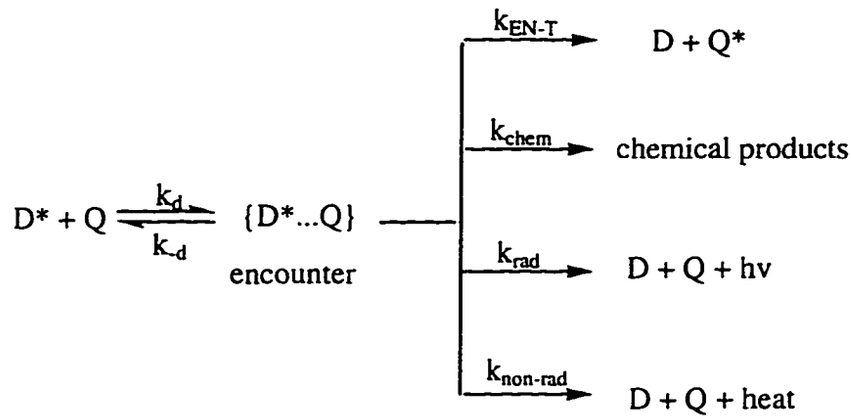

Figure 1.3 Typical bimolecular deactivation processes of an excited state molecule.

1.2 Quenching Mechanisms Involving Metal Complexes

1.2.1 Stern-Volmer Plot and Quenching Rate Constants

The kinetic aspects of the interaction between an excited state and a quencher in solution have been extensively discussed.[16] The quenching processes are usually studied by two classes of experimental methods: continuous irradiation and pulse excitation (flash photolysis). The measurable quantities are the quantum yield of the photoreaction, the emission intensity (under steady state or pulse excitation) and the lifetime (under pulse excitation). In the absence of the quencher, the lifetime of the excited state (τ^0) is defined by the following relationship:

$$\tau^0 = \frac{1}{\sum k_i} \qquad (1.5)$$

where the superscript ^{0} designates the quantities in the absence of quencher, and $\sum k_i$ represents the summation of the first order rate constants of a given unimolecular process that causes the disappearance of the excited state.

The quantum yield for each process is defined as the ratio between the number of moles of species (photons or molecules) produced and the number of einsteins (1 einstein = 1 mole of photons) that have been absorbed. If the excited state is directly reached by irradiation, the quantum yield of a specific process i (Φ_i^0) can be given as:

$$\Phi_i^0 = \frac{k_i}{\sum k_i} = \tau^0 k_i \qquad (1.6)$$

For the excited state which is not directly populated by absorption, the calculation of quantum yield is more complicated. For example, the quantum yield of emission from the lowest spin-forbidden excited state (phosphorescence quantum yield Φ_{phos}) can be expressed by the following equation:

$$\Phi^0_{phos} = \eta_{ISC}\, k_{phos}\, \tau^0_{phos} \qquad (1.7)$$

In eq. 1.7, η_{ISC} is the efficiency of population of this excited state from the state populated by light absorption:

$$\eta_{ISC} = \frac{k_{ISC}}{\sum k_i} \qquad (1.8)$$

In the presence of a quencher Q, the number of excited state deactivation modes increases, therefore the lifetime (τ) is shortened to:

$$\tau = \frac{1}{\sum k_i + k_q\,[Q]} \qquad (1.9)$$

where k_q represents the sum of the bimolecular rate constants of different types of quenching processes which might happen simultaneously.

Dividing eq. 1.5 by eq. 1.9, a common form of the Stern-Volmer equation can be derived:

$$\frac{\tau^0}{\tau} = 1 + k_q \tau^0 [Q] \qquad (1.10)$$

Thus a plot of τ^0/τ vs [Q] gives a straight line with slope equal to $k_q \tau^0$. The bimolecular quenching constant, k_q, can thus be calculated from the slope divided by τ^0. The Stern-Volmer equation can also be written in other forms, such as in ratio of quantum yields, or emission intensities in the absence and presence of quencher. It should be mentioned that when the donor D and quencher Q can give rise to a chemical or physical association, DQ, in their ground state, lifetime measurements have the advantage of giving directly the rate constant, k_q, from the straight line of Stern-Volmer plot, while intensity and quantum yield plots result in quadratic upward curvature.[16]

1.2.2 Quenching Mechanisms

In a fluid solution, the most important bimolecular processes are collisional energy transfer (the simultaneous deactivation of the originally excited molecule D* to its ground state D, and the promotion of the quencher Q to its excited state Q*, eq. 1.11), and electron transfer (electron transfers from D* to Q, or *vice versa*, eqs. 1.12-13). Occasionally, atom transfer process also occurs (eq. 1.14):

$D^* + Q \longrightarrow D + Q^*$	collisional energy transfer	(1.11)
$D^* + Q \longrightarrow D^+ + Q^-$	oxidative electron transfer	(1.12)
$D^* + Q \longrightarrow D^- + Q^+$	reductive electron transfer	(1.13)
$D^* + A\text{-}B \longrightarrow D\text{-}A + B$	atom transfer	(1.14)

From the thermodynamic point of view, the ability of an excited state to undergo energy transfer is related to the excited state energies E_t (also referred to as zero-zero spectroscopic energy level E^{0-0} for the appropriate transition) of the donor-acceptor pair; and the ability to undergo electron transfer is related to the excited state reduction and oxidation potentials of D^+/D^* and D^*/D^- couples.

Figure 1.4 shows schematically some quantities that characterize an excited state from the point of view of energy and electron transfer processes.

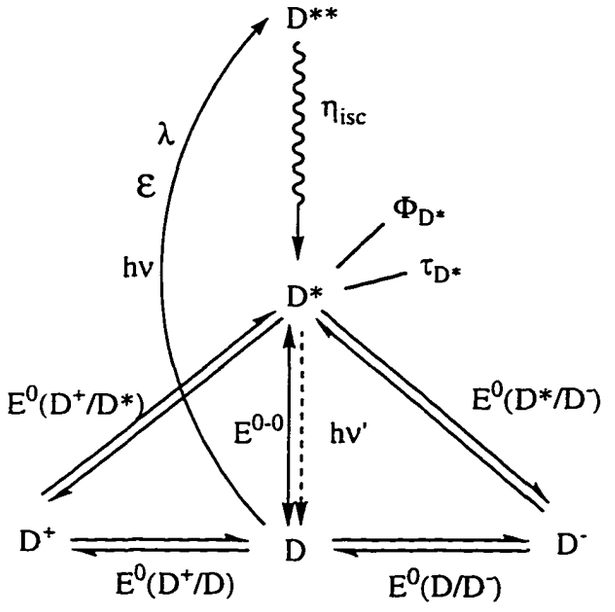

Figure 1.4 Schematic diagram showing the molecular quantities relevant for energy and electron transfer processes.
D* represents the lowest excited state which involved in the quenching processes (usually has different multiplicity from the ground state), D** represents the excited state with same multiplicity as ground state.

Energy transfer requires that the excited state energy level of the acceptor be below that of the donor (i.e. substantially endergonic energy transfer processes are forbidden).[17]

The most important energy transfer mechanism for transition metal complexes in-fluid solution is the contact exchange process; it requires that there be a favorable overlap of the wave functions between the donor and the acceptor. For the collisional energy transfer to be facile, the Wigner spin conservation rule[18] must be satisfied; the spin states produced by coupling of the spins of D* and Q in D*/Q (i.e. $S_{D^*} + S_Q$, $S_{D^*} + S_Q - 1$, ..., $|S_{D^*} - S_Q|$) must yield at least one spin state which is in common with the spin states produced by coupling of the spins of D and Q* in the final complex D/Q* (i.e. $S_D + S_{Q^*}$, $S_D + S_{Q^*} - 1$, ..., $|S_D - S_{Q^*}|$).

Electron transfer has assumed great importance for its role in solar energy applications.[6,8] Assuming the excited state energy is available as free energy for the excited state redox process, the reduction and oxidation potentials of an excited state are given by the following equations:

$$E^0(D^+/D^*) = E^0(D^+/D) - E^{0\text{-}0} \qquad (1.15)$$

$$E^0(D^*/D^-) = E^0(D/D^-) + E^{0\text{-}0} \qquad (1.16)$$

where $E^0(D/D^-)$ and $E^0(D^+/D)$ are the reduction and oxidation potentials of the ground state molecule, and can often be obtained by cyclic voltammetry methods.[19] Such an assumption is justified provided the "Stokes shift" (the shift between absorption and emission) is quite small, i.e. the excited state has approximately the same size, shape, solvation, and thus the entropy content, as the ground state. The above equations show that the excited state D* is a better reductant and a better oxidant than the corresponding ground state molecule. This can be seen clearly from the pictorial diagram, Figure 1.5.

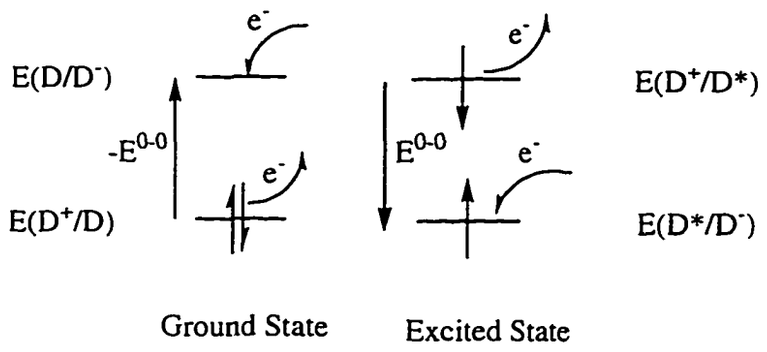

Figure 1.5 Electronic configurations for a ground state and its excited state.

It has been discovered that for complexes which are coordinatively unsaturated, or where the unpaired electron density in the excited state is not located on an inner d orbital, an atom transfer from the quencher to the metal complex can also occur.[20]

Atom transfer is thermodynamically allowed if the bond energy for D-A is greater than that for A-B, and therefore is likely to occur when quenchers A-B have small bond energies. The majority of excited states of complexes are coordinately saturated and have unpaired electrons in the d electron manifold of states. These d orbitals are not frontier orbitals that penetrate to the outer periphery of the atom, resulting in poor access of the quencher A-B to the unpaired electrons in the excited state complex. For these reasons the atom transfer pathway involving coordination complexes is not very commonly observed.

1.2.3 Determination of Quenching Mechanisms

1.2.3.4 Energy Transfer vs Electron Transfer

The quenching process(es) taking place in a system will depend on the specific properties of the excited state and the quencher. For example, in the quenching of $*[Ru(bpy)_3]^{2+}$ by Tl^{3+}, energy transfer (EN-T, eq. 1.17) and reductive electron transfer (eq. 1.18) are thermodynamically not allowed, whereas oxidative electron transfer (eq. 1.19) is thermodynamically very favorable. Thus. there is little doubt that the quenching takes place by eq. 1.19.

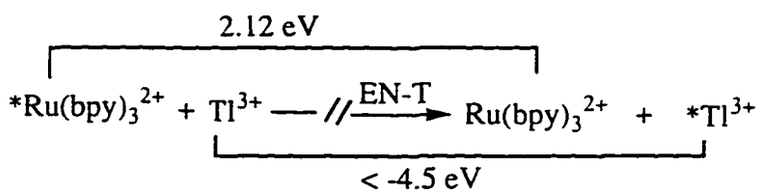

(1.17)

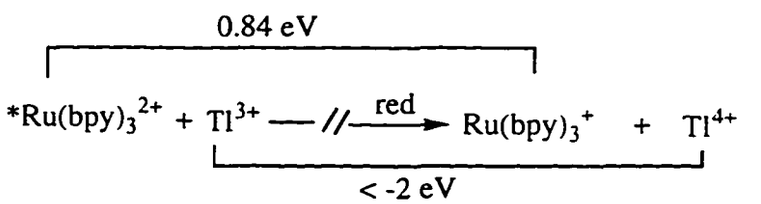

(1.18)

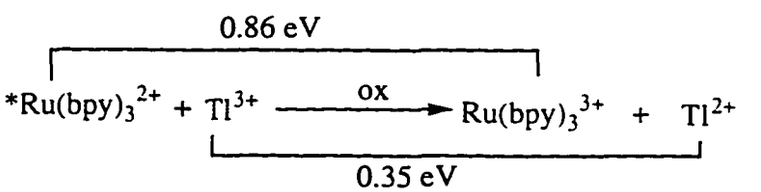

(1.19)

In other cases however, more than one quenching mechanism may be thermodynamically allowed. For example, with Fe^{3+} as a quencher of $*[Ru(bpy)_3]^{2+}$ both energy transfer (eq. 1.20) and oxidative electron transfer (eq. 1.22) are thermodynamically allowed.[8] Thus, a careful quenching product study is needed in order to discriminate these mechanisms.

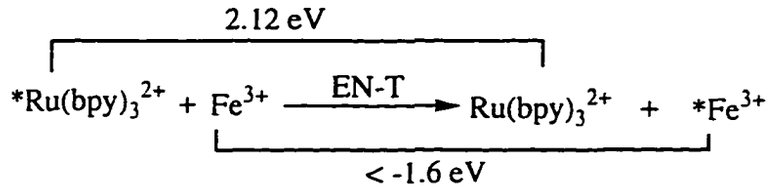

(1.20)

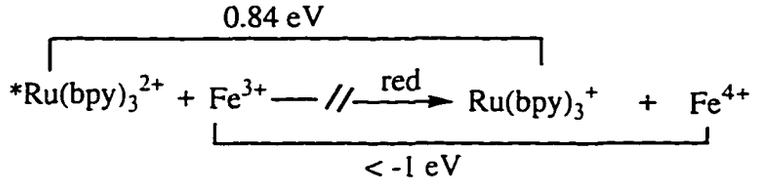

(1.21)

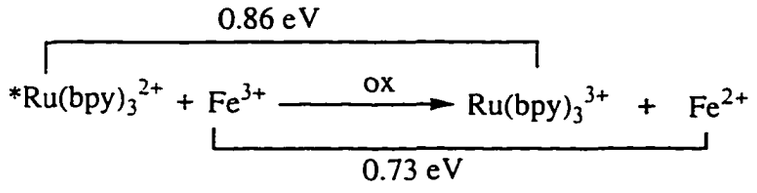

(1.22)

The establishment of the actual quenching mechanism is by no means a trivial exercise. In a large number of quenching cases involving coordination compound donors or acceptors, it is possible that quenching takes place by electron transfer rather than energy transfer, but experimental investigations have not been sufficiently detailed to enable the mechanism to be definitely assigned. The strongest evidence to support the occurrence of oxidative and reductive quenching mechanisms is the direct observation of redox products. These observations can be performed in a few cases with continuous irradiation[21,22] on irreversible redox systems and more often, in flash photolysis experiments (e.g. in the system of $*[Ru(bpy)_3]^{2+} + S_2O_8^{2-}$.[23,24] Usually, the redox products decay rapidly either by back electron transfer reactions to reform the starting materials (reversible redox) or by secondary reactions to form other products. This recombination can be avoided by the addition of a radical scavenger, a technique which can also be used for reversible redox systems under continuous irradiation. For example, $EDTA^{2-}$ irreversibly scavenges $[Ru(bpy)_3]^{3+}$ (the primary oxidative electron transfer product of $*[Ru(bpy)_3]^{2+}$), even

within the solvent cage, due to the opposite charge types of the two species.[10] This allows the accumulation of reduced quencher product Q^-. For reductive quenching $[Co(NH_3)_6]^{3+}$ is introduced, since it will scavenge any kinetically free $[Ru(bpy)_3]^+$ product with 100% efficiency,[25,26] allowing the accumulation of the oxidized quencher Q^+. Failure to observe the redox product indicates that: (i) the quenching occurs *via* energy transfer, and/or (ii) electron transfer quenching is followed by very efficient cage recombination (See note 29 in reference[26]). For the energy transfer process, the observation of transient absorption or luminescence corresponding to the acceptor excited state is adequate evidence. In cases where the quencher excited states are non-absorbing or non-luminescent, assignments to energy transfer mechanisms have to rest on the observation of sensitized photoreaction from the appropriate acceptor excited states (that is, the excited state of the acceptor is populated by the energy transferred from the excited state of another molecule, often referred to as a sensitizer) .

1.2.3.5 Electron Transfer vs Atom Transfer

As an alternative to electron transfer (ET) followed by nucleophilic attack, atom transfer (AT) can also yield similar products:[20]

$$\text{ET:} \quad D^* + RX \longrightarrow D^+ + RX^- \tag{1.22}$$

$$RX^- \xrightarrow{\text{fast}} R\cdot + X^- \tag{1.23}$$

$$D^+ + X^- \longrightarrow DX \tag{1.24}$$

$$\text{AT:} \quad D^* + RX \longrightarrow DX + R\cdot \tag{1.25}$$

Strong evidence for the ET pathway comes from the direct observation of intermediate D^+ by laser flash photolysis, provided that D^+ absorbs and has lifetime long enough so that it can be detected. Failure to observe the intermediate will require more careful analysis on the quenching rate constants in correlation with other thermodynamic properties of the quenchers. For the AT pathway, the value of k_q should correlate with both the R-X bond energy and the stability of the radical (R·), while for ET it should be governed by the reduction potential of E(RX/RX$^-$).

Irradiation of binuclear d^8 complexes, such as $[Pt_2(pop)_4]^{4-}$ (where pop = μ-pyrophosphite-P,P', see Figure 1.6 for its lantern-type structure, and Figure 1.7 for the hole formation on a Pt center at an open coordination site in the excited state), in the presence of organic halides, RX, yields products that can be rationalized in terms of both AT and ET.[27] In some cases the AT and ET pathways are indistiguishable. For example, the k_q values for ArX decrease markedly according to the order I > Br > Cl. This can be accommodated by either pathway because the C-X bond energy increases and the reduction potential decreases from ArI, ArBr, to ArCl. In the following cases, however, the AT pathway is strongly suggested. The reduction potential for n-BuBr (-2.27 V vs SCE) is only a little higher than for ArBr (-2.32 V vs SCE) , but the k_q value for n-BuBr is about 10 times larger (4.4×10^7 M^{-1} s^{-1}, compared to 4.0×10^6 M^{-1} s^{-1} for ArBr). This supports the AT pathway because the $C(sp^3)$-Br bond in n-BuBr should be much easier to break than the $C(sp^2)$-Br bond in ArBr. The remarkable increase of k_q from n-BuBr (4.4×10^7 M^{-1} s^{-1}) to t-BuBr (>10^9 M^{-1} s^{-1}), despite the similarity of their reduction potentials (-2.23 and -2.19 V vs SCE respectively), also indicates the AT mechanism, since the t-Bu· radical is much more stable than n-Bu· radical.

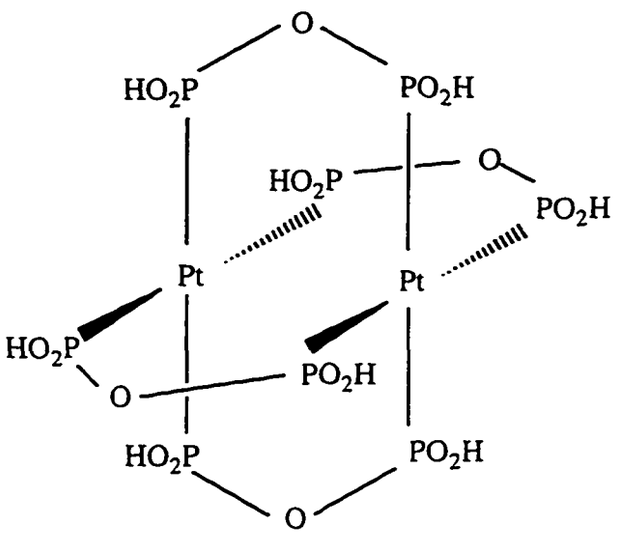

Figure 1.6 Schematic diagram of $[Pt_2(pop)_4]^{4-}$ structure.

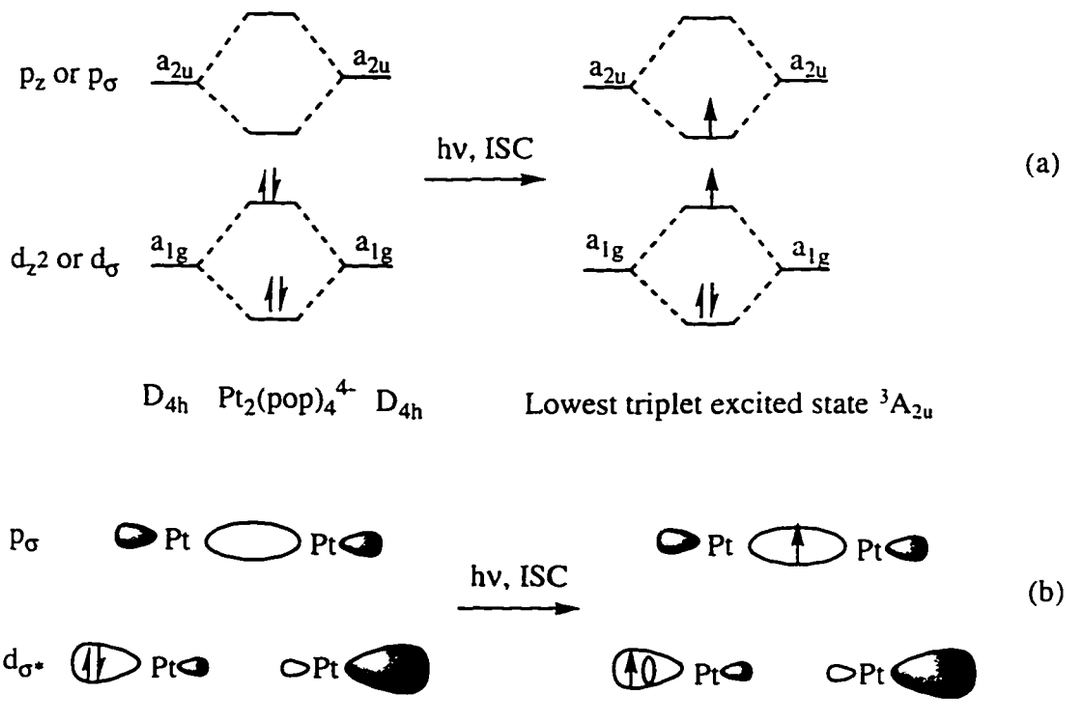

Figure 1.7 Energy diagram of ground state and triplet excited state $[Pt_2(pop)_4]^{4-}$. (a) Simplified molecular orbital diagram, and (b) Pictorial representation of ground state and triplet excited state for a face-to-face d^8 $[Pt_2(pop)_4]^{4-}$.

1.3 Photochemistry of Co(III) Complexes

1.3.1 Photoreactions (Redox/Substitution/Isomerization)

In general, Co^{3+} (d^6) complexes are kinetically inert compared to most of the other first-row series transition metal ions.[15] Therefore the coordination compounds of cobalt(III) have served for many years as ideal systems in which to study the mechanisms of photoinduced processes[16] before subsequent thermal reaction occurs. Six coordinate cobalt(III) complexes are often low spin (with the exception of very weak field ligands, such as F^-) and diamagnetic. Their photoreactions usually include three principal types:

(i) Photoredox reactions (can be intramolecular or intermolecular processes), which involve changes in oxidation number of metal and/or ligand(s);

(ii) Photosubstitution reactions (most commonly photoaquations), which involve changes in the composition of the coordination shell;

(iii) Photoisomerization reactions (such as linkage isomerization), which involve changes in the arrangement of the ligands.

For Co(III) complexes, owing to the high oxidation number of the central metal ion and the reducing properties of the usual ligands, the reactions of the first type always consist of an electron transfer from the ligand(s) to the metal (LMCT), followed by the solvation of the labile Co(II) complex (metallofragment) generated. Am(m)ine complexes were especially thoroughly examined as model compounds for LMCT photochemical investigation.[28]

Figure 1.7 shows the qualitative (Tanabe-Sugano) energy level diagram of d^6 ions in O_h symmetry,[29] where the ground state configuration, t_{2g}^6, gives rise to the term $^1A_{1g}$. The lowest excited configuration (in most cases), $t_{2g}^5e_g$, gives rise to the singlet states $^1T_{1g}$ and $^1T_{2g}$ and to the corresponding triplets $^3T_{1g}$ and $^3T_{2g}$. The $^5T_{2g}$ and ^5E_g states result from the higher energy excited configurations $t_{2g}^4e_g^2$ and $t_{2g}^3e_g^3$ respectively.

Notice from Figure 1.8 that for ligand with a range of low ligand field strength (small Δ), the lowest excited state may be $^5T_{2g}$, rather than the common situation of $^3T_{1g}$.

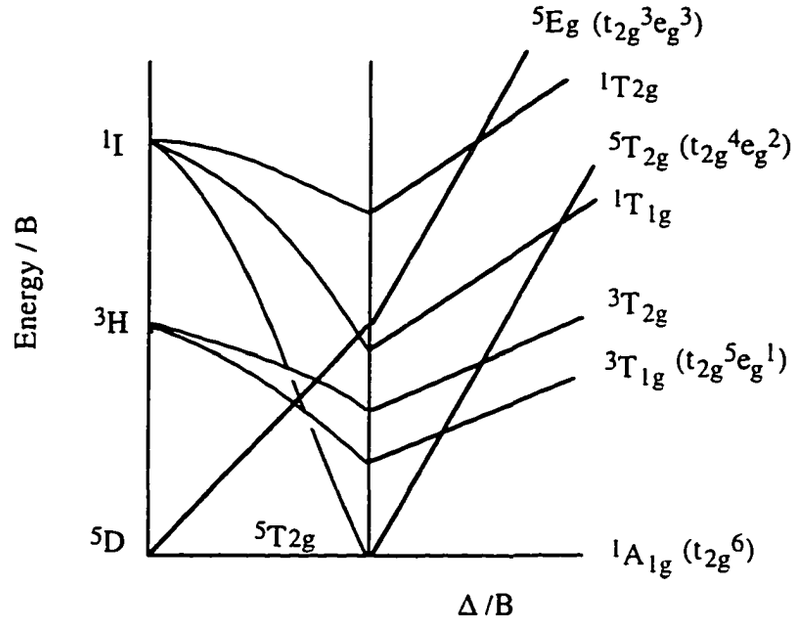

Figure 1.8 Qualitative (Tanabe-Sugano) energy level diagram of d^6 ions in O_h symmetry.
Δ is the crystal field splitting, B is Racah parameter. ^1I, ^3H, ^5D are Russell-Saunders terms[29] for the free ion.

Irradiation into the LF band of Co(III) am(m)ine complexes results in photoaquation with low quantum yield (e.g. $\emptyset \approx 10^{-4}$), while irradiation into the CT band can result in both intramolecular photoredox (with much higher yield, e.g. $\emptyset \approx 0.3$) and photo aquation reactions.[13,28,30,31] For example:

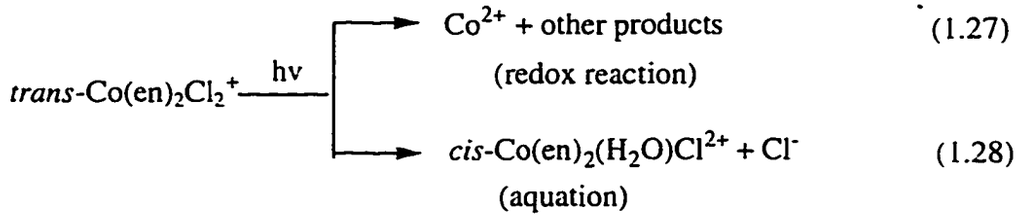

(1.27)

(1.28)

In the presence of inorganic anions (such as halide X^-, especially when X = I), Co(III) am(m)ine complexes can also undergo intermolecular electron transfer via the formation of an ion pair:[32,33]

$$\{[Co(NH_3)_6]^{3+}, X^-\} + 6\ H_3O^+ \xrightarrow{hv} [Co(H_2O)_6]^{2+} + 6\ NH_4^+ + X\cdot \quad (1.29)$$

ion pair

Photoinduced linkage isomerization of Co(III) ammine complexes has also been observed when one of the ligands has non-equivalent donor atoms X and Y, such as thiocyanate and nitrite ligands,[34-38] eqs: 1.30-1.31:

$$[Co(NH_3)_5SCN]^{2+} \xrightarrow{hv} [Co(NH_3)_5NCS]^{2+} \quad (1.30)$$

$$[Co(NH_3)_5NO_2]^{2+} \xrightarrow{hv} [Co(NH_3)_5ONO]^{2+} \quad (1.31)$$

1.3.2 Radical Pair Models

Mechanistic discussions of photoredox reactions of cobalt(III) complexes are commonly formulated in terms of "radical pair" models.

1.3.2.1 The Limiting Radical Pair Model of Adamson

In 1958 Adamson[32,39] proposed a simple radical pair model which he claimed accounted for most of the features of the photoredox chemistry of cobalt complexes. Using $Co^{III}L_5(X^-)$ as an example, the Adamson model can be summarized below:

$$Co^{III}L_5(X^-) \xrightarrow{h\nu} \{Co^{II}L_5, \cdot X\} + \Delta E \quad \text{(radical pair, RP, formation)} \qquad (1.32)$$

$$\{Co^{II}L_5, \cdot X\} \longrightarrow Co^{III}L_5(X^-)$$

$$\text{(primary RP recombination, for small } \Delta E) \qquad (1.33)$$

$$\{Co^{II}L_5, \cdot X\} \longrightarrow \{Co^{II}L_5\,(S)\,\cdot X\}$$

$$\text{(solvent separated RP, for large } \Delta E) \qquad (1.34)$$

$$\{Co^{II}L_5\,(S)\,\cdot X\} \longrightarrow Co^{2+} + \cdot X \quad \text{(redox)} \qquad (1.35)$$

$$\{Co^{II}L_5\,(S)\,\cdot X\} \longrightarrow Co^{III}L_5S + X^- \quad \text{(aquation of } X^-) \qquad (1.36)$$

where the primary reaction for absorption in a charge transfer (CT) band is the formation of a cage species via homolytic fission (eq.1.32). The quantity ΔE represents the amount of light energy absorbed in excess of that necessary for the electron transfer, and it determines to some extent the magnitude of the quantum yields for either aquation or redox. If ΔE is small (i.e., the kinetic energies of $\cdot X$ and the cobalt entity are low), then primary recombination of the cage partners is favorable (eq.1.33). For large ΔE , $\cdot X$ may diffuse far enough from the cobalt entity for a solvent (S) molecule to separate the radical and metal ion (eq.1.34). Following reaction 1.34 the original reaction partners may then diffuse apart with or without electron transfer back to $\cdot X$, leading to aquation of X^- (eq. 1.36) and the redox reaction (eq. 1.35) of the complex respectively.

Some definite inferences may be made on the basis of this radical pair model:

(i) the redox quantum yield (Φ_{Co2+}) should be wavelength dependent, and decrease with an increase in solvent viscosity;

(ii) the total quantum yield ($\Phi_{Co2+} + \Phi_{aq}$) should increase with increasing excitation energy;

(iii) the ratio of yields ($\Phi_{Co2+} : \Phi_{aq}$) should be independent of wavelength;

(iv) the photoaquation process involves only the ligand photo-oxidized (i.e., the ligand aquated is the ligand photooxidized in the primary step).

Some of the above predictions have been observed.[28,33] There are some inferences, however, which do not appear to have universal validity. For example, on irradiations of $Co(NH_3)_5NO_2^{2+}$, photoredox decomposition has been found to be accompanied by linkage isomerization of NO_2^- but not by aquation; and for $Co(NH_3)_5N_3^{2+}$, ammonia aquation, but no azide aquation has been found.[35-37]

Despite the apparent inadequacies, this model is useful as the simplest limiting model for radical pair behavior but there is potential for radical pair complexity.

1.3.2.2 The Modified Model Allowing for Secondary Radical Pair Recombination

The photochemistry of $Co(NH_3)_5NO_2^{2+}$ has been investigated by Balzani and coworkers.[35] The complex was shown to undergo simultaneous redox decomposition as well as nitro-nitrito linkage isomerization, regardless of whether CT or LF bands were irradiated. The redox quantum yield decreases with the increase of irradiation wavelength. The quantum yield ratio of photoredox to the linkage isomerization photoreaction, however, remains constant at all irradiation wavelengths, indicating that the same photoreactive intermediate is involved for both reactions. To explain the formation of the linkage isomer, a process which allows secondary recombination of solvent separated radical pair was suggested:

$$\{Co^{II}(NH_3)_5\,(S)\cdot NO_2\} \longrightarrow Co^{III}(NH_3)_5(NO_2) + S$$

(secondary RP recombination without isomerization) (1.37)

$$\{Co^{II}(NH_3)_5\,(S)\cdot NO_2\} \longrightarrow Co^{III}(NH_3)_5(ONO) + S$$

(secondary RP recombination with isomerization) (1.38)

Thus, an alternative to the Adamson mechanism was suggested in which reaction 1.36 (not eq. 1.33) is replaced by eqs. 1.39-1.40:

$$\{Co^{II}L_5\,(S)\cdot XY\} \longrightarrow Co^{III}L_5XY + S \quad (1.39)$$

$$\{Co^{II}L_5\,(S)\cdot XY\} \longrightarrow Co^{III}L_5YX + S \quad (1.40)$$

This model can account for the observation of the wavelength and solvent dependence of the $[Co(NH_3)_5NO_2]^{2+}$ photoisomerization (Ø increases with irradiation energy and viscosity), as well as the wavelength independence of the quantum yield ratio of redox and linkage isomerization.[37] It can also explain the photoisomerization of $[Co(NH_3)_5SCN]^{2+}$ to give thermodynamically more stable linkage isomer $[Co(NH_3)_5NCS]^{2+}$.[34,38] The above interpretation is inconsistent, however, with the effect of glycerol on the product distribution from excited $[Co(NH_3)_5SCN]^{2+}$: the yield of Co^{2+} decreases with increasing viscosity as expected, but the $[Co(NH_3)_5(NCS)]^{2+}$ yield decreases too, though more gradually, while the $[Co(NH_3)_5(H_2O)]^{3+}$ yield remains essentially constant and low.[34]

The above two models postulated photoreaction via a radical pair species. This radical pair has been suggested to evolve through a caged form with a "memory" of its precursor state (Adamson) to a solvent-separated species that has lost this memory and can recombine to form the thermodynamically stable linkage isomer (Balzani). Although none

of the radical pair models discussed above can be regarded as well established, the weight of evidence as well as considerations of logic strongly support the view that the primary products of excited state decomposition are radical pair species. Clearly, additional probing of the nature and the behavior of radical pair species is necessary.

1.3.3 Experimental Attempts at Observing Radical Pairs Spectroscopically

A variety of techniques have been used to characterize primary radicals. Flash photolysis, one of the pulse techniques, is probably one of the most dependable, since this technique may permit analytical observations to be made within the radical pair lifetime. One limitation has been that transients are usually detected by means of changes in the optical spectrum, and not all radicals absorb more strongly than the substrates irradiated. In many cases, weakly absorbing radicals can be readily detected and characterized by means of their reactions with simple scavenging substrates. For example, ·NCS absorbs significantly only in the deep ultraviolet (ca. 330 nm with $\varepsilon_{330} = 900\ M^{-1}\ cm^{-1}$),[40] but is very readily detected after its association with NCS^- to form $(NCS)_2^{-\cdot}$, which absorbs strongly at 475 nm with molar absorptivity about $7600\ M^{-1}\ cm^{-1}$.[40]

Kirk and Langford made an attempt to observe the radical pair spectroscopically in picosecond flash photolysis experiments on the N- and S-bonded linkage isomers of the thiocyanatopentamminecobalt(III) system.[41] Their photochemistry has been reported in some detail, and in addition, both linkage isomers meet the criteria necessary for successful ps work, namely a strong absorption band at the excitation wavelength of 355 nm for both isomers. What was seen in those experiments was a short lived transient absorbance, which was assigned to the triplet state on the basis that its band maximum depended on the ligand field strength of the ligands.[42] There was no clear evidence for a longer lived radical pair, although there was a weak long-lived signal in the region 425-475 nm, which appears

to be the same for both complexes. Is this the radical pair absorption band? If not, is this because the radical pair lifetime is too short to be detected, or are the absorption energies outside the range of observation? If it is the radical pair, it is important to increase the molar absorptivity and absorption maximum so that it can be detected in the observation window from 400 to 700 nm. The results in Chapter 3 and 4 bear directly on these questions.

1.4 Kinetic Salt Effects

1.4.1 Ionic Strength Effect

1.4.1.1 Theory of Electrolyte Solutions

As mentioned earlier, collisional quenching in a fluid solution requires the formation of an encounter complex in the solvent cage. Such a situation is common when coordination complexes are involved.

In general, for a bimolecular process in solution a simple kinetic scheme can be established:

$$A + Q \underset{k_{-d}}{\overset{k_d}{\rightleftharpoons}} \{A \ldots Q\} \xrightarrow{k_t} \text{Products} \qquad (1.41)$$

where k_d is the bimolecular rate constant for diffusion together of the reactants to give the precursor (encounter) complex, k_{-d} is the unimolecular rate constant for dissociation of the precursor complex, and k_t is the unimolecular rate constant of the reactive step within the precursor complex. Applying the steady state assumption to the precursor complex leads to a rate law with an overall bimolecular rate constant k_q,

$$k_q = k_d \left[\frac{k_t}{k_t + k_{-d}} \right] \qquad (1.42)$$

Three distinct kinetic regimes can be considered:

(i) the diffusional pre-equilibrium regime, which is defined by the condition $k_t << k_{-d}$. In this case eq. 1.42 reduces to $k_q = (k_d/k_{-d})k_t = K_{eq}\, k_t$, here $K_{eq} = k_d/k_{-d}$ is the association constant of the precursor complex. The reaction rate is much lower than diffusion, with k_t being the rate determining step. Most bimolecular reactions belong to this class.

(ii) the diffusion-controlled regime, this occurs when $k_t >> k_{-d}$. Here $k_q = k_d$ and the rate determining step is diffusion together of the reactants.

(iii) the intermediate regime, often referred to as "nearly diffusion controlled". Within this regime the full equation must be used and the reaction rates are lower than diffusion controlled and moderately sensitive to k_t.

The Debye-Smoluchowski treatment of the diffusion of charged particles has been used by Chiorboli and co-workers[43] who give the relevant equations in c.g.s. units. The converted equations (in SI units) are shown below:

$$k_d = \frac{\dfrac{2000 k_B T N}{3\eta}\left[2 + \dfrac{r_A}{r_Q} + \dfrac{r_Q}{r_A}\right]}{\displaystyle a \int_a^{\infty} r^{-2} \exp\left[\frac{W(r,\mu)}{k_B T}\right] dr} \qquad (M^{-1}\, s^{-1}) \qquad (1.43)$$

where $W(r, \mu)$ is given according to Debye-Hückel theory by

$$W(r, \mu) = \frac{Z_A Z_Q e^2}{8\pi\varepsilon^0 D}\left[\frac{\exp(\beta\sigma_A\sqrt{\mu})}{1 + \beta\sigma_A\sqrt{\mu}} + \frac{\exp(\beta\sigma_Q\sqrt{\mu})}{1 + \beta\sigma_Q\sqrt{\mu}}\right]\frac{\exp(-\beta r\sqrt{\mu})}{r}$$

$$= \frac{Z_A Z_Q e^2}{8\pi\varepsilon^0 D} \; f(r,\mu) \qquad \text{(J)} \qquad (1.44)$$

here $f(r,\mu)$ and β are defined by:

$$f(r,\mu) = \left[\frac{\exp(\beta\sigma_A\sqrt{\mu})}{1 + \beta\sigma_A\sqrt{\mu}} + \frac{\exp(\beta\sigma_Q\sqrt{\mu})}{1 + \beta\sigma_Q\sqrt{\mu}} \right] \frac{\exp(-\beta r\sqrt{\mu})}{r} \qquad (1.45)$$

$$\beta = \sqrt{\frac{8\pi N e^2 \rho_s}{4\pi\varepsilon^0 D k_B T}} \qquad (\text{mol}^{-1}\,\text{kg}\,\text{m}^{-2})^{1/2} \quad (1.46)$$

In these equations, k_B is Boltzmann's constant ($1.381\text{x}10^{-23}$ J K^{-1}), N is Avogadro's number ($6.022\text{x}10^{23}$ mol^{-1}), e is the electron charge ($1.602\text{x}10^{-19}$ C), ε^0 is vacuum permittivity ($8.854\text{x}10^{-12}$ J^{-1} C^2 m^{-1}), D is the static dielectric constant of the solvent (78.54 for water), ρ_s is the solvent density (For water at 298 K, ρ_s = 997 kg m^{-3}), η is the solvent viscosity (for water at room temperature, η = 1.002 cP = $1.002\text{x}10^{-3}$ N s m^{-2}), T is the temperature, Z_A and Z_Q are the respective charges of the reactants, the variable r is the distance separating the two reactants, r_A and r_Q are the radii of the reactants, $a = r_A + r_Q$, σ_A (or σ_Q) is the radius (in meters, m) of reactant A (or Q) plus that of the dominant counterion present in the ionic atmosphere, and μ is the ionic strength, which is the function of charge (Z) and concentration (m) of the ions present:

$$\mu = \frac{1}{2}\sum_i Z_i^2 \, m_i \qquad (\text{mol kg}^{-1}) \qquad (1.47).$$

The rate constant for the separation of encounter pairs, k_{-d}, can be determined from the Eigen equation:

$$k_{-d} = \frac{\frac{k_B T}{2\pi\eta a^2}\left[\frac{1}{r_A}+\frac{1}{r_Q}\right]\left[\exp\frac{W(a,\mu)}{k_B T}\right]}{\int_a^{\infty} r^{-2}\exp\left[\frac{W(r,\mu)}{k_B T}\right]dr} \quad (s^{-1}) \qquad (1.48)$$

The value W(a, μ) is obtained from eq. 1.44 by setting r equal to a.

The expression for the equilibrium constant K_{eq} is obtained by combining eq. 1.43 and eq. 1.48 as follows:

$$K_{eq} = \frac{k_d}{k_{-d}} = \frac{4000\pi N a^3}{3}\exp\left[\frac{-W(a,\mu)}{k_B T}\right] \quad (M^{-1}) \qquad (1.49)$$

Eqs. 1.43 and 1.48 (for k_d, k_{-d}) are referred to as the Debye-Eigen (DE) equations, and eq. 1.49 is the well-known Fuoss equation[44] for the stability constant of ion pairs.

The expressions for k_d and k_{-d} are found to give reasonably reliable results despite some fairly severe approximations, such as treating participating ions as rigid spheres, considering only the pure electrostatic interaction between charged species, and the neglect of hydrogen bonding between solvent and/or substrates.[45] The calculations for rate constants are nontrivial, however, as one needs to evaluate the DE integal over the interaction distance, which can be done numerically.

1.4.1.2 Commonly Used Simplified Equations

To avoid the tedious integration, one can apply the Taylor expansion ($r^0 = a$) of the exponential term in the above equations:

$$\exp(-\beta r\sqrt{\mu}) = \exp(-\beta a\sqrt{\mu}) - \beta\sqrt{\mu}\,(r-a)\exp(-\beta a\sqrt{\mu}) + \ldots \qquad (1.50)$$

If the first and second terms are retained, then substitution into eq. 1.44 (with assumption of $\sigma_A = \sigma_Q = a$) followed by further substitution into eqs. 1.43 and 1.48 leads to eq. 1.51:

$$k_d = k_d^0 \exp\left[\frac{W(a,0)\beta a\sqrt{\mu}}{k_B T\,(1 + \beta a\sqrt{\mu})}\right]$$

$$= k_d^0 \exp\left[\frac{2A' Z_A Z_Q \sqrt{\mu}}{1 + \beta a\sqrt{\mu}}\right] \qquad (M^{-1}\,s^{-1}) \qquad (1.51)$$

where A' is the Debye-Hückel coefficient:

$$A' = \sqrt{2\pi N\rho}\left[\frac{e^2}{4\pi\varepsilon^0 D k_B T}\right]^{1/3} \qquad (mol^{-1}\,kg)^{1/2} \qquad (1.52)$$

k_d^0 is the rate constant at zero ionic strength,

$$k_d^0 = \frac{\dfrac{2000 k_B T N}{3\eta}\left[2 + \dfrac{r_A}{r_Q} + \dfrac{r_Q}{r_A}\right]\dfrac{W(a,0)}{k_B T}}{\exp\left[\dfrac{W(a,0)}{k_B T}\right] - 1} \qquad (M^{-1}\,s^{-1}) \qquad (1.53)$$

and W(a,0) is the $W(r,\mu)$ at distance a and zero ionic strength, and can be derived from eq. 1.44 to give:

$$W(a,0) = \frac{Z_A Z_Q e^2}{4\pi\varepsilon^0 D a} \qquad (J) \qquad (1.54)$$

Taking logarithms of both sides of eq. 1.51 leads to the Debye-Hückel-Brønsted equation (DHB):

$$\log k = \log k^0 + 2A\, Z_A Z_Q \left[\frac{\sqrt{\mu}}{1 + \beta a\sqrt{\mu}}\right] \qquad (1.55)$$

where $A = A' \log_{10}(e)\ (\text{mol}^{-1}\ \text{kg})^{1/2}$. At room temperature in aqueous solution, $A \approx 0.509$, $2A \approx 1$. Therefore eq. 1.55 is usually simplified further to

$$\log k = \log k^0 + Z_A Z_Q \left[\frac{\sqrt{\mu}}{1 + \beta a\sqrt{\mu}}\right] \qquad (1.56)$$

which is the well known Extended Debye-Hückel equation.

In water at 298 K, the constant $\beta = 3.3 \times 10^9\ (\text{mol}^{-1}\ \text{kg m}^{-2})^{1/2}$. For reactions between simple ions, the value of a is often close to 0.3 nm = 3×10^{-10} m. Therefore $\beta a \approx 1.0\ (\text{mol}^{-1}\ \text{kg})^{1/2}$, which further reduces eq. 1.56 to

$$\log k = \log k^0 + Z_A Z_Q \left[\frac{\sqrt{\mu}}{1+\sqrt{\mu}}\right] \qquad (1.57)$$

In very dilute solutions ($< 10^{-3}$ mol kg^{-1}), the above equation can be further simplified to give the familiar Debye-Brønsted limiting equation

$$\log k = \log k^0 + Z_A Z_Q \sqrt{\mu} \qquad (1.58)$$

The Debye-Hückel eqs. 1.55-1.58 are widely used in exploring the **ionic strength** dependence of a bimolecular rate constant in dilute solutions. These equations predict a positive salt effect (i.e. rate constant increases with ionic strength) if A and Q carry charges of the same sign, a negative salt effect (i.e. rate constant decreases with ionic

strength) if the charges are of opposite sign, and a zero salt effect if one or both of the reactants are uncharged. Moreover the effect depends on the charges of the ions and may be very large. The well known Livingston diagram[46] illustrates the successes of the theory (Figure 1.9).[47] From Figure 1.9 we see no reason to doubt that inter-ionic effects on reaction rates will, at sufficiently low concentrations, be entirely long range and nonspecific. They will be correctly described by the Debye-Hückel equations and depend on ionic strength alone. As the concentration of ions increases, however, deviations from the equation may become increasingly significant and eventually dominant as both short-range and specific interactions become more important.

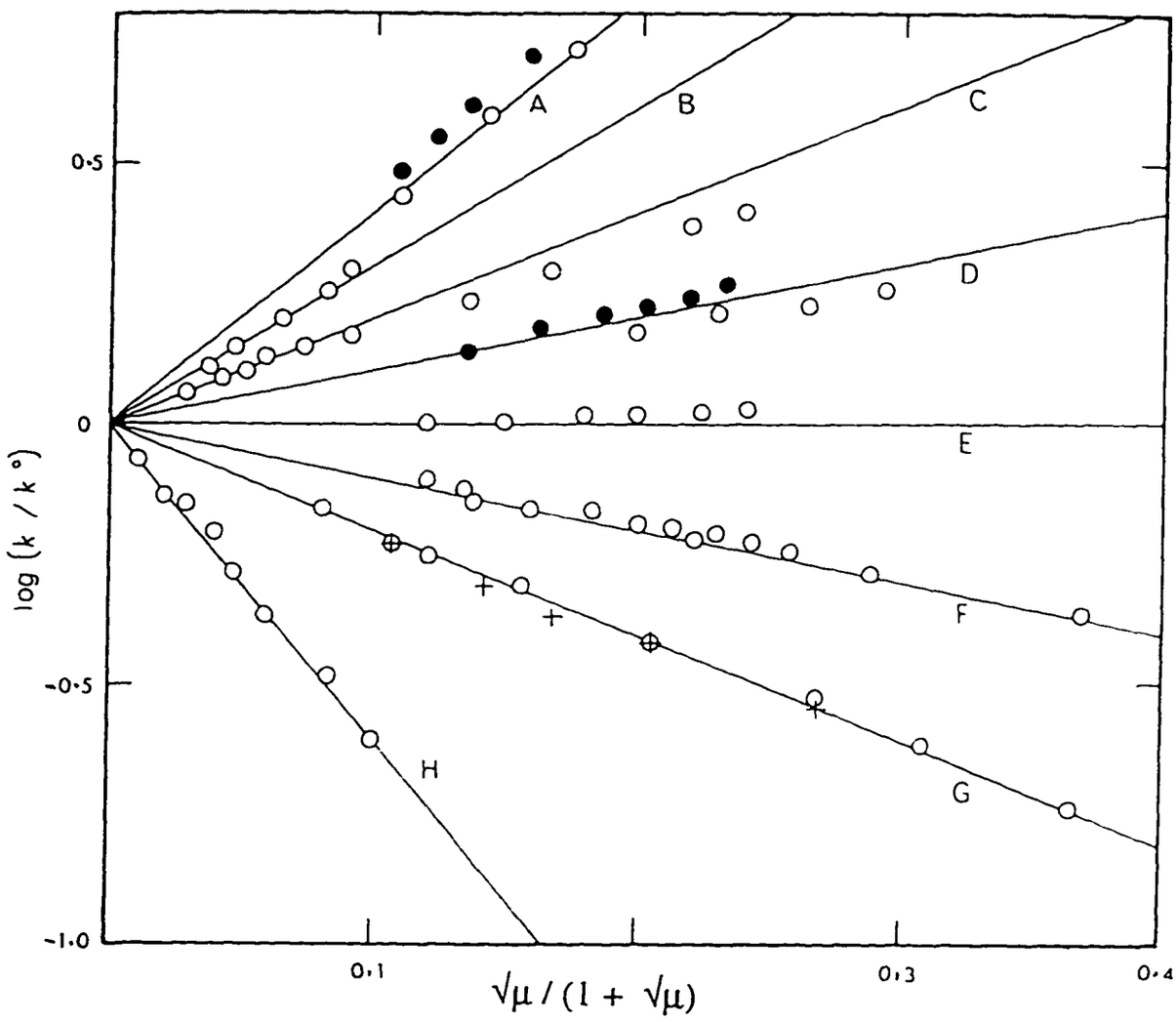

Figure 1.9 Modernized Livingston diagram.
The lines are drawn with the appropriate values of the slope $2AZ_AZ_Q$. (A) $[Co(NH_3)_5Br]^{2+}$ + Hg^{2+}, • added $Ba(NO_3)_2$, o added KNO_3; (B) $[Mo(CN)_8]^{3-}$ + I^-; (C) $BrCH_2COO^-$ + $S_2O_3^{2-}$, K^+ salt; (D) • $EtOOC{\cdot}COO^-$ + OH^-, added KCl; o $Me_3N^+(CH_2)_2O{\cdot}COMe$ + H^+, added KBr; (E) $C_{12}H_{22}O_{11}$ + H^+, from $HClO_3$; (F) $Me_3N^+(CH_2)_2O{\cdot}COMe$ + OH^-, added KBr; (G) $[Co(NH_3)_5Br]^{2+}$ + OH^-, o added NaBr, + added KNO_3; (H) $[Co(C_2O_4)_3]^{3-}$ + Fe^{2+} (modified from reference [47]).

1.4.2 Olson-Simonson Effect

After re-examining the influence of salts on the rates of certain chemical reactions, Olson and Simonson[48] concluded that for reactions between ions of *like* sign, it is not the ionic strength that is significant, but the concentration of the ions of opposing charge to that of the reactants. This is known as the **Olson-Simonson effect**. For example, they found that the rate of reaction between $[Co(NH_3)_5Br]^{2+}$ and Hg^{2+} depended on the concentration of ClO_4^-, irrespective of whether the cation was Na^+ or La^{3+}. i.e. the rate is determined by the concentration of the ion of opposite sign, and when the latter is kept constant the rate is not influenced by a change in ionic strength brought about by changing the ionic charge of the supporting counterion.

The Olson-Simonson effect has since been noticed for other systems with reactants of like charge such as the thermal reactions between $[Co(sep)]^{3+}$ and $[Cr(H_2O)_6]^{2+}$,[49] $[Mo(CN)_8]^{3-}$ and I^-,[50] $S_2O_8^{2-}$ and $[Fe(CN)_6]^{4-}$,[51,52] $Etox^-$ and OH^-,[53] $CO_2CH_2CO_2C_2H_5^-$ and OH^-,[54] $[Fe(CN)_6]^{4-}$ and $[Fe(CN)_6]^{3-}$,[55] $S_4O_6^{2-}$ disproportionation to give $S_3O_6^{2-}$ and $S_5O_6^{2-}$,[56] and quenching of excited state $^*[Ru(bpy)_3]^{2+}$ by $[Co(sep)]^{3+}$.[57]

1.4.3 Specific Ion Effects

In addition to the Olson-Simonson effect, **specific ion effects** were also observed, particularly for multivalent reactants. The specific ion effects indicate that within a given charge type, the accelerating influence on the reactions varies with the nature of the ions of opposing charge to that of the reactants, even though the ionic strength or concentration of the electrolytes is kept constant. Viewed from another perspective, the example of the racemization of $[Cr(ox)_3]^{3-}$ illustrates this effect. As can be seen from Table 1.1, the cation concentration needed to obtain a given rate constant decreases dramatically with increasing cation charge ($[K^+] : [Ca^{2+}] : [La^{3+}] = 500 : 16 : 1$).[47] Due to this reason

any rate constant or equilibrium constant obtained needs to state the electrolyte, not just ionic strength.[58]

Table 1.1 First-order rate constants k (25 °C) for the racemization of $[Cr(ox)_3]^{3-}$ with added salts.

Added salt	None	0.5 M KCl	0.0016 M $CaCl_2$	0.0001 M $LaCl_3$
10^3k, s^{-1}	0.175	0.213	0.233	0.222

Specific cation effects, with rate constant trends such as $Li^+ < Na^+ < K^+ < Cs^+$ for alkalis and $Mg^{2+} < Ca^{2+} < Sr^{2+} < Ba^{2+}$ for alkaline-earths, have been reported for a number of thermal electron transfer reactions occuring between two anions; $[Fe(CN)_6]^{3-}$ and $[Fe(CN)_6]^{4-}$,[59] $[MnO_4]^{2-}$ and $[MnO_4]^-$,[60] $S_2O_8^{2-}$ and $[Fe(CN)_6]^{4-}$,[51] $S_2O_8^{2-}$ and $S_2O_3^{2-}$,[61] $S_2O_8^{2-}$ and I^-,[62] $S_2O_8^{2-}$ and $[Mo(CN)_8]^{4-}$,[63] $S_2O_8^{2-}$ and $[Fe(CN)_6]^{4-}$,[52] $[Fe(CN)_6]^{3-}$ and SO_3^{2-},[64] $[M(CN)_8]^{3-}$ and SO_3^{2-} (M = Mo, W),[65] $Co^{II}O_4W_{12}O_{36}^{6-}$ and $Co^{III}O_4W_{12}O_{36}^{5-}$,[66] $[W(CN)_8]^{3-}$ and As^{III}.[67]

There are also some examples of specific anion effects on the thermal electron transfer reactions between two cations; $[FeL_3]^{3+}$ and $[OsL_3]^{2+}$ (L = bpy and its derivatives),[68] $[FeL_3]^{3+}$ and $[OsL_3]^{2+}$ (L = 4,4-dimethyl-2,2'-bipyridyl),[69] $[Co(NH_3)_6]^{3+}$ and $[Co(NH_3)_6]^{2+}$.[70]

Only a few examples have been reported for specific ion effects involving the quenching reactions of excited state complexes; $*[Ru(bpy)_3]^{2+}$ and $[Co(sep)]^{3+}$,[57] $*[Ru(bpy)_3]^{2+}$ and MV^{2+},[43,71,72] $*[(Mo_6Cl_8)Cl_6]^{2-}$ and $[IrCl_6]^{2-}$,[73] $*[Pt_2(pop)_4]^{4-}$ and $[Mo(CN)_8]^{4-}$.[74]

1.4.3.1 Semi-empirical Debye-Hückel Equation for Specific Ion Effects

A semi-empirical method of extending the Debye-Hückel treatment to take account of specific interactions was presented[47] by introducing specific interaction coefficients $B_{i,j}$, which are defined by the equation

$$-\log f_i = A\, Z_i\, F(\mu) - \Sigma_j\, B_{i,j}\, C_j \qquad (1.59)$$

where f_i is the activity coefficient of the ion i, and $F(\mu)$ is some function of the ionic strength μ. The summation extends over all ions of concentration C_j of charge opposite to the ion i. This is due to the fact that oppositely charged ions will approach more closely to one another, resulting in the more intense and the more specific interactions. If the specific interactions between two oppositely charged ions on close approach are repulsive, $B_{i,j}$ will be positive, while if the interactions are attractive $B_{i,j}$ will be negative. For very strong interactions, $B_{i,j}$ can be estimated by the following equation:

$$B_{i,j} \approx -K_{eq}\, f_{ion}^2 / \ln 10 \qquad (1.60)$$

where f_{ion} is the mean free ion activity coefficient, and K_{eq} is the association constant which can be calculated by the Fuoss equation (eq. 1.49).[44]

Two opposing sequences (α and β) of specific interaction coefficients are found for alkali metal, alkaline-earth metal and tetraalkylammonium salts. For anions of weak acids which offer a site of high charge density, such as OH^-, F^- and acetate, $B_{i,j}$ values become increasingly positive with the increasing size of "bare" cation, giving an α (or growth) sequence with cation size. For Cl^-, Br^-, I^- ions and oxyanions with a well-dispersed charge, the opposite is true, giving a β (or decline) sequence with cation size. As can be seen from the Table 1.2,[47] the smaller the anion, the stronger the α sequence, while the larger the anion, the stronger the β sequence.

Table 1.2 Specific interaction coefficients, $B_{i,j}$,[a] for some 1:1 and 1:2 electrolytes at 25 °C.

	α sequence[b]			β sequence[b]			
Cation \ Anion	OH^-	F^-	$CH_3CO_2^-$	Cl^-	I^-	NO_3^-	ClO_4^-
Li^+	-0.22	-	0.16	0.19	0.30	0.18	0.30
Na^+	-0.09	0.06	0.20	0.13	0.18	0.03	0.11
K^+	0.12	0.11	0.23	0.09	0.13	-0.10	-0.48
Cs^+	0.30	0.19	0.24	0.00	-0.01	-0.13	-
NH_4^+	-	-	-	0.09	-	-0.07	-0.10
NMe_4^+	0.5	0.2	0.46	-0.14	-0.4	-	-
NEt_4^+	0.5	0.5	0.39	-0.11	-0.5	-	-
NPr_4^+	0.5	0.5	0.29	-0.11	-0.9	-	-
NBu_4^+	-	0.7	-	0.2	-1.6	-	-0.15
Mg^{2+}	-	-	0.13	0.69	0.95	0.65	1.01
Ca^{2+}	-2.4	-	0.2	0.63	0.85	0.39	0.88
Sr^{2+}	-0.3	-	0.6	0.59	0.82	0.30	0.71
Ba^{2+}	-0.1	-	0.5	0.53	0.76	-0.10	0.65

[a] $B_{i,j}$ (kg mol^{-1}), defined by eq. 1.59; [b] Except for alkyl ammonium cations

According to the Brønsted-Bjerrum relation:

$$k = k^0 \left[\frac{f_A \, f_Q}{f_X} \right] \qquad (1.61)$$

where f_A, f_Q, and f_X are the activity coefficients of reactants A, Q, and the activated complex X. Substituting eq. 1.59 to eq. 1.61 gives

$$\log k = \log k^0 + 2A \, Z_A \, Z_Q \, F(\mu) + \sum_j B_{A,j} \, C_j + \sum_i B_{Q,i} \, C_i - \sum_k B_{X,k} \, C_k \qquad (1.62)$$

where C_j, C_i, C_k represent concentrations of ions with opposite charge to ion A, Q, and X respectively.

Using the knowledge of specific interaction coefficients along with some speculation about charge distribution in activated complexes, one can make some rationalizations and predictions about the specific ion effects on rate constants.

For example, for anion-anion reactions such as the reaction between bromoacetate ($BrCH_2COO^-$) and hydroxide (OH^-), the rate constant will be

$$\log k = \log k^0 + 2A \, F(\mu) + (B_{BrCH_2COO,c} + B_{OH,c} - B_{X,c}) \, C_c \qquad (1.63)$$

where C_c is the concentration of cation.

The OH^- anion shows a strong α sequence; the bromoacetate anion, by analogy with the acetate anion, would be expected also to have an α (growth) sequence. The activated complex, with a dispersed charge and a partially detached bromide ion is likely to display a β (decline) sequence. The net effect of (growth + growth - decline) is a growth sequence in the rate constant, as is indeed observed. For a 1 M added cation, the rate constants are in the ratio[47] 1 : 1.19 : 1.25 : 1.4 : 1.7 for $Li^+ : Na^+ : K^+ : Rb^+ : Cs^+$.

The extended Debye-Hückel equation (with $B_{i,j}$ parameters) also provides a reasonable explanation of salt effects on other types of reaction (e.g. cation-anion, cation-cation), as illustrated in Pethybridge's paper.[47]

1.4.3.2 Water Structure

The observed specific salt effects have been attributed to the influence of salt ions on solvent structure and their participation in the transition state of the reactions. Theories of water structure fall into one of two general classes, uniform and mixture models. Uniform models propose that each water molecule has the same molecular environment as every other water molecule in the liquid. These are clearly inappropriate for the present purposes of dealing with interactions with charged species. By far the greater number of models are mixture models and these have been extensively used in rationalizing the properties of water and aqueous solutions. According to mixture models liquid water contains two or more distinguishable species. Frank and Wen[75,76] proposed the "flickering cluster" model which has received much experimental support.[77-81] In liquid water, as shown in Figure 1.10, there are non-bonded monomers and short-lived liquid clusters (half-life about 10 ps) of varying extent consisting of highly hydrogen-bonded molecules. The water molecules can be considered as in dynamic equilibrium between clusters and monomers, $(H_2O)_{cluster} \rightleftharpoons (H_2O)_{monomer}$. This equilibrium can be altered by changes in temperature or pressure. For instance, with an increase in temperature the extent of inter-molecular hydrogen bonding decreases, the equilibrium shifts to the right, and the "structure of water" breaks down. Conversely with a decrease in temperature the equilibrium shifts to the left, and the structure increases. The structure of water can also be affected by the addition of solute. A solute which causes the shift to the left is termed a structure-maker, and a solute which has an effect in the opposite direction is called a structure-breaker. The structure maker will slow down the diffusion rate of reactants, and *vice versa* for the structure breaker. These effects can be detected experimentally by observing the changes of water properties, such as transport properties (measured by reorientation time, viscosity, conductivity), spectroscopic properties (e.g.

NMR chemical shift δ), and thermodynamic properties (e.g. heat capacity C_p, entropy ΔS, enthalpy ΔH etc).[81-84] Interestingly, bulky organic ions often result in a different influence than observed for inorganic ions, as will be discussed later.

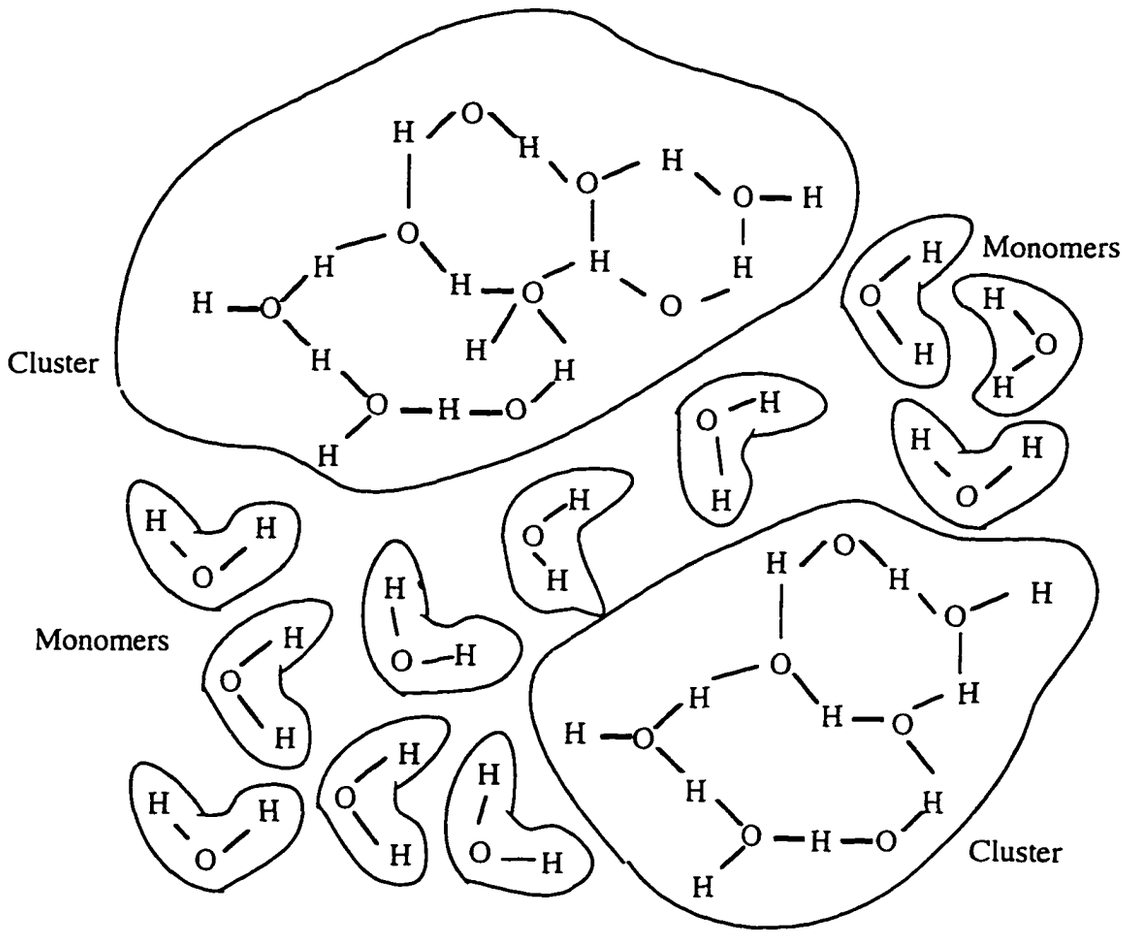

Figure 1.10 Frank-Wen flickering cluster model of liquid water.

1.4.3.3 Electrostatic Interaction between Inorganic Ions and Water Molecules

It was reported that a 0.1 M solution of CsCl is more fluid than pure water at the same temperature, while the viscosity of water increased with the addition of LiCl. In order to explain these phenomena, Frank and Wen[76] proposed a model which identifies three zones of water structure around each ion (Figure 1.11). The inner-most zone A is the hydration shell which contains water molecules polarized, immobilized, and electrostricted by the ion. The bulk water zone C extends from the outer sphere to infinity and includes those water molecules which have essentially the same arrangement as in pure water. The intermediate region B is the one in which the water is less ice-like, (i.e. more randomly organized than "normal" bulk water), and the extent of zone B increases with increasing ion size and contracts with decreasing ion size.

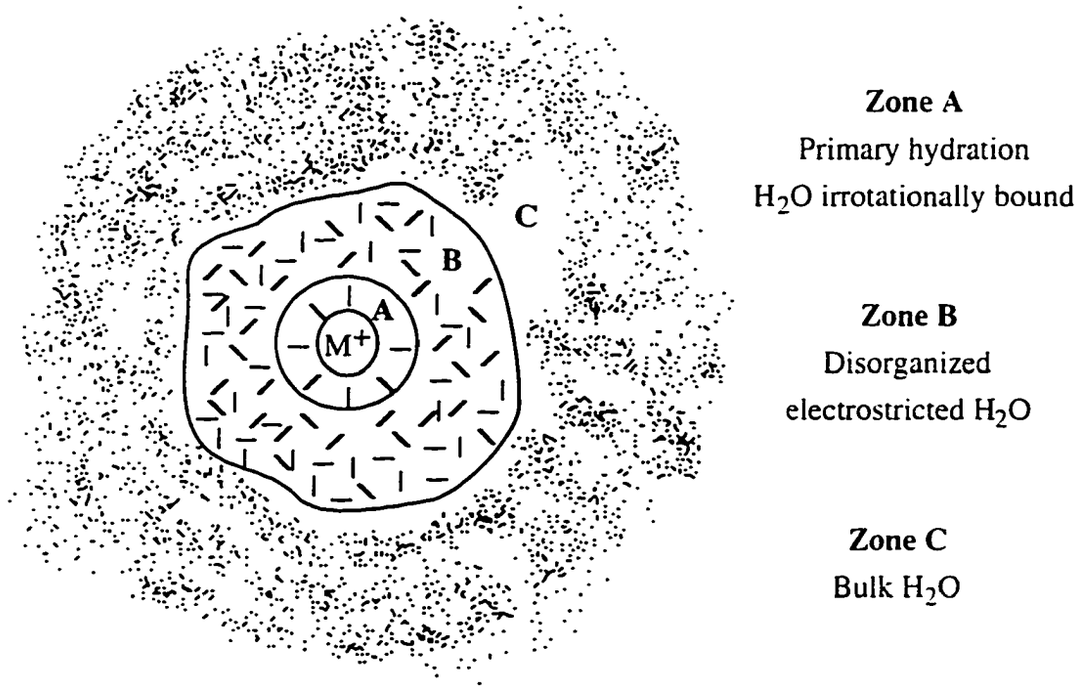

Figure 1.11 Frank-Wen zone model of water in the neighbourhood of a simple cation.

In cases of cations with low charge-density (large size, such as Cs^+ and Ba^{2+} which have relatively weak electrostatic fields), zone B "encroaches" on zone A (perhaps to the extent of extinguishing it altogether), resulting in a smaller zone A thereby causing a net decrease in water structure (C_p decreases, δ shifts to high field, and ΔS increases). This effect becomes more noticeable as cation size increases. Such cations are referrred to as structure breakers. In cases of cations of high charge-density (small size, such as Li^+) zone A "encroaches" on zone B. This effect is stronger for the smaller or the more highly charged ions, resulting in a net structural increase around these cations. Such cations are (electrostrictive) structure makers.

According to this model, anions such as F^- are structure makers, and other halide anions are structure breakers (larger size, more structure breaking); NO_3^- and ClO_4^- are strong structure breakers, and OH^- a structure maker.

1.4.3.4 Hydrophobic Interaction between the Bulky Organic Alkylammonium Ions and Water Molecules

A great deal of interest has been aroused by the often strange properties of large alkylammonium salts in aqueous solutions.[53,55,76,85,86] It has been found that there is a close link between the properties of large alkylammonium ions and those of non-polar solutes. For example, the partial molar volumes $V^{\phi}(R_4N^+Br^-)$ increases through the series R = Me < Et < n-Pr < n-Bu < n-amyl.[86]

It was suggested[76,87,88] that water molecules will form cage-like structures to "hide" the hydrocarbon chains of R_4N^+ ion (guest) inside the cage (host), and by doing so they will reduce the number of voids. The interactions between host (the water lattice) and guest (the ion) are weak van der Waals forces (hydrophobic interaction, i.e. non-

electrostatic effects), and the stability of the structure depends on the extent of occupancy of the cages by the guest. The larger the non-polar group in the guest molecule, the bigger the cavity required. Due to the relative feebleness of both the polarizability and electrostatic influences, the guest molecule is relatively incapable of producing and transmitting the disruptive influences on the water structure, therefore they protect part of the cage boundary from the high-energy attack of bulk water molecules which tries to disrupt the structure. The extent of structure making for alkylammonium ions according to the above model follows the order, $Me_4N^+ < Et_4N^+ < n\text{-}Pr_4N^+ < n\text{-}Bu_4N^+$, and this order agrees with most experimental observation. Actually, Me_4N^+ is just small enough so that the water structure around the ions is still under the influence of charge and therefore is usually classed as an electrostrictive structure breaker (*cf.* cation of Cs^+), whereas in the Et_4N^+ ion the structure enhancement by the ethyl groups only slightly overshadows the electrostrictive structure breaking due to the charge, therefore Et_4N^+ is a weak structure maker and has very little effect on the structure of water. When the alkyl group R is larger than Et, however, the properties are dominated by the hydrophobic alkyl groups, therefore bulky organic ions such as Bu_4N^+ and Pr_4N^+ are strong structure makers due to the nonelectrostatic effects.

Notice that the trends of the size effects observed for the large alkylammonium cations are in the opposite direction to the simple alkaline or alkaline-earth cations. The structure making ability of ions increases with the size of bulky organic ions, but decreases with that of inorganic ions. i.e. a large alkylammonium cation is a structure maker, while a large inorganic cation is a structure breaker.

Obviously the hydrophobic structure forming of water due to bulky organic ions is quite different from the electrostrictive structure forming effects of the lithium cation mentioned in the previous section. Consequently, the structure that is formed around organic ions may not be similar to the structure of the cluster caused by inorganic ions, or that existing in pure water at low temperature.

1.4.3.5 Involvement of the Electrolyte Ions in the Reaction

It is noticed that added anions have the greatest influence on the rate of reaction between two cations, and *vice versa* for cations. For the involvement of cations in anionic reactions, two possible mechanisms have been proposed in the literature, and are shown in Figure 1.11.[59]

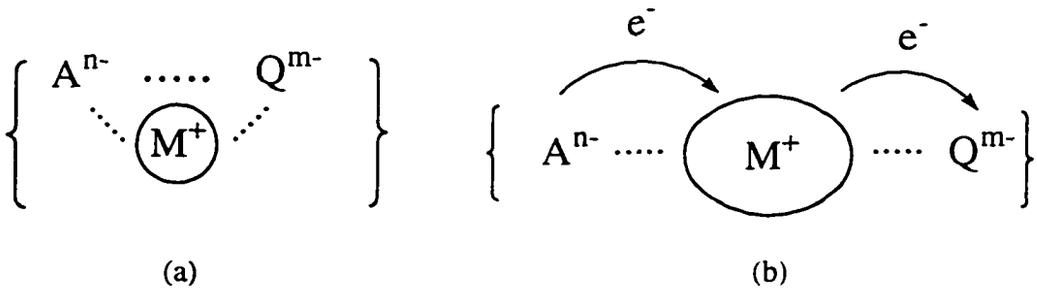

Figure 1.11 Involvement of cations in the transition state of the reaction between anions A^{n-} and Q^{m-}. (a) triangular, and (b) linear ion triplets.

In both cases the cation M^+ facilitates the approach of the two anions in the solution forming an activated complex, and the assisting cation can be involved in the transition state in two arrangements:

(i) triangular arrangement. In this arrangement the cation is off-center (i.e. triangular arrangement among reactant anions and the cation, see Figure 1.11(a)) and reactions occur either directly from one anion to the other or through solvent. The cation is acting as a charge buffer to reduce the electrostatic repulsion between the reacting anions, enabling them to approach each other more closely, and lowering the activation barrier for the reaction.

(ii) linear arrangement. This mechanism suggests that the activated complex would be described as a linear triplet with the structure shown in Figure 1.11(b), i.e. the cation

serves as a bridge between the two anions. One important property of the "bridging ion" is its ability to "conduct" an electron: it can transfer an electron from the reducing agent, eg. A^{n-}, to the bridge cation, with a simultaneous transfer of an electron from the bridge to the oxidizing agent, eg. Q^{m-}. It must be made clear, however, that this outer sphere "double exchange" bridge differs completely from an inner-sphere halide or cyano bridge between metal centers.

In the linear arrangement, polarizability should play a dominant role in catalyzing the reaction. The larger the cation, the larger the polarizability, and the greater the expected reaction rate. The triangular arrangement could also show a linear relationship to size and polarizability, but should be somewhat weaker. Therefore, a linear relationship between rate constant and polarizability of cations may serve as evidence for the formation of ion triplet, and this has been reported in the literature.[63,64,73,74] A similar effect of ligand polarizability was considered in describing the electron transfer between metal ions bridged by organic ligands.[89,90]

Specific ion effects can be very complicated in reactions involving transition metal complexes. One way to eliminate the specific ion effect is to make all measurements in solutions that contain a swamping excess of an inert salt such as 3 M sodium perchlorate.[47] This "swamping technique" has been widely adopted in the kinetic and thermodynamic studies of substitution and redox reactions of complex ions, although not used in this thesis because of the interests in specific ion effects.

1.4.4 Summary

(i) The Debye-Eigen equations can be used to explain the influences of ionic strength on observed rate constants, but a tedious numerical integration is involved in the

calculation. Simplified forms of the Debye-Eigen equation are more commonly used for the reactions in dilute electrolyte solution.

(ii) Olson-Simonson effects are commonly observed in reactions between ions of like charge.

(ii) Specific salt effects on rate constants are due to the influence of the added ions on solvent structure. Inorganic ions change the solvent structure through electrostrictive interactions, while bulky organic ions change the solvent structure through hydrophobic interactions with the solvent molecules. The added ions often participate in the transition state of the reactions by the formation of an ion triplet. A semi-empirical Debye-Hückel theory (using measured $B_{i,j}$ parameters) can be used to explain specific ion effects on simple reactions.

CHAPTER TWO

EXPERIMENTAL

2.1 Materials

All chemicals used were analytical grade reagents purchased from Aldrich, ACP Chemicals Inc., BDH Chemicals, Fisher Scientific Company Ltd., Sigma, or Strem. Most of these chemicals were used without further purification, except the solvents for spectroscopic analysis, which were dried over 4Å molecular sieves. Organo pure water was prepared using a SYBRON / Barnstead Nanopure-A purifying system. Some alkylammonium salts were prepared and purified as mentioned below.

Di- and tri-methylamine hydrochloride, Me_2NH_2Cl and Me_3NHCl, were recrystallized from $CHCl_3$ and dried under vacuum in a desiccator containing P_2O_5. Diethylamine hydrochloride Et_2NH_2Cl was prepared by diffusing hydrogen chloride HCl gas from a cylinder into an Erlenmeyer flask containing 98% diethylamine solution with vigorous stirring. The crude powder was washed with acetone, and recrystallized from ethanol. The final fluffy white product was washed with ether and dried in the vacuum desiccator. Methylamine hydrochloride $MeNH_3Cl$ was prepared by slowly mixing equi-molar portions of concentrated HCl solution (12 M) and methyl amine $MeNH_2$ (40%) in cold ethanol keeping the temperature under 10 °C. To isolate the crude product the solvent was removed using a rotary evaporator. The compound was recrystallized from ethanol to give white crystals, which were then dried in the vacuum desiccator.

2.2 Instrumentals and Techniques

2.2.1 Elemental and Products Analysis

2.2.1.1 C, H, N, S Analyses

C, H, N, S analyses were performed by Canadian Microanalytical Service Ltd. (Delta, Vancouver, British Columbia).

2.2.1.2 Co^{2+} Analysis

Cobaltous ion Co^{2+} was determined according to a literature procedure[91] by forming the blue complex ion $Co(NCS)_4^{2-}$ in a water-DMSO-acetone solution and measuring the absorbance at 625 nm in a 10 cm glass cell. The calibration curve for product analysis for the photochemical reaction of the *trans-/cis*-Co(III)diisothiocyanatotetraam(m)ine complexes in $2x10^{-3}$ M $HClO_4$ solution was $A_{625} = 1.865x10^4 [Co^{2+}] - 0.082$ (10 points) with correlation coefficient R = 0.9997, and the calibration line for $Co(tacn)(NCS)_3$ system (in $8x10^{-4}$ M $HClO_4$ aqueous DMSO (1/1.5 v/v) solution) was $A_{625} = 2.02x10^4 [Co^{2+}] - 0.001$ (6 points) with correlation coefficient R = 0.9999. The difference can be attributed to solvent effect on the Co^{2+}/NCS^- equilibrium constant.

2.2.1.3 NCS^- Analysis

Free thiocyanate ion NCS^- was determined by adding a 2.00 ml aliquot of the irradiated and blank (dark) solution to a 25.00 ml actinic glass volumetric flask containing 10.00 ml of 0.1 M ferric nitrate in 0.5 M $HClO_4$, and measuring the absorbance due to the resulting ferric thiocyanate complex at 450 nm.[92] The calibration line was $A_{450} = 3.596x10^3 [NCS^-] + 0.0740$ (8 points) with correlation coefficient R = 0.99996.

2.2.1.4 NH_3 Analysis

To measure the ammonia yields, efficiently stirred solutions were irradiated in 1-cm rectangular cuvettes and the pH monitored continuously by an Ingold LOT combination electrode interfaced to a PDP-11 computer using a program written in PASCAL by A.D. Kirk. To maintain a constant pH value of the solution, a standard acid (0.09427 M $HClO_4$)

was added from a 200-μL stepping motor buret, and the amount of acid added was recorded periodically . This permitted measurements of the ammonia released by the photoredox reaction. Since the pK_a value of thiocyanic acid HSCN is ca. -1,[93] and is much lower than that of NH_4^+ ($pK_a = 14 - pK_{b,NH_3} = 14 - 4.75 = 9.25$), i.e. NCS^- is a much weaker base (10^{10} times weaker) than NH_3. Therefore there is no interference by released NCS^- at pH 3-4.

2.2.1.5 $(NCS)_2^{-\cdot}$ Analysis

The quantum yield of the intermediate $(NCS)_2^{-\cdot}$ was estimated from laser flash photolysis data. With a laser beam of 6 mm diameter, and a sample window of 4 x 8 mm (Figure 2.1), the moles of photon incident on the sample (n_{photon}) can be calculated using eq. 2.1:

$$n_{photon} = \frac{E}{N\ h\ c\ /\ \lambda}\ S_{eff} \qquad (2.1)$$

where E is the laser pulse energy (30 or 60 mJ), N is Avogadro's number, h is Plank's constant (6.63×10^{-34} J s), c is the speed of light in vacuum (3.00×10^8 m s^{-1}), λ is the irradiation wavelength (355 nm), and S_{eff} is the effective area of the solution irradiated by the laser beam ($S_{eff} = \{4x6\}/\{\pi\,(3)^2\} = 0.85$).

The absorption of $(NCS)_2^{-\cdot}$ was detected using a Xe-lamp as the light source with an average beam width (b) of 2 mm. According to the Beer-Lambert absorption law (eq. 1.2), the fraction of the laser light absorbed by the sample solution, f_a, can be calculated by:

$$f_a = \frac{I_0' - I_t}{I_0} = \frac{I_0\ 10^{-\varepsilon [Co] a} - I_0\ 10^{-\varepsilon [Co] (a+b)}}{I_0}$$

$$= 10^{-\varepsilon [Co] a} (1 - 10^{-\varepsilon [Co] b}) \qquad (2.2)$$

where a = (0.7 cm- 0.2 cm) / 2 = 0.25 cm, b = 0.2 cm, ε and [Co] are the molar absorptivity at irradiation wavelength and the concentration of the Co(III) sample respectively.

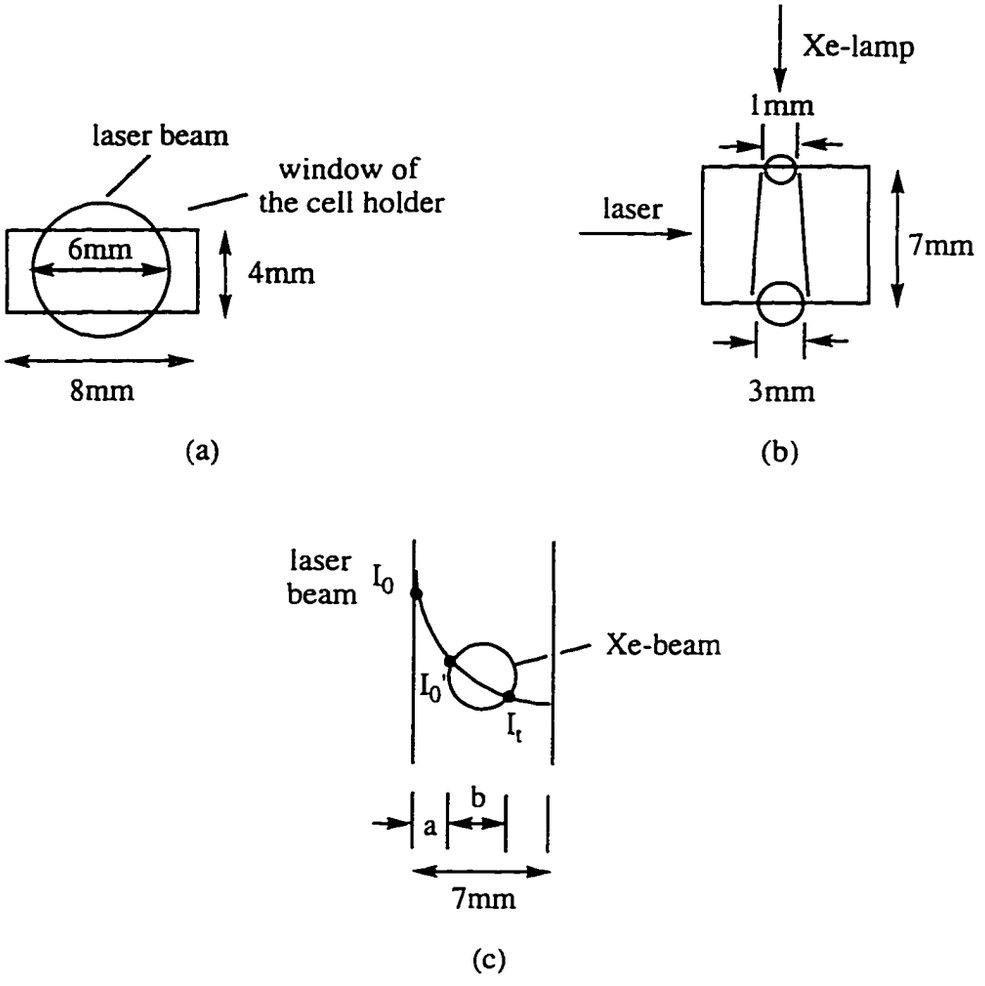

Figure 2.1 Schematic diagrams of laser flash photolysis system.

The number of moles of $(NCS)_2^{-\cdot}$ produced can be obtained by eq. 2.3:

$$n_{(NCS)_2^{-\cdot}} = \frac{A_{(NCS)_2^{-\cdot}}\, V}{\varepsilon_{(NCS)_2^{-\cdot}}\, l} \qquad (2.3)$$

where $n_{(NCS)_2^{-\cdot}}$, $A_{(NCS)_2^{-\cdot}}$, and $\varepsilon_{(NCS)_2^{-\cdot}}$ represent the moles, absorbance and the molar absorptivity of $(NCS)_2^{-\cdot}$; l is the irradiation path length (0.6 cm), and V is the volume in which $(NCS)_2^{-\cdot}$ was detected ($V = 0.4 \times 0.7 \times 0.6\ cm^3 = 1.7 \times 10^{-4}$ L).

Finally the quantum yield of $(NCS)_2^{-\cdot}$ can be estimated from the above equations to give:

$$\Phi_{(NCS)_2^{-\cdot}} = \frac{n_{(NCS)_2^{-\cdot}}}{n_{photon}\, f_a} \qquad (2.4)$$

or, $$\Phi_{(NCS)_2^{-\cdot}} = \frac{0.49\, A_{(NCS)_2^{-\cdot}}}{f_a} \qquad \text{(when E = 30 mJ)} \qquad (2.5)$$

2.2.2 Chromatography

2.2.2.1 HPLC

An ion pair reversed phase HPLC technique, successfully optimized to obtain rapid separations of all the peaks of interest,[94,95] was used. A Varian 5000 liquid chromatograph was used in conjunction with a 25x0.46 cm Chromatographic Sciences ODS2 10 μm C_{18} column. For cobalt(III) cationic complexes, the ion interaction reagent, 25 mM sodium hexanesulfonate (Aldrich, 98%), and the modifier, 20 mM triethylamine hydrochloride (Aldrich, 98%), were dissolved in organo-pure water and in 95% HPLC grade methanol respectively. These eluents were adjusted to pH 3.5 (unless otherwise specified), and filtered through a 0.45 μm Micro Sep membrane filter. A flow rate of 2 mL min^{-1} was used in all systems. The best separations for the $Co(tacn)(NCS)_3$ system

were obtained by using a 30% isocratic combination of these two eluents. Peaks were detected by a Varichrom variable-wavelength detector at 310 nm (unless otherwise specified), which is close to the band maximum of most of the reactants and products.

For highly charged anionic complexes such as $[Co(CN)_5X]^{3-}$ (X = CN, Cl, Br, N_3, I), the procedure was similar to the above, except that 25 mM of o-octylammonium was used as interaction reagent and 25 mM of sodium citrate as modifier. The pH of the eluent was adjusted to 6.5 to ensure that the citrate was present as the 3- species. Eluents were made up using the water and 50% v/v aqueous methanol respectively. It was found that an 80% isocratic combination of the eluents gave the best separations at detecting wavelength of 240 nm.

The above technique gave rapid and good separation of all the peaks of interest. Peak areas were determined by the cutting and weighing of photocopies.

The amount of starting material decomposed can be obtained by the following method:

For reaction	$R \xrightarrow{h\nu} P$			(2.6)
$t_{h\nu} = 0$	c_R^0	0	(mol L^{-1})	
$t_{h\nu} > 0$	$c_R = c_R^0 - c_P$	c_P	(mol L^{-1})	

$$S_R = \int_0^t A\,dt = \int_0^t (\varepsilon_R\, c_R'\, l')\,dt = \varepsilon\, l' \int_0^t c_R\,dt = \varepsilon\, l'\, c_R\, t_w \qquad (2.7)$$

where S_R and t represent the area and the retention time on HPLC, A, ε_R are the absorbance and the molar absorptivity of compound A at the detecting wavelength, l' is the pathlength of light, c_R' represents the concentration of reactant at retention time of t, t_w is the width of HPLC peak which should be a constant for a given compound.

Thus,

$$c_R = c_R^0\left[\frac{S_R}{S_R^0}\right] \qquad (2.8)$$

where S_R^0 represents the HPLC peak area of starting material before the irradiation.

2.2.2.2 Ion Exchange Chromatography

The cationic charge and isomeric purity of the complexes synthesized were monitored using SP Sephadex C-25 cation exchange column (5 x 50 mm) chromatography. Small amounts of the solids were dissolved in water and the cations were absorbed onto the column. Elution was performed with aqueous 0.05 M LiCl. Divalent cations eg. $[Co(NCS)(NH_3)_5]^{2+}$ or *cis*-$[Co(NCS)(NH_3)_4(OH_2)]^{2+}$ were not eluted under such conditions and remained at the top of the column. *Trans*-$[Co(NCS)_2(NH_3)_4]^+$ was readily eluted as a rose-pink band followed more slowly by *cis*-$[Co(NCS)_2(NH_3)_4]^+$ as an orange band. "Chromatographically pure" indicates that only one band was observed on elution and no observable divalent ion residue remained.

2.2.3 X-Ray

2.2.3.1 X-Ray Powder Diffraction

The X-ray powder diffraction photographs of $K_3[Co(CN)_5X]$ complexes (X = CN, Cl, Br, N_3, I) were taken by A.D. Kirk, using a Guinier camera with Cu - Kα line (λ = 1.542 Å) radiation, in Bern, Switzerland.

2.2.3.2 X-Ray Crystallography

A crystal of *trans*-$[Co(NH_3)_4(NCS)_2](NO_3)$ with approximate dimensions 0.15x0.2x0.3 mm was mounted in a random orientation and centered with 25 reflections

(28 - 56° in 2θ), at 20 °C, using an Enraf Nonius CAD-4 automatic diffractometer with Cu (λ = 1.542 Å) radiation. A data set of 570 reflections was collected: h ($\overline{12}$ - 12), k (0 - 12), l (0 - 5) and of these, 338 were used for the analysis (SHELXS direct method) and refinement (SHELXS least squares). Co in the cation and N(4) and O(1) of the nitrate anion were located at special positions. The final refinement converged with an R-factor of 10.7% for Co and S anisotropic and all ammonia H atoms in their calculated positions.

2.2.4 pH, Electroanalytical Techniques, and Conductivity Measurements

2.2.4.1 pH Measurements

The pH of solutions was determined within ± 0.01 pH units with a Fischer "Accumet" 910 digital pH meter and Ingold LOT electrode calibrated with appropriate buffers.

2.2.4.2 Differential Pulse Polarogram

The differential pulse polarography experiments were performed using Princeton Applied Research Model 174A Polarographic Analyzer, with an EG & G PARC Model 303A SMDE (Static Mercury Dropping Electrode) as working electrode, standard Ag/AgCl as reference electrode, and a shiny inert platinum wire as a counter electrode. The cell used was a standard glass polarography cell. The polarograms were recorded with a Hewlett Packard 7040A X-Y Recorder. The parameters were set as follows: potential scan rate 10 mV s^{-1}, scan range from 0 to -1.5 V, modulation amplitude 50 mV, current clock (drop time) 0.5 s, and low pass filter time constant 0.3 s. 0.10 M KNO_3/0.010 M $HClO_4$ aqueous solutions of 5.0×10^{-4} M $K_3[Co(CN)_5X]$ (X = I, N_3, Br, Cl, CN) were used. To avoid the interference of oxygen waves at -0.1 V and -1.0 V vs Ag/AgCl in 0.10 M

KNO_3/0.010 M $HClO_4$ media at room temperature, all solutions were deaerated by nitrogen for 4 min before the scans, and N_2 was passed over the surface of the solution during the recording to prevent re-entry of oxygen. By using the Un-Plot-It (Silk Scientific Inc.) automated digitizing system MS-DOS software and a Hewlett Packard 7475A plotter the original polarograms were then scanned and stored into a computer disk. Final polarograms were generated and analyzed using Igor software on a Macintosh IIci computer.

For irreversible waves, such as observed for these complexes, the estimation of $E_{1/2}$ values is difficult. Hibbert has suggested that the shape of an irreversible polarographic wave can be approximated by the following equation[96]

$$E = E_{1/2} + \frac{RT}{\alpha\ n\ F} \ln\left[\frac{i_d - i}{i}\right] \qquad (2.9)$$

where E is the potential at any point in the rising portion of the current vs potential polarogram curve, R is the universal gas constant, F is the Faraday constant, T is temperature, and α is the transfer coefficient (in the strictly reversible case $\alpha = 1$, the more irreversible the reaction, the nearer α approaches zero), n is the number of electrons involved in the reduction equation, i is the current flowing at the potential E, i_d is the average diffusion current, which can be related by the Ilkovic equation to the parameters of the dropping mercury electrode and the properties of the electroactive species in solution. The Ilkovic equation is:

$$i_d = 607\ n\ D^{1/2}\ C\ m^{2/3}\ t^{1/6} \qquad (2.10)$$

where D is the diffusion coefficient of the reducible ion in solution, C is the concentration of the reactant, m is the mass of mercury flowing, and t is the drop time.

2.2.4.3 Conventional Conductivity Measurements

Conductivity measurements of 1.0×10^{-3} M solutions at room temperature were carried out with automatic temperature compensation using a CDM 83 conductivity meter. The electrode used was a conventional dipping probe with cell constant of 1.065 cm^{-1}, manufactured by Radiometer Copenhagen Electrochemical Measuring Instruments.

2.2.5 Spectroscopy

2.2.5.1 UV/Vis

Routine spectrum: UV/Vis spectra were run on a Philips PU 8740 UV/Vis Spectrophotometer or Cary 5 / Cary 1 UV-Vis-NIR Spectrophotometer using 1 cm quartz cells. All solutions were filtered through 0.45 μm and / or 0.20 μm Micro Sep membrane filters to minimize the scattering effect of particles. The spectral data were transferred to a Macintosh IIci and evaluated using the Igor Pro 2.0.2 Program (WaveMetrics, Inc.).

The generation of product spectrum: For the following reaction:

$$R \xrightarrow{h\nu} P \qquad (2.11)$$

$t_{h\nu} = 0$	c_R^0	0	(mol L^{-1})
$t_{h\nu} > 0$	$c_R = c_R^0 - c_P$	c_P	(mol L^{-1})
	ε_R	ε_P	(L mol^{-1} cm^{-1})

$$A_{total}^0 = c_R^0 \varepsilon_R l \qquad (2.12)$$

$$A_{total} = (c_R^0 - c_P) \varepsilon_R l + c_P \varepsilon_P l = c_R^0 \varepsilon_R l + (\varepsilon_P - \varepsilon_R) c_P l \qquad (2.13)$$

If pathlength l = 1 cm, the total absorbance change ΔA would be:

$$\Delta A = A_{total} - A_{total}^0 = (\varepsilon_P - \varepsilon_R)\, c_P \tag{2.14}$$

Therefore, the product spectrum can be generated by eq. 2.15:

$$\varepsilon_P = \varepsilon_R + \frac{\Delta A}{c_P} \tag{2.15}$$

where $c_P = c_R^0 - c_R$ and can be obtained by other methods (e.g. HPLC).

K_{IP} determination: In the case where ion pairs (IP) form,

$$C + T \rightleftharpoons^{K_{IP}} IP \tag{2.16}$$

where C, T, and IP represent cation, anion, and ion pair respectively.

Assuming [T] >> [C], the ion pair association constant (K_{IP}) can be obtained experimentally using the Benesi-Hildebrand treatment as follows:

$$A = A_C + A_T + A_{IP} \tag{2.17}$$

$$\begin{aligned} A - A_T &= A_C + A_{IP} \\ &= \varepsilon_C [C] + \varepsilon_{IP} [IP] \\ &= \varepsilon_C \{[C]^0 - [IP]\} + \varepsilon_{IP} [IP] \\ &= A_C^0 - \varepsilon_C [IP] + \varepsilon_{IP} [IP] \end{aligned} \tag{2.18}$$

where A is the overall absorbance, A_i and ε_i are absorbance and molar absorptivity for i species. Rearranging eq. 2.18 gives:

$$\begin{aligned} [IP] &= \frac{A - A_T - A_C^0}{\varepsilon_{IP} - \varepsilon_C} \\ &= \frac{\Delta A}{\varepsilon_{IP} - \varepsilon_C} \end{aligned} \tag{2.19}$$

where ΔA is the absorbance change due to the ion pair formation. By definition, the ion pair association constant K_{IP} can be written as:

$$K_{IP} = \frac{[IP]}{[C]\,[T]} = \frac{[IP]}{\{[C]^0 - [IP]\}\,[T]} \qquad (2.20)$$

where ^{0} designates the quantities in the absence of any ion pair. Substituting eq. 2.19 into eq. 2.20 and rearranging the equation leads to:

$$\Delta A = \frac{\{\varepsilon_{IP} - \varepsilon_C\}\,[C]^0\,[T]}{\frac{1}{K_{IP}} + [T]} \qquad (2.21)$$

The K_{IP} value can thus be determined by a non-linear least squares computer fit to equation 2.21 of a plot of ΔA vs [T].

The generation of ion pair spectrum: In order to obtain the ion pair spectra, rearrange eq. 2.21 to give:

$$\varepsilon_{IP} = \varepsilon_C + \frac{\Delta A\,(1 + K_{IP}\,[T])}{K_{IP}\,[C]\,[T]}$$

$$= \frac{A_C^0}{[C]^0} + \frac{(A - A_C^0 - A_T)\,(1 + K_{IP}\,[T])}{K_{IP}\,[C]\,[T]} \qquad (2.22)$$

Therefore the ion pair spectra at each anion concentration [T] can be generated from the spectra of cation, anion, and of combined solutions, together with the K_{IP} value obtained from eq. 2.21. See Chapter 3 for examples.

2.2.5.2 FT-IR

Infrared spectra were obtained in KBr pellets by using a Bruker IFS-25 FT-IR spectrophotometer coupled with an IBM PS/2 Model 50-Z computer.

2.2.5.3 NMR

^{1}H NMR, ^{13}C NMR, ^{31}P NMR, and ^{195}Pt NMR were run on a Bruker AMX 360 MHz NMR spectrometer, or a Bruker B-ACS60 300 MHz NMR spectrometer. The chemical shifts (δ ppm) were reported relative to tetramethylsilane (TMS) for ^{1}H NMR and ^{13}C NMR, and 85% $H_3\underline{P}O_4$ for ^{31}P NMR.

2.2.5.4 Emission / Excitation Spectra

The emission / excitation spectra were obtained from an Aminco SPF 125 double monochromator spectrofluorometer, using a 1 cm silica fluorescence cell. The light source is a Xenon lamp.

2.2.6 Photochemical Procedures

2.2.6.1 Steady State Light Intensity Measurements

Ferrioxalate actinometry[97,98] was used for steady state light intensity measurement at 360 or 370 nm wavelengths. A solution of 3.0 ml of 0.050 M ferrioxalate $[Fe(C_2O_4)_3]^{3-}$ solution (filtered through a 0.45 μm Micron Sep membrane filter) was irradiated for an appropriate time (10 to 150 seconds), depending on the light intensity. $[Fe(C_2O_4)_3]^{3-}$ underwent photochemical reaction to produce free Fe^{2+} as shown below:[99]

$$[Fe(C_2O_4)_3]^{3-} \xrightarrow{h\nu} Fe^{2+} + 2\,C_2O_4^{2-} + C_2O_4^{-} \quad (2.23a)$$

$$[Fe(C_2O_4)_3]^{3-} + C_2O_4^{-} \longrightarrow Fe^{2+} + 3\,C_2O_4^{2-} + 2\,CO_2 \quad (2.23b)$$

$$\text{i.e.} \quad 2\,[Fe(C_2O_4)_3]^{3-} \xrightarrow{h\nu} 2\,Fe^{2+} + 5\,C_2O_4^{2-} + 2\,CO_2 \quad (2.23)$$

After irradiation, the entire solution was quantitatively transferred into a 25.00 mL actinic glass volumetric flask, 6.00 mL of developer (0.1% 1,10-phenanthroline, 0.75 M sodium acetate in 0.2 M H_2SO_4) was added, mixed well and stood in the dark for about 30 min. to allow the reaction of Fe^{2+} with 1,10-phenanthroline to be complete. The absorbance in a 1 cm rectangular cell was measured at 510 nm, where the $Fe(phen)_3^{2+}$ product absorbs. The incident light intensity (einstein s^{-1}) was calculated using the following equation:

$$I_0 = \left[\frac{A_p - A_d}{\varepsilon_{510}\, l}\right]\left[\frac{V_T}{\varnothing\, f_a\, t}\right] \quad (2.24)$$

where A_p and A_d are the absorbances of the photolysed and the blank solution at 510 nm respectively. $V_T = 2.500\times10^{-2}$ L, $\varepsilon_{510} = 1.105\times10^{4}$ M^{-1} cm^{-1} is the molar absorptivity of $Fe(phen)_3^{2+}$ complex at 510 nm, l = 1 cm is the path length of the cell, $\varnothing$ is the known quantum yield value of Fe^{2+} production by ferrioxalate at the appropriate wavelength ($\varnothing_{360}$ = 1.28. For $\lambda_{irradiation} < 436$ nm, $\varnothing_{Fe2+} > 1$ due to the secondary thermal reaction, eq. 2.23b),[99] $f_a = 1\text{-}10^{-A}$ is the fraction of the light absorbed by original ferrioxalate solution, where A is the absorbance of the ferrioxalate solution at the wavelength of photolysis, and t is the time of photolysis.

It was reported that higher concentrations of ferrioxalate (0.15 M) required longer time for equilibriation. Several methods were recommended to solve this problem.[100] The addition of excess phenanthroline is applied here ([phen]:[Fe^{2+}] > 20) and 30 min. reaction time is more than adequate to reach the full absorbance.

2.2.6.2 Steady State Photolysis

An HBO 100 W mercury lamp was used as the light source for steady state measurements of quantum yield. The light was filtered through a Corning CS 7-60 filter and a monochromator set at 360 or 365 nm, with 5 cm of water as an infrared absorber. The lamp intensity was measured by ferrioxalate actinometry to be in the range of $1\text{-}10\text{x}10^{-8}$ einstein s^{-1} for the studies of diisothiocyanato am(m)ine cobalt(III) and triisothiocyanato tacn cobalt(III) systems, or $2.4\text{x}10^{-9}$ einstein s^{-1} during the studies of $[Pt_2(pop)_4]^{4-}$ quenching. As a check, the light intensity was continuously monitored with an Alphametrics Model P111OS silicon diode detector and Model 1020 meter. Solutions were irradiated with magnetic stirring (for diisothiocyanatoam(m)inecobalt(III) and $Co(tacn)(NCS)_3$ systems) or nitrogen bubbling (for $[Pt_2(pop)_4]^{4-}$ system) in 1 cm rectangular glass spectrophotometer cells held in a thermostatted cell compartment at 20.0 ± 0.1 °C or 22.0 ± 0.01 °C for the isothiocyanatoam(m)inecobalt(III) and $[Pt_2(pop)_4]^{4-}$ systems respectively. For diisothiocyanatoam(m)inecobalt(III) most of the studies were carried out in aqueous $2.0\text{x}10^{-3}$ M $HClO_4$ solution, and the concentration of complexes was typically $2\text{x}10^{-3}$ M. For $Co(tacn)(NCS)_3$ studies, the solvent used was $8\text{x}10^{-4}$ M $HClO_4$ aqueous DMSO (1/1.5 v/v) solution unless otherwise specified, and the concentration of the complex was typically $5.30\text{x}10^{-4}$ M. For the studies in $[Pt_2(pop)_4]^{4-}$ system, the concentration of $[Pt_2(pop)_4]^{4-}$ was typically $3\text{x}10^{-5}$ M and that of quencher $[Co(CN)_5X]^{3-}$ ranged from $1\text{-}2\text{x}10^{-4}$ M, in 0.50 M cation concentration and 0.010 M $HClO_4$ media with continuous N_2 degassing. The solutions were photolyzed to conversions less than 15% (unless otherwise specified) to avoid secondary photolysis.

2.2.6.3 Laser Flash Photolysis

A GCR-12 Spectra Physics Nd:YAG laser with harmonic generator / Spectra Physics Model PHS-1 wavelength separator was used for flash photolysis studies. The

laser pulse characteristics were 355 nm with 7 ns half-width. The laser pulse energy was measured by a thermal detector (Molectron J50) / Tektronix 2445 oscilloscope.

Conductivity measurement: The laser pulse energy at 355 nm was 40 mJ. The DC-conductivity quartz flow cell involves three equally spaced (0.7 cm apart) Pt electrodes each 0.5 mm in diameter and 10 mm long. The dimensions of the cell are 0.7x0.7x3 cm. The two outer electrodes are connected to a 50 ohm resistor and a variable resistor, producing a Wheatstone bridge network in conjunction with the resistance of the solution, as shown in Figure 2.2. A 150 V square wave DC pulse of approximately 4 ms duration is applied to the central electrode, and the Wheatstone bridge balanced through the use of the variable resistor. The baseline signal is further controlled by varying the timing of the laser pulse relative to the potential pulse so that triggering is on the flattest portion of the 4 ms pulse. The laser beam is directed through a 0.6x0.4 cm window irradiating the solution between the two upper electrodes. The resulting change in the conductivity due to photoreaction is detected through the imbalance of the bridge and measured as a voltage. The transient conductivity data after excitation are amplified using a two-stage amplifier with gain settings of 1, 10, and 30 before being relayed to a Tektronix TDS-520 digital scope. The timing of the laser pulse and data acquisition is set by a custom pulse generator and synchronizer operated with a Standford Research Systems DG-535 delay generator. The experimental system is integrated to a Macintosh IIci computer and the acquisition and analysis programs were written by L. Netter and A.D. Kirk using Labview 2.2 (National Instruments). These programs control the sequencing of the laser pulses and shutters along with data transfer from the Tektronix TDS-520 and mathematical transformation of the data.

The absorbance of the solution used was adjusted to ~ 0.3 at 355 nm, and pH adjusted to 3.5. About 50 mL of the solution was pumped from the reservoir through the cell using a peristaltic pump with a flow rate of approximately 40 mL min^{-1}. Under such conditions the possibility of the secondary photolysis is minimized.

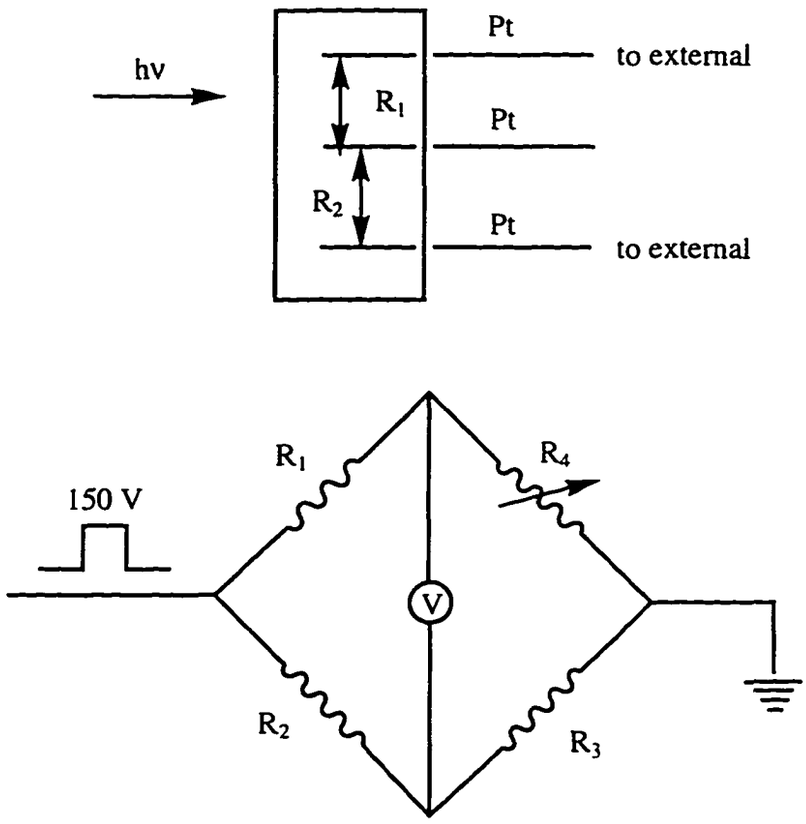

Figure 2.2 Wheatstone network for laser flash conductivity measurement.

Transient absorption measurements at fixed wavelength: The laser pulse energy was set at 30 mJ for diisothiocyanatoam(m)inecobalt(III) system, and 60 mJ for $Co(tacn)(NCS)_3$ system (unless otherwise specified). A 150 W Oriel Xe-arc lamp and a CVI Model Digikrom 240 monochromator were used together with two 435 nm cut off filters. One filter, placed between the lamp and sample, minimized photolysis of the sample while the other, set in front of the monochromator, cut off both environmental and scattered light. Solutions in 7 x 7 mm quartz cells closed by rubber septa were adjusted to an absorbance of about 0.3 at 355 nm. Between laser shots the solution was deaerated and

stirred, if necessary, by N_2 bubbling which was paused during data collection. The solutions were irradiated at 355 nm for 10 laser shots and the $(SCN)_2^{-\cdot}$ transient absorption signal was detected at 475 nm. Data were collected by a TDS 520 Tektronix oscilloscope.

Transient absorption spectra: Nanosecond time resolved absorption spectra were obtained using the same procedures but detection involved the use of an intensified dual diode array system (Princeton Instruments DIDA 700/RG, detector controller ST116, ISA Spectrometer HR-320 and high voltage gating pulse generator PG200). The solutions were stirred by passing N_2 gas between each shot.

The picosecond flash photolysis was carried out by D.M. Kneeland, exciting with a 1-1.5 mJ, 30 ps pulse at 355 nm, using the facilities at Concordia University in Montreal. Transient absorption was probed by means of a double-beam OMA system employing a 30 ps probe light pulse of effective wavelength in the range 400 to 700 nm.

2.2.6.4 Emission Lifetime Measurements

Principles: A PTI PL 2300 Nitrogen Laser of output energy 1.5 mJ at 337 nm was used with a repetition rate of 3 Hz at 18.5 kV. As fill gas, 99.999% ultra pure grade nitrogen was further purified by passing through a Hydrocarbon Trap and a 13 X molecular sieve Moisture Trap (Chromatographic Specialties Inc.). The laser pulse was filtered through a Corning CS 7-54 filter before reaching the solution.

Cell design: At the N_2 laser wavelength (337 nm) $[Pt_2(pop)_4]^{4-}$, the complex which is to be studied, has a much smaller molar absorptivity than the quencher $[Co(CN)_5I]^{3-}$. In order to quench the lifetime of $*[Pt_2(pop)_4]^{4-}$ to half of its initial value, the quencher concentration should be about 10^{-3} M, while the concentration of $[Pt_2(pop)_4]^{4-}$ should be about $3x10^{-4}$ M to achieve an absorbance of 0.3 at 337 nm. Under such conditions the iodo complex would absorb 90% of the light, possibly leading to the photolysis of the quencher, as well as serious inner filter effects in the Stern-Volmer study. Therefore it was considered desirable to find a way of irradiating $[Pt_2(pop)_4]^{4-}$ at its

emission maximum of about 370 nm. Quinine sulfate in ethanol has a strong absorption between 320 nm and 340 nm (log $\varepsilon = 4$) and emits at 370 nm, where $\varepsilon([Pt_2(pop)_4]^{4-}) \gg \varepsilon([Co(CN)_5I]^{3-})$, and has a fluorescence lifetime of 19.2 ns,[101] short enough to avoid distortion of the 9 μs emission decay curve of $*[Pt_2(pop)_4]^{4-}$, and can thus be used as a wavelength shifter. The absorbance of quinine sulfate solution (in ethanol) at 337 nm was adjusted to 3.0 (ca. 3×10^{-4} M), and fresh solution was used for each quenching experiment. Such a high absorbance was necessary, as quinine solution undergoes partial bleaching during the laser pulse, leading to a smaller than expected absorption with dilute solutions. This results in a low level of emission intensity from the quinine and consequently low level of excitation of $[Pt_2(pop)_4]^{4-}$ solution.

Emission arrangement: Two 1-cm fluorescence cells were used and placed in line with the laser beam. The one which faces the laser beam contained quinine solution, and the one behind this was the sample cell containing 2.60 mL of $[Pt_2(pop)_4]^{4-}$ solution (see Figure 2.3). Both cells were held in a thermostatted cell compartment connected to a MGW Lauda RC 6 refrigerating bath, with the temperature maintained at 22.0 ± 0.1 °C. Nitrogen was passed through a 0.010 M $HClO_4$ solution and bubbled into the working solution for degassing and mixing after the addition of quencher. By focusing the laser on the quinine sulfate solution, 370 nm fluorescence was generated which in turn excited preferentially the $[Pt_2(pop)_4]^{4-}$ solution. The resulting emission from the $[Pt_2(pop)_4]^{4-}$ solution was first filtered by a Corning CS 3-72 glass filter, then a $K_2Cr_2O_7$ solution filter to remove any radiation of wavelength shorter than 500 nm, and finally a neutral density filter to avoid overloading the photomultiplier and distorting the signal. The emission decay was detected at right angles to the laser beam by a Jarrel-Ash 82-410 monochromator (set at 514 nm for $[Pt_2(pop)_4]^{4-}$ system) / Hamamatsu R928 GaAs photomultiplier / Tektronix 2230 digital storage oscilloscope detector system (connected with 200 ohm load resister) with a GPIB interface to an ATARI 1040 microcomputer. Lifetimes were evaluated by weighted linear regression on a plot of ln(intensity) versus time[102] over 1024 channels of decay using a

fitting program written by A.D. Kirk. A schematic diagram of the experimental set up for the emission lifetime described above is shown in Figure 2.3.

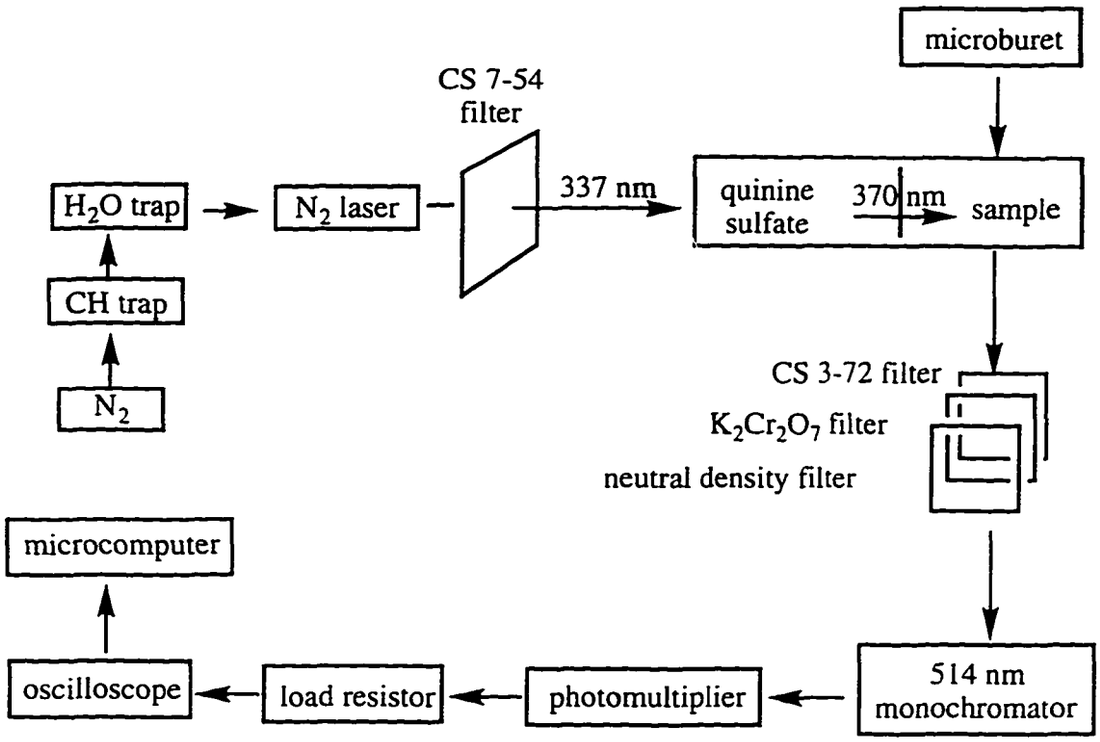

Figure 2.3 Experimental set-up for emission lifetime measurement.

Data collection: Solutions of MCl ($M = Li^+$, Na^+, K^+, Cs^+), $M'Cl_2$ ($M' = Mg^{2+}$, Ca^{2+}, Sr^{2+}, Ba^{2+}), $R_nNH_{4-n}Cl$ (R = H, Me, Et, n-Pr, n = 0-3), or K_nX ($X = Br^-$, NO_3^-, SO_4^{2-}, $[Co(CN)_6]^{3-}$, n = 1-3) electrolytes (0.500 M in cation concentration unless otherwise mentioned) were prepared by dissolving accurately weighed amounts in 0.010 M $HClO_4$ aqueous solution. The solutions were kept in polyethylene bottles to avoid leaching of impurities from glass containers.[103] $[Pt_2(pop)_4]^{4-}$ solution was freshly prepared by dissolving the complex in the appropriate electrolyte solution (except when biacetyl was used as a quencher, where the experiment was conducted in aqueous solution in the absence of electrolytes) until an absorbance of about 1 (in a 1-cm quartz cell) at 370 nm

was achieved. The solution was then purged with nitrogen until the lifetime reached an upper limit constant value. The quencher, also dissolved in the appropriate chloride salt solution, was delivered into the $[Pt_2(pop)_4]^{4-}$ solution in 5 - 20 μL aliquots by a microburet fitted with a capillary tube. The final absorption of quencher was less than 50% of the total absorption even at the maximum quencher concentrations used. For each aliquot of quencher added, the lifetime, τ, was determined a minimum of 5 times. For each experiment, the maximum quencher added reduced the lifetime of $*[Pt_2(pop)_4]^{4-}$ to approximately half of its initial value in 7 - 12 aliquots, and the quenching rate constant k_q was obtained from a Stern-Volmer plot of τ^0/τ vs [Q]. Each quenching experiment was carried out for 2 to 5 times, and the average rate constant value was reported.

2.3 Synthesis of the Coordination Complexes

2.3.1 Co(III)diisothiocyanatotetraam(m)ine Complexes, *Trans-/Cis*-$[Co(NCS)_2(NH_3)_4]ClO_4$ and *Trans-/Cis*-$[Co(NCS)_2(en)_2]ClO_4$

2.3.1.1 *Trans*-$[Co(NCS)_2(NH_3)_4]ClO_4$

A solution of $CoCl_2 \cdot 6H_2O$ (24 g) and NH_4NCS (76 g) in 200 ml of 10% aqueous ammonia was air oxidized for 6 hours at 40 °C to give 8 g red powder (compared to the previously reported[104] 13 g). This material contained $[Co(NCS)(NH_3)_5]^{2+}$ as well as *trans*- and *cis*-$[Co(NCS)_2(NH_3)_4]^+$.

The red powder (6 g) was dissolved in 200 ml of 0.1 M acetic acid at 80 °C. On addition of 15 g of $NaNO_3$ to the hot solution, an orange precipitate of impure $[Co(NCS)(NH_3)_5](NO_3)_2$ deposited (2 g, containing some $[Co(NCS)_2(NH_3)_4]NO_3$). This was filtered from the hot solution, and washed with ethanol and acetone.

The mother liquor deposited about 1.8 g of slightly impure *trans*-$[Co(NCS)_2(NH_3)_4]NO_3$ which was washed with ethanol and acetone. This was recrystallized as the perchlorate salt from 120 ml 0.1 M acetic acid at 80 °C by addition of $NaClO_4 \cdot H_2O$ (15 g). Three crops of orange-red *trans*-$[Co(NCS)_4(NH_3)_4]ClO_4$ were collected; one from the hot solution (0.72 g), one after 30 min. at room temperature (0.3 g), and one on standing at room temperature (0.3 g) overnight. The products were washed with ethanol only. The purest of these was the first.

2.3.1.2 *Cis*-$[Co(NCS)_2(NH_3)_4]ClO_4$

$[Co(CO_3)(NH_3)_4]NO_3$ was prepared according to published procedures.[105,106] A 5 g sample of this compound was converted to *cis*-$[Co(NH_3)_4(OH_2)_2]_2(SO_4)_3$ using the method of Springborg and Schäffer.[107] The diaqua product was dissolved in 50 ml of 0.5 M acetic acid and 7 g of NaNCS was added. The solution was then heated to about 70 °C for 10 min. (care, some decomposition occurs), filtered to remove any oxide precipitate, and 15 g of $NaNO_3$ added to the hot solution. Fine red crystals of *cis*-$[Co(NCS)(NH_3)_4(OH_2)](NO_3)_2$ were deposited (3.4 g) and these were collected and washed with a little H_2O. This product was recrystallized (3.1 g yield) from 0.1 M acetic acid (80 ml, 80 °C) by addition of 10 g $NaNO_3$ and washed with ethanol, then acetone. The original mother liquor slowly deposited a further 1 g of impure *cis*-$[Co(NCS)_2(NH_3)_4]NO_3$ on long standing.

The dinitrate salt of the aqua thiocyanato tetraammine cobaltate was converted to the dithiocyanate complex, *cis*-$[Co(NCS)(NH_3)_4(OH_2)](NCS)_2$, by metathesis. A 2.1 g sample of *cis*-$[Co(NCS)(NH_3)_4(OH_2)](NO_3)_2$ was dissolved in 80 ml of 0.1 M acetic acid at 80 °C and 5 g of NaNCS was added. The solution was cooled rapidly in ice to give about 1 g of red product which was washed with ethanol only. The mother liquor

deposited a small amount of *cis*-$[Co(NCS)_2(NH_3)_4]NCS$ on standing overnight at room temperature.

The *cis*-$[Co(NCS)(NH_3)_4(OH_2)](NCS)_2$ obtained was further converted to *cis*-$[Co(NCS)_2(NH_3)_4]NCS$ by thermal dehydration in an oven at 75 °C for 3 hours. The crude orange dithiocyanate product was recrystallized as the perchlorate salt by dissolving in 80 ml 0.1 M acetic acid at 80 °C and the addition of 10 g $NaClO_4 \cdot H_2O$. The product deposited from the hot solution was collected at 40 °C and washed with 95% ethanol and acetone to give chromatographically pure, tan coloured, *cis*-$[Co(NCS)_2(NH_3)_4]ClO_4$ (0.51 g).

2.3.1.3 *Trans*- and *Cis*-$[Co(NCS)_2(en)_2]ClO_4$

5 g *trans*-$[Co(en)_2Cl_2]ClO_4$ (obtained by Krishnamurthy's method[108]) was dissolved in 70 ml 0.1 M $HClO_4$. 7 g of NH_4NCS was added and after heating to 80 °C for 2 h, was cooled to room temperature and allowed to stand overnight (because the *trans* isomer forms very slowly). A mixture of *trans-/cis*-$[Co(NCS)_2(en)_2]NCS$ (4 g) was obtained, to which acetone was added with vigorous stirring. The red solid (mainly *cis* isomer) and blue solution (mainly *trans*) were separated by filtration. The 3 g crude *cis* isomer was washed with acetone until the filtrate was colorless, dissolved in 0.1 M HAc and converted to 2.5 g *cis*-$[Co(NCS)_2(en)_2]NO_3$ by reaction with 5 g $NaNO_3$. It was recrystallized as the pinkish *cis*-$[Co(NCS)_2(en)_2]ClO_4$ (2.5 g) from hot 0.1 M HAc solution with the addition of 20 g $NaClO_4 \cdot H_2O$.

To obtain the pure *trans*- complex, water was added to the blue acetone solution until the volume was tripled and the color of the solution turned to orange. With heating and stirring, 30 g $NaNO_3$ was added to the above solution until a pinkish solid (*cis* isomer) appeared. The *cis* isomer was filtered off and the filtrate was cooled to room temperature gradually, and left to stand overnight. 0.12 g of red needle crystals of

trans-$[Co(NCS)_2(en)_2]NO_3$ were obtained and recrystallized as the perchlorate salt, *trans*-$[Co(NCS)_2(en)_2]ClO_4$ (0.1 g), from hot HAc/$NaClO_4$ solution.

2.3.2 Co(III)(1,4,7-triazacyclononane)triisothiocyanato Complexes, Co(tacn)$(NCS)_3$, Co(tacn)$(NCS)_3$·3DMSO, and Co(Me_3tacn)$(NCS)_3$

2.3.2.1 Co(tacn)$(NCS)_3$

Tacn·3HCl can be synthesized according to literature method,[109] and was kindly provided by I. Mackay. 0.80 g (3.3 mmol) of tacn·3HCl was mixed with a stoichiometric amount of freshly prepared sodium ethoxide in ethanol. The resulting sodium chloride was filtered off, leaving the free amine in ethanol. $CoCl_2$, 0.65 g (5 mmol) and 1.5 g KNCS (15 mmol) were then added to this solution and air was bubbled through the mixture until the color turned from blue to brownish (ca. 12 h). After removing the excess reactants by extraction with 0.1 M aqueous hydrochloric acid, a tan precipitate was obtained. After filtration, this crude product was dissolved into the minimum amount of DMSO and the filtered solution was then added dropwise into a 100-fold volume of water. The orange powder that formed was washed with water, ethanol, and ether and was dried under vacuum. The total yield was 0.62 g (52%). The compound was soluble in DMSO, DMF and pyridine, but insoluble in nonpolar solvents as well as in ethanol, THF, acetonitrile, ethyl acetate, formamide and water. It was stable in air and in DMSO or aqueous/DMSO solutions.

2.3.2.2 Co(tacn)$(NCS)_3$·3DMSO

Red crystals were obtained by dissolving the above tan powder into DMSO and evaporating in a stream of air overnight. After carefully washing with cold DMSO and

drying under vacuum, these monoclinic crystals were found by elemental analysis to be $Co(tacn)(NCS)_3 \cdot 3DMSO$.

2.3.2.3 $Co(Me_3tacn)(NCS)_3$

An analogous preparation starting with N,N',N''-trimethyltriazacyclonane, a yellowish oil prepared by the reaction of free tacn with excess HCOOH/HCHO,[110] gave a crude tan product of which the solubility in all solvents tried was not improved compared with $Co(tacn)(NCS)_3$. It was therefore not explored further.

2.3.3 Potassium Acidopentacyano Cobaltate (III) Complexes, $K_3[Co(CN)_5X]$ (X = N_3, I, Br, Cl)

Literature methods were used for the synthesis of the precursor $[Co(NH_3)_5N_3]Cl_2$[111] and $K_3[Co(CN)_5N_3] \cdot 2H_2O$.[112] The latter complex was carefully recrystallized to remove potassium chloride.[113] Flor and Casabo's method was used for the syntheses of acidopentacyano cobaltate(III) complexes,[114] but further purification was needed, especially for the chloro complex. The crude product was dissolved in a minimum amount of water (for the bromo- and iodo- complexes) or 50% ethanol (for the chloro-complex) and filtered. The filtrate became oily when mixed with cold ethanol (0 °C). The purest products were obtained with an oily filtrate, rather than powder, when mixed with EtOH. After being vigorous stirred in the ethanol solution, the oily product was broken into smaller droplets, and the supernatant was discarded. The above process (+ cold EtOH, stir, and discard supernatant) was repeated until the filtrate was finally solidified. The final precipitate was then filtered, washed with cold ethanol, acetone, and ether, and vacuum dried in a desiccator. For the chloro complex, the above purification procedure seems to be relatively inefficient, resulting in a low product yield.

2.3.4 Potassium Tetrakis(μ-pyrophosphite-P,P')diplatinate(II) Dihydrate, $K_4[Pt_2(\mu\text{-}P_2O_5H_2)_4]\cdot 2H_2O$

The complex was prepared by modifying a literature procedure.[115] Fresh 97% phosphorous acid H_3PO_3 stored under nitrogen was used in the synthesis. A solution of 0.8 g of K_2PtCl_4 and 3.0 g of H_3PO_3 in 4 to 5 ml H_2O was heated for about 3 hrs in a 100 °C glycerol bath with continuous stirring. A small stream of N_2 gas was blown into the solution to prevent any air oxidation. The water content of the solution was replenished periodically to prevent the solution from evaporating to dryness. During the heating process the color of the solution gradually changed from red to brown, then to yellow-green. Instead of being dried in an oven which led to a low product yield, the solution was left in the 100 °C bath and dried by N_2 flow. The solid was treated with methanol and acetone to remove unreacted H_3PO_3. The crude product was purified by dissolving in a minimum amount of degassed water, and filtering through a medium porosity filter (10 to 20 μm), and a 0.45 μm Micron Sep membrane filter. Degassed methanol followed by acetone were quickly added to this bright yellow solution. Some very fine powder formed, and the solution was degassed, sealed, and cooled in a refrigerator overnight. The yellow-green, fine powder obtained was filtered through a fine porosity filter, under N_2, to prevent the complex from being oxidized. The powder was then washed with methanol, acetone, ether, and vacuum dried. Yield 45%. The dry sample was air-stable, and solutions in degassed water were stable for several hours. Aerated solutions gradually turned purple or even black within an hour.

CHAPTER THREE

PHOTOREDOX BEHAVIOUR OF *TRANS*- AND *CIS*-DIISOTHIOCYANATOTETRAAM(M)INECOBALTATE(III) COMPLEXES

3.1 Introduction

Following on from Kirk and Langford's attempts to observe a putative Co^{II} radical pair species (see section 1.3.3),[41] the *trans-* and *cis-* isomers of $[Co(NCS)_2(NH_3)_4]^+$ and $[Co(NCS)_2(en)_2]^+$ were chosen for study because of their potential to give transient Co(II) fragments capable of being seen by laser flash photolysis. The presence of a remaining NCS^- ion in the Co(II) fragment provides filled and empty π^* orbitals in the intermediate, so that intense CT transitions could assist a spectroscopic search for the radical pair. Both steady state and laser flash photolysis (LFP) methods were used in the work. As will be seen in this Chapter, the search for a radical pair was not successful. Instead, a strong transient owing to $(NCS)_2^{-\cdot}$ dominated the spectrum. Furthermore, a significant thiocyanate effect was observed for the first time, which led to intensive studies on the reaction mechanisms.

3.2 Results

3.2.1 Characterization of *Trans-/Cis-*$[Co(NCS)_2(NH_3)_4]ClO_4$ and *Trans-/Cis-*$[Co(NCS)_2(en)_2]ClO_4$

3.2.1.1 UV/Vis Spectra

Table 3.1 gives the wavelengths of peak maxima (λ_{max}) and molar absorptivity values at maximum absorption (ε_{max}) obtained from UV/Vis spectra as well as the physical appearance of *trans-/cis-*$[Co(NCS)_2(NH_3)_4]ClO_4$ and *trans-/cis-*$[Co(NCS)_2(en)_2]ClO_4$ compounds in aqueous solution. The redox quantum yield $\emptyset(Co^{2+})$ at 20 °C and 360 nm irradiation wavelength, and the molar percentage of residual NCS^- are listed in Table 3.2.

Table 3.1 Colour and UV/Vis data of *trans-/cis*-$[Co(NCS)_2(NH_3)_4]^+$ and *trans-/cis*-$[Co(NCS)_2(en)_2]^+$ complexes in aqueous solution.

Complexes	$\lambda_{max,1}(\varepsilon_1)^a$	$\lambda_{max,2}(\varepsilon_2)^a$	$R = \frac{\varepsilon_1}{\varepsilon_2}$	colour
trans-$[Co(NCS)_2(NH_3)_4]^+$	325(2960)	525(281)	10.5	pink
cis-$[Co(NCS)_2(NH_3)_4]^+$	311(2830)	506(276)	10.2	orange
trans-$[Co(NCS)_2(en)_2]^+$	324(3260)	510(296)	11.0	orange-red
cis-$[Co(NCS)_2(en)_2]^+$	309(2980)	490(362)	8.2	orange

[a] nm (L mol^{-1} cm^{-1}).

Table 3.2 Redox quantum yield $\Phi(Co^{2+})$ in pH 2.7 solution and molar percentage of residual NCS^- in *trans-/cis*-$[Co(NCS)_2(NH_3)_4]^+$ and *trans-/cis*-$[Co(NCS)_2(en)_2]^+$ complexes.

Complexes	$\Phi(Co^{2+}) / H^{+a}$	% Residual NCS^-
trans-$[Co(NCS)_2(NH_3)_4]^+$	0.065	2.5
cis-$[Co(NCS)_2(NH_3)_4]^+$	0.082	2.6
trans-$[Co(NCS)_2(en)_2]^+$	0.009	2.5
cis-$[Co(NCS)_2(en)_2]^+$	0.003	4.9

[a] $\lambda_{irrad.}$ = 360 nm, T = 20.0 °C.

3.2.1.2 Single Crystal X-ray Structure Determination of *Trans*-$[Co(NCS)_2(NH_3)_4]NO_3$

A sample of the nitrate salt of the *trans*-$[Co(NCS)_2(NH_3)_4]NO_3$ (most rapidly eluted from Sephadex C-25 with 0.05M LiCl) was crystallized from water by slow evaporation to give red monoclinic crystals. The crystallographic parameters were: elemental formula $C_2H_{12}N_7S_2O_3Co$; molecular weight 305.2; space group C2/c (No. 15); $\underline{a}$ = 12.733(3), $\underline{b}$ = 13.017(3), $\underline{c}$ = 7.397(1)Å; β = 95.95(1)°; V = 1219.5 Å^3; D_m = 1.638 g/cm^3 (flotation); D_c = 1.662 g/cm^3 for Z = 8. Table 3.3 gives the atomic positional coordinates for the non-hydrogen atoms and Table 3.4 gives some of the more interesting bond lengths and angles.

Table 3.3 Atomic positional coordinates for *trans*-$[Co(NCS)_2(NH_3)_4]NO_3$.

Atom	x / a	y / b	z / c
Co	0.2500	0.2500	0.5000
S	0.4088(6)	0.3958(6)	1.035(1)
N(1)	0.311(2)	0.307(2)	0.721(3)
N(2)	0.107(2)	0.286(2)	0.568(3)
N(3)	0.240(2)	0.113(2)	0.612(3)
C(1)	0.350(2)	0.338(2)	0.854(4)
N(4)	0	0.495(3)	0.2500
O(1)	0	0.394(2)	0.2500
O(2)	0.076(2)	0.536(2)	0.334(2)

Table 3.4 Bond lengths and angles for *trans*-$[Co(NCS)_2(NH_3)_4]NO_3$.[c]

Atoms	Bond Lengths (Å)	Atoms	Bond Angles (Å)
Co - N(2)	2.00(2)	N(1)[a] - Co - N(2)	89.6(8)
Co - N(3)	1.98(2)	N(1)[a] - Co - N(3)	91.5(8)
Co - N(1)[a]	1.88(2)	N(2) - Co - N(3)	90.5(8)
C(1) - S(1)	1.65(3)	C(1) - N(1)[a] - Co	177(3)
C(1) - N(1)	1.13(2)	N(1)[a] - C(1) - S(1)	173(3)
N(4) - O(1)[b]	1.31(4)	O(2) - N(4) - O(1)[b]	116(2)
N(4) - O(2)[b]	1.22(2)	O(2) - N(4) - O(2')	127(4)

[a], N atom of NCS ligand. [b], In the NO_3^- anion. [c], See Figure

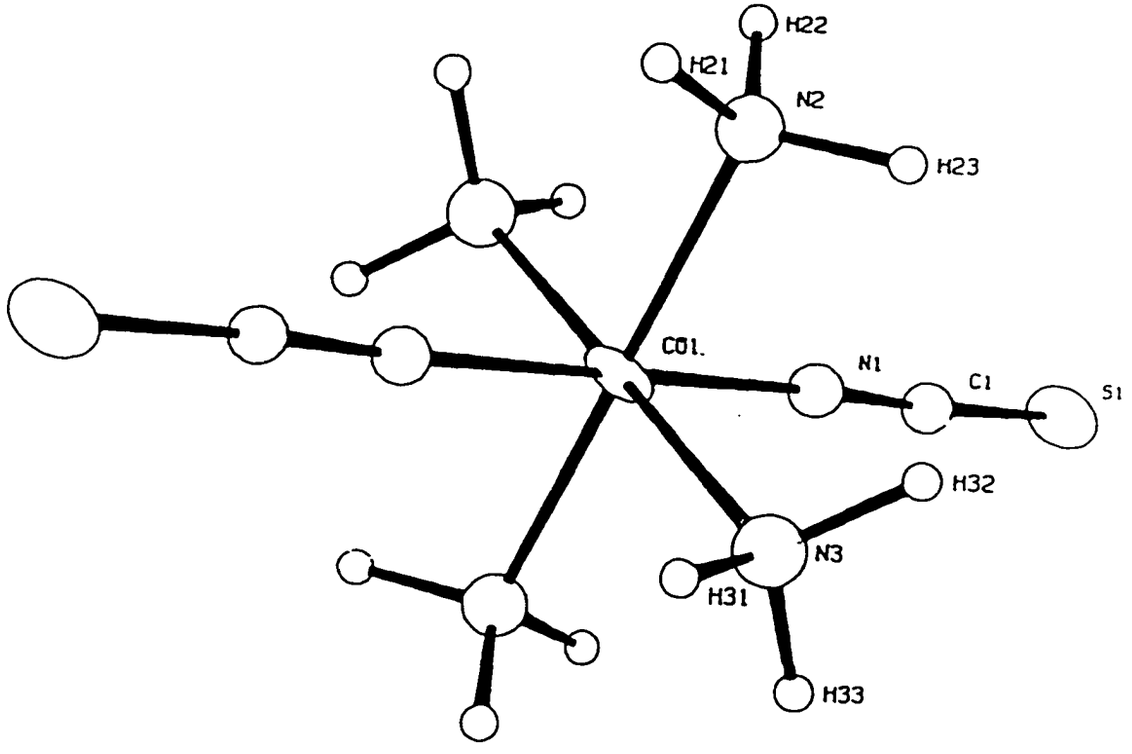

Figure 3.1 X-Ray structure of *trans*-$[Co(NCS)_2(NH_3)_4]^+$.

As can be seen in Figure 3.1, the compound has the thiocyanate ligands in a *trans* relationship and the thiocyanates are N-bonded. Also notice from Table 3.1 that the ratios of the UV/Vis molar absorptivity maxima for the two ligand field bands in all four complexes are very similar to each other (R = 8.2 to 10.5), close to the literature report of isothiocyanato complex, $[Co(NH_3)_5(NCS)]^{2+}$ (R = 8.3),[116] and inconsistent with the reported S-bonded complex where R = 211.[38,116] These results indicate that the binding mode of thiocyanate should be the same in all four complexes, i.e. they are all N-bonded to the cobalt(III) center.

3.2.2 Steady State Studies of *Trans-/Cis-* Diisothiocyanato Tetraam(m)ine Cobaltate(III) Complexes

3.2.2.1 Photoproducts of *trans*-$[Co(NCS)_2(NH_3)_4]^+$ Photolysis

On irradiation at 360 nm in acidic medium, both ammine isomers give Co^{2+}, thiocyanate and ammonium ions by direct analysis . Most of the Co(III) containing photoproduct complexes can be detected by reversed phase HPLC techniques, and identified using the authentic complex, as shown and explained in Figure 3.2. The results suggest that the following processes (3.1)-(3.3) occur,

$$\textit{trans}\text{-}[Co(NCS)_2(NH_3)_4]^+ \xrightarrow{h\nu} Co^{2+} + xNCS^- + yNH_3 \quad \text{(redox products)} \qquad (3.1)$$

$$+ \textit{cis}\text{-}[Co(NCS)(NH_3)_4(H_2O)]^{2+} \quad (NCS^- \text{ aquation}) \qquad (3.2)$$

$$+ \textit{trans-/cis}\text{-}[Co(NCS)_2(NH_3)_3(H_2O)]^+ \quad (NH_3 \text{ aquation}) \qquad (3.3)$$

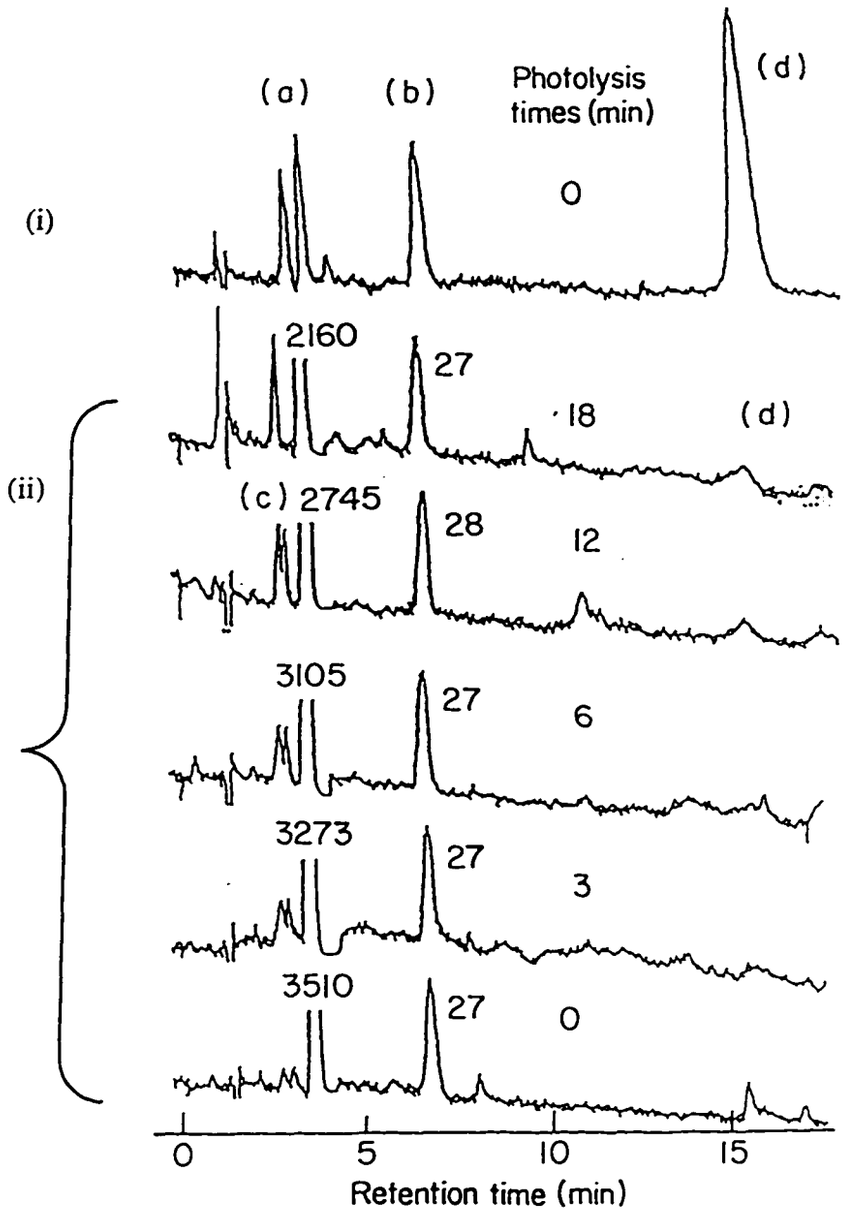

Figure 3.2 Reversed-phase HPLC results on (i) *cis*-$[Co(NCS)(NH_3)_4(H_2O)]^{2+}$ containing *trans*-$[Co(NCS)_2(NH_3)_4]^+$ and *cis*-$[Co(NCS)_2(NH_3)_4]^+$, (ii) photolysis of *trans*-$[Co(NCS)_2(NH_3)_4]^+$ at 360 nm. The photolysis times and relative peak heights are marked on the graph. Peak (b) is clearly an impurity and does not increase on photolysis. Peak identities are: (a) *trans*-$[Co(NCS)_2(NH_3)_4]^+$, (b) *cis*-$[Co(NCS)_2(NH_3)_4]^+$, (c) *trans-/cis*-$[Co(NCS)_2(NH_3)_3(H_2O)]^+$, (d) *cis*-$[Co(NCS)(NH_3)_4(H_2O)]^{2+}$.

Since the aquation products might be formed by Co^{2+} catalysed solvation, the effect of Co^{2+} was explored. A concentrated $CoCl_2$ solution was added into a photolysed solution containing the above species until final $[Co^{2+}]$ = 30% of the concentration of the starting complex. This solution was thermolysed at room temperature for up to 40 min in the dark, then re-analyzed chromatographically. The peaks obtained via HPLC were the same as for a Co^{2+}-free solution, discounting the Co^{2+} catalysis of the thermal reactions on the experimental time scale. The two product peaks labelled (c) in Figure 3.2 could only be tentatively identified as the ammonia aquation products, *trans-/cis*-$[Co(NCS)_2(NH_3)_3(H_2O)]^+$, on the basis of the similar retention times to the 1+ charge complex. If this is correct, the aquation involves not only the photooxidized ligand (that is NCS^-), but also the auxiliary NH_3 ligand, which is inconsistent with Adamson's model (section 1.3.2.1),[28] but has been observed in other systems (eg. $[Co(NH_3)_5N_3]^{2+}$).[34-36] The amount of all aquations (about 3% of the total quantum yield) indicates that they are not major processes.

3.2.2.2 Relationship of Ø(NCS^-), Ø(NH_3) and Ø(Co^{2+}) on the Irradiation of Cobalt(III) Isothiocyanato Ammine Complexes

In the steady state studies of the ammine complexes the ratio of thiocyanate anion quantum yield Ø(NCS^-) to Co^{2+} quantum yield Ø(Co^{2+}) is found to be about 2 to 1 (Table 3.5), and ammonia quantum yield Ø(NH_3) to Co^{2+} quantum yield Ø(Co^{2+}) is around 3 to 1, both inconsistent with the ratios 1:1 and 4:1 predicted by the chemical stoichiometry of eqs. 3.4-3.5:

$$*[Co(NCS)_2(NH_3)_4]^+ \longrightarrow Co^{2+} + (NCS)_2^{-\cdot} + 4NH_3 \qquad (3.4)$$

$$(NCS)_2^{-\cdot} + (NCS)_2^{-\cdot} \longrightarrow (NCS)_2 + 2NCS^-$$

$$k_5 = 1.2 \times 10^9\ M^{-1}s^{-1}\ (pH3)\ ^{117} \qquad (3.5)$$

Table 3.5 The ratio of $\emptyset(NCS^-) : \emptyset(Co^{2+})$ for the photolysis of *trans-/cis*-$[Co(NCS)_2(NH_3)_4]^+$ complexes in H^+ (pH 2.7) and 50% glycerol/H^+ aqueous solution.

	$\emptyset(NCS^-) : \emptyset(Co^{2+})$	
Complexes	in H^+	in 50% glycerol/H^+
cis-$[Co(NCS)_2(NH_3)_4]^+$	2.2 ± 0.1	2.1 ± 0.1
trans-$[Co(NCS)_2(NH_3)_4]^+$	2.0 ± 0.1	2.0 ± 0.3

In a few exploratory experiments, similar results for the $\emptyset(NH_3) : \emptyset(Co^{2+})$ ratio were obtained for other isothiocyanatoammine Co(III) compounds and these are listed in Table 3.6.

Table 3.6 The ratio of $\emptyset(NH_3) : \emptyset(Co^{2+})$ for the photolysis of some isothiocyanatoammine Co(III) complexes.

	$\emptyset(NH_3) : \emptyset(Co^{2+})$	
Complexes	Experimental	Stoichiometric expectation
cis-$[Co(NCS)_2(NH_3)_4]^+$	3.1 ± 0.1	4
cis-$[Co(NCS)(H_2O)(NH_3)_4](NO_3)_2$	3.1 ± 0.1	4
$[Co(NCS)(NH_3)_5](NO_3)_2$	3.9 ± 0.1	5

3.2.2.3 Influence of Medium on the Quantum Yield of Co(II) upon the Irradiation of *Trans-/Cis-* Diisothiocyanato Tetraam(m)ine Cobaltate(III) Complexes

Thiocyanate Effect:

Added thiocyanate increases the redox yield markedly in a non-linear fashion as shown in Figures 3.3-3.4. It also forms ion pairs with all four complex cations studied. The ion pair constants of all four cationic complexes with thiocyanate anion were obtained by spectroscopic methods as described in section 2.2.5.1. Typical spectra are shown in Figures 3.5-3.6, and values of the ion pair constant K_{IP} are included in Table 3.11 for comparison.

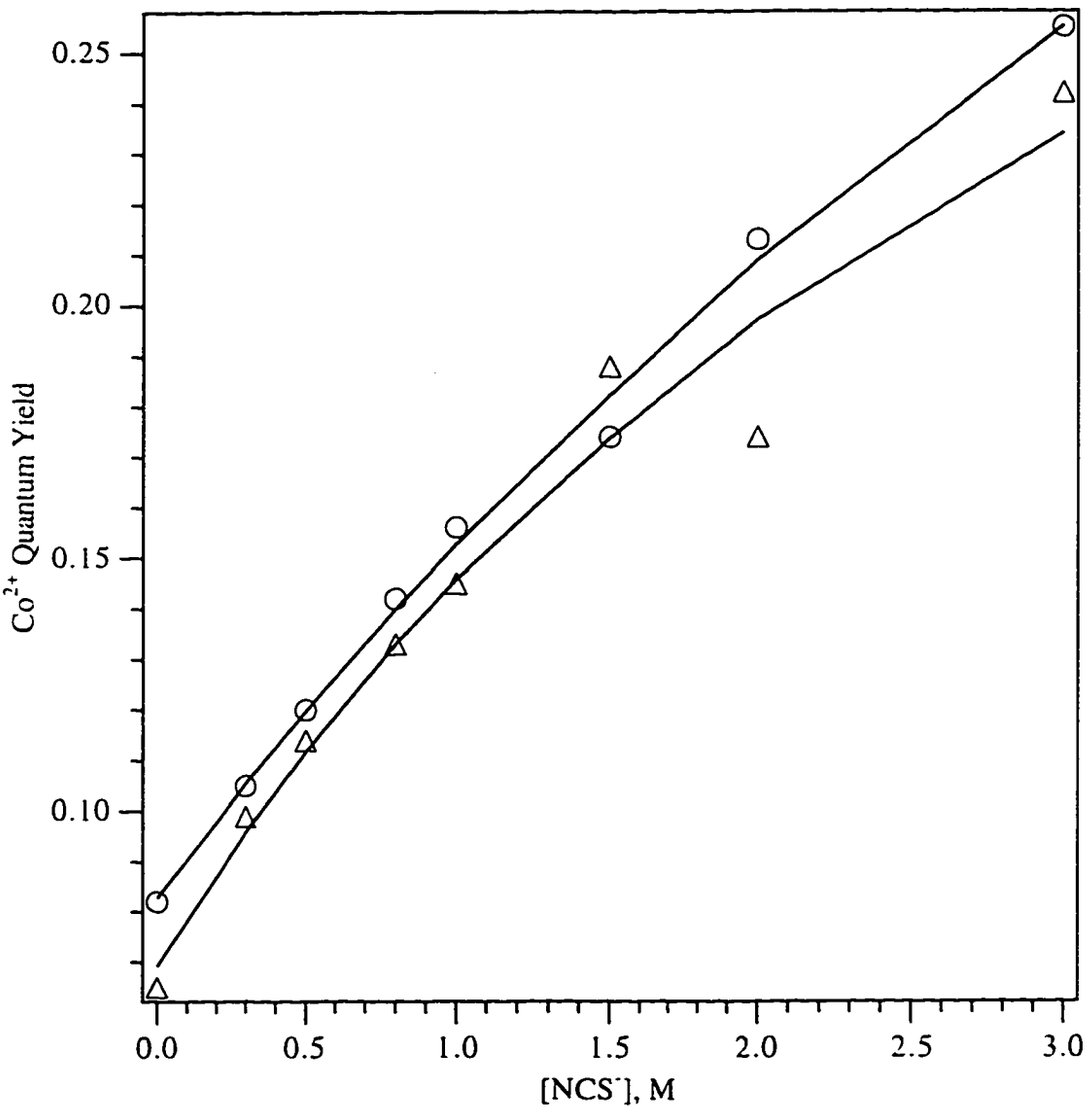

Figure 3.3 Quantum yield of Co^{2+} from $[Co(NCS)_2(NH_3)_4]^+$ vs $[NCS^-]$. Δ *trans-* isomer; O *cis-* isomer. Markers are experimental points and solid lines are the fits to the two models discussed in the text.

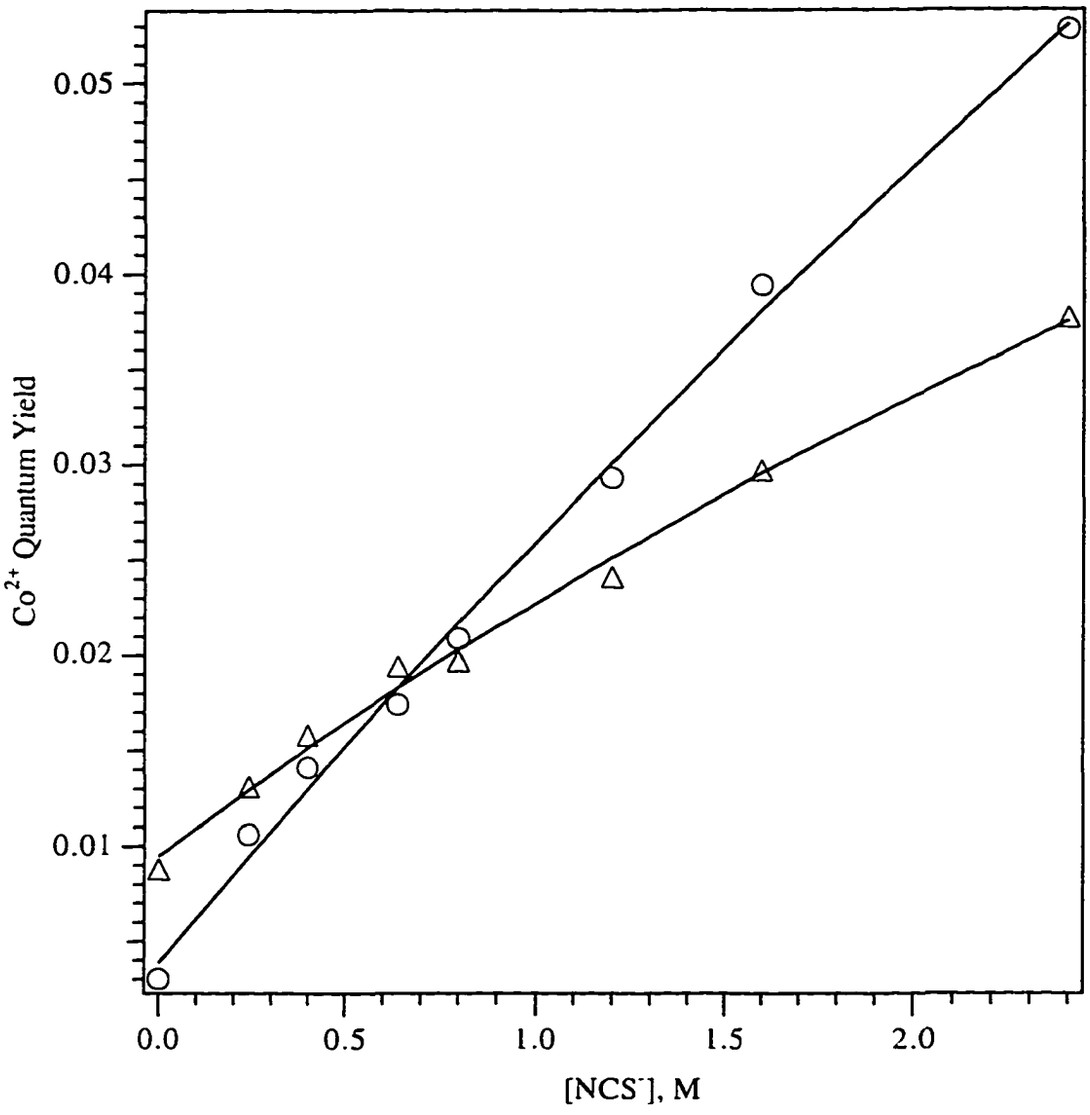

Figure 3.4 Quantum yield of Co^{2+} from $[Co(NCS)_2(en)_2]^+$ vs $[NCS^-]$.
Δ *trans*- isomer; O *cis*- isomer. Markers are experimental points and solid lines are the fits to the two models discussed in the text.

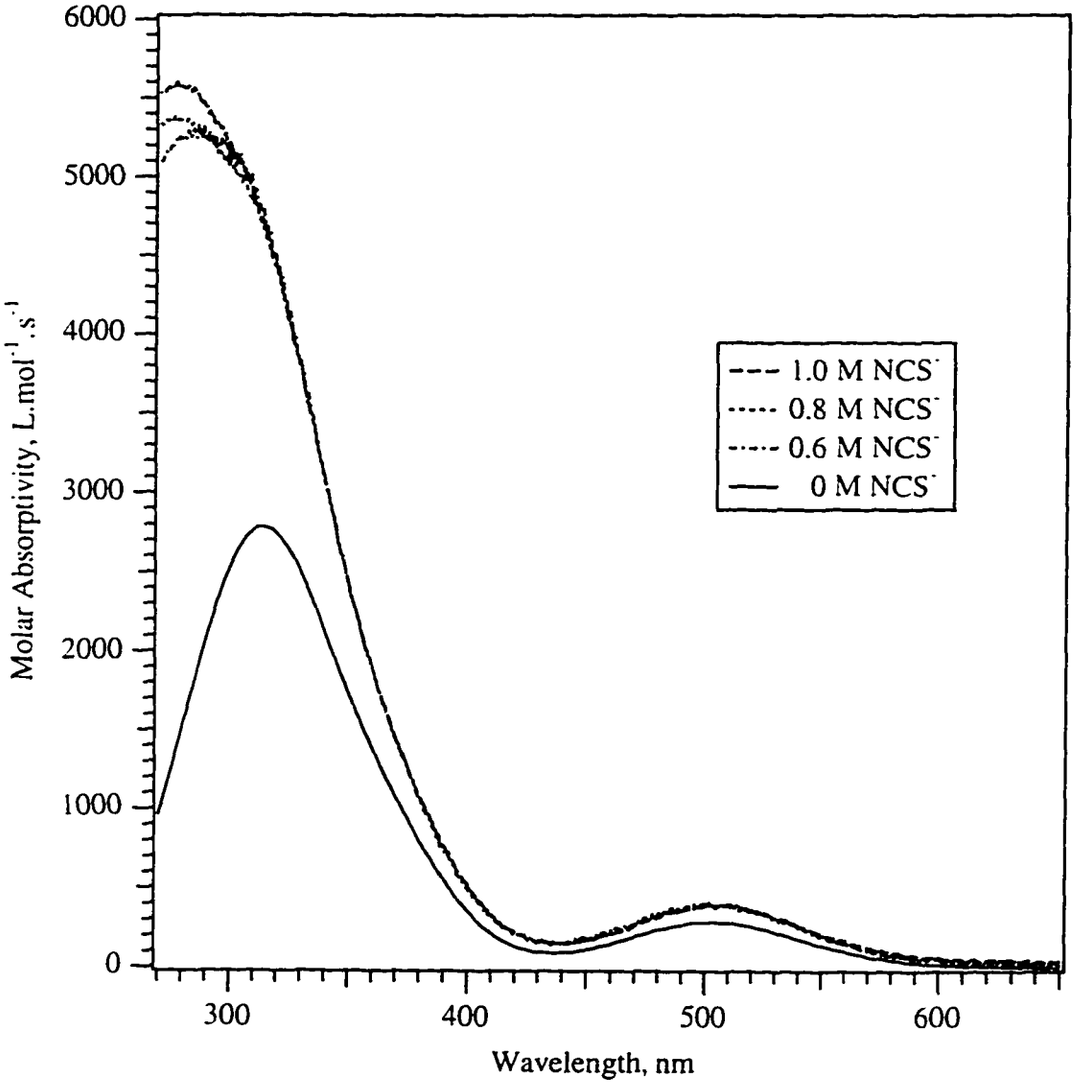

Figure 3.5 UV/Vis spectrum of *cis*-$[Co(NCS)_2(NH_3)_4]^+$ (solid line) compared to the spectra of ion pair (IP) {*cis*-$[Co(NCS)_2(NH_3)_4]^+$, NCS^-} calculated from data obtained for different thiocyanate concentrations (dotted lines).

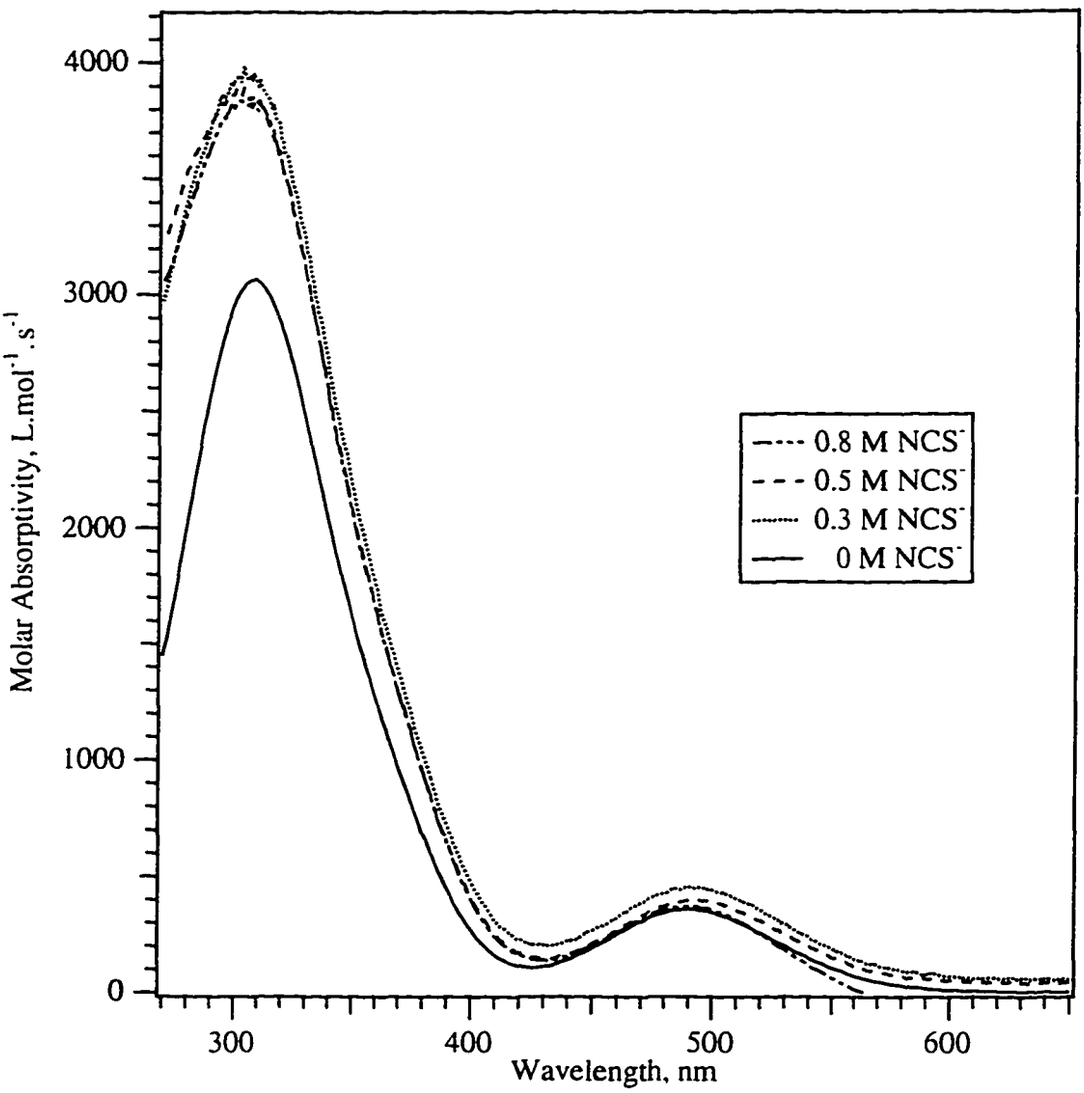

Figure 3.6 UV/Vis spectrum of *cis*-$[Co(NCS)_2(en)_2]^+$ (solid line) compared to the spectra of ion pair (IP) {*cis*-$[Co(NCS)_2(en)_2]^+$, NCS^-} calculated from data obtained for different thiocyanate concentrations (dotted lines).

Other Medium Effects:

In pH 2.7 aqueous solutions, for ionic strength range from 0.0036 to 0.086 M, $\emptyset(Co^{2+})$ of 0.082±0.001 for the *cis*-$[Co(NCS)_2(NH_3)_4]^+$ isomer was observed. This indicates that there is no charge effect. It was also found that O_2 and pH had no obvious effect (< 5% variation) on the redox of the Co(III) complexes. There is no change in the UV/Vis spectra with the addition of either Cl^- or Ac^-.

Table 3.7 shows that, in high concentrations of LiCl, no significant variation in $\emptyset(Co^{2+})$ was observed. But $\emptyset(Co^{2+})$ did decrease in 2 M sodium acetate solution (ca.10-20%) with and without NaNCS present. In 50% glycerol solution, $\emptyset(Co^{2+})$ was further decreased by a factor of about 2.

Table 3.7 $\emptyset(Co^{2+})$ on irradiation of *trans-/cis*-$[Co(NCS)_2(NH_3)_4]^+$ complexes at 360nm in various media.

Media	*trans*-$[Co(NCS)_2(NH_3)_4]^+$	*cis*-$[Co(NCS)_2(NH_3)_4]^+$
in H^+ (pH = 2.7)	0.065±0.001	0.082±0.001
0.5M LiCl/H^+	0.062±0.002	0.077±0.001
2M LiCl/H^+	0.068±0.002	0.085±0.001
2M NaAc/H^+	0.055±0.001	0.065±0.002
50% Glycerol/H^+	0.035±0.001	0.047±0.001
0.5M NCS^-/H^+	0.114±0.001	0.120±0.003
2M LiCl/0.5M NCS^-/H^+	-	0.122±0.003
2M NaAc/0.5M NCS^-/H^+	0.101±0.001	0.106±0.002
50% Glycerol/0.5M NCS^-/H^+	0.035±0.001	0.047±0.001

3.2.3 LFP Studies for *Trans-/Cis*-$[Co(NCS)_2(NH_3)_4]^+$ Isomers

3.2.3.1 Transient Spectra

Unfortunately no transient was seen corresponding to the Co(II) radical pair species. Instead a strong transient signal corresponding to the dithiocyanate radical ion,[40,118] $(NCS)_2^{-\cdot}$, was observed at 10 ns for both isomers (Figure 3.7). As shown in Figure 3.8, in H_2O solution the radical absorption for the *trans-* isomer is almost absent at 50 ps, even by 1 ns no strong absorption is observed. In contrast, for the *cis-* isomer, this radical appears within the 50 ps duration of the laser flash and remains constant up to 1 ns.

In concentrated sodium acetate buffer solution, similar results were obtained to those in H_2O solution: almost no absorption by $(NCS)_2^{-\cdot}$ was observed for the *trans-* isomer even up to 5 ns delay, but was detected in the *cis-* isomer although the signals were weaker than in H_2O solution (Figure 3.9).

When excess thiocyanate ion was introduced to the solutions, strong absorptions were observed in both isomers (Figure 3.10), slightly stronger for the *cis-* isomer. The absorbance maximum at 475 nm declines at 5 ns timescale in *cis-* isomer, but it is not apparent whether or not this is due to experimental error. With the addition of NCS^-, the intensity of this transient absorption increases gradually (Figure 3.11). In addition, a weak transient which decays in about 50 ps is seen at around 600 nm for both isomers. It is assigned as a ligand field state,[41] triplet or quintet, and is not involved in the redox photochemistry; for example, in Figures 3.9(a), 3.10(a), no additional contribution to $(NCS)_2^{-\cdot}$ absorbance is seen as this LF peak decays.

It is interesting to note that a shift of wavelength maximum from 475 nm to 450 or 440 nm was observed in ns flash photolysis experiments with the presence of concentrated LiCl or NaAc solutions (Figures 3.12(a)-(c)). On addition of NCS^- to the above solutions,

the A_{max} shifts back to 470 nm in the case of Cl^- (Figure 3.12(e)), but in Ac^- / $\dot{N}CS^-$ solution A_{max} remains blue shifted at 455 nm, Figure 3.12(f).

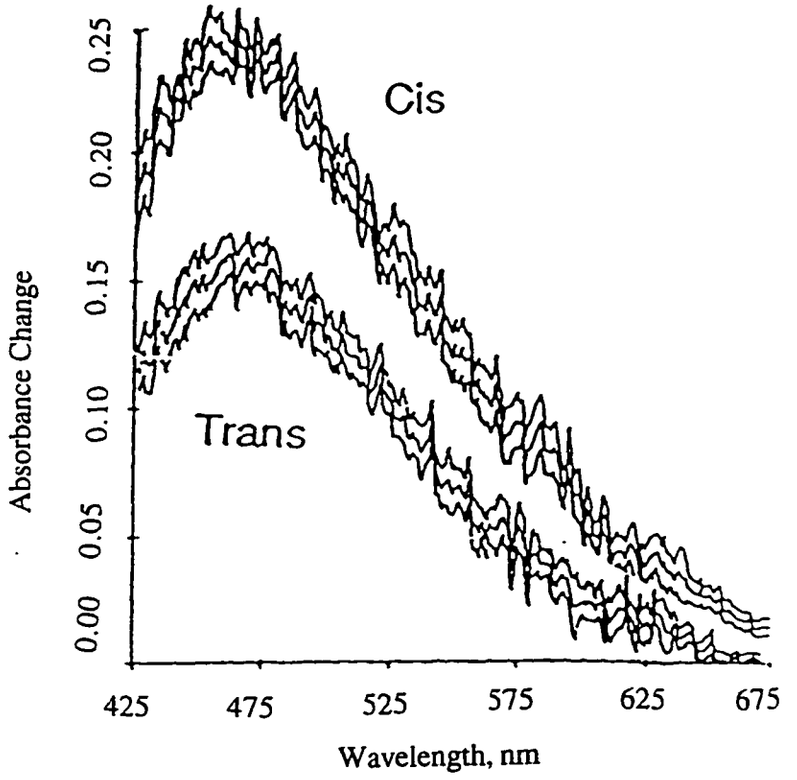

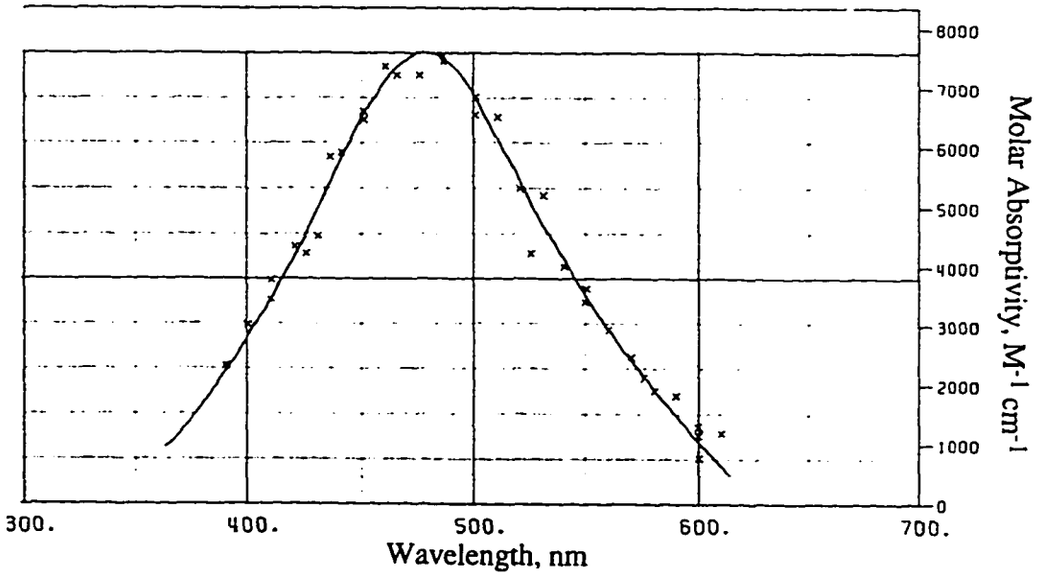

Figure 3.7 Observed (a) and literature reported (modified from reference [40]) spectra (b) of $(NCS)_2^{\cdot-}$. Data courtesy of D.M. Kneeland.

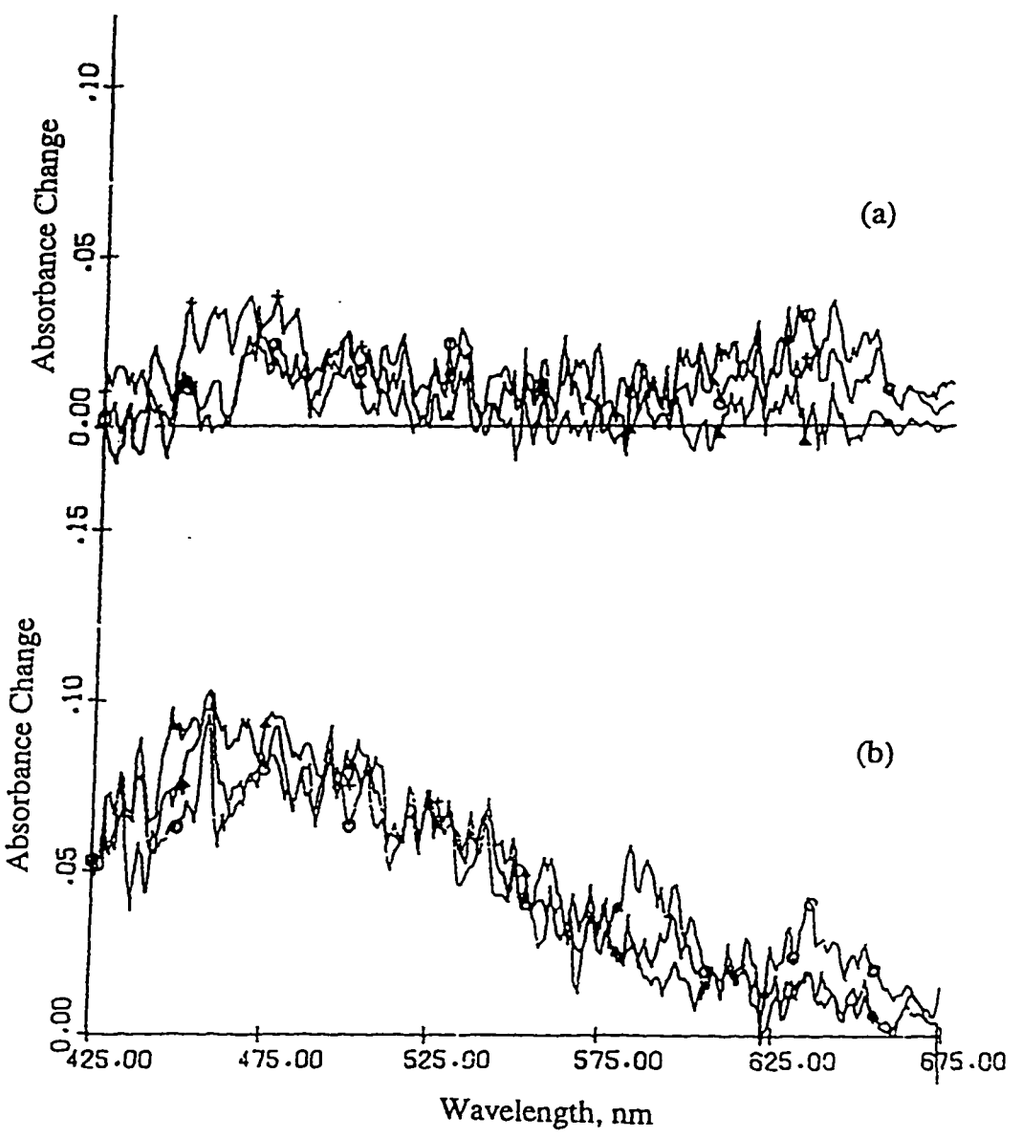

Figure 3.8 Time dependent transient absorption spectra of (a)*trans*- and (b) *cis*-$[Co(NCS)_2(NH_3)_4]^+$ in water.
o 50 ps; Δ 500 ps; + 1 ns. Data courtesy of D.M. Kneeland.

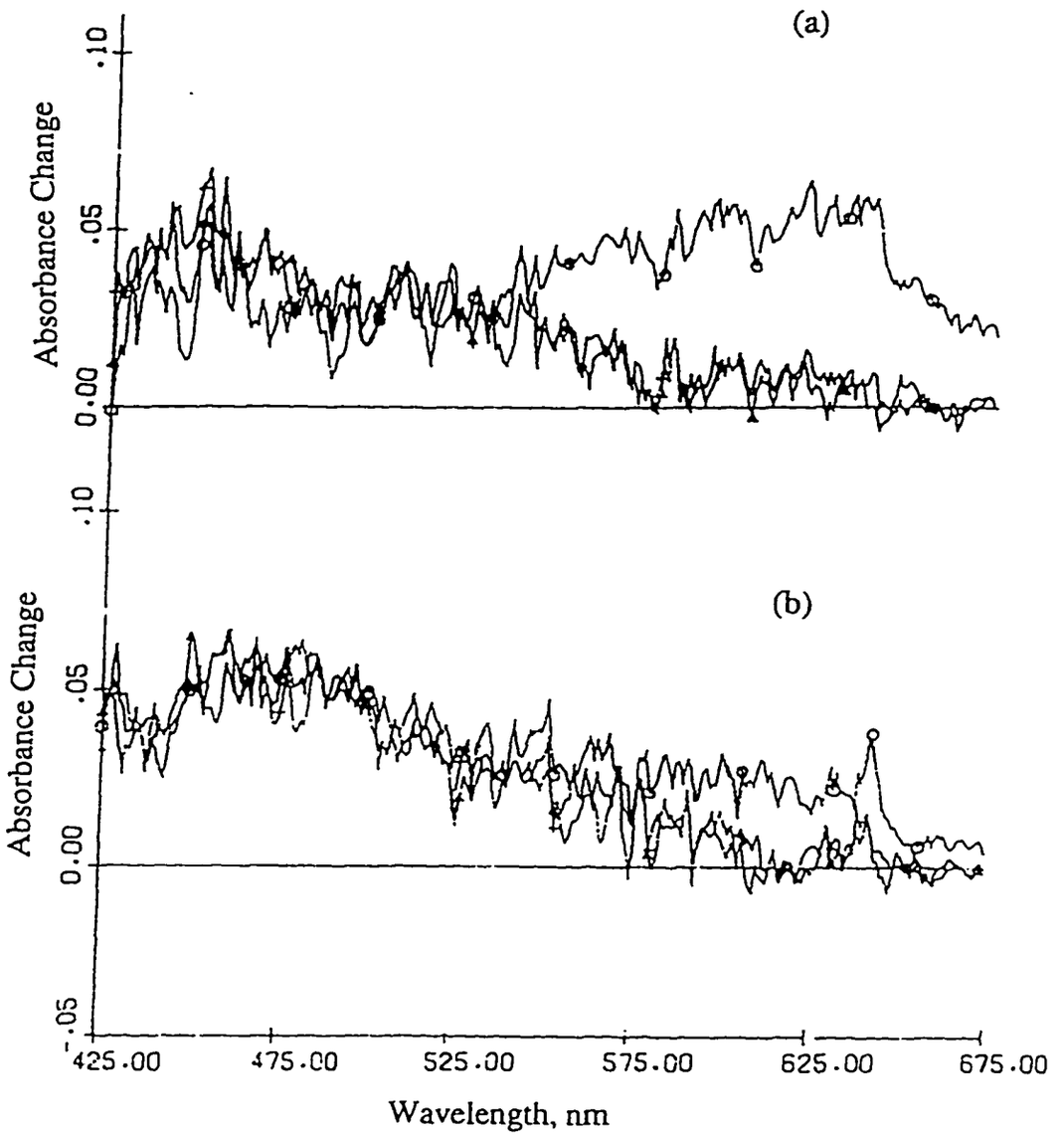

Figure 3.9 Time dependent transient absorption spectra of (a)*trans*- and (b) *cis*-$[Co(NCS)_2(NH_3)_4]^+$ in 2 M NaAc / pH7 buffer solution. o 20 ps; Δ 1 ns; + 5 ns. Data courtesy of D.M. Kneeland.

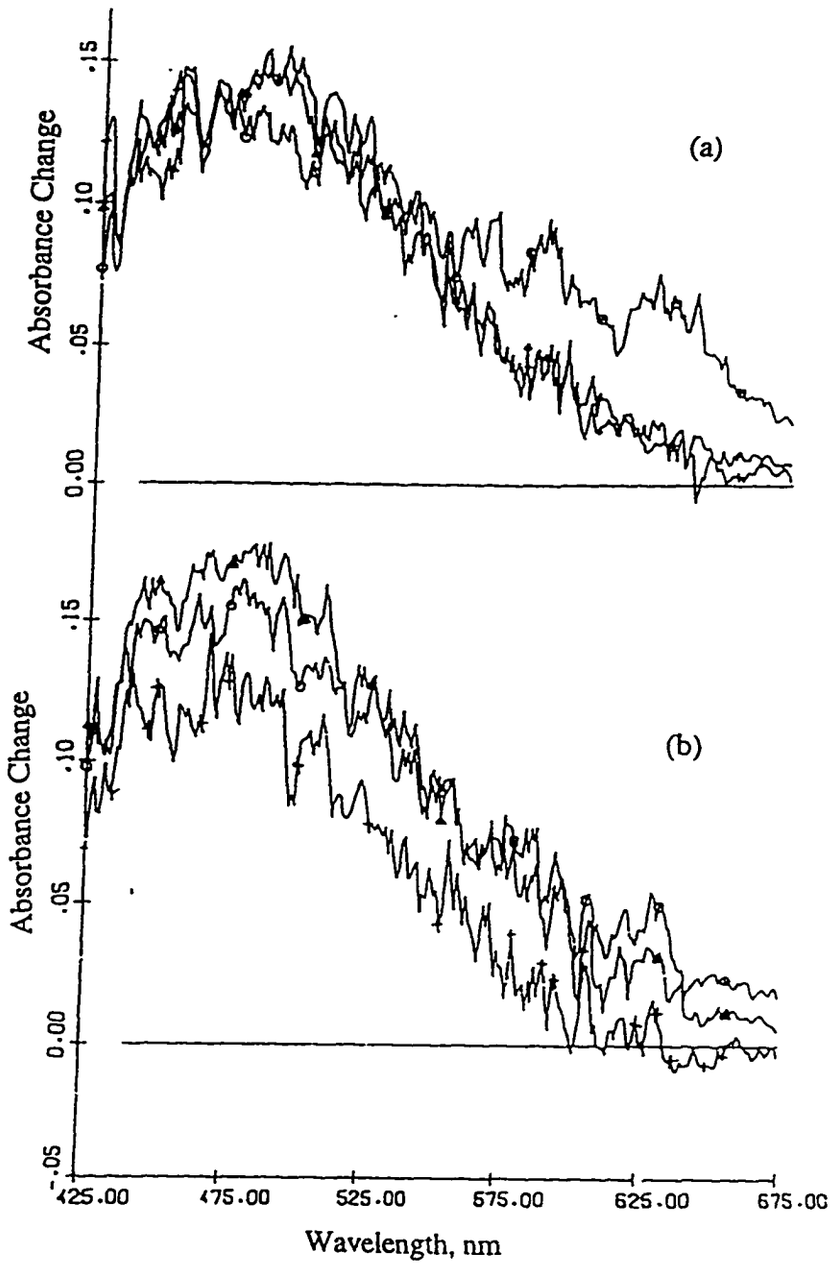

Figure 3.10 Time dependent transient absorption spectra of (a) *trans*- and (b) *cis*-$[Co(NCS)_2(NH_3)_4]^+$ in 2 M NaAc/2 M NCS^-/pH7 buffer solution. o 20 ps; Δ 1 ns; + 5 ns. Data courtesy of D.M. Kneeland.

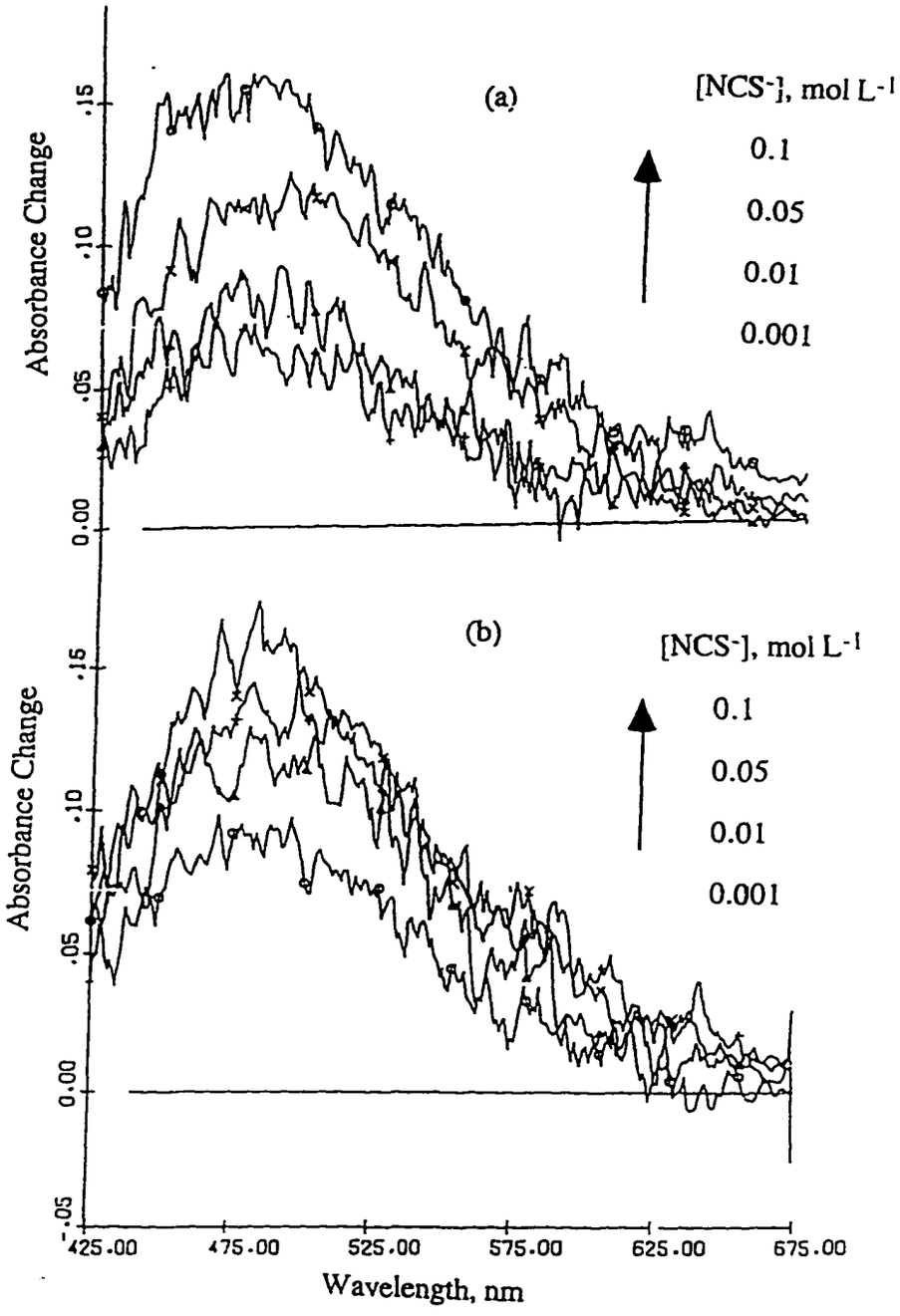

Figure 3.11 $(NCS)_2^{-\cdot}$ spectra in different NCS^- concentrations.
(a) *trans*-$[Co(NCS)_2(NH_3)_4]^+$, (b) *cis*-$[Co(NCS)_2(NH_3)_4]^+$.
Data courtesy of D.M. Kneeland.

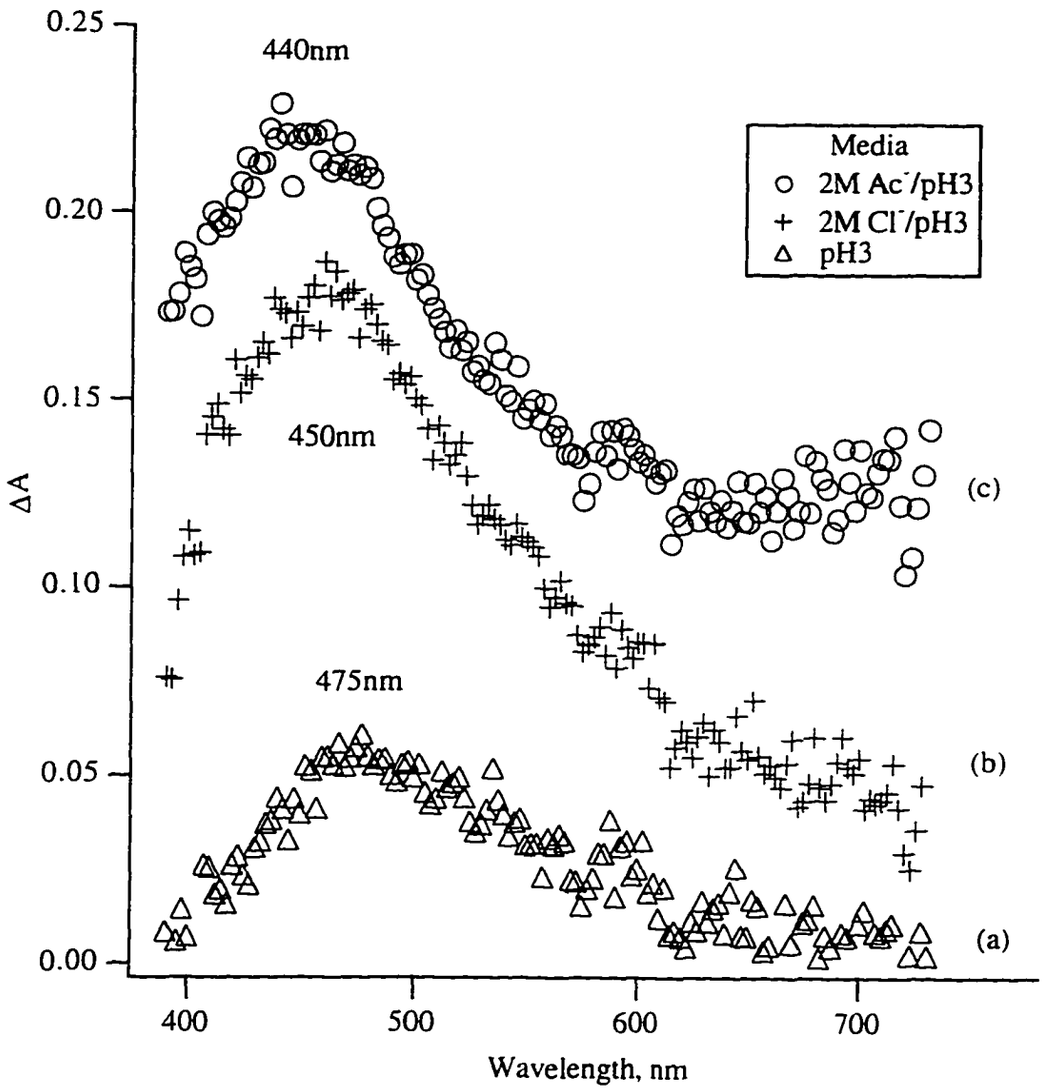

Figure 3.12A Transient spectra generated from *cis*-$[Co(NCS)_2(NH_3)_4]^+$ in different media (ns data, gate delay 40 ns).
(a) pH3, (b) 2 M Cl^-/pH3, (c) 2M Ac^-/pH3.

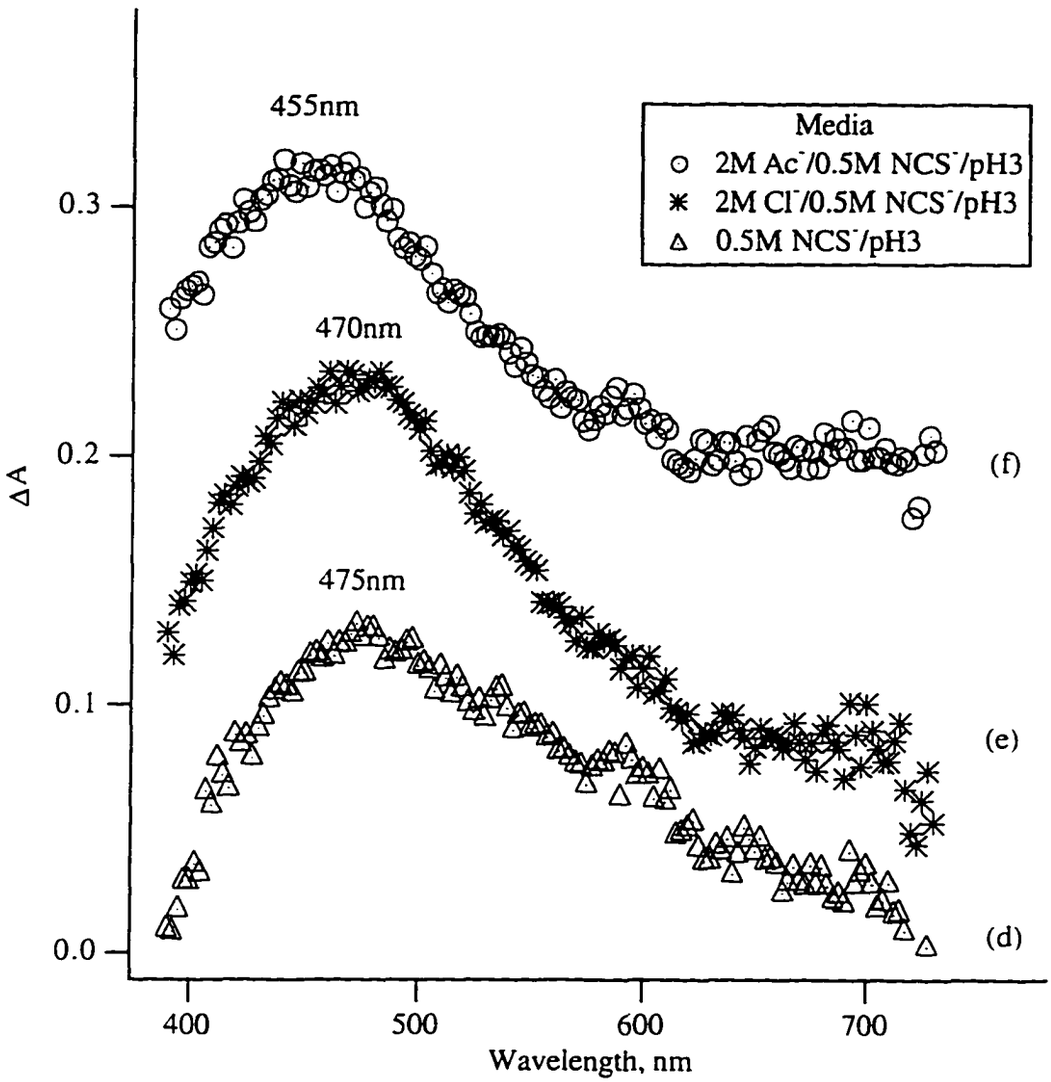

Figure 3.12B Transient spectra generated from *cis*-$[Co(NCS)_2(NH_3)_4]^+$ in different media (ns data, gate delay 40 ns). (d) 0.5 M NCS^-/pH3, (e) 2M Cl^-/0.5 M NCS^-/ pH3, (f) 2M Ac^-/0.5 M NCS^-/pH3.

3.2.3.2 Fixed Wavelength (λ = 475 nm) Observation

The LFP data collected at fixed λ (475 nm) confirmed the steady state observations that oxygen, pH, and $NaClO_4$ have no effect on the redox reaction. The presence of halide anions and acetate anion does effect A_{475} though. For example, A_{475} decreased slightly in 2 M Cl^-, approximately 30% in the presence of 2 M AC^-, and even more (85%) in the presence of 10^{-2} M I^- (Table 3.8). In 50% glycerol/H^+ solution, A_{475} decreased ca. 40% and the transient decay time $t_{1/2}$ was longer (50 μs) compared to that in the other media (20 to 30 μs). In the case of neutral atom-cation radical pairs, lifetimes are largely a function of solvent viscosity.[119]

As can be seen from Table 3.8, the amount of transient formed increased markedly when excess NCS^- was introduced into the solution. It was also found that A_{475} increased more than $\emptyset(Co^{2+})$ with the addition of NCS^-. For example, in *cis*-$[Co(NCS)_2(NH_3)_4]^+$ complex, as [NCS^-] increased from 0 to 0.8 M, the transient absorbance increased 2.3 times (from 0.07 to 0.16 with $[Co(III)]_0 = 7.8 \times 10^{-4}$ M) while $\emptyset(Co^{2+})$ increased only 1.7 times (from 0.082 to 0.142).

Table 3.8 Transient absorption and decay half-life at 475 nm on the irradiation of *trans-/cis*-$[Co(NCS)_2(NH_3)_4]^+$ complexes at 355 nm in various media (ns data).

	cis-$[Co(NCS)_2(NH_3)_4]^+$		*trans*-$[Co(NCS)_2(NH_3)_4]^+$
Conditions	A_{475}	$t_{1/2}$[a]	A_{475}[b]
in H^+ (pH = 2.7)	0.044	25	0.020
2 M $NaClO_4/H^+$	0.043	37	0.018
2M $NaClO_4$/pH=6.86 buffer	0.046	31	0.018
2M LiCl/H^+	0.042	21	-
2M NaAc/H^+	0.029		0.015
50% Glycerol/H^+	0.026	48	0.012
0.01M KI/10^{-3} M NCS^-	-	-	0.0034[c]
0.001M NCS^-/H^+	0.048	33	0.021[c]
0.01M NCS^-/H^+	0.049	27	0.022[c]
0.05M NCS^-/H^+	0.051	30	-
0.1M NCS^-/H^+	0.060	29	0.023[c]
0.5M NCS^-/H^+	0.091	19	0.038[c]
2M LiCl /0.5M NCS^-/H^+	0.085	24	-
2M NaAc/0.5M NCS^-/H^+	0.065	24	-
50% Glycerol/0.5M NCS^-/H^+	0.061	51	-

[a] for $(NCS)_2^{-\cdot}$ in μs; [b] laser power different, 20.5 mJ; [c] in 2 M $NaClO_4$/pH 6.86 buffer and $[NCS^-]$ indicated in the table

3.3 Discussion

3.3.1 Photoproducts and Photoreaction Stoichiometry

It is clear that, like other Co(III) systems studied, the main photoreaction is redox reaction to produce Co^{2+} and release am(m)ine, together with a complex mixture of oxidised species. In the present work this has not been investigated in detail, but the observations of the thiocyanate radical ion absorbance suggest that one of the final products is likely to be thiocyanogen. According to the literature,[120,121] the formation of $(NCS)_2^{-\cdot}$ from NCS· and NCS^- occurs with a nearly diffusion controlled rate constant (7.0×10^9 M^{-1} s^{-1}), and the equilibrium constant is 2×10^5 M^{-1}. Thus even fairly low concentrations of free thiocyanate can form the $(NCS)_2^{-\cdot}$ radical.

$$SCN^- + NCS\cdot \rightleftharpoons (NCS)_2^{-\cdot} \qquad K_6 = 2 \times 10^5\ M^{-1} \qquad (3.6)$$

Once $(NCS)_2^{-\cdot}$ is formed, it will undergo disproportionation ($k = 10^9$ M^{-1} s^{-1} at pH 3-7)[117] to give thiocyanate and thiocyanogen, as shown earlier in eq. 3.5.

In acid solution the formation of $(SCN)_2$ is much faster than its hydrolysis,[122] reaction (3.7):

$$(SCN)_2 + H_2O \rightleftharpoons H^+ + SCN^- + HOSCN \qquad K_7 = 6 \times 10^{-13}\ M \qquad (3.7)$$

The subsequent hydrolysis of HOSCN proceeds with a small rate constant of about 70 s^{-1}, reaction (3.8).[122]

$$HOSCN + H_2O \longrightarrow HSO_2^- + HCN + H^+ \qquad (3.8)$$

Therefore, reactions 3.7-3.8 should be negligible in acidic solution.

There are clear indications of complexity, however. The results obtained showed that the quantum yield of NH_3 is less than expected, while that of NCS^- is higher than

would be predicted from stoichiometry. i.e. the final reaction stoichiometry appears to be closer to:

$$[Co^{III}(NCS)_2(NH_3)_4^+] \xrightarrow{h\nu} Co^{2+}(aq) + 2NCS^- + 3NH_3 + \text{oxidised ammonia} \quad (3.9),$$

than to the naive expectation based on observation of the dithiocyanato radical ion as a primary redox species. These results suggest that somehow ammonia may react with $(NCS)_2^{-\cdot}$ or its products $(NCS)_2$ to form NCS^- and ammonia oxidation products. It is known that $NCS\cdot$ and $(NCS)_2^{-\cdot}$ are moderately strong oxidants with redox potential $E^0(SCN\cdot/SCN^-) = 1.62$, and $E^0[(SCN)_2^{-\cdot}/SCN^-] = 1.33$.[123] Thiocyanogen is a weaker oxidant with $E^0[(SCN)_2/SCN^-] = 0.77$ V (all vs NHE).[124] It has been reported that $(NCS)_2^{-\cdot}$ can oxidize[117] the NH_3 analogues, aniline ($C_6H_5NH_2$) and N,N-dimethylaniline ($C_6H_5N(CH_3)_2$) which have a rich electron supply in the aryl, with rate constants of about 10^8 M^{-1} s^{-1} as shown below:

$$(NCS)_2^{-\cdot} + C_6H_5NH_2 \longrightarrow 2\,NCS^- + C_6H_5NH\cdot + H^+$$
$$k_{10} = 1.0\times10^8\ M^{-1}\ s^{-1}\ (pH = 10) \quad (3.10)$$

$$(NCS)_2^{-\cdot} + C_6H_5N(CH_3)_2 \longrightarrow 2\,NCS^- + [C_6H_5N(CH_3)_2]^{+\cdot} + H^+$$
$$k_{11} = 1.3\times10^8\ M^{-1}\ s^{-1}\ (pH = 13\text{-}14) \quad (3.11)$$

The redox potential for one-electron oxidation by amino radical $NH_2\cdot$ was not available, but it is believed to be similar to that of the sulfite radical, $SO_3^{-\cdot}$, which is a mild oxidant with a one-electron redox potential of 0.84 V vs NHE at pH 3.6, or 0.63 V at pH 7.[117] Since $(NCS)_2^{-\cdot}$ actually reacts with SO_3^{2-} to give $SO_3^{-\cdot}$ as reported (eq.3. 12),[117] then it would be expected that $(NCS)_2^{-\cdot}$ should also be able to oxidize NH_2^- to give $NH_2\cdot$ (eq. 3.13):

$$(NCS)_2^{-\cdot} + SO_3^{2-} \longrightarrow 2\,NCS^- + SO_3^{-\cdot}$$

$$k_{12} = 1.1 \times 10^8\ M^{-1}\ s^{-1}\ (pH = 13\text{-}14) \qquad (3.12)$$

$$(NCS)_2^{-\cdot} + NH_2^- \longrightarrow 2\,NCS^- + NH_2^{\cdot} \qquad (3.13)$$

Direct evidence of $(NCS)_2^{-\cdot}$ oxidizing NH_3 molecule, however, has not been found. In fact, Endicott has reported that the redox potential of NH_3^+/NH_3 or NH_3^+/NH_4^+ was estimated to be either $E^0(NH_3^+/NH_3) = 2.7$, or $E^0(NH_3^+/NH_4^+) = 3.3$,[28] both of which are much greater than that of the $(NCS)_2^{-\cdot}/NCS^-$ or $NCS^{\cdot}/NCS^-$ couples. This indicates that NH_3 can not be oxidized by $NCS^{\cdot}$ nor by $(NCS)_2^{-\cdot}$ radicals. Nevertheless, such oxidation is implied by these results and by those for several other ammine Co(III) compounds,[4,13,19] and an explanation is offered in section 4.3.4.

Also in agreement with literature precedent is the observation that the redox decomposition is accompanied by minor photoaquation of both thiocyanate and ammonia.

3.3.2 The Intrinsic Redox Yield and the Effect of Impurity NCS^-

The reversal of the order of redox yield, $\Phi(Co^{2+}) / H^+$, in en analogues, i.e. smaller $\Phi(Co^{2+})$ in *cis*- than in *trans*-isomer compared to the ammine complexes, led to a suspicion that the intrinsic photoredox yield and its variation amongst this group of complexes might be a result of NCS^- impurity in the starting complexes, since NCS^- has been shown to increase $\Phi(Co^{2+})$. To explore whether the $\Phi(Co^{2+})$ for the complexes alone might be distorted by impurity $[NCS^-]$ levels, the mole percentages of NCS^- residues in these complexes were determined. From Table 3.2, it is quite clear that, although the residual NCS^- in *cis*-$[Co(NCS)_2(en)_2]^+$ is greater than that in *trans*-$[Co(NCS)_2(en)_2]^+$, a

smaller quantum yield was obtained in *cis*-$[Co(NCS)_2(en)_2]^+$. Again, the residual NCS^- in the en analogue is similar to or even larger than that of the ammine series, while the quantum yield in the former series is much smaller than in the latter. More significant yet, the LFP data (Table 3.8) shows no obvious increase in the transient absorbance of $(NCS)_2^{-\cdot}$ even when $[NCS^-]$ is 0.05 M ($[NCS^-] : [Co^{3+}] > 100$). Hence, the effects of these small levels of thiocyanate impurity can be neglected.

3.3.3 Ligand Effect

As the ligand changed from monodentate NH_3 to bidentate en ($H_2NCH_2CH_2NH_2$), the ligand effect was remarkable:

(i) the photoredox yield $\Phi(Co^{2+})$ decreased dramatically, about 7 and 27 fold for the *trans-* and *cis-* isomers respectively (Table 3.2);

(ii) for the ammine compounds without added NCS^- ion, $\Phi(Co^{2+})$ for *cis-* isomer was larger than that for *trans-* isomer (see Figure 3.3); in contrast, $\Phi(Co^{2+})$ for *cis*-$[Co(NCS)_2(en)_2]^+$ was less than that for *trans*-$[Co(NCS)_2(en)_2]^+$ (Figure 3.4);

(iii) $\Phi(Co^{2+})$ for *cis*-$[Co(NCS)_2(en)_2]^+$ increased more dramatically with added NCS^- than did $\Phi(Co^{2+})$ for *trans*-$[Co(NCS)_2(en)_2]^+$ (Figures 3.3-3.4).

The smaller redox quantum yield in en complexes is often found in the literature,[31] and can be related to the chelate effect of the en ligand. Bidentate ligands such as en stabilize the Co(III) oxidation state (compare the reduction potentials for reactions 3.14 and 3.15),[13] and one end detached bidentates are expected to be able to re-coordinate to the Co^{II}-fragment. This increases the chance of radical pair recombination, and results in a smaller quantum yield. A suitable explanation for the ligand geometry effect in the above observations, (ii) and (iii), is still required.

$$[Co(NH_3)_6]^{3+} + e^- \rightleftharpoons [Co(NH_3)_6]^{2+} \qquad E(Co^{III}/Co^{II}) = 0.06\ V \qquad (3.14)$$

$$[Co(en)_3]^{3+} + e^- \rightleftharpoons [Co(en)_3]^{2+} \qquad E(Co^{III}/Co^{II}) = -0.26\ V \qquad (3.15)$$

3.3.4 Anion Effects (Cl^-, I^-, and Ac^-)

(i) Cl^- Effect:

The blue shift of the transient absorption maximum A_{max} in the presence of Cl^- can be explained by the formation of $ClNCS^{-\cdot}$:

$$Cl^- + NCS\cdot \rightleftharpoons ClNCS^{-\cdot} \qquad K_{16} = 6.7 \qquad (3.16)$$

According to the literature,[125] the equilibrium constant of the above reaction is $K_{16} = 6.7$. In the presence of Cl^- in the solution, the ·NCS radical ($\lambda_{max} = 330$ nm, $\varepsilon_{330} = 900\ M^{-1}\ cm^{-1}$)[121] generated from complex will react both with Cl^- in the bulk and the thiocyanate in the metallofragment, forming $ClNCS^{-\cdot}$ (Figure 3.12(a))[40] and $(NCS)_2^{-\cdot}$ transients. The absorption maximum λ_{max} should thus be between 390 nm ($\lambda_{max,ClNCS^{-\cdot}}$) and 475 nm ($\lambda_{max,(NCS)_2^{-\cdot}}$), which agrees with the experimental observation of $\lambda_{max,obs}$ = 450 nm.

In the Cl^-/NCS^- solution, however, Cl^- can no longer compete with NCS^- in the solution due to the small equilibrium constant of K_{17}:[125]

$$(NCS)_2^{-\cdot} + Cl^- \rightleftharpoons ClNCS^{-\cdot} + NCS^- \qquad K_{17} = 3.3 \times 10^{-5} \qquad (3.17)$$

Here

$$\frac{[(NCS)_2^{-\cdot}]}{[ClNCS^{-\cdot}]} = \frac{[NCS^-]}{K_{17}\,[Cl^-]} = \frac{0.5}{(3.3\times10^{-5}) \times 2} = 7500 \qquad (3.186)$$

which means $(NCS)_2^{-\cdot}$ is the dominant transient species in the solution, so λ_{max} shifts back to 475 nm.

(ii) I^- Effect:

I^- acts similarly to Cl^- but with more pronounced effect due to its stronger affinity for the NCS· radical:[126]

$$(NCS)_2^{-\cdot} + I^- \rightleftharpoons INCS^{-\cdot} + NCS^- \qquad K_{19} = 400 \qquad (3.19)$$

Therefore when $[I^-] = 10^{-2}$ M and $[NCS^-] = 10^{-3}$ M,

$$\frac{[(NCS)_2^{-\cdot}]}{[INCS^{-\cdot}]} = \frac{[NCS^-]}{K_{19}\,[I^-]} = \frac{10^{-3}}{(400)\ x(10^{-2})} = 2.5x10^{-4} \qquad (3.20)$$

or,

$$[INCS^{-\cdot}] = 4000 \times [(NCS)_2^{-\cdot}] \qquad (3.21)$$

that is, $[INCS^{-\cdot}] \gg [(NCS)_2^{-\cdot}]$. According to Figure 3.13, a result of $\varepsilon_{475,INCS^{-\cdot}}/\varepsilon_{475,(NCS)_2^{-\cdot}} = 3800 / 7600 = 0.5$ would be expected, which is much larger than that observed experimentally with and without added I^- at same thiocyanate concentration: 0.0034 / 0.021 = 0.16. This is due to the further reaction of $INCS^-$ with excess I^-:[126]

$$INCS^{-\cdot} + I^- \rightleftharpoons I_2^{-\cdot} + NCS^- \qquad K_{22} = 55 \qquad (3.22)$$

Thus,

$$\frac{[I_2^{-\cdot}]}{[INCS^{-\cdot}]} = \frac{K_{22} \times [I^-]}{[NCS^-]} = \frac{55 \times 10^{-2}}{10^{-3}} = 550 \qquad (3.23)$$

This means that in the above solution, $I_2^{-\cdot}$ (λ_{max} = 390 nm, $\varepsilon_{390} = 9400$ $M^{-1}cm^{-1}$)[40] is the dominant species. This gives a ratio of $\varepsilon_{475,I_2^{-\cdot}}/\varepsilon_{475,(NCS)_2^{-\cdot}} =$ 1400/7600 = 0.18, which is very close to the experimental value of 0.16.

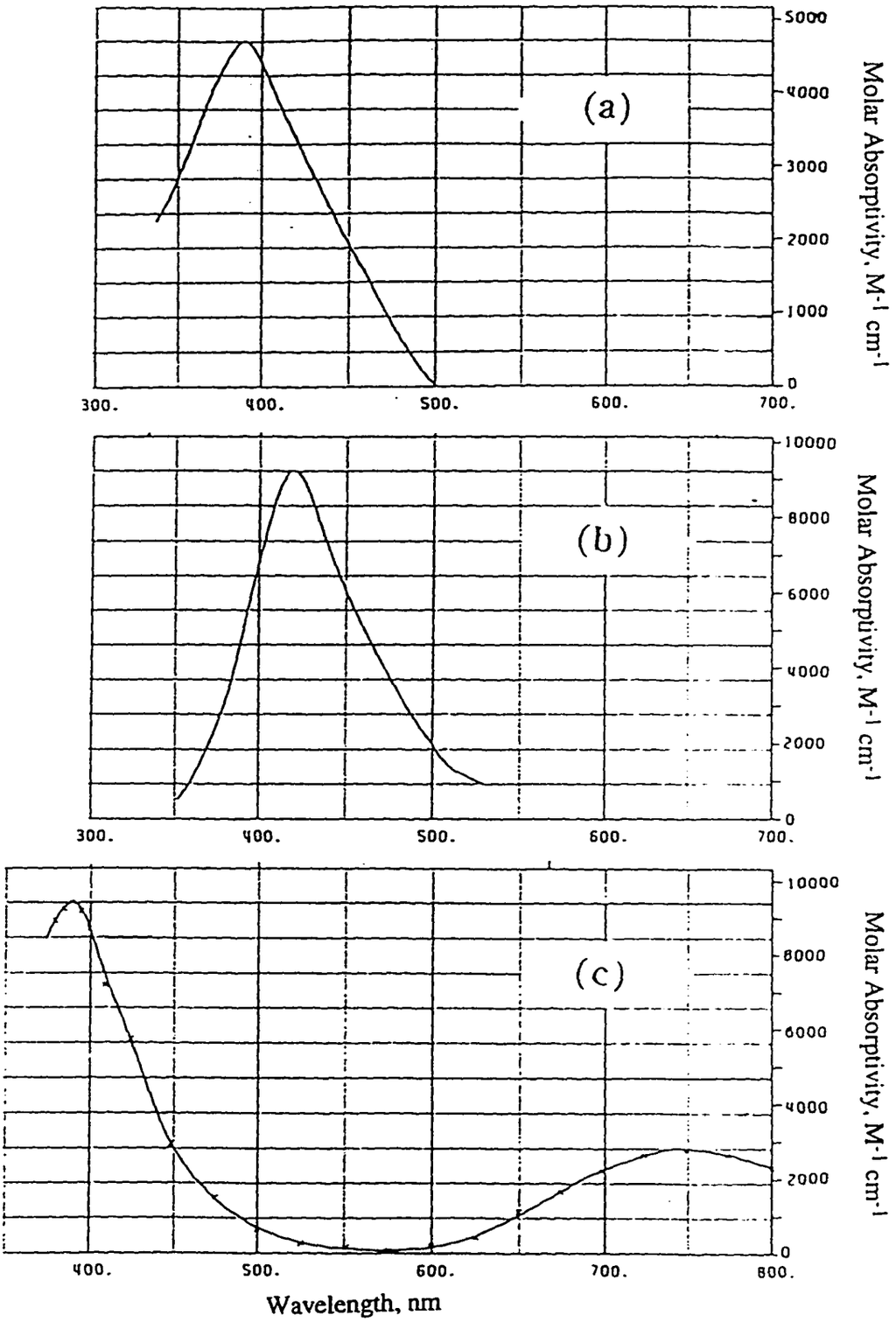

Figure 3.13 Transient spectra. (a) $ClNCS^{-\cdot}$, (b) $INCS^{-\cdot}$, (c) $I_2^{-\cdot}$. (Modified from reference [40]).

(iii) The Acetate Effect:

Both steady state and LFP results show that acetate reduces the redox yields and the efficiency of production of the intermediates. It is suggested that acetate may compete with SCN^- for the $SCN\cdot$ radical and form $AcNCS^{-}\cdot$ transient (though not reported in the literature), eqs. 3.24-3.25:

$$Ac^- + \cdot NCS \rightleftharpoons AcNCS^{-}\cdot \qquad (3.24)$$

$$(NCS)_2^{-}\cdot + Ac^- \rightleftharpoons AcNCS^{-}\cdot + NCS^- \qquad (3.25)$$

According to the literature (See Table 3.9, also Figure 3.13),[125-127] definite trends are observed for the transient species $XNCS^{-}\cdot$, as X^- changes from the smaller Cl^- to larger I^-. Both λ_{max} and ε_{max} increase, as well as the equibrium constant K_{eq} for the following equation:

$$(NCS)_2^{-}\cdot + X^- \rightleftharpoons NCS^- + XNCS^{-}\cdot \qquad (3.26)$$

Table 3.9 UV/Vis data for the transients $XNCS^{-}\cdot$ and equilibrium constants K_{eq} for the scavenging of $(NCS)_2^{-}\cdot$ radical by halide anions X^- (X = Cl, Br, I).

Radicals [a]	λ_{max}, nm	ε_{max}, L mol^{-1} cm^{-1}	K_{eq}[b]
$ClNCS^{-}\cdot$	390	4700	3.3×10^{-5}
$BrNCS^{-}\cdot$	400	7300	9.1×10^{-3}
$INCS^{-}\cdot$	420	9200	400

[a] results obtained from references [125-127]; [b] the equilibrium constant for eq. 3.26.

Since both Ac^- and I^- have relatively larger sizes ("soft" anions) compared to Cl^- and Br^-, a similar magnitude of ε_{max} and K_{eq} for $AcNCS^{-\cdot}$ compared to $INCS^{-\cdot}$ might be expected. Therefore, a large excess of Ac^- will likely scavenge the $NCS\cdot$ or $(NCS)_2^{-\cdot}$ radicals to form $AcNCS^{-\cdot}$, resulting in the blue shift of λ_{max} and the decrease of A_{475}. The decrease of the $\Phi(Co^{2+})$ in the presence of Ac^- suggests that $AcNCS^{-\cdot}$ may decay more slowly than $(NCS)_2^{-\cdot}$ and hence increase the possibility of the back reaction.

3.3.5 Mechanisms

3.3.5.1 Without Added Thiocyanate Anion

The observation of a distinct viscosity effect both in steady state and transient studies supports the presence of a radical pair intermediate in the photoredox pathways of the ammine complexes. The picosecond studies bear on the question of the mechanism of the photoreaction in the absence of added thiocyanate. The difference in rise time for the *trans-* and *cis-*$[Co(NCS)_2(NH_3)_4]^+$ isomers in water or acetate buffer is interesting. It suggests that in the *cis-* isomer having the two thiocyanate ions needed to form $(NCS)_2^{-\cdot}$ are adjacent, leads to the prompt appearance of the transient signal during the 50 ps laser pulse. In the *trans-* isomer, rotation or diffusion is required to bring the two thiocyanate species together. This would give a slower appearance of the transient and also allow recombination to compete more effectively in the *trans-* isomer, accounting for its lower quantum yield. Figure 3.14 shows the schematic diagram of the above proposed mechanisms (For simplicity A represents NH_3 ligand).

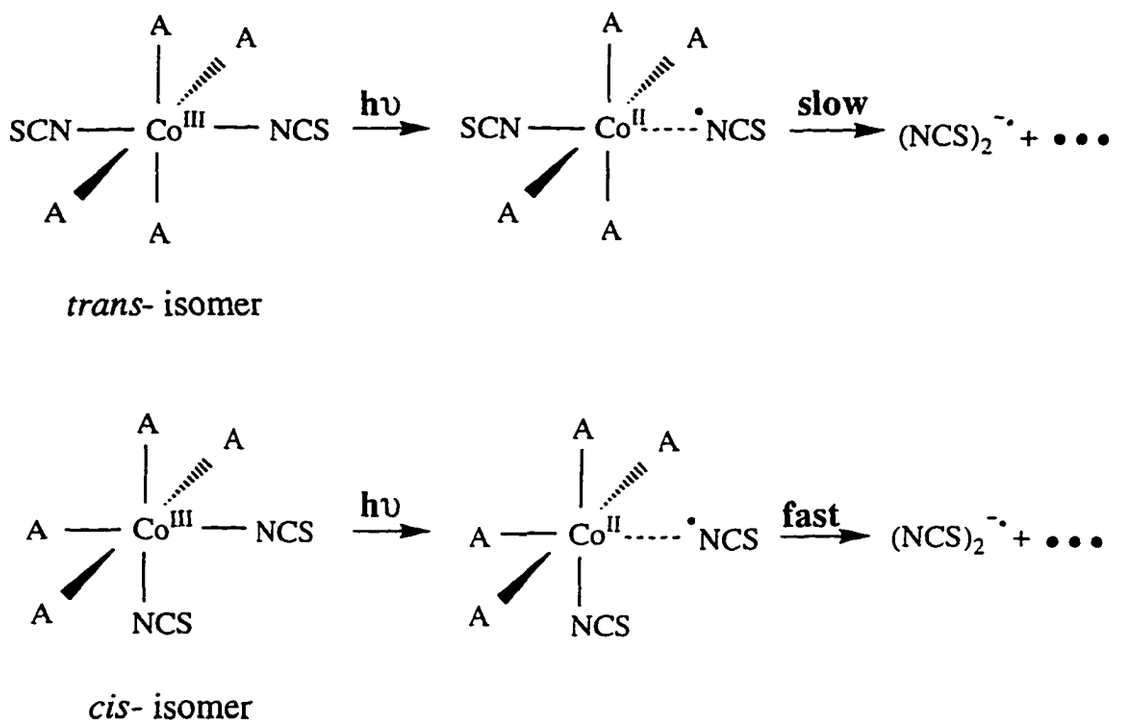

Figure 3.14 Proposed mechanism of *trans-/cis*-$[Co(NCS)_2(NH_3)_4]^+$ photoredox in NCS^- free solution.

3.3.5.2 With Added Thiocyanate Anion

The steady state results are consistent with the LFP (ps & ns) observations in showing that for all complexes studied there is a significant increase in redox quantum yields on addition of thiocyanate to the solutions. These results are summarised in Tables 3.7-3.8 and Figures 3.3-3.4 and 3.11. The enhancement of $\emptyset(Co^{2+})$ by NCS^- can be accounted for by two models, kinetic and ion pair models, which could, of course, operate simultaneously.

Kinetic model: In this model the NCS^- is considered a good scavenger for NCS· radical (eq. 3.28). The sequence of primary processes would be (for simplicity the am(m)ine and one NCS ligand are not included in the complex formula):

$$Co^{III}\text{-}NCS^+ \xrightarrow{\Phi_{RP}} \{Co^{II}, \cdot NCS\} \qquad (3.27)$$

(Formation of the radical pair (RP) in the cage)

$$\{Co^{II}, \cdot NCS\} \longrightarrow Co^{III}\text{-}NCS^+ \text{ (Recombination of the RP)} \qquad (3.28)$$

$$\{Co^{II}, \cdot NCS\} \longrightarrow Co^{2+} + (NCS)_2^{-\cdot} \qquad (3.29)$$

(Capture of NCS^- from Co^{II} fragment and separation of $(NCS)_2^{-\cdot}$ from the cage)

$$\{Co^{II}, \cdot NCS\} + NCS^- \longrightarrow Co^{2+} + (NCS)_2^{-\cdot} \qquad (3.30)$$

(Formation of $(NCS)_2^{-\cdot}$ with NCS· radical in the cage by scavenging of NCS^- from the medium)

Applying a steady state analysis to this scheme gives

$$\Phi(Co^{2+}) = \frac{a_0 (a_1 + [NCS^-])}{a_2 + [NCS^-]} \qquad (3.29)$$

here, $a_0 = \Phi_{RP}$, $a_1 = k_{29}/k_{30}$, $a_2 = (k_{28} + k_{29})/k_{30}$. The fit parameters for the four complexes are listed in Table 3.10. Assuming that $k_{30} = 1 \times 10^{10}$ L mol^{-1} s^{-1} (i.e. of the order of diffusion controlled), for the first time the radical pair lifetimes, $\tau_{RP} = 1/(k_{28} + k_{29}) = 1/(a_2 k_{30})$, can be estimated to be on the order of tens of picoseconds as listed in Table 3.10.

Table 3.10 Kinetic model fit for *trans-/cis*-$[Co(NCS)_2(NH_3)_4]^+$ and *trans-/cis*-$[Co(NCS)_2(en)_2]^+$ complexes in the presence of thiocyanate.

Complexes	a_0	a_1	a_2	τ_{RP}, ps[a]
trans-$[Co(NCS)_2(NH_3)_4]^+$	0.46 ± 0.16	0.61 ± 0.29	4.1 ± 2.8	25 ± 20
cis-$[Co(NCS)_2(NH_3)_4]^+$	0.73 ± 0.17	0.94 ± 0.15	8.3 ± 2.9	12 ± 5
trans-$[Co(NCS)_2(en)_2]^+$	0.14 ± 0.06	0.60 ± 0.12	9.1 ± 5.1	11 ± 6
cis-$[Co(NCS)_2(en)_2]^+$	0.41 ± 0.24	0.16 ± 0.05	17.3 ± 11.7	6 ± 4

[a] Assuming that $k_{30} = 1 \times 10^{10}$ L mol^{-1} s^{-1}.

Ion pair model: An alternative "Ion Pair" (IP) model, however, could also operate. Here, the complex forms an ion pair with thiocyanate which will have a thiocyanate ion poised to scavenge thiocyanate radical generated photochemically from the intramolecular charge transfer in the complex, and will also introduce the possibility of a new intermolecular charge transfer process leading to an external thiocyanate radical:

$$[Co(NCS)_2(NH_3)_4]^+ + NCS^- \rightleftharpoons \{[Co(NCS)_2(NH_3)_4]^+, NCS^-\} \quad K_{IP} \quad (3.32)$$

$$[Co(NCS)_2(NH_3)_4]^+ + h\nu \longrightarrow \text{Product} \quad \emptyset^0 \quad (3.33)$$

$$\{[Co(NCS)_2(NH_3)_4]^+, NCS^-\} + h\nu \longrightarrow \text{Product} \quad \emptyset_{IP} \quad (3.34)$$

The fraction of light absorbed by complex C^+, f^0, is:

$$f^0 = \frac{\varepsilon_{C^+}[C^+]}{\varepsilon_{C^+}[C^+] + \varepsilon_{IP}[IP]} = \frac{1}{1 + b\,K_{IP}[NCS^-]} \quad (3.35)$$

where b represents the ratio of molar absorptivity of ion pair (IP) to the complex (C^+) at 360 nm, $b = \varepsilon_{IP}/\varepsilon_{C+}$, which can be obtained from UV/Vis spectra (Figures 3.5-3.6).

The redox quantum yield $\Phi(Co^{2+})$ can be expressed as:

$$\Phi(Co^{2+}) = f^0 \Phi^0 + (1-f^0) \Phi_{IP} \qquad (3.36)$$

Substituting eq. 3.35 into eq. 3.36 leads to:

$$\Phi(Co^{2+}) = \frac{a_0 + a_1 [NCS^-]}{1 + a_2 [NCS^-]} \qquad (3.37)$$

where, $a_0 = \Phi^0$, $a_1 = b\ K_{IP}\ \Phi_{IP}$, $a_2 = b\ K_{IP}$.

This model fits the data for all four complexes just as well as the kinetic model as it gives the same mathematical equation (Figures 3.3 and 3.4 show that the fits obtained for the two models overlap one other). The three parameters that now result from the fit yield the quantum yield of photoproduct Co^{2+} from the ion pair, Φ_{IP}, and the ion pair equilibrium constant, K_{IP}. The results are listed in Table 3.11.

Table 3.11 Ion pair model fits for *trans-/cis*-$[Co(NCS)_2(NH_3)_4]^+$ and *trans-/cis*-$[Co(NCS)_2(en)_2]^+$ complexes in the presence of thiocyanate. For simplicity T = NCS^-.

Items	*trans*-$[CoT_2(NH_3)_4]^+$	*cis*-$[CoT_2(NH_3)_4]^+$	*trans*-$[CoT_2(en)_2]^+$	*cis*-$[CoT_2(en)_2]^+$
$a_0 = \emptyset^0$	0.069±0.011	0.083±0.004	0.0095±0.0007	0.0038±0.0009
a_1	0.095±0.029	0.079±0.008	0.016±0.002	0.024±0.002
a_2	0.25±0.17	0.12±0.04	0.11±0.06	0.06±0.04
$\emptyset_{IP}=a_1/a_2$	0.4 ± 0.3	0.7 ± 0.2	0.2 ± 0.1	0.4 ± 0.3
$K_{IP}=a_2/b$	0.19 ± 0.13	0.09 ± 0.03	0.08 ± 0.04	0.05 ± 0.03
K_{IP}[a]	0.34±0.25[b]	0.14±0.07[b]	0.09±0.07[b]	0.60±0.07

[a] K_{IP} values obtained by UV/Vis spectroscopical method, see section 2.2.5.1;
[b] Ionic strength was maintained at 0.8 M with $NaClO_4$ / NaNCS

The quantum yields $\emptyset_{IP}$ found are in the range 0.15 to 0.66, considerably larger than the intrinsic yields $\emptyset^0$, showing that either or both of the inner or outer sphere ion pair photolysis mechanisms mentioned above are operating to increase the photoredox efficiency.

The ion pair equilibrium constants K_{IP} obtained from the fits lie in the range 0.1 to 0.2. This is consistent with most of the K_{IP} data obtained from the UV/Vis spectra. The values estimated from this model are in good agreement with published values for similar cobalt(III) am(m)ine systems under similar conditions (Table 3.12)[128-131] when the charge effect has been taken into account (K_{IP} for a system where $Z_A Z_Q = -1$ should be about 1.7 or 1.4 smaller than that for $Z_A Z_Q = -4$ or -3 respectively based on the Fuoss equation 1.49). In fact, the ion pair constant can also be calculated using the Fuoss equation with the parameters listed in section 1.4.1.1 and $r_{complex} = 0.25$ nm, $r_{NCS^-} = 0.46$ nm, $\mu = 0.8$

M, $\sigma_A = \sigma_Q = a = 0.71$ nm, $Z_AZ_Q = -1$ to have a value of $K_{eq} \approx 1$. All of these results support the feasibility of this modelling.

Table 3.12 Ion pair constant, K_{IP}, for some cobalt(III) am(m)ine complexes obtained from the literature.

Complexes	Anions	K_{IP}	μ, M[a]	Z_AZ_Q[b]	references
$[Co(NH_3)_5(NCS)]^{2+}$	CO_3^{2-}	0.9±0.3	1.0	-4	129
$[Co(NH_3)_5(NCS)]^{2+}$	SO_4^{2-}	0.8±0.3	1.0	-4	129
$[Co(NH_3)_6]^{3+}$	Cl^-	0.20	0.9	-3	128,130
$[Co(NH_3)_6]^{3+}$	Br^-	0.20	0.9	-3	130
$[Co(NH_3)_5(H_2O)]^{3+}$	SCN^-	0.43	1.0	-3	131
trans-$[Co(SCN)_2(en)_2]^+$	SCN^-	0.3	3	-1	128

[a] ionic strength; [b] charge product.

Although these aspects imply that the ion pair model is likely to operate here, it is impossible to distinguish rigorously between the two models based on the experimental results obtained so far. Further investigation is necessary and will be discussed in Chapter four.

3.4 Conclusions

(i) Photoredox reaction is the dominant process for both *trans*- and *cis*-$[Co(NCS)_2(NH_3)_4]^+$, but with complicated reaction stochiometry.

(ii) O_2, pH, and ionic strength have little effect on the redox quantum yield, but anion effects brought about by halides and acetate were observed. Increasing medium viscosity retards the photoredox process.

(iii) Ligand effects are observed as the neutral ligand is changed from NH_3 to en. The photochemical yields decrease markedly, but the order of *trans*- and *cis*- isomer yields in the absence of NCS^- can not be explained by the Figure 3.14 mechanism.

(iv) In the absence of NCS^-, a mechanism with nearly concerted elimination of $(NCS)_2^{-\cdot}$ in the *cis*-$[Co(NCS)_2(NH_3)_4]^+$ isomer is proposed. Diffusion or rotation is necessary to bring the two NCS species together in the *trans*-$[Co(NCS)_2(NH_3)_4]^+$ isomer.

(v) In the presence of NCS^-, the great enhancement of redox quantum yield can be explained equally well by both kinetic model and ion pair model. The kinetic model gives a radical pair lifetime in the range of 6 to 25 ps. The K_{IP} values estimated from the ion pair model agree with data obtained by UV/Vis methods and with published values for similar systems .

CHAPTER FOUR

SYNTHESIS AND THIOCYANATE PHOTOSUBSTITUTION OF (1,4,7-TRIAZACYCLONONANE)-TRIISOTHIOCYANATO COBALTATE(III). YIELD ENHANCEMENT BY ADDED THIOCYANATE

4.1 Introduction

As was reported in Chapter three, a significant increase in photoredox yields occurs on irradiation of diisothiocyanatotetraam(m)inecobalt(III) complexes in the presence of thiocyanate. This raised questions regarding the role of inner and outer sphere (or intra and intermolecular) electron transfer in the primary process, and the mechanism of scavenging by thiocyanate ion in these systems. It was found in Chapter 3 that those results can be fit equally well in terms of thiocyanate ion scavenging of the thiocyanate radical from an initial caged radical pair having a lifetime of tens of picoseconds (the kinetic model), or in terms of photolysis of a thiocyanate/cobalt complex ion pair (the ion pair model). There was no firm basis on which to distinguish the two.

In this chapter an approach to exploring this issue will be reported. A zero charged complex was chosen for study since it would not form ion pairs, turning off any ion pair mechanism, while remaining susceptible to thiocyanate enhancement of its redox yield by a scavenging mechanism. The approach requires a thermally stable triam(m)inetri(iso)thiocyanatocobalt(III) complex. Ligand Field Theory and literature data suggested such a goal might be difficult to reach as increasing the number of weak field ligands destabilizes Co(III) complexes. Such compounds tend to be insoluble and few appear to be known. The closest described[132] is $Co(dan)(SCN)_3$, where dan = 1,4,7-triazaheptane, which has been reported to be prone to thermal solvolysis. As a more promising target, $Co(tacn)(NCS)_3$ (where tacn = 1, 4, 7 - triazacyclononane) was chosen based on the probable stability of the $Co(tacn)^{3+}$ moiety. This complex was synthesized, characterized, and its thermal stability and photochemical behavior is reported.

4.2 Results

4.2.1 Characterization of Co(III)(1,4,7-triazacyclononane)-triisothiocyanato Complexes, $Co(tacn)(NCS)_3$, and $Co(tacn)(NCS)_3 \cdot 3DMSO$

The compound $Co(tacn)(NCS)_3$ was characterized by elemental analysis , NMR, IR, UV/Vis and conductivity. Elemental analysis: Found (calcd) for $Co_1C_9H_{15}N_6S_3$: C% 29.88 (29.83), H% 4.07 (4.17), N% 22.65 (23.19), S% 27.06 (26.54). ^1H NMR (d_6-DMSO): δ 2.59 (6.6H, C$\underline{H}_2$), 2.98 (5.4H, C$\underline{H}_2$), 7.94 (2.8H, N$\underline{H}$). (Compare tacn·3HCl in d_6-DMSO: δ 3.4 (12.0H, C$\underline{H}_2$), 4.3 (6.6 H, br, N$\underline{H}$+$\underline{H}$Cl); or in D_2O: δ 3.4 (12.0H, $\underline{C}H_2$)). ^{13}C NMR (d_6-DMSO): δ 51.2 ($\underline{C}H_2$), 139.1 (N$\underline{C}$S). (Compare tacn·3HCl in D_2O: δ 42.1 ($\underline{C}H_2$)). FT-IR, cm^{-1}: 3440 (s, br) ν(NH); 3100 (s, br) ν(CH); 2100 (s) ν(CN); 1620(w) δ(NH); 1340 (w) δ(CH); 815 (w) ν(CS); 485 (m, single sharp) δ(NCS). UV/Vis in $8x10^{-4}$ M $HClO_4$ aqueous DMSO (1/1.5 v/v) solution: λ_{max},nm (ε, M^{-1} cm^{-1}): 507 ($5.10x10^2$), 342 ($3.85x10^3$), $\varepsilon_{342}/\varepsilon_{507} = 7.55$ (Figure 4.1). Conductivity μS/cm: 2.6, compare to NaCl: 31.1, $CaCl_2$: 39.6 (all corrected for solvent).

$Co(tacn)(NCS)_3 \cdot 3DMSO$: Found (Calcd) for $Co_1C_{15}H_{33}N_6S_6O_3$: C% 30.13 (30.19), H% 5.49 (5.57), N% 14.25 (14.08) and S% 30.87 (32.32).

The elemental analysis and NMR results establish the identity of this compound and its purity, which is confirmed by chromatography (*vide infra*). The large positive chemical shift of N$\underline{H}$, $\Delta\delta = 7.9\text{-}4.3 = 3.6$ in the complex indicates that coordination to the cobalt(III) center of the tacn nitrogen reduces its electronic density and deshields its proton, shifting δ to the lower field. The two C$\underline{H}_2$ peaks found in the ^1H NMR of the complex compared with the one found in the free ligand reveal the magnetic inequivalency of the C$\underline{H}_2$-C$\underline{H}_2$ protons expected upon coordination. The very small conductivity compared to that of NaCl (1:1 electrolyte) and $CaCl_2$ (1:2 electrolyte) demonstrates that the complex synthesized is a

neutral molecule in solution. Figure 4.2 shows the schematic diagram of $Co(tacn)(NCS)_3$ complex.

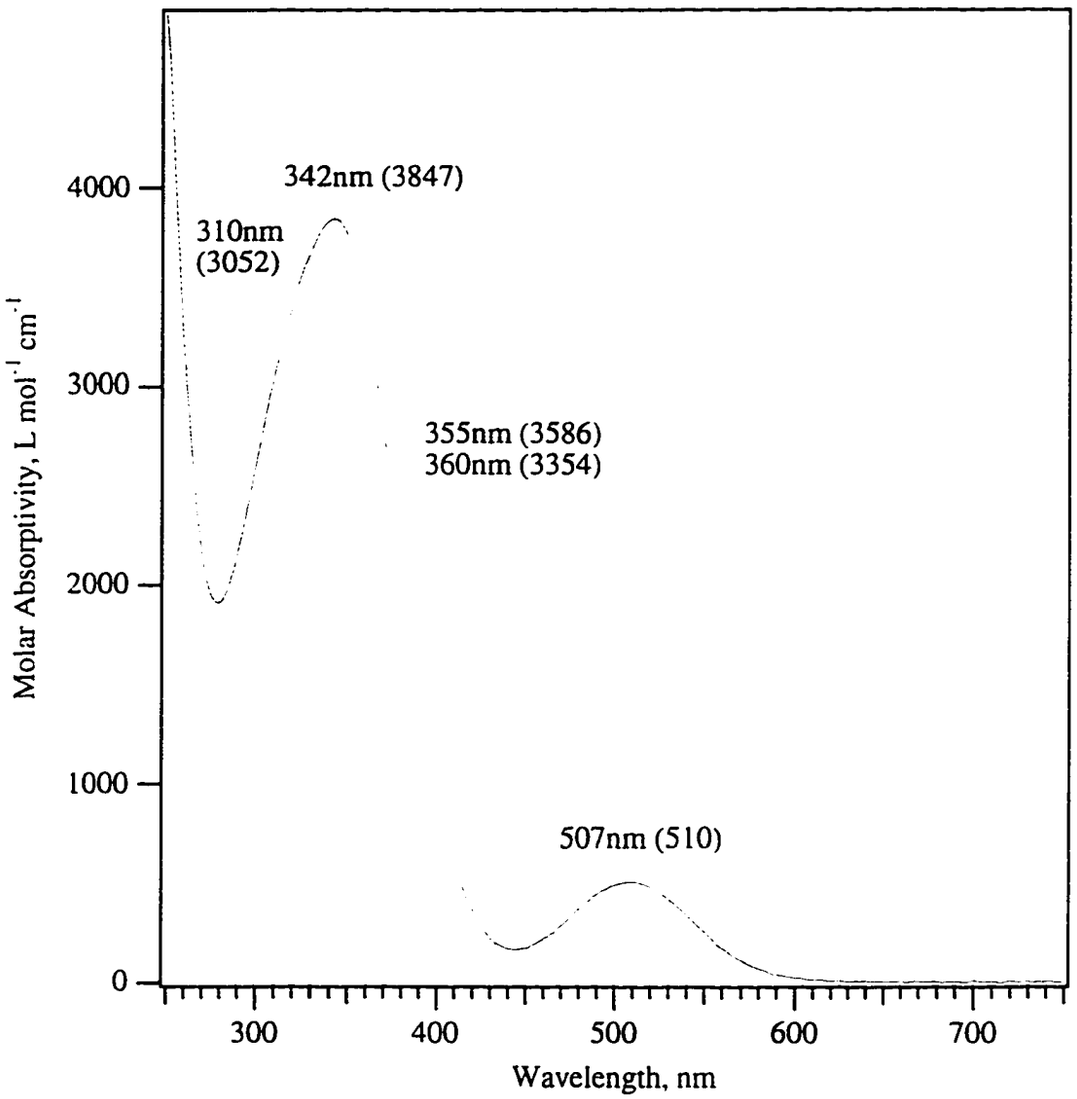

Figure 4.1 Electronic absorption spectrum of $Co(tacn)(NCS)_3$ in $8x10^{-4}$ M $HClO_4$ aqueous DMSO (1/1.5 v/v) solution.

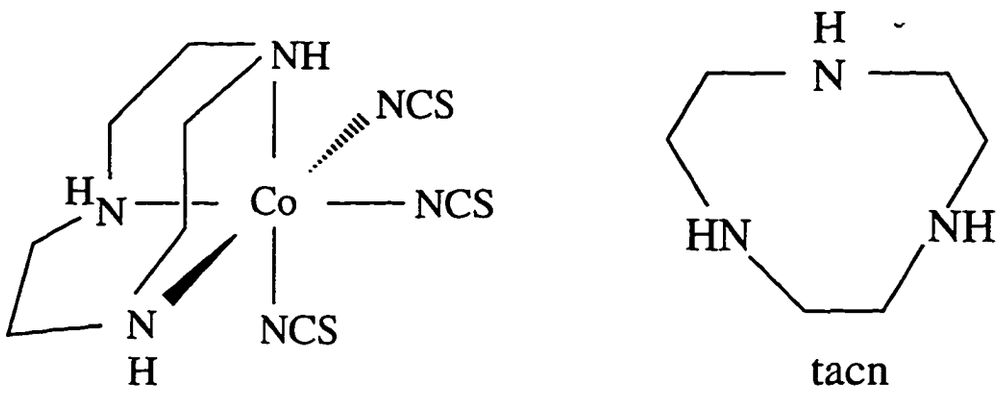

(a) (b)

Figure 4.2 Schematic diagram of (a) $Co(tacn)(NCS)_3$ complex, and (b) tacn ligand.

The bonding mode of the thiocyanate ligands can be decided spectroscopically. In the IR spectrum the bands observed at 815 (ν(CS), N-bonded), 485 cm^{-1} (δ(NCS), N-bonded) and the absence of bands in the range 690-720 (ν(SC), S-bonded) and near 420 cm^{-1} (δ(SCN), S-bonded) show that they are N-bonded.[133] The ratio of the UV/Vis molar absorptivity maxima for the two ligand field bands, L_1 and L_2 in increasing energy, is 7.6 in this compound, similar to the range (8.2-10.5) for other N-bonded cobalt(III) isothiocyanate am(m)ine analogues reported in Chapter 3, and far smaller than is found in the only S-bonded type reported (211).[38,116] These results suggest that the thiocyanate is N-bonded to the cobalt(III) center in the complex synthesized here.

This compound is thermally stable in aqueous/DMSO solutions. No kinetic studies of the thermal reaction were deemed necessary, as solutions were stable at room temperature over several hours, sufficient that no interference, before, during or after irradiation occured from thermal processes involving reactant or products.

4.2.2 Photoproducts and Quantum Yields

The complex underwent both photoredox and photosubstitution reactions on steady state irradiation at 360 nm and 22 °C in 1.0 M sodium thiocyanate in 8 x 10^{-4} M $HClO_4$ aqueous DMSO (1/1.5 v/v) medium. The photoredox quantum yield, $\emptyset(Co^{2+})$, was found to be 0.0008 (Table 4.1), much smaller than that for its analogues *cis-/trans*-$[Co(NCS)_2(en)_2]^+$ (0.026 and 0.023 respectively) and *cis-/trans*-$[Co(NCS)_2(NH_3)_4]^+$ (0.153 and 0.146 respectively) under similar conditions (Chapter 3). In the absence of added thiocyanate, $\emptyset(Co^{2+})$ was too small to be measured .

On laser flash photolysis of all solutions, the transient signal corresponding to the dithiocyanate radical ion $(NCS)_2^{-\cdot}$ (λ_{max} = 475, ε = 7.6 x 10^3 M^{-1} cm^{-1})[40] was observed. The absorption was very weak in the absence of added thiocyanate ion, and increased almost linearly with its addition. Figure 4.3 shows the transient absorption decay obtained in 1.82 M NCS^- / 8x10^{-4} M $HClO_4$ aqueous DMSO (1/1.5 v/v) solution. and the fit to the second-order decay with a first half-life of 31 μs. The permanent absorption change observed does not correspond to the product formation at 475 nm (refer to Figure 4.7). It is likely due to the experimental artifact, or the contribution of other long lived species which absorb at this wavelength.

Figure 4.4 shows the estimated quantum yield of dithiocyanate radical $\emptyset((NCS)_2^{-\cdot})$ as a function of thiocyanate concentration. These estimates were based on the observed absorbance change at 475 nm, the laser pulse energy, the solution absorbance at 355 nm and the geometry of the beam intersection region for the analysing and laser beams, see section 2.2.1.5 for details. The concentration dependence can be relied on in this calculation, but the absolute yields may be subject to systematic errors and to an assessment of ±10% relative uncertainty. For 1 M thiocyanate ion, Figure 4.4 gives a $\emptyset((NCS)_2^{-\cdot})$ of 0.036 which is just over 50% larger than $\emptyset$(total) of 0.022 for disappearance of starting material measured chromatographically (Table 4.1). In the absence of thiocyanate, the corresponding yields are about 0.004 and 0.012 respectively so that photosubstitution has

about three times (0.012/0.004 = 3) the quantum yield of the photoredox intermediate $(NCS)_2^{-\cdot}$.

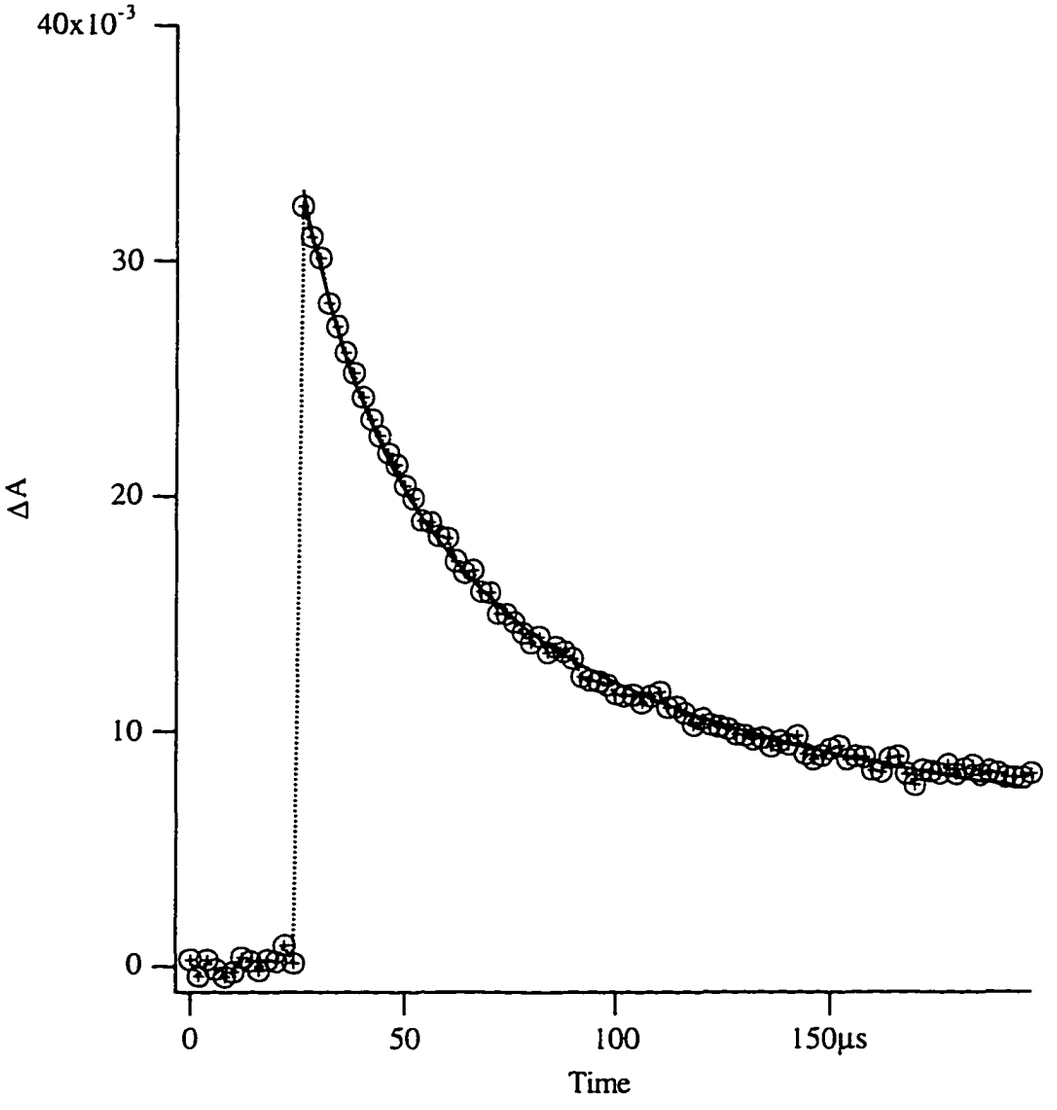

Figure 4.3 The decay of the $(NCS)_2^{-\cdot}$ transient absorption at 475 nm in 1.82 M NCS^- / $8x10^{-4}$ M $HClO_4$ aqueous DMSO (1/1.5 v/v) solution.
Markers, experimental points. Solid line, fit to the second order decay.

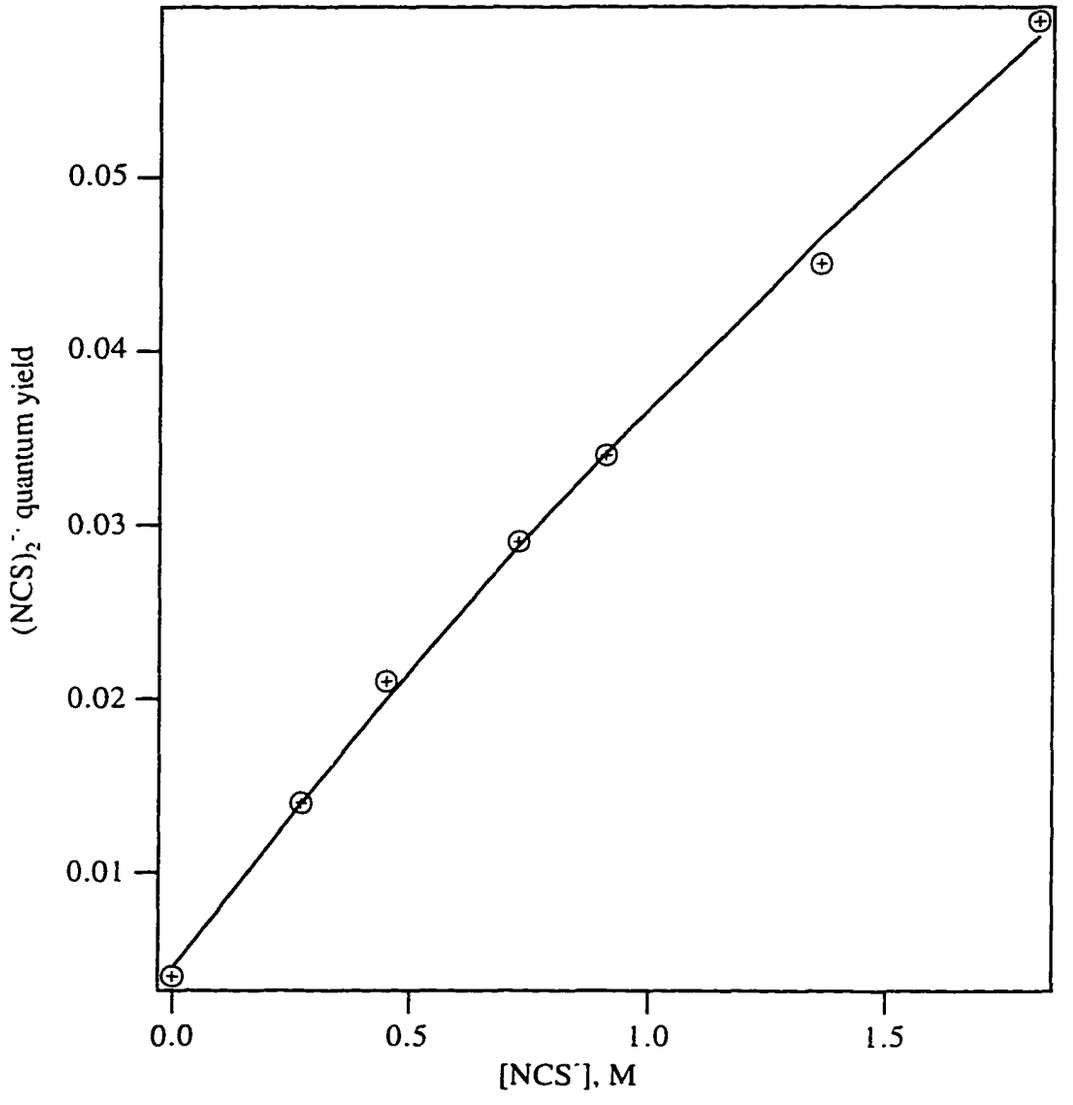

Figure 4.4 Quantum yield of $(NCS)_2^{-\cdot}$ from $Co(tacn)(NCS)_3$ vs $[NCS^-]$ by laser flash photolysis experiment.
Marker, experimental points. Line, fit to the kinetic model discussed in the text.

Table 4.1 Typical quantum yields for the photolysis of $Co(tacn)(NCS)_3$ in $8x10^{-4}$ M $HClO_4$ aqueous DMSO (1/1.5 v/v) with and without added NCS^-.

Quantum yields[a]	$[NCS^-] = 0$ M	$[NCS^-] = 1.0$ M
$\emptyset(Co^{2+})$	-	0.0008±0.0003 (4)
$\emptyset_{total}$	0.012±0.005 (6)	0.022±0.002 (4)
$\emptyset((NCS)_2^{-\cdot})$	0.004	0.036

[a] Irradiation wavelength: 360 nm (steady state) or 355 nm (LFP). The numbers of determinations are listed in the bracket.

These results indicate that pure $Co(tacn)(NCS)_3$ is rather photoredox inert, but that the addition of thiocyanate can enhance its yield of photoredox intermediates, and the main concurrent photosubstitution reaction (commented on in the following) is also enhanced under these conditions. In all cases photosubstitution dominates; e.g. in 1 M NCS^- solution, about 96% photosubstitution product (1 - 0.0008/0.022 = 0.96) is found with 4% Co^{2+} photoredox product (0.0008/0.022 = 0.04).

A study of these predominant photosubstitution reactions was therefore undertaken using HPLC chromatography to analyse the photoproducts, coupled with UV/Vis difference spectroscopy and some thermal kinetics experiments.

As shown in Figure 4.5, an unphotolyzed solution of starting complex gave a major peak (A) at a retention time (t_R) of 3.6 min and two small impurity peaks, B (it may be an injection artifact, not a true impurity peak) and C. These impurity peaks corresponded to less than 4% of the total peak area. On irradiation of the complex in the absence of thiocyanate, a clear product peak, B, grew in at the expense of the starting material, which it just preceeded in the elution sequence (at t_R = 2.7 min). The area of peak B increased

with irradiation time (Figure 4.5(a)-(c)). At higher conversions it became evident that two additional peaks, C at t_R = 8.3 min and coincident with the second impurity peak mentioned above, and a new peak (D), t_R = 5.4 min, were also being produced. No other peaks appeared for conversions less than 15%. Because of the small size of peaks C and D, it was not possible to decide from their growth kinetics alone whether they were secondary or primary photolysis products, see discussion. In contrast, in the presence of 1 M thiocyanate, the behaviour was simpler: peak B again grew but with a faster rate than in the absence of added thiocyanate, peak C remained essentially constant at the impurity level while D did not appear (Figure 4.5(d)). The significance of Figure 4.5(e)-(f) will be discussed in section 4.3.1.

Figure 4.6 shows clearly the linear relationship of the disappearance of the starting material (peak A) and the growth of products (peaks B, C, D) with irradiation time. It also shows that in the presence of thiocyanate, the starting complex (peak A) disappeared at a rate increased by about 30%, and peak B grew at about five times the rate in the absence of added thiocyanate.

During these sequences of irradiations, the UV/Vis spectral changes were monitored, Figure 4.7. Without thiocyanate, Figure 4.7(a), reasonable isosbestic points were seen at 335, 411, 454 and 545 nm. A peak grew in at 290 nm. It should be noted that, at the irradiation wavelength of 360 nm, ΔA was negative, showing that products were less strongly absorbing than the starting complex. This relates later to the question of possible secondary photolysis. With 1 M thiocyanate, similar isobestic points were seen at 365, 383, 460 and 537 nm, and a similar peak grew in at 290 nm with much greater absorbance. For both sets of conditions, the ligand field band of the product was red shifted relative to the starting material, indicating the replacement of a stronger field ligand by a weaker one (e.g. NCS^- replaced by solvent DMSO or water, since ligand field strength $NCS^- > H_2O >$ DMSO)[15]. The band developed at 290 nm is consistent with a charge transfer transition from DMSO/H_2O to cobalt(III).

To obtain calculated absorption spectra for the photoproduct mixtures obtained in the two sets of experiments, both difference absorption spectra (Figure 4.7(a)-(b)) were combined with the percent conversion data for the starting complex measured chromatographically, see section 2.2.2.1 and 2.2.5.1 for details. The results are shown in Figure 4.8(a)-(b), and displayed in terms of apparent molar absorptivity to emphasize that they correspond to some undetermined mixture of product absorption spectra, not to a single compound.

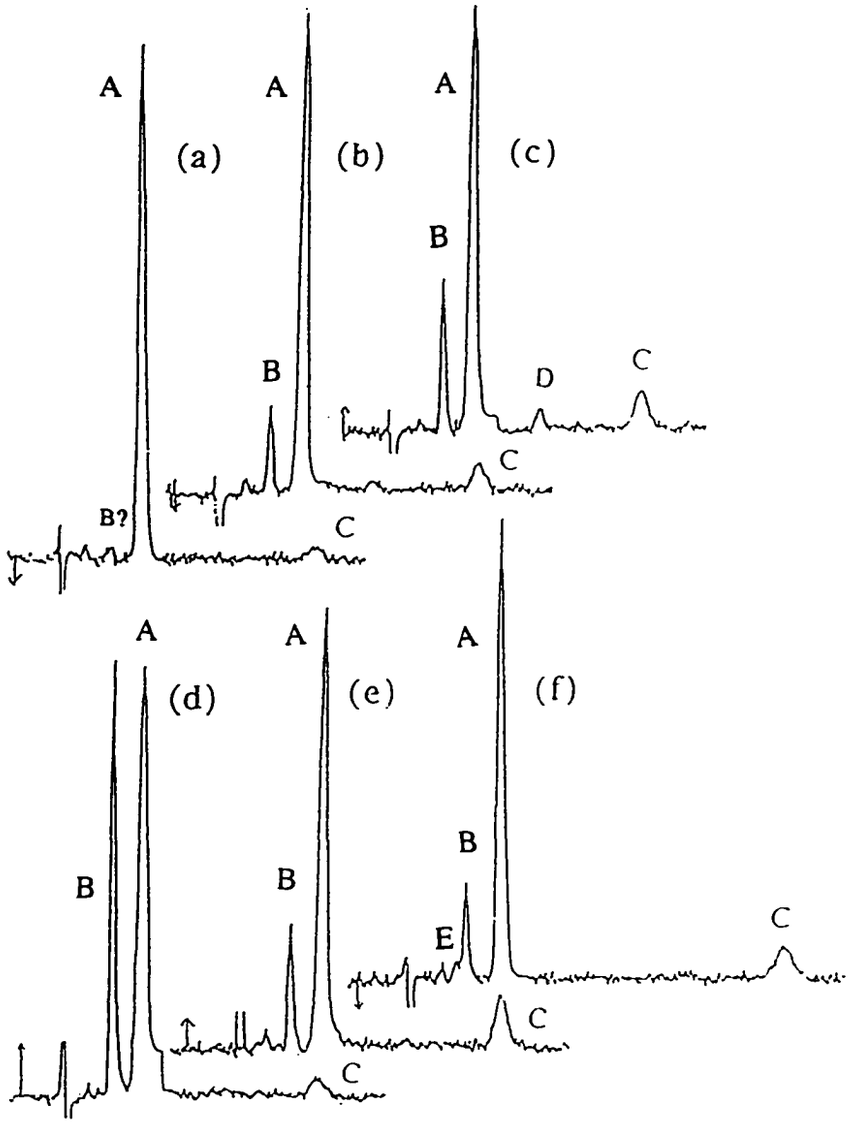

Figure 4.5 Reversed-phase HPLC analysis of 5.30×10^{-4} M $Co(tacn)(NCS)_3$ photolysed at 360 nm with and without added thiocyanate ion. Sensitivity in absorbance units full scale: Peak A, 0.1; Peak B, C, D and E, 0.05. (a) DMSO/H^+ solvent, $t_{hv} = 0$ min; (b) DMSO/H^+ solvent, $t_{hv} =$ 15 min; (c) DMSO/H^+ solvent, $t_{hv} = 30$ min; (d) 1 M NCS^-/DMSO/H^+ solvent, $t_{hv} = 20$ min; (e) neat DMSO solvent, $t_{hv} = 22$ min; (f) DMSO/H^+ solvent, $t_{hv} = 30$ min, eluent's pH = 9.

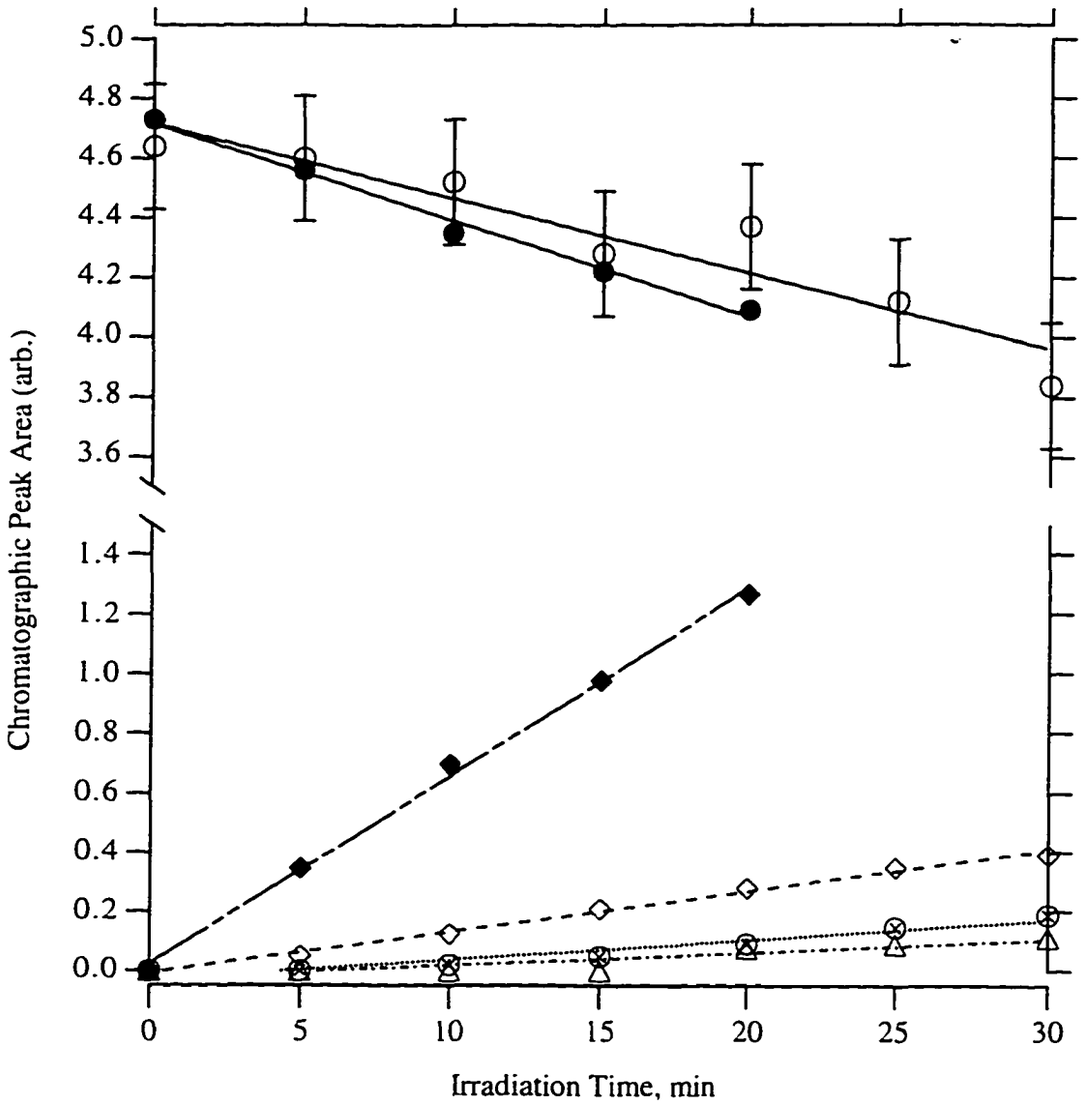

Figure 4.6 Plot of reactant disappearance and products appearance as function of irradiation time. Peak areas obtained from HPLC results on the photolysis of 5.30×10^{-4} M $Co(tacn)(NCS)_3$.
Markers, experimental; lines, theoretical fittings. Standard deviation based on a norm of 5 measurements. Letter in parentheses identifies corresponding chromatographic peak.

- O $Co(tacn)(NCS)_3$ (A) without added NCS^-;
- ◊ $[Co(tacn)(NCS)_2(DMSO)]^+$ (B) without added NCS^-;
- ⊗ $[Co(tacn)(NCS)(DMSO)_2]^{2+}$ (C) without NCS^-;
- Δ $[Co(tacn)(NCS)_2(H_2O)]^+$ (D) without NCS^-;
- • $Co(tacn)(NCS)_3$ (A) in 1 M NCS^-
- ♦ $[Co(tacn)(NCS)_2(DMSO)]^+$ (B) in 1 M NCS^-.

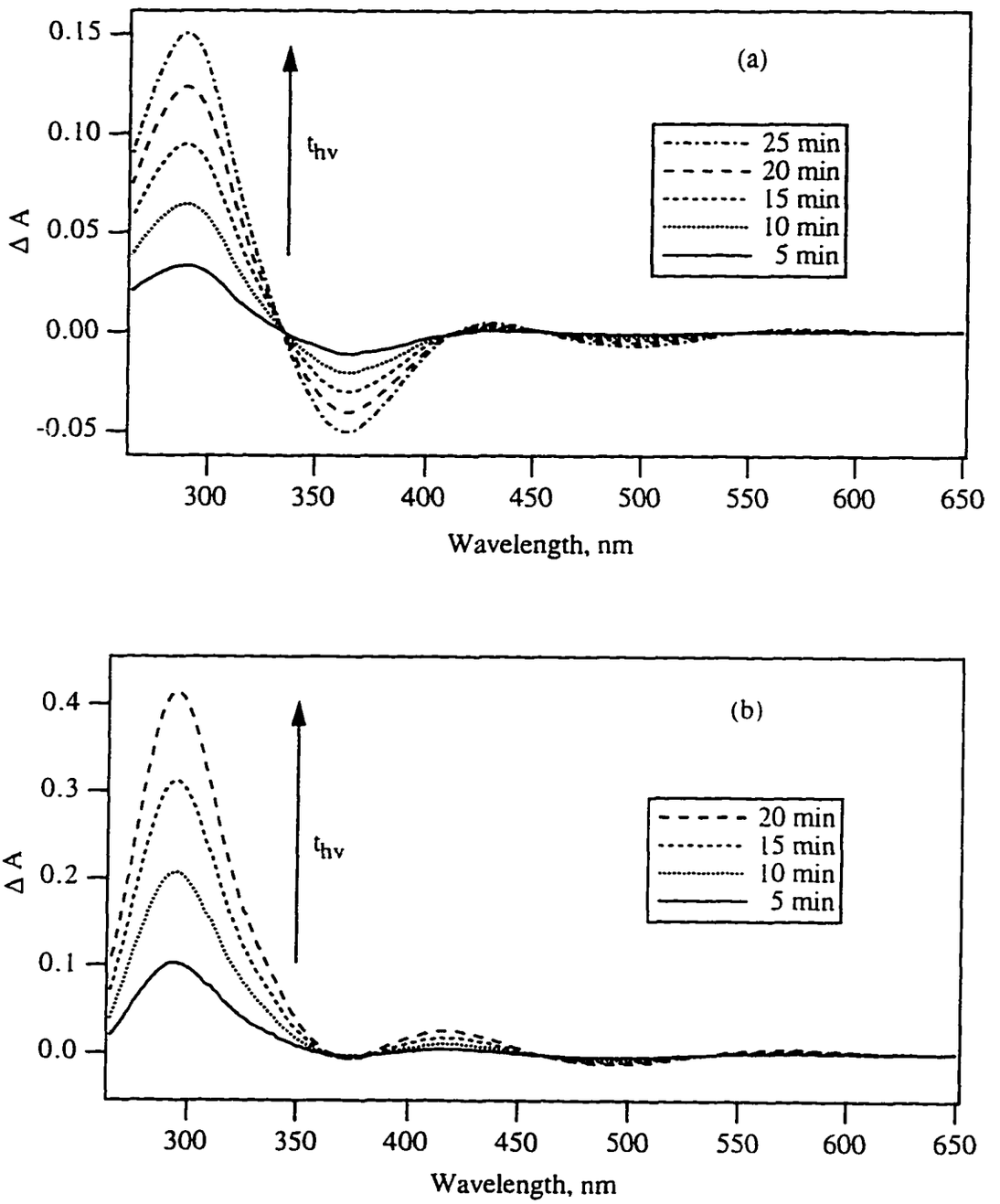

Figure 4.7 Absorbance changes for photolysis of 5.30×10^{-4} M $Co(tacn)(NCS)_3$ measured against an unphotolyzed aliquot for different irradiation times as shown in the figures. (a) in 8×10^{-4} M $HClO_4$ aqueous DMSO (1/1.5 v/v) solution, (b) in 1M $NCS^-/8 \times 10^{-4}$ M $HClO_4$ aqueous DMSO (1/1.5 v/v) solution.

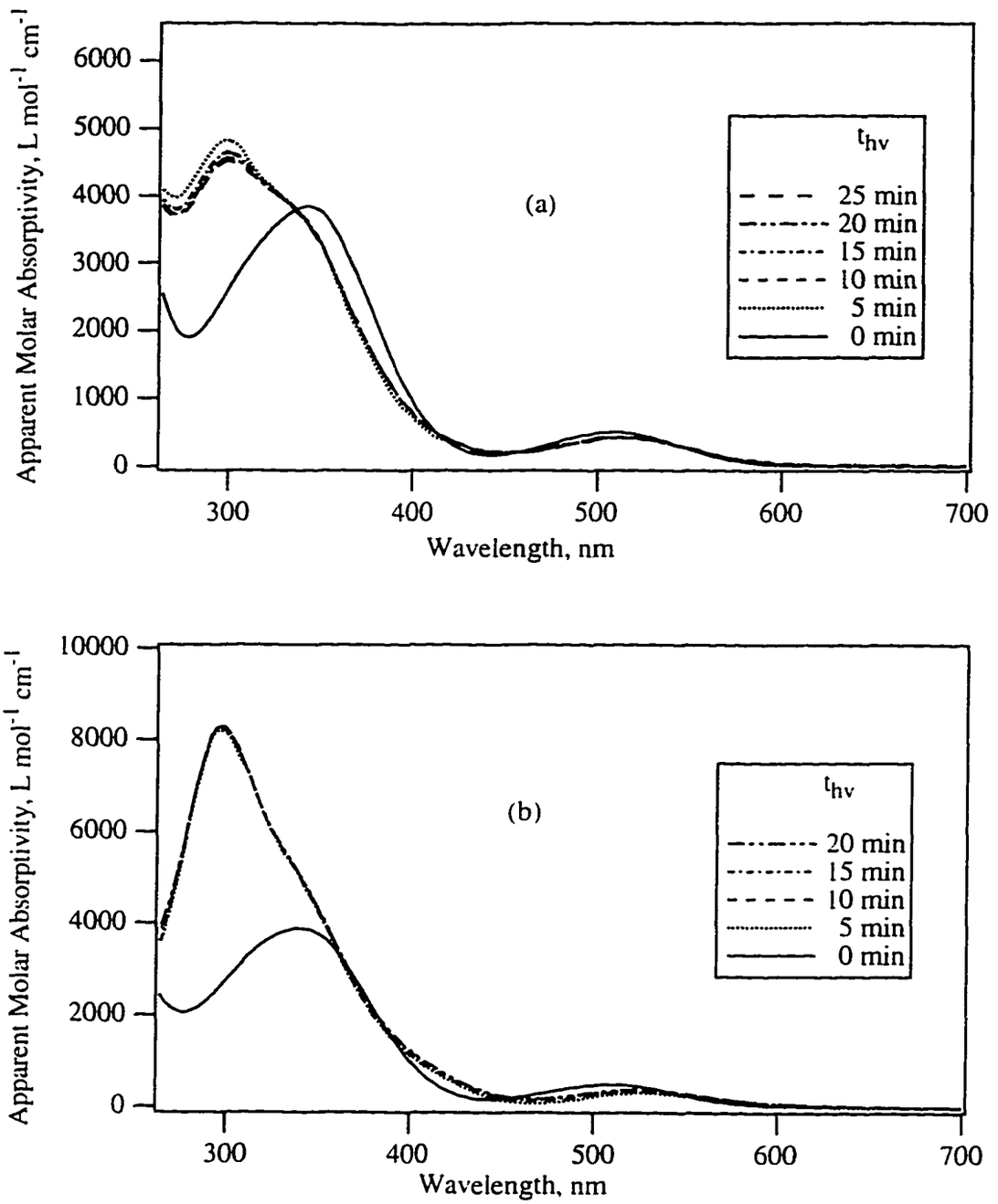

Figure 4.8 Electronic absorption spectrum of $Co(tacn)(NCS)_3$ (solid line) and apparent molar absorptivity of product (dashed lines) calculated for the data of Figure 4.6 with the measured percentage conversions of $Co(tacn)(NCS)_3$ from HPLC. Assuming $Co(tacn)(NCS)_3 \xrightarrow{h\nu}$ product mixture. (a) in $8x10^{-4}$ M $HClO_4$ aqueous DMSO (1/1.5 v/v) solution, (b) in 1M NCS^-/ $8x10^{-4}$ M $HClO_4$ aqueous DMSO (1/1.5 v/v) solution.

Note that the displacement of the tacn ligand at one or more coordination sites is unlikely. Any dangling N of tacn will be likely to recoordinate back, which does not lead to a final change in chemical structure. Due to the thermal stability of the photoproducts the possible formation of protonated, partially coordinated, tacn species can also be excluded, though protonated amine was formed in photoreactions of other polyamine analogues. Linkage isomerization is another possibility to be considered; here one would expect the product $Co(tacn)(NCS)_2(SCN)$. Small amounts of this species would be hard to detect (it would likely elute with the starting material under the chosen chromatographic conditions) and therefore would have been missed.

To further explore the mechanism, a 1.19×10^{-4} M $Co(tacn)(NCS)_3$ solution in 8×10^{-4} M $HClO_4$ aqueous DMSO (1/1.5 v/v) medium, $A_{355} = 0.39$, was flashed with 40 mJ of 355 nm light and the transient conductivity change compared with the blank without the $Co(tacn)(NCS)_3$ complex. A conductivity increases on a μs timescale was observed (Figure 4.9), demonstrating the generation of ionic products by photolysis. Together with other experimental data this supports ligand substitution (not isomerization) as the major process. Due to the complexity of the products in the absence of added thiocyanate, however, it does not eliminate the possibility of the linkage isomer being a minor process.

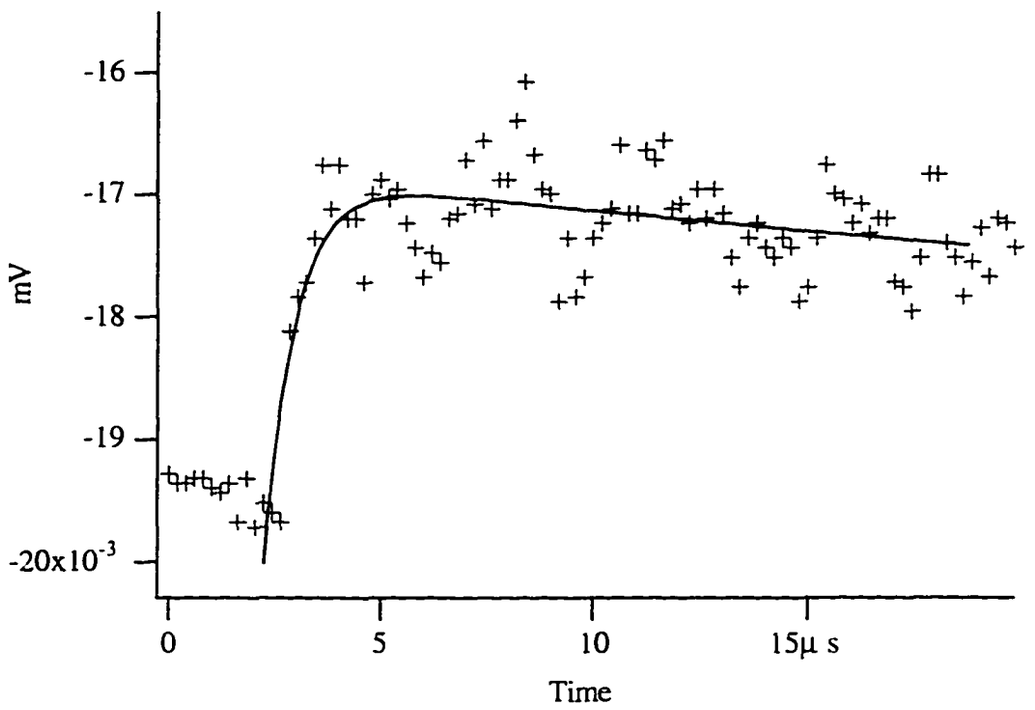

Figure 4.9 Time dependence of solution conductivity on the photolysis of $Co(tacn)(NCS)_3$ in $8x10^{-4}$ M $HClO_4$ aqueous DMSO (1/1.5 v/v) solution using LFP at 355 nm.

4.3 Discussion

4.3.1 Identification of Photosubstitution Products

4.3.1.1 The Identification of the Major Product

The identification of the main product chromatography peak B was as follows. It was likely to correspond either to the product seen spectroscopically, Figure 4.7, with UV/Vis $\lambda_{max} \approx 290$ nm, or to the photoredox product $[Co(NCS)_4]^{2-}$ which has λ_{max} at 320 nm and apparent $\varepsilon_{320} = 7.68$, 9.08, or 11.4 x 10^3 M^{-1} cm^{-1} in 0.5, 1.0 or 2.0 M NCS^- solution. (Note that these spectral data do not exhibit the very high molar absorptivity ratio for the second to first ligand field bands expected for the linkage isomer.) Several pieces of evidence support the first assignment. Table 4.2 (#1 to #3) shows that the peak height observed for B was reduced as the HPLC detection wavelength was changed from 300, 310 to 320 nm, as would be expected for a product with $\lambda_{max} \approx 290$ nm. Next, injection of authentic $[Co(NCS)_4]^{2-}$ did not give any peak in the chromatogram, presumably because of its lability and interactions with the components of the eluent. This indicates that the 310 nm peak detected can not be $[Co(NCS)_4]^{2-}$. Similarly, when chloride anion was added into the photolyzed solution, no change in optical spectrum or in chromatographic peak height of B was observed (Table 4.2, #4 and #6), owing to the equilibrium:

$$[Co(NCS)_4]^{2-} + 4Cl^- \overset{K_1}{\rightleftharpoons} [CoCl_4]^{2-} + 4NCS^- \qquad (4.1)$$

The logarithms of stability constants of $[CoCl_4]^{2-}$ and $[Co(NCS)_4]^{2-}$ in DMSO are known to be $\log\beta_4([CoCl_4]^{2-}) = 9.05$ and $\log\beta_4([Co(NCS)_4]^{2-}) = 6.76$ respectively.[134] Therefore in pure DMSO the equilibrium constant for eq. 4.1 can be calculated:

$$K_1 = \frac{[CoCl_4^{2-}]\,[NCS^-]^4}{[Co(NCS)_4^{2-}]\,[Cl^-]^4}\,\frac{[Co^{2+}]}{[Co^{2+}]} = \frac{\beta_4([CoCl_4]^{2-})}{\beta_4([Co(NCS)_4]^{2-})} = 195 \qquad (4.2)$$

The relatively large K_1 indicates that chloride competes effectively with thiocyanate in the equilibrium to consume $[Co(NCS)_4]^{2-}$ and produce $[CoCl_4]^{2-}$ species with ε_{310} almost zero. The appearance of 310 nm peak at the chromatogram with and without the addition of Cl^- excludes the possibility of peak B being $[Co(NCS)_4]^{2-}$. Lastly, in the absence of thiocyanate, the photoredox of the complex was barely detectable, but the major product (peak B) still appeared under these conditions.

These observations rule out the redox product $[Co(NCS)_4]^{2-}$ and point to a photosolvation product, $[Co(tacn)(NCS)_2S]^+$, where S could be either water or DMSO.

Table 4.2 HPLC peak heights after 16 min irradiation of 5.30×10^{-4} M $Co(tacn)(NCS)_3$ (A) in 1 M NCS^- / 8×10^{-4} M $HClO_4$ aqueous DMSO (1/1.5 v/v) solution at 360 nm, and photoproducts $[Co(tacn)(NCS)_2(DMSO)]^+$ (B), $[Co(tacn)(NCS)(DMSO)_2]^{2+}$ (C).

Chromatographic # and conditions [a]		Peak Height, cm		
#	Conditions	A	B	C
1	λ_{det}, nm = 300	20.2	9.1	0.6
2	λ_{det}, nm = 310	23.2	8.2	0.6
3	λ_{det}, nm = 320	25.1	6.8	0.7
4	no added Cl^-, room temp.	22.7	6.8	0.7
5	no added Cl^-, heated at 80°C for 30 min	23.1	3.2	0.9
6	in 1M added $[Cl^-]$, room temp.	20.6+sh	6.9	0.7
7	in 1M added $[Cl^-]$, heated at 80°C for 30 min	22.8+sh	2.9	1.2

[a] $\lambda_{det\ (HPLC)}$ = 310 nm except as specified for #1 and #3.

The identity of S was explored by irradiation in dry DMSO solution. Peak B behaved almost in the same manner no matter whether or not there was water in the solvent (Figure 4.5(e)). As additional evidence, no band shift occurred in the UV/Vis spectrum of an extensive photolysed solution (60 % conversion) on addition of ammonia. Aquo Co(III) complexes show a red shift under these conditions owing to the acid/base equilibrium:

$$[Co(tacn)(NCS)_2(H_2O)]^+ \underset{+\,H^+}{\overset{+\,OH^-}{\rightleftharpoons}} Co(tacn)(NCS)_2(OH)^0 \qquad (4.3)$$

These results show that peak B is the DMSO substituted product, $[Co(tacn)(NCS)_2(DMSO)]^+$. Notice that the calculated total product spectra of Figure 4.8 have the same $\lambda_{max} \approx 300$ nm and two shoulders at ca. 320 nm and 335 nm, indicating the formation of the same major species in the absence and presence of added thiocyanate. The apparent molar absorptivity is much higher at λ_{max} in the presence of thiocyanate than in its absence. The peak at 300 nm apparently corresponds to an overlap of $[Co(tacn)(NCS)_2(DMSO)]^+$ with the more strongly absorbing ion pair $\{[Co(tacn)(NCS)_2(DMSO)]^+, NCS^-\}$. The shoulder at 320 nm can arise from the small amounts of Co^{2+}.

4.3.1.2 The Identification of the Minor Products

The identities of the minor products (C and D) were explored by a series of reaction studies. Both have to be photoproducts because their peak height did not increase on standing at room temperature in the dark up to 1.5 h. On heating of a photolyzed thiocyanate-containing aqueous DMSO solution at 80 °C for 30 min, the height of peak B decreased, while peaks A (starting material) and C both increased (Table 4.2, compare #4 with #5, and #6 with #7). This experiment was consistent with expectations for the

thermal reaction of peak B, which can re-anate to starting material on heating with thiocyanate, or can solvate a further thiocyanate ligand, consistent with C as the di-DMSO product. The t_R of 8.4 min is about the value to be expected for a 2+ ion of type $[Co(tacn)(NCS)(DMSO)_2]^{2+}$, and this same peak was also developed in the solution when no water was present in the solvent. The remaining product is peak D at a retention time of 5.4 min. This peak did not appear in the chromatography when pure DMSO was used as solvent (Figure 4.5(e)). The retention time of 5.4 min suggests a singly charged cation and an obvious candidate is $[Co(tacn)(NCS)_2(H_2O)]^+$. To explore for an aquo ligand, the eluent pH was changed from 3.5 to 9.0; peak D then disappeared, while a new peak E, appeared at t_R = 2.4 min, prior to $[Co(tacn)(NCS)_2(DMSO)]^+$ (Figure 4.5(f)). This is consistent with the formation of a zero charged complex $[Co(tacn)(NCS)_2(OH)]$ in the basic solution, according to:

$$[Co(tacn)(NCS)_2(H_2O)]^+ \xrightarrow{+ OH^-} [Co(tacn)(NCS)_2(OH)] \qquad (4.4).$$

An alternate possibility that D = $Co(tacn)(NCS)(DMSO)(H_2O)^{2+}$ is less likely since this doubly-charged cation and its conjugate base form should have longer retention times than observed. It can be concluded that peak D is the aquation product $[Co(tacn)(NCS)_2(H_2O)]^+$.

The elution order for the photoproduct peaks implied by these results is reasonable. Peaks generally elute in order of increasing charge and greater ligand hydrophobicity. The only exception observed is for the starting complex, which has zero charge and could be expected to be the first peak eluted. Complicated elution sequences were also discovered in other tacn/thiocyanate complexes, and were similarly attributed to the importance of hydrophobicity in the interactions involved.[135]

4.3.2 Primary vs Secondary Photolysis, and Reaction Stoichiometry

Are C and D primary photoproducts or do they result from secondary photolysis of B? Figure 4.7(a) and (b) show definitively that at the irradiation wavelength of 360 nm, the products absorb less strongly than the reactant, therefore, significant secondary photolysis under these circumstances would be most unusual. The calculation based on a simple theory[136,137] show the secondary photolysis is a major contributor only if B had a much larger photoreaction quantum yield than A, which is very unlikely due to the similarity of these complexes. For example, for the worse case 15% conversion of starting complex A, and given $\varepsilon_{A,360nm} = 3.3x10^3\ M^{-1}\ cm^{-1}$, $\varepsilon_{B,\ 360nm} = 2.5x10^3\ M^{-1}\ cm^{-1}$ (from Figure 4.8(a)), the calculation shows that the fraction of the secondary photolysis is only 6% if assuming $\Phi_B = \Phi_A = 0.012$, and 0.6 only if $\Phi_B = 10\ \Phi_A$. This calculation and the linear time dependence of these product peaks, Figure 4.6, indicate that C and D are primary products, and suggest that the photochemistry in the absence of thiocyanate follows a number of parallel paths involving substitution of one or more ligands.

There is also stoichiometric evidence for such complexity. Figure 4.6 shows chromatographic peak area versus photolysis time curves. Ideally one would use isolated authentic samples of each product to calibrate these data, but these were not available. Peak area is proportional to ε_{det} at 310 nm, the HPLC detector wavelength, and the corresponding molar absorptivity of photoduct mixtures is calculated (sections 2.2.5.1 and 2.2.2.1) and shown in Figure 4.8. Figure 4.8(a) indicates that $\varepsilon_B/\varepsilon_A = 1.4$ while Figure 4.8(b) gives a value of 2.3 for the same ratio in 1 M thiocyanate. The first value is likely too low because the photoproduct mix known to occur probably has lower absorbance than pure B due to the presence of C and D, while the second value is likely too high because of intensity enhancement owing to the formation of the ion-pair $\{B^+, NCS^-\}$. In 1 M thiocyanate, only one product, B, is formed to any significant extent and from Figure 4.6, the rate of decrease in the complex, A, should match the rate of increase in the product, B.

This will occur if $\varepsilon_B/\varepsilon_A = 2.0$. It seems reasonable to accept this value as a calibration factor consistent with the spectral data and to use it to convert the areas in Figure 4.6 into molar quantities together with the assumption that $\varepsilon_B = \varepsilon_C = \varepsilon_D$ at 310 nm. On summing B, C, and D for the photolysis in the absence of thiocyanate it becomes clear that about 55% of the complex has simply disappeared without leading to observed products. This could occur if triply charged products, which would not elute under these HPLC conditions, were being formed, or if $\varepsilon_B > \varepsilon_C$ and ε_D. The course of the photoreaction is thus complicated in the absence of added thiocyanate, and leads to a multitude of products formed in parallel, while the addition of thiocyanate removes this complexity, moving the system closer to a simple A $\longrightarrow$ B behaviour. The reason is likely to be the thiocyanate scavenging of highly reactive radical pair species to produce $(NCS)_2^{-\cdot}$ which results in a simplification of the products found.

4.3.3 Mechanism of Photosubstitution

Photosubstitution is clearly the main photoreaction pathway of $Co(tacn)(NCS)_3$ for irradiation at 360 nm and photoredox reaction is relatively minor. Both pathways are more efficient and the photochemistry is less complex in the presence of added thiocyanate. The accepted models for cobalt(III) photochemistry recognize the possibility of formation of both redox and substitution products by a radical pair mechanism,[32,138] together with photosubstitution occuring via internal conversion to low-lying ligand field states, triplet and/or quintet in nature. Such metastable states have been observed by sub-picosecond transient absorption spectroscopy.[139]

The question immediately arises as to whether the observed redox and substitution modes occur in parallel or consecutively. For the reaction in the absence of added thiocyanate this is not obvious; the photosubstitution yield is higher than the yield of $(NCS)_2^{-\cdot}$ but this is misleading as the initial radical pair species does not give an

observable transient absorption. The photosubstitution observed is complicated, involving more than one ligand loss, and this is quite unlike the usual photoreaction from ligand field excited states. This leads one to suspect that a complex redox mechanism is operating.

In contrast, the reaction in thiocyanate looks like a clean consecutive process and it is suggested to occur also through the radical pair mechanism, supplemented with a thiocyanate scavenging step. This can be represented in a simplified manner as:

$$Co(tacn)(NCS)_3 + h\nu \xrightarrow{\Phi_{RP}} \{Co^{II}, \cdot NCS\} \qquad (4.5)$$

(Radical pair (RP) formation)

$$\{Co^{II}, \cdot NCS\} \longrightarrow Co(tacn)(NCS)_3$$

(RP recombination + Linkage isomerization) (4.6)

$$\{Co^{II}, \cdot NCS\} \longrightarrow Co^{II} + (NCS)_2^{-\cdot}$$

(Capture of NCS^- from a Co(II) fragment with separation of $(NCS)_2^{-\cdot}$ from the cage) (4.7)

$$\{Co^{II}, \cdot NCS\} + NCS^- \longrightarrow Co^{II} + (NCS)_2^{-\cdot}$$

(Scavenging by NCS^-) (4.8)

$$Co^{II} + (NCS)_2^{-\cdot} \longrightarrow \text{substitution products} \qquad (4.9)$$

$$Co^{II} \longrightarrow Co^{2+} \text{ and other redox products} \qquad (4.10)$$

To reduce their complexity, Co^{II} has been used in these equations to represent the reduced cobalt complex in its various possible solvated forms. It therefore represents a

distribution of species that may vary with time and origin; for example Co^{II} will likely not be the same on the product sides of equations 4.7 and 4.8. The scavenging of NCS· from the radical pair by NCS^-, reaction (4.8), has been added to account for the product yield enhancement caused by thiocyanate ion. The back electron transfer reaction (4.9) that leads to substitution products has been represented as occuring in the bulk in order to be consistent with the observation that the decay of $(NCS)_2^{-}\cdot$ occurs with second order kinetics (Figure 4.3). Due to the limited amount of information it is impossible to get an exact k_9 value. However, k_9 can be estimated based on the assumption that $[Co^{II}]^0 = [(NCS)_2^{-}\cdot]^0$ in equation 4.9.

Since

$$[(NCS)_2^{-}\cdot]^0 = \frac{\Delta A((NCS)_2^{-}\cdot)^0}{\varepsilon_{475}\, l}$$

$$= \frac{0.033}{7600 \times 0.7}$$

$$= 6.2\times10^{-6}\ M \qquad (4.11)$$

This, together with the observed first half-life for this second order decay ($t_{1/2}$ = 31 μs), the rate constant for reaction (4.9) can be estimated to be:

$$k_9 \approx \frac{1}{t_{1/2}\,[(NCS)_2^{-}\cdot]^0}$$

$$= \frac{1}{(31\times10^{-6})\,(6.2\times10^{-4})}$$

$$= 5\times10^{9}\ M^{-1}\,s^{-1} \qquad (4.12)$$

Assuming the correctness of the assumption, k_9 is about five times faster than that of the bulk reaction of two $(NCS)_2^{-}\cdot$ radicals to thiocyanogen ($k = 1\times10^{9}\ M^{-1}\,s^{-1}$ for

eq. 3.5).[117] This partly explains the low overall redox yield and the finding of photosubstitution via a redox intermediate in this system.

The other part of the explanation is suggested by a comparison of the redox vs substitution yields and recombination rates for the series of complexes shown in Table 4.3. As the amine ligand becomes more robust to substitution, the redox efficiency goes down, the substitution efficiency goes up, and the half-life of the thiocyanate transient in the bulk increases. This suggests that the factor determining the partition of the radical species to redox or substitution products, either in the caged pair or in the bulk, is the rate of substitution of the strongest field ligands (am(m)ine ligands) in the Co(II) fragment. The more rapidly they are completely solvated, the more back electron transfer is disfavoured and overall redox dominates over photosubstitution.

Table 4.3 Photoredox yields and $(NCS)_2^{-\cdot}$ transient decay kinetics for Co(III)-am(m)ine-isothiocyanato analogues.

Complexes	$\emptyset(Co^{2+})^a$	$\emptyset((NCS)_2^{-\cdot})^a$	$\frac{\emptyset((NCS)_2^{-\cdot})}{\emptyset(Co^{2+})}$	$t_{1/2}$, μs^b
cis-$[Co(NCS)_2(NH_3)_4]^+$	0.153[c]	0.32	2.1	8
cis-$[Co(NCS)_2(en)_2]^+$	0.026[c]	0.067	2.6	23
$Co(tacn)(NCS)_3$	0.0008	0.036	39	31

[a] in 1 M NCS^-/DMSO/H^+ solution; [b] $t_{1/2}$ is the first half-life of a second order decay in 1.82 M NCS^-/DMSO/H^+ solution; [c] no DMSO.

4.3.4 Radical Pair Scavenging by Thiocyanate

The data provides a clear distinction between the earlier kinetic and ion pair models of the photochemistry. For this system, no ion-pair will form for the neutral starting complex. The redox and substitution yields can be attributed to the mechanism given above, because it has already been shown in section 4.3.2 that even though the primary photoproduct B does form an ion pair, secondary photolysis does not occur. Therefore, the increase in yield with thiocyanate concentration arises from the kinetic scavenging of the radical pair intermediates by the thiocyanate, reaction (4.8). Notice here that these intermediates may be considerably more complicated than implied by reaction (4.5). Attention has been drawn to the complexity of the photochemistry with no added thiocyanate, and literature reports consistently refer to complicated stoichiometry, often indicative of oxidation of the am(m)ine ligands, etc. in these systems, as mentioned in Chapter 3. These radical pair species, represented misleadingly as $\{Co^{II},\cdot NCS\}$, may therefore involve oxidization of ligands other than thiocyanate, and perhaps even solvent. The added thiocyanate is believed to simplify matters by acting as electron donor to the various oxidizing species to form NCS· and lead to the less reactive $(NCS)_2^{-\cdot}$, thus reducing the photoredox complexity.

The above kinetic scheme allows an estimate of the radical pair yield and lifetime, for, applying a steady state analysis to the radical pair species:

$$\emptyset((NCS)_2^{-\cdot}) = \frac{a_0\,(a_1 + [NCS^-])}{a_2 + [NCS^-]} \qquad (4.13)$$

where, $a_0 = \emptyset_{RP}$, $a_1 = k_7/k_8$, $a_2 = (k_6 + k_7)/k_8$.

Fitting the data of Figure 4.4 to this equation gave a radical pair yield at infinite thiocyanate concentration of 0.29 ± 0.10, of similar magnitude to the tetraammine and bisethylenediamine isothiocyanato systems (Chapter 3). The rate constant ratios were k_7/k_8

$= 0.12 \pm 0.03$ and $(k_6 + k_7)/k_8 = 8.0 \pm 3.3$. If k_8 is about 10^{10} M^{-1} s^{-1} (the diffusion controlled rate constant estimated from Debye-Eigen equation 1.43), then a radical pair lifetime $1/(k_6 + k_7)$ of about 12 ps is obtained, again in good agreement with the values estimated similarly for the other systems (Table 4.4). The rate constants obtained based on this model are in descending order; $k_6 = a_2k_8 - k_7 = 7 \times 10^{10}$ $s^{-1} > k_8 = 10^{10}$ M^{-1} $s^{-1} > k_9 = 5 \times 10^9$ M^{-1} $s^{-1} > k_7 = a_1k_8 = 1 \times 10^9$ s^{-1}, and the values are reasonable for the unimolecular and bimolecular processes involved.

Table 4.4 Comparison of the radical pair quantum yield and lifetime obtained for Co(III)-am(m)ine-isothiocyanato analogues with *cis* NCS^- ligands from the kinetic model fit.

Complexes	$\emptyset_{RP}$	τ_{RP}, ps
cis-$[Co(NCS)_2(NH_3)_4]^+$	0.73 ± 0.17	12 ± 5
cis-$[Co(NCS)_2(en)_2]^+$	0.41 ± 0.24	6 ± 4
$Co(tacn)(NCS)_3$	0.29 ± 0.10	12 ± 6

The net mechanism for the photolysis of $Co(tacn)(NCS)_3$ complexes with and without added NCS^- anion is summarized in a schematic diagram, Figure 4.10.

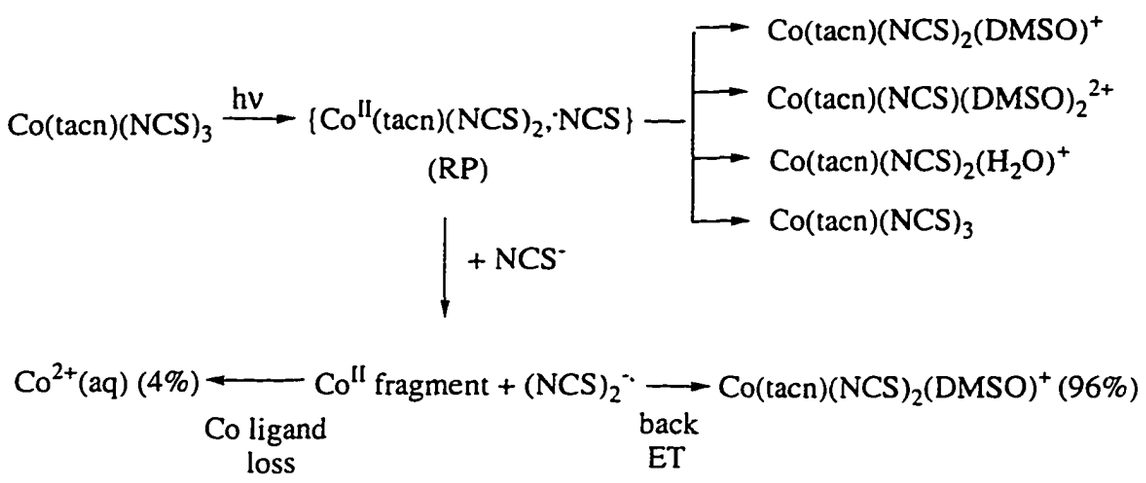

Figure 4.10 Mechanistic scheme of the photolysis of $Co(tacn)(NCS)_3$ with and without added NCS^-.

The similarity in behaviour, Table 4.4, for the charged and uncharged systems of am(m)ine isothiocyanato cobalt(III) complexes implies that thiocyanate scavenging processes are likely to be important in both. However, for the charged complexes, the ambiguities concerning ion-pair photolysis that prompted the present study partially remain.

4.4 Conclusions

(i) The photochemistry of $Co(tacn)(NCS)_3$ in thiocyanate free solution consists largely of photosubstitution processes with barely detectable redox reaction. Under these conditions reactions proceed via a profile of different radical pair species and give rise to a complicated mixture of products that results in part from complex solvolysis reactions which have been clarified by this study.

(ii) Added thiocyanate simplifies matters by scavenging radical pair species to form $(NCS)_2^{-\cdot}$ which then accepts back an electron from solvolysed cobalt(II) fragments to

cleanly give about 96% photosubstitution product, and enhances both redox and substitution products significantly. A lifetime for the radical pair species is estimated by kinetic modelling to be about 12 ps.

4.5 Final Remarks

The results obtained from Chapter 3 and Chapter 4 show that:

The small signal in the 425-475 nm region reported by Kirk and Langford[41] is proved to be the transient $(NCS)_2^{-\cdot}$ species, not radical pair. The radical pair continues to elude direct detection even at picosecond timescale.

Both photosubstitution and redox products result from radical pair mechanism. The ligand field excited state does not contribute significantly to the formation of products in these systems.

The reaction manner of Co(III) is more complicated than described in the equations from Adamson's radical pair model or the other models discussed here. The complexity, however, can be eliminated by the addition of thiocyanate anion. These new results provide a better understanding of the radical pair and its complexity and provide additional insights on the mechanism of the photoredox reactions of Co(III) complexes. The thiocyanate scavenging technique can also be used in the studies of other Co(III) am(m)ine systems, such as $[Co(NH_3)_5X]^{2+}$ (X can be halide or other acido anions).

Rapid loss of the stronger field ligands (i.e. am(m)ine ligand) from the Co(II) fragment tends to favor redox reaction over photosubstitution. This finding may help to design systems that selectively control the ratio of photoredox to photosubstitution reactions.

The kinetic model fit provides the estimated radical pair lifetime of ca. 10 ps, indicating that it is too short to be detected with the Concordia University picosecond laser

flash photolysis system (30 ps pulse). Therefore, it is necessary to use femtosecond laser flash system to observe the radical pair transient. Unfortunately, this has to be done elsewhere since the femtosecond system available here can only be used for the observation of transient emission, and not transient absorption spectra.

If further shift of the λ_{max} of a radical pair to the longer wavelength is needed, one can chose the cobalt amine complexes with ligands of even lower π^* energy than thiocyanate anion (e.g. halide anions Cl^-, Br^-, or I^-). The corresponding Co^{III} complex can be stabilized by introducing multidentate (e.g. tn) or macrocyclic ligand (e.g. [13]-aneN_4) instead of ammine ligand. For instance, compounds with macrocyclic and iodo ligands, such as $[Co([13]aneN_4)I_2]^+$, could be tried in a future search for the radical pair using a femtosecond laser system.

CHAPTER FIVE

SALT EFFECTS AND QUENCHING MECHANISMS OF THE EXCITED STATE TETRAKIS(μ-PYROPHOSPHITE-P,P')-DIPLATINATE(II) BY ACIDOPENTACYANOCOBALTATE(III) COMPLEXES

5.1 Introduction

Chapter 3 and 4 deal with the mechanism of photosubstitution and photoredox reactions of cobalt(III) complexes, and it was found that the substitution product was produced via redox (radical pair) mechanism. Earlier work, including from this laboratory, suggests that efficient photosubstitution in $[Co(CN)_5X]^{n-}$ (X = CN^-, N_3^-, Cl^-, Br^-, I^-, OH^- and H_2O) system takes place via the ligand field state ($^3T_{1g}$) and that anation by aqueous thiocyanate solution can occur producing N and S-bonded linkage isomers.[140] The study of competition of solvent substitution with anation and linkage isomer formation[141] showed evidence of specific cation catalysis by various alkali metal cations. It was found that this cation effect was interesting but hard to study with precision due to the experimental limitation associated with the chromatographic analysis of the aquation and anation products. A system was thus sought in which the physical aspects of specific cation catalysis could be better studied.

The famous platinum pop (usually denoted as $[Pt_2(pop)_4]^{4-}$) complex, $K_4[Pt_2(\mu\text{-}P_2O_5H_2)_4]$ and a series of pentacyanocobaltate(III) complexes $[Co(CN)_5X]^{3-}$ were chosen for a careful study of salt effects between the excited state and ground state reactants due to the following reasons:

(i) the triplet excited state of $[Pt_2(pop)_4]^{4-}$ has a lifetime of ~9 μs which is long enough to be conveniently measured using nitrogen laser system;

(ii) the reaction involves two highly charged anions, 4- and 3-, therefore the reaction rate should be very sensitive to changes in the ionic atmosphere of the solution;

(iii) there are a large number of simple cations available for studying the specific cation effects on the reactions between anions.

The significant salt effects observed as well as the reaction mechanisms involved will be reported in this Chapter.

5.2 Results

5.2.1 Characterization of the Complexes

5.2.1.1 Acidopentacyanocobaltate(III) Complexes, $[Co(CN)_5X]^{3-}$ (X = N_3, I, Br, Cl)

Elemental analysis was not applicable since these compounds form refractory nitrides and carbides when combusted and give irreproducible analytical results.[114,142,143] The identity and purity of the complexes were therefore established by HPLC (single peak with retention time of 6.5, 7.0, 8.0, and 12.1 min. for X = N_3, Cl, Br, and I respectively), electronic absorption spectra (Figure 5.1) as well as X-ray powder diffraction. The UV/Vis spectra were found to be in good agreement with literature data (Table 5.1). The stronger absorptions ($\varepsilon \geq 10^3$ M^{-1} cm^{-1}) in the near UV are due to charge transfer transitions (eg. X $\longrightarrow$ Co), and the weaker absorptions at longer wavelength (around 390 nm for azido, bromo, and chloro complexes, and 400_{sh} and 500 nm for iodo complex) are due to spin-allowed d-d transitions, $^1A_1 \longrightarrow {}^1E$, of the complexes.[144-146] X-ray powder diffraction results (Table 5.2) showed that each of the above complexes has a line pattern similar to potassium hexacyano cobaltate(III), $K_3[Co(CN)_6]$, and the samples were found to be free of potassium halide, which is highly distinguishable if present. The result for KCl salt is also included in Table 5.1 for comparison. Except for KCl, which is primitive cubic with a lattice constant of 310 pm, the patterns of the complexes were not indexed and the lattice constants were not calculated because of the lower symmetry of the complexes.

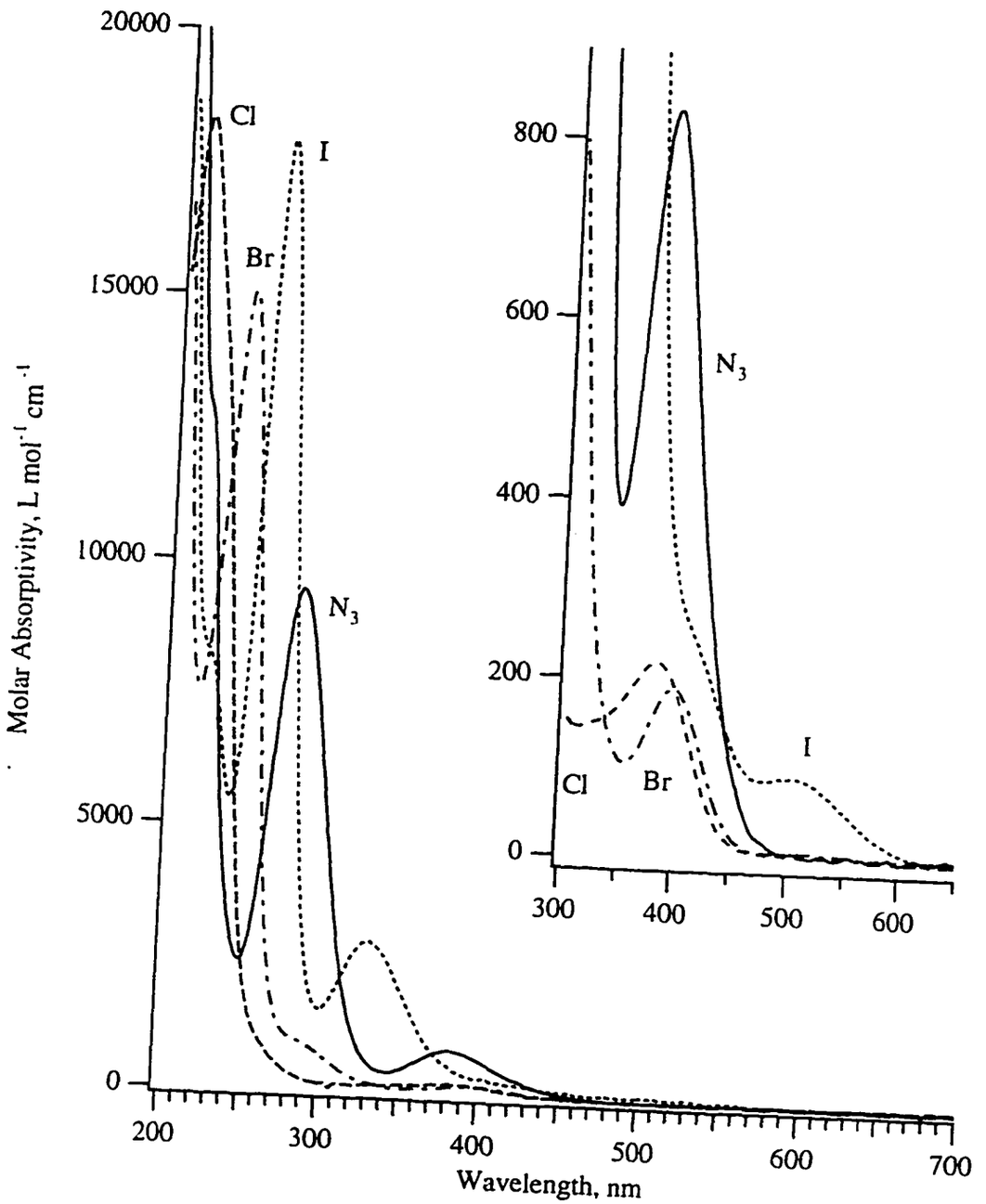

Figure 5.1 Electronic absorption spectra of $[Co(CN)_5X]^{3-}$ (X = N_3, I, Br, Cl) in aqueous solution.

Table 5.1 Electronic absorption spectra data λ_{max}, nm (ε) of $[Co(CN)_5X]^{3-}$ complexes in aqueous solution at room temperature.

X	this work	Ref.[144]	Ref.[103]	Ref.[114]
N_3	220_{sh} (1.23×10^4)		220_{sh} (1.08×10^4)	
	281 (9.48×10^3)		280 (8.36×10^3)	
	382 (824)		380 (749)	380 (600)
I	223_{sh} (8.27×10^3)			
	262 (1.79×10^4)	260 (1.75×10^4)		
	331 (2.85×10^3)	330 (2.95×10^3)	334 (2.93×10^3)	
	408_{sh} (2.67×10^2)	~440_{sh} (~200)	408 (255)	440_{sh} (200)
	500 (93)	500 (95)	500 (107)	
Br	242 (1.71×10^4)	242 (1.32×10^4)		
	290_{sh} (1.02×10^3)	295 (822)		
	397 (190)	395 (170)	398 (172)	398 (177)
Cl	210 (1.83×10^4)	224 (1.61×10^4)		
	384 (215)	392 (200)	390 (201)	390 (200)

Table 5.2 X-ray powder diffraction results for $K_3[Co(CN)_5X]$ complexes (X = Cl, Br, I, N_3, CN) and KCl salt (for comparison).

Compounds	4θ (°)[a]
$K_3[Co(CN)_6]$	43.3, 44.6, 58.5, 61.2, 68.5, 88.5, 97.8
$K_3[Co(CN)_5Cl]$	44.0, 44.4, 59.0, 61.5, 68.9
$K_3[Co(CN)_5Br]$	43.9, 44.6, 58.5, 61.2, 68.1, 97.0
$K_3[Co(CN)_5I]$	42.9, 43.2, 53.1, 60.8, 62.7
$K_3[Co(CN)_5N_3]$	39.0, 41.0, 43.9, 58.1, 64.2, 66.8, 75.2, 85.0
KCl	56.9, 81.0, 100.5, 117.0, 133.0, 147.8
(hkl)[b]	(100), (110), (111), (200), (210), (211)

[a] Cu-Kα, λ = 1.542 Å, [b] Miller index.

5.2.1.2 Potassium Tetrakis(μ-pyrophosphite-P,P')-diplatinate(II) Dihydrate Complex, $K_4[Pt_2(\mu\text{-}P_2O_5H_2)_4]\cdot 2H_2O$

The electronic absorption spectrum of $[Pt_2(pop)_4]^{4-}$ complex in aqueous solution is shown in Figure 5.2. λ_{max}, nm (ε, M^{-1} cm^{-1}): 245 (3.1×10^3), 271 (1.5×10^3), 304_{sh} (1.0×10^3), 368 (3.4×10^4), 453 (115), which is in good agreement with literature data of 244, 270 (1.4×10^3), 303 (8.5×10^2), 368 (3.5×10^4), 452 (1.2×10^2).[147] These absorption bands have been assigned as 5d ⟶ $6p_z$ transitions (271 and 244 nm bands), d ⟶ d transition (303 nm), fully allowed $^1A_{1g}$ ⟶ $^1A_{2u}$ transition (368 nm), and spin-forbidden $^1A_{1g}$ ⟶ $^3A_{2u}$ transition (450 nm).[148-150] Excitation of a room temperature aqueous solution at 330, 370, or 452 nm results in an intense green emission at 514 nm,

which originates from the $^3A_{2u}$ excited state,[149,151] and is rather long-lived (lifetime $\tau \geq 9$ μs in aqueous solution at 22.0 °C). ^{31}P NMR: δ 68.9 ppm, $^1J(^{31}P\text{-}^{195}Pt) = 3076$ Hz. The ^{195}Pt NMR of the prepared compound confirmed this value of the $^{31}P\text{-}^{195}Pt$ coupling constant.

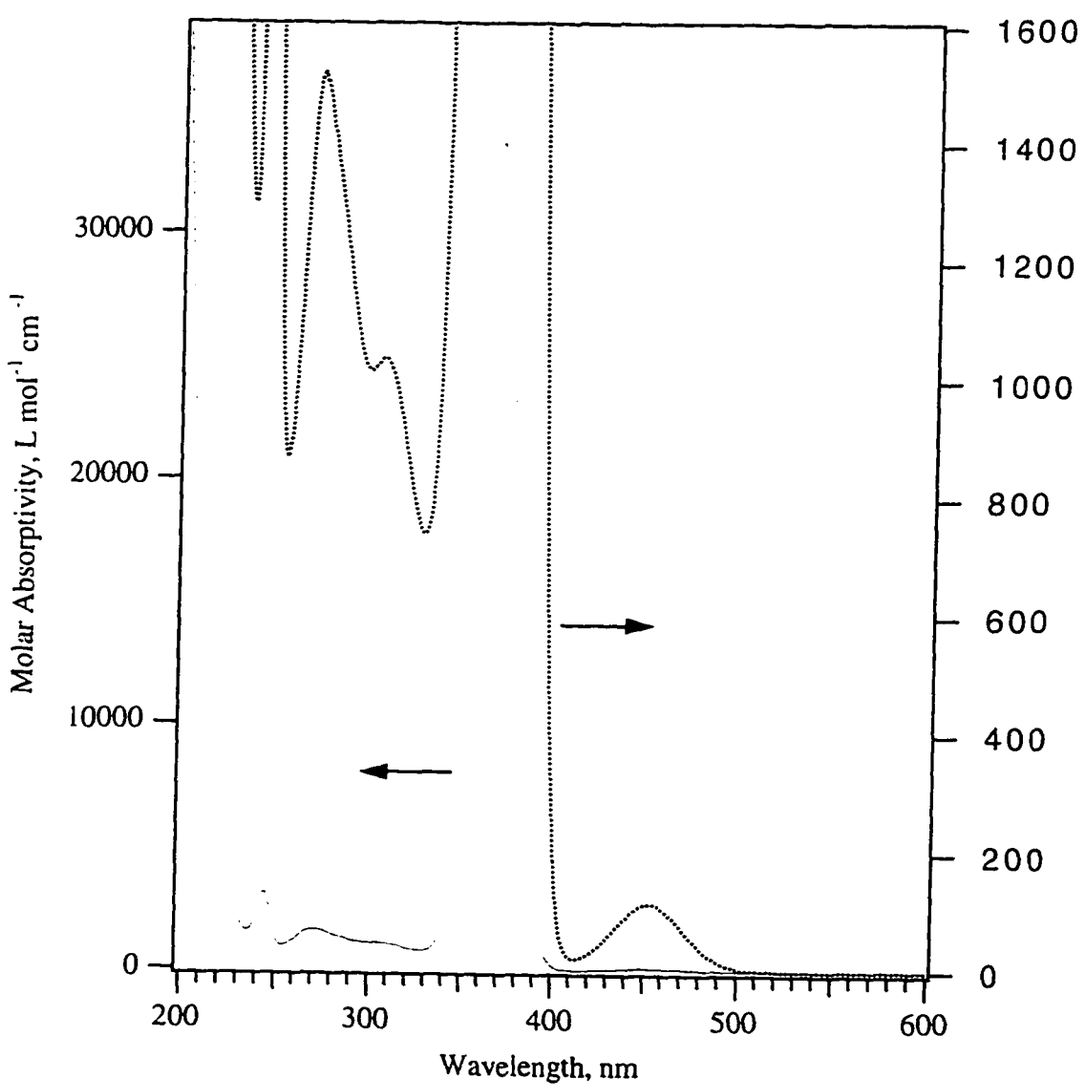

Figure 5.2 Electronic absorption spectra of $[Pt_2(pop)_4]^{4-}$ in aqueous solution.

5.2.2 Redox Potential of $K_3[Co(CN)_5X]$ (X = I, N_3, Br, Cl, CN) Complexes in Aqueous Acidic Solution

The results of differential pulse polarography of the cobalt complexes $K_3[Co(CN)_5X]$ are shown in Figure 5.3(a). Except for CN, each complex shows two unsymmetrical peaks. This indicates that the complexes were reduced irreversibly in two steps. Similar literature studies of pentacyanocobaltate(III) complexes at the dropping mercury electrode[152,153] concluded that these reductions occur irreversibly by the processes: $[Co^{III}(CN)_5X]^{3-} + e^- \longrightarrow [Co^{II}(CN)_5X]^{2-}$, and $[Co^{II}(CN)_5X]^{2-} + e^- \longrightarrow Co^{I}$ (complex).

In order to obtain the $E_{1/2}$ values of these irreversible reductions, the normal polarograms, Figure 5.3(b), were generated by numerically integrating (trapezoidal) the differential pulse curves using Igor program.

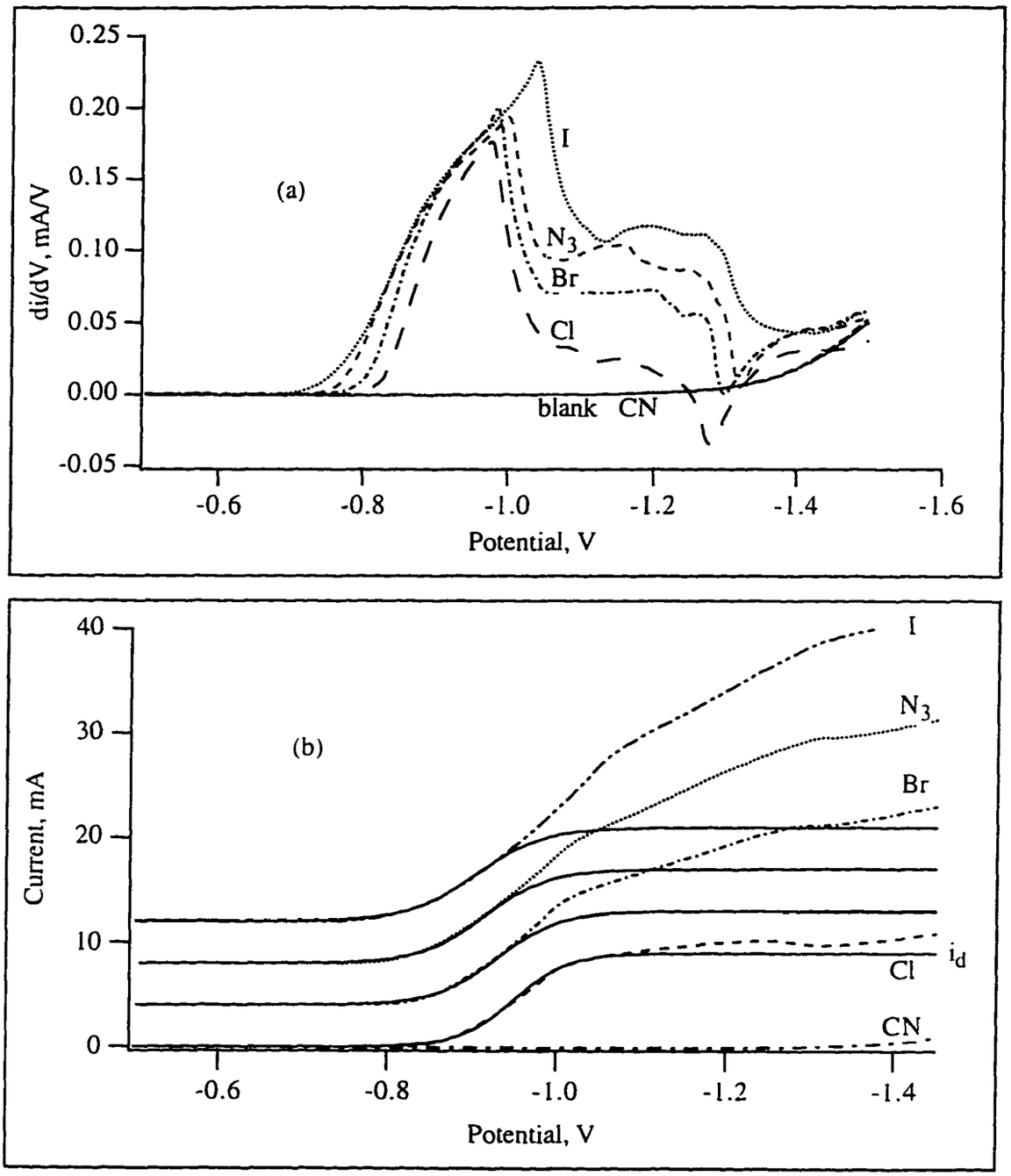

Figure 5.3 Polarography of 5.0×10^{-4} M $K_3[Co(CN)_5X]$ (X = I, N_3, Br, Cl, CN) in 0.10 M KNO_3 and 0.010 M $HClO_4$ aqueous solution. (a) Differential pulse polarography, and (b) Normal polarography generated from (a) by integration, and computer fittings.
I, N_3, Br waves are offset vertically by 12, 8, 4 mA respectively.

Due to the fact that in an irreversible wave the current does not rise steeply as for a reversible process, and to avoid partial inclusion of the second reduction step, only the front portions of the normal polarogram curves were used for computer fitting to eq. 2.9. All $[Co(CN)_5X]^{3-}$ complexes are of the same electrolyte type, undergo the same type of electron reduction process, and the waves were measured at the same complex concentration using the same instrument at the same temperature. These complexes should therefore have very similar values for the diffusion current (i_d) (see eq. 2.10) for the first reduction step. Both Figure 5.3(a) and (b) suggest that the reduction of the $[Co(CN)_5Cl]^{3-}$ complex is less complicated than other analogues in that a second reduction step does not interfere with the first one. Therefore the i_d value was taken from the fittings of the first wave of the $[Co(CN)_5Cl]^{3-}$ complex, and computer fits using eq. 2.9 with this i_d value were performed on the first waves of the acidopentacyanocobalt complexes (see Figure 5.3(b)). The $E_{1/2}$ values and corresponding transfer coefficient α were thus estimated for $[Co(CN)_5I]^{3-}$, $[Co(CN)_5N_3]^{3-}$, $[Co(CN)_5Br]^{3-}$, and $[Co(CN)_5Cl]^{3-}$ complexes respectively, as summarized in Table 5.3. The cyano complex is very stable and could not be reduced before the onset of water reduction, which is consistent with literature findings.[153]

Table 5.3 The estimated half-wave potentials $E_{1/2}$ and the transfer coefficient α of 5.0×10^{-4} M $[Co(CN)_5X]^{3-}$ complexes (X = I, N_3, Br, Cl) in 0.10 M KNO_3/0.010 M $HClO_4$ aqueous solution at room temperature.

X	$E_{1/2}$, V vs Ag/AgCl	$E_{1/2}$, V vs SCE	$E_{1/2}$, V vs NHE	α	$E_{1/2}$, V vs SCE[153]
I	-0.90	-0.92	-0.68	0.65	-0.71
N_3	-0.91	-0.93	-0.69	0.68	-1.37[a]
Br	-0.93	-0.95	-0.71	0.70	-0.71
Cl	-0.95	-0.97	-0.73	0.80	-0.86

[a] For $2e^-$ reduction process, Co^{III} to Co^{I}.

The $E_{1/2}$ values obtained here have more negative values than Makis' results,[153] where 3 M of KCl was used as supporting electrolyte and Tween-80 was used as a maximum suppressor. This is consistent with literature observations that the presence of maximum suppressor (which is necessary for normal polarography but can be avoided in more accurate differential pulse polarographic techniques) and the higher concentration of electrolyte would both shift the $E_{1/2}$ towards a more positive direction.[153,154]

The $E_{1/2}$ values decrease in the order $[Co(CN)_5I]^{3-} > [Co(CN)_5Br]^{3-} > [Co(CN)_5Cl]^{3-} >> [Co(CN)_6]^{3-}$, a sequence that can be explained by ligand field theory. When Co(III) (d^6) is reduced to Co(II) (d^7), the electron accepted will occupy the anti bonding orbital e_{2g}. The ligand field strength, Δ, of the ligand lies in the sequence CN » Cl > Br > I (section 1.1.1),[15] which can be related to the stability of the electron in the e_g orbital, that is; CN « Cl < Br < I. The $[Co(CN)_6]^{3-}$ complex should therefore be a very weak oxidant and the oxidizing ability should increase from chloro to bromo to iodo complex. When compared to $E([Pt_2(pop)_4]^{3-}/^*[Pt_2(pop)_4]^{4-}) < -1.5$ V vs SCE in H_2O,[155]

it is obvious that the cobalt complexes (except the cyano complex) are all thermodynamically able to oxidatively quench the excited state $*[Pt_2(pop)_4]^{4-}$.

5.2.3 Quenching Rate Constants

In a thoroughly deaerated aqueous solution with no quencher, $[Pt_2(pop)_4]^{4-}$ has a lifetime of 9.7 μs in pure water, which is in good agreement with the literature.[148,156,157] The lifetime was shortened to 8-9 μs in acidic media, but no effect was observed on addition of Cl^- within the experimental error of ± 0.1 μs in the lifetime measurement. No self-quenching of phosphorescence was observed under these experimental conditions, where $A_{370} \approx 1$ and $[Pt_2(pop)_4^{4-}] \approx 3 \times 10^{-5}$ M. This is consistent with the report by Kalyanasundaram[158] that no self-quenching occurs up to a $[Pt_2(pop)_4]^{4-}$ concentration of 10^{-4} M (i.e. $A_{370} = 3.4$). Buffer solution was not introduced due to the reported decomposition of $[Pt_2(pop)_4]^{4-}$ in pH 7 buffer.[159] Instead, the quenching study was performed in a 0.010 M $HClO_4$ medium to ensure that more than 90% of platinum-pop exists as undissociated (or protonated) 4- anion (pK_a values, $pK_{a1} = 3.0$, $pK_{a2} = 8.0$, for $[Pt_2(pop)_4]^{4-}$ have been reported).[156]

$$[Pt_2(P_2O_5H_2)_4]^{4-} \rightleftharpoons [Pt_2(P_2O_5H_2)_3(P_2O_5H)]^{5-} + H^+ \qquad K_{a1}$$

$$[Pt_2(P_2O_5H_2)_3(P_2O_5H)]^{5-} \rightleftharpoons [\,Pt_2(P_2O_5H_2)_2(P_2O_5H)_2]^{6-} + H^+ \qquad K_{a2}$$

The kinetics of the reaction have been analyzed quantitatively to study: (i) the ionic strength effect in the presence of potassium cation (KCl) at various concentrations, (ii) the anion effect and the Olson-Simonson effect when potassium salts of various anions with different charge types, such as KCl, KBr, KNO_3, K_2SO_4, and $K_3[Co(CN)_6]$ are present, (iii) the specific cation effects when 0.500 M cation solutions of MCl, $M'Cl_2$, or $R_nNH_{4-n}Cl$ are present (M = Li^+, Na^+, K^+, Cs^+; M' = Mg^{2+}, Ca^{2+}, Sr^{2+}, Ba^{2+}; R = H, Me, Et, n-Pr; n = 0-3).

According to the Stern-Volmer (SV) equation (eq. 1.10, see Introduction 1.2.1), the quenching rate constant k_q can be calculated from the slope of SV plot (i.e. τ^0/τ vs quencher concentration [Q], see Figures 5.4 for a typical SV-plot) divided by the initial lifetime τ^0. The values of the log of the quenching rate constant, log k_q, for each of the cobalt complexes in the presence of each cation, are listed in Tables 5.4-5.7.

The second-order rate constants for quenching the excited state $[Pt_2(pop)_4]^{4-}$ by the cobalt complexes are found to be in the range 10^7 to 10^9 M^{-1} s^{-1} at a 0.500 M cation concentration. These constants decrease across the complex series; $[Co(CN)_5I]^{3-}$ > $[Co(CN)_5N_3]^{3-}$ > $[Co(CN)_5Br]^{3-}$ > $[Co(CN)_5Cl]^{3-}$. The hexacyanocobaltate $[Co(CN)_6]^{3-}$ had no quenching effect in combination with any of the cations.

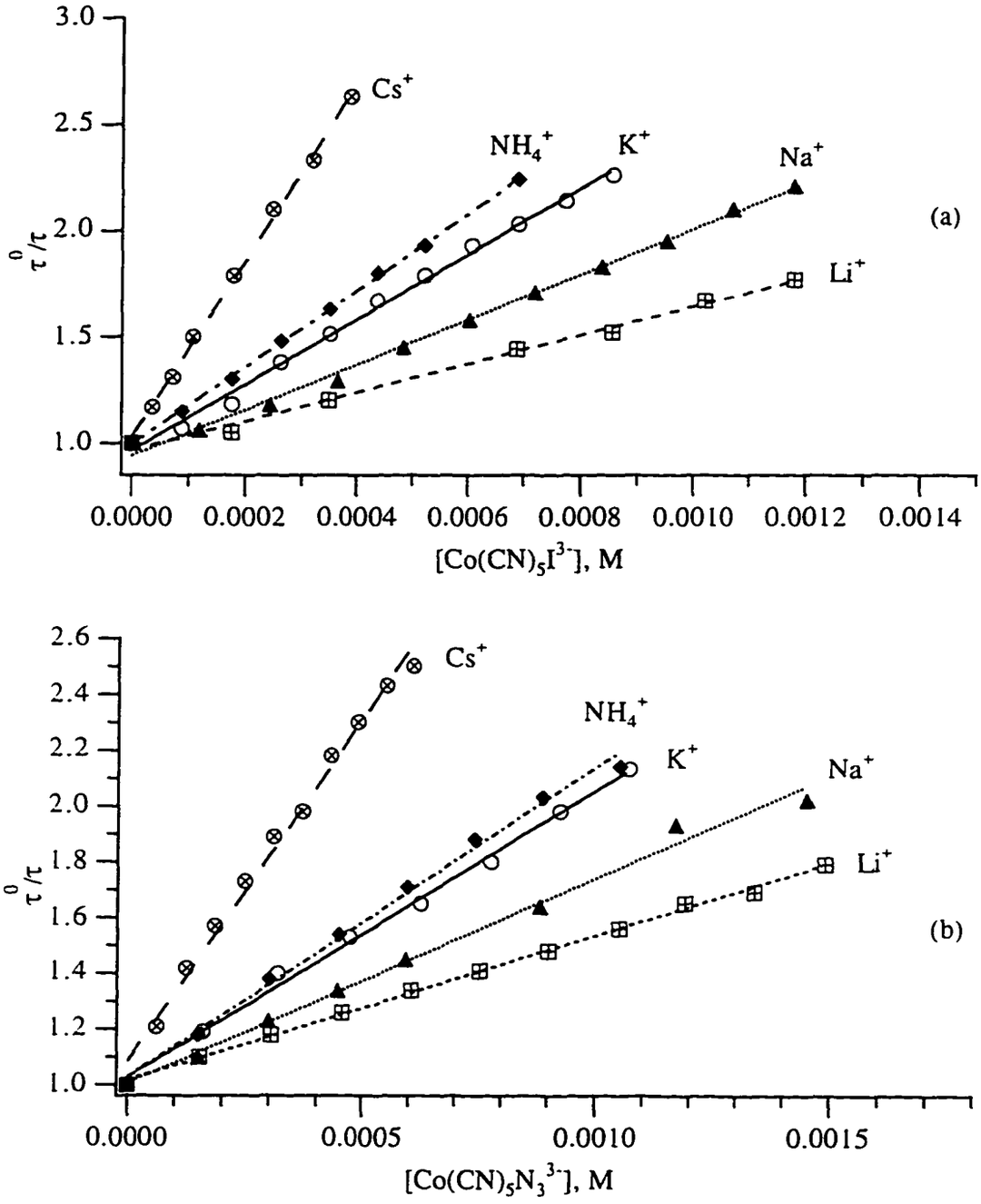

Figure 5.4 Stern-Volmer plot of $*[Pt_2(pop)_4]^{4-}$ with $[Co(CN)_5X]^{3-}$ (X = I, N_3) in 0.5 M MCl (M = Li^+, Na^+, K^+, NH_4^+, Cs^+) and 0.01 M $HClO_4$ aqueous solution. (a) X = I, (b) X = N_3.
Markers, experimental points; Lines, fits to the Stern-Volmer equation 1.10.

Table 5.4 log k_q at 22 °C for quenching of photo-excited $*[Pt_2(pop)_4]^{4-}$ by $[Co(CN)_5I]^{3-}$ at various concentrations of KCl, in 0.010 M $HClO_4$ aqueous solution.

[KCl], M	$\mu^{1/2}$, $M^{1/2}$	log k_q	[KCl], M	$\mu^{1/2}$, $M^{1/2}$	log k_q
0.10	0.33	7.72±0.02	0.50	0.71	8.33±0.03
0.15	0.40	7.79±0.05	0.60	0.78	8.47±0.01
0.20	0.46	8.04±0.01	0.80	0.90	8.61±0.01
0.30	0.56	8.12±0.01	-	-	-

Table 5.5 log k_q at 22 °C for the quenching of the excited state $*[Pt_2(pop)_4]^{4-}$ by $[Co(CN)_5I]^{3-}$ with different electrolytes in 0.010 M $HClO_4$ aqueous solution.

Electrolytes	$[K^+]$, M	μ, M	log k_q
KCl	0.50	0.51	8.33±0.03
KBr	0.50	0.51	8.60±0.01
KNO_3[a]	0.50	0.51	8.30±0.02
K_2SO_4	0.50	0.76	8.28±0.01
$K_3[Co(CN)_6]$	0.50	1.01	8.36±0.01

[a] KNO_3 itself quenches $*[Pt_2(pop)_4]^{4-}$, log k_q = 5.9 at 22 °C.

Table 5.6 log k_q at 22 °C for quenching of photo-excited $*[Pt_2(pop)_4]^{4-}$ with $[Co(CN)_5X]^{3-}$ (X = N_3, I, Br) in the presence of 0.500 M MCl (M = Li^+, Na^+, K^+, NH_4^+, Cs^+) and 0.010 M $HClO_4$ aqueous solution.

X \ M	Li^+	Na^+	K^+	NH_4^+	Cs^+
I	7.91±0.01	8.10±0.01	8.33±0.03	8.35±0.01	8.70±0.01
N_3	7.73±0.06	7.91±0.03	8.10[a]	8.13±0.04	8.46[a]
Br	7.39±0.02	7.59±0.01	8.02±0.03	7.99±0.02	8.41±0.04
Cl	6.8±0.2	7.12±0.12	7.48±0.05	-	7.84±0.01

[a] Two coincident measurements. The rest are based on 3-5 measurements.

Table 5.7 Effect of cations on log k_q at 22 °C for the quenching of photo-excited $*[Pt_2(pop)_4]^{4-}$ with $[Co(CN)_5I]^{3-}$ in the presence of 0.500 M $M'Cl_2$, $R_nNH_{4-n}Cl$ ($M' = Mg^{2+}$, Ca^{2+}, Sr^{2+}, Ba^{2+}. R = H, Me, Et. n = 0-3) in 0.010 M $HClO_4$ aqueous solution.

M'	log k_q	$R_nNH_{4-n}^+$	log k_q	$R_nNH_{4-n}^+$	log k_q
Mg^{2+}	8.26 ± 0.01	NH_4^+	8.35 ± 0.01	$EtNH_3^+$	8.33[a]
Ca^{2+}	8.38 ± 0.01	$MeNH_3^+$	8.43 ± 0.01	$Et_2NH_2^+$	8.31[a]
Sr^{2+}	8.49 ± 0.01	$Me_2NH_2^+$	8.51 ± 0.02	Et_3NH^+	8.19 ± 0.01
Ba^{2+}	8.56 ± 0.01	Me_3NH^+	8.54[a]	$n\text{-}PrNH_3^+$	8.29 ± 0.02

[a] Two coincident measurements. The rest are based on 3-5 measurements.

The effect of ionic strength on the quenching rate constant was studied using $[Co(CN)_5I]^{3-}$ in KCl solutions with the results shown in Table 5.4 (Figure 5.5). Quenching efficiency increased with an increase in ionic strength, μ, as expected for two species having like charge. For comparisions with theory, the diffusion controlled rate constants k_d, k_{-d} and ion pair constant K_{eq} between the reactants $*[Pt_2(pop)_4]^{4-}$ and $[Co(CN)_5I]^{3-}$ in KCl/H^+ media were calculated according to the Debye-Eigen (DE) equation (see section 1.4.1.1) and are listed in Table 5.8. Parameters used for the calculation of k_d, k_{-d} and K_{eq} were as used earlier in section 1.4.1.1 except as follows: radii of the reactants and the main counter ion $r_A = r_{[Pt_2(pop)_4]^{4-}} = 0.43$ nm, $r_Q = r_{Co\text{-}I} =$ 0.47 nm, $r_{K^+} = 0.13$ nm, and temperature T = 295 K. The radii of $[Pt_2(pop)_4]^{4-}$ and $[Co(CN)_5I]^{3-}$ ions were obtained from $r = 0.5(d_x d_y d_z)^{1/3}$, where d_x, d_y, d_z are the dimensions measured along the three molecular axes of space filling models generated by Chem-3D . DE equations were numerically integrated over a range going from $r = a = r_A + r_Q$ to 30a with increments of 0.0145a, at which $(\exp[W(r, \mu)/k_BT]-1) < 1 \times 10^{-10}$. The effect of variation in the cation radius on the calculation of diffusion-controlled rate constants is very small and can be neglected in comparision to the observed specific cation effects. For example, the difference of calculated k_d is only 2% when the counter ion is Cs^+ or K^+ whereas the experimental quenching rate constant k_q in Cs^+ is 2.3 times that in K^+. A similar phenomenon was also observed in literature.[43,45]

Table 5.8 Ionic strength effect on the experimental quenching rate constant k_q, calculated diffusion controlled rate constants k_d, k_{-d} and ion pair constant K_{eq} of the reaction between $*[Pt_2(pop)_4]^{4-}$ and $[Co(CN)_5I]^{3-}$ in KCl/0.010 M $HClO_4$ aqueous solution.

μ, M	k_q, M^{-1} s^{-1}	k_d, M^{-1} s^{-1} [a]	k_{-d}, s^{-1} [b]	K_{eq} [c]
0.11	5.25×10^7	7.6×10^8	2.6×10^{10}	0.03
0.16	6.17×10^7	1.2×10^9	2.3×10^{10}	0.05
0.21	1.10×10^8	1.7×10^9	2.1×10^{10}	0.08
0.31	1.32×10^8	2.5×10^9	1.8×10^{10}	0.14
0.51	2.14×10^8	3.7×10^9	1.4×10^{10}	0.27
0.61	2.95×10^8	4.1×10^9	1.2×10^{10}	0.34
0.81	4.07×10^8	4.7×10^9	1.0×10^{10}	0.47

[a] calculated form eauation 1.43, [b] calculated from equation 1.48, [c] from equation 1.49. See sections 1.4.1.1 and 5.2.3 for the theory and parameters used in the calculations.

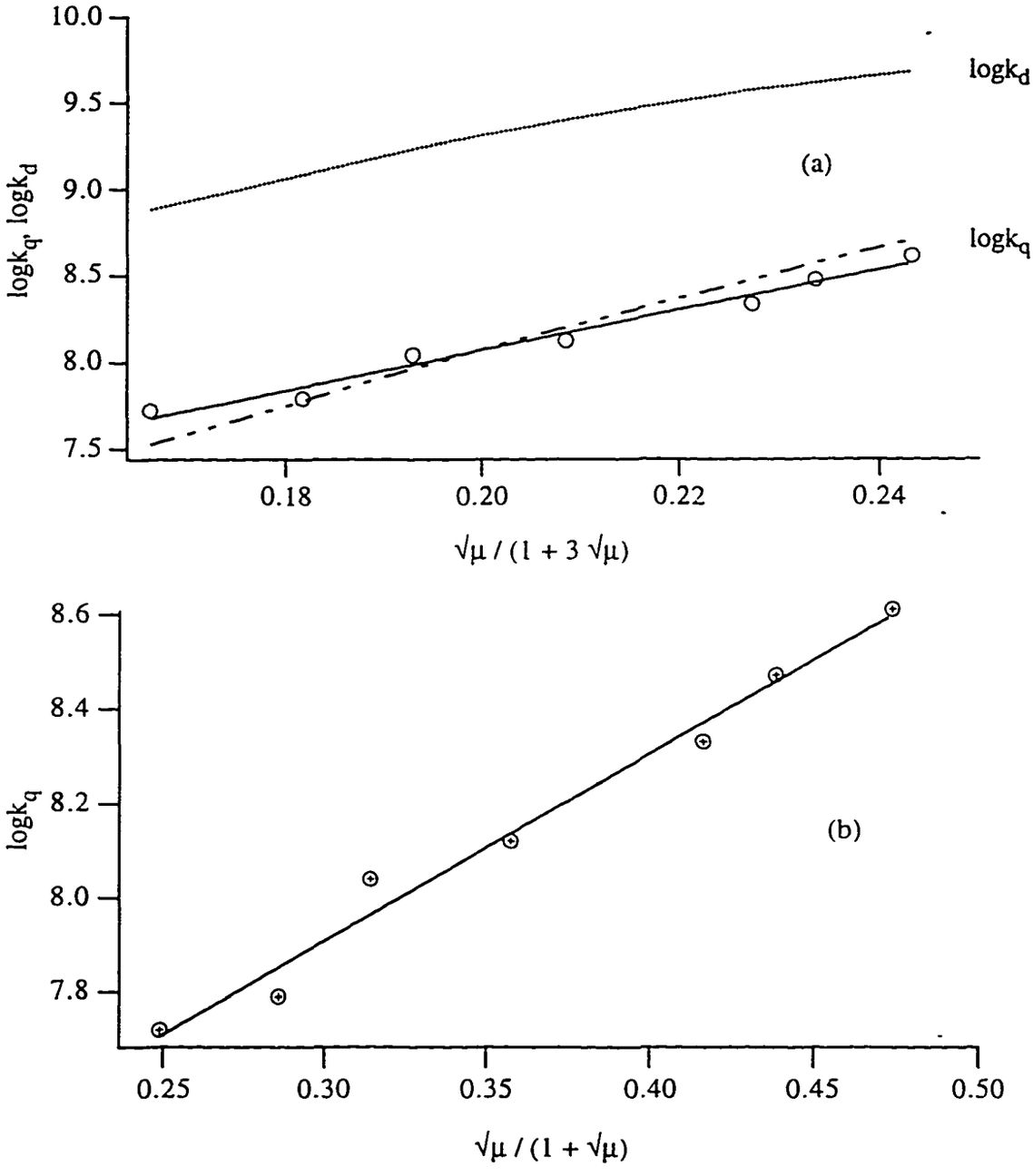

Figure 5.5 Correlation of log k_q and log k_d to the ionic strength for the quenching of $*[Pt_2(pop)_4]^{4-}$ by $[Co(CN)_5I]^{3-}$ in various concentrations of KCl in 0.010 M $HClO_4$ aqueous solution.

Markers, experimental points. Lines: (a) Dotted line, calculated log k_d values using eq. 1.43; Dashed line, log k_q fit using eq. 1.42 and DE eqs. 1.43, 1.48 with $k_t = 1.2 \times 10^9$ s^{-1}; Solid line, log k_q fit using DHB eq. 1.56. (b) log k_q fit using Debye-Hückel eq. 1.57.

The Olson-Simonson effect and the anion effect were tested at 0.5 M cation concentration by comparing the results in 0.50 M KNO_3 or KBr, 0.25 M K_2SO_4, and 0.167 M $K_3[Co(CN)_6]$ electrolytes. The results are shown in Table 5.5.

Specific cation effects were observed in the quenching rate constants such that $Li^+ < Na^+ < K^+ < Cs^+$, and $Mg^{2+} < Ca^{2+} < Sr^{2+} < Ba^{2+}$, as shown in Tables 5.6-5.7. For the series of alkaline and alkaline earth metal cations, the logarithm of the rate constants was linear either with the crystal radius of the cation, r_C,[124] the cation-water distance (d_{M-O}),[160] or the polarizability (α) of the cation (Tables 5.9-5.10, Figures 5.6(a)-(c)).[161-163] Poor linear correlation was found, however, for log k_q vs the reciprocal of either the Stokes radius, r_S,[164] or the hydrated radius of the cation, r_h (Figures 5.6(d)-(e)).[164]

Table 5.9 Various radii (nm) for alkali (M^+) and alkaline earth (M^{2+}) cations.

Cations	r_C [a]	d_{M-O} [b]	r_S [c]	r_h [d]
Li^+	0.068	0.208	0.238	0.382
Na^+	0.097	0.2356	0.184	0.358
K^+	0.133	0.2798	0.125	0.331
Cs^+	0.167	0.3139	0.119	0.329
Mg^{2+}	0.066	0.209	0.347	0.428
Ca^{2+}	0.099	0.242	0.309	0.412
Sr^{2+}	0.112	0.26	0.309	0.421
Ba^{2+}	0.134	0.29	0.288	0.404

[a] r_C, the cation crystal radii, ref. [124]; [b] d_{M-O}, the cation-water distance, ref. [160]; [c] r_S, the Stokes radii, ref. [164-166]; [d] r_h, the hydrated radii, ref. [164]

Table 5.10 Polarizability (α, cm^3/mol) of alkali (M^+), alkaline-earth (M^{2+}), and alkylammonium $R_nNH_{4-n}^+$ cations.

Cations	α [161]	α [163]	$R_nH_{4-n}N^+$	α [167]
Li^+	3.0×10^{-26}	2.8×10^{-26}	NH_4^+	2.26×10^{-24}
Na^+	1.9×10^{-25}	1.5×10^{-25}	$MeNH_3^+$	3.99×10^{-24}
K^+	8.9×10^{-25}	7.9×10^{-25}	$Me_2NH_2^+$	5.74×10^{-24}
Cs^+	2.6×10^{-24}	2.26×10^{-24}	Me_3NH^+	7.47×10^{-24}
Mg^{2+}	1.0×10^{-25}	7.2×10^{-26}	$EtNH_3^+$	5.79×10^{-24}
Ca^{2+}	5.5×10^{-25}	4.7×10^{-25}	$Et_2NH_2^+$	9.36×10^{-24}
Sr^{2+}	1.02×10^{-24}	7.7×10^{-25}	Et_3NH^+	1.28×10^{-23}
Ba^{2+}	1.86×10^{-24}	1.5×10^{-24}	$n\text{-}PrNH_3^+$	7.62×10^{-24}

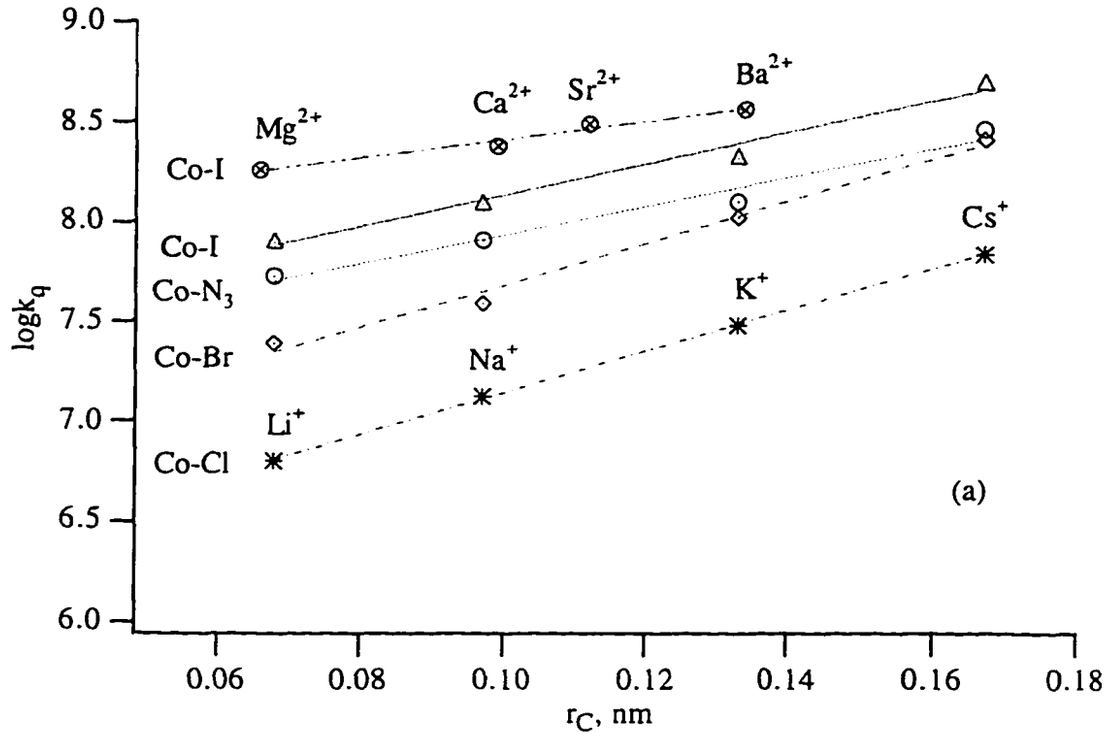
9.0
8.5
8.0
7.5
7.0
6.5
6.0
logk$_q$
Mg^{2+}
Ca^{2+}
Sr^{2+}
Ba^{2+}
Co-I
Co-I
Co-N$_3$
Co-Br
Co-Cl
Li$^+$
Na$^+$
K$^+$
Cs$^+$
(a)
0.06
0.08
0.10
0.12
0.14
0.16
0.18
r$_C$, nm

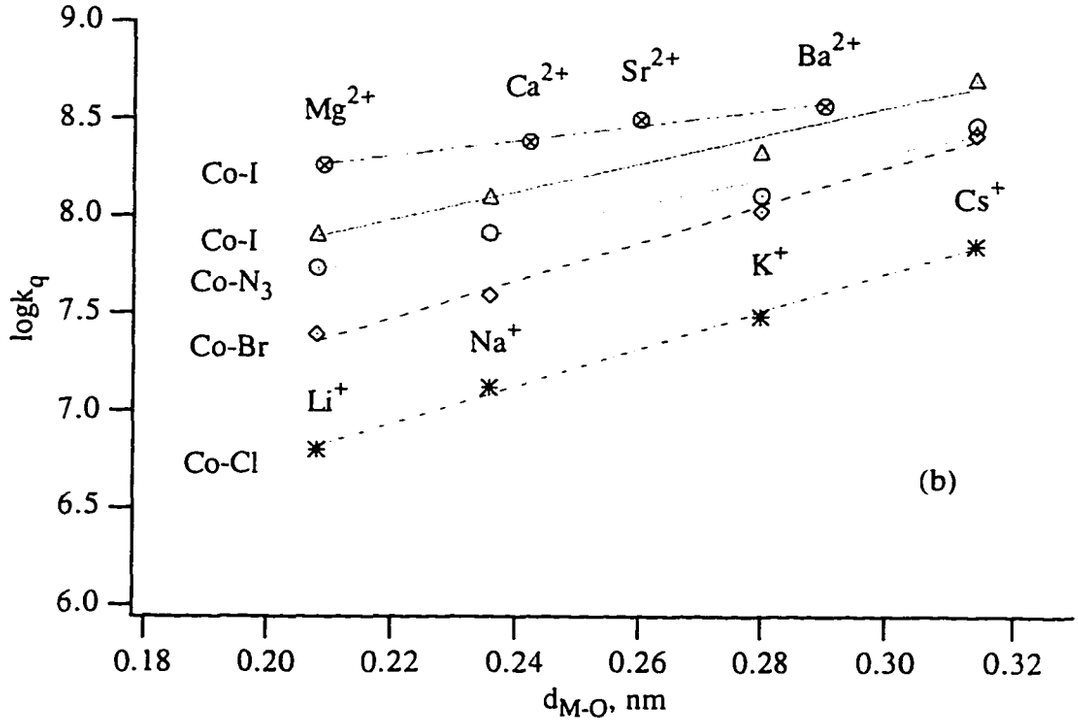
9.0
8.5
8.0
7.5
7.0
6.5
6.0
logk$_q$
Mg^{2+}
Ca^{2+}
Sr^{2+}
Ba^{2+}
Co-I
Co-I
Co-N$_3$
Co-Br
Co-Cl
Li$^+$
Na$^+$
K$^+$
Cs$^+$
(b)
0.18
0.20
0.22
0.24
0.26
0.28
0.30
0.32
d$_{M-O}$, nm

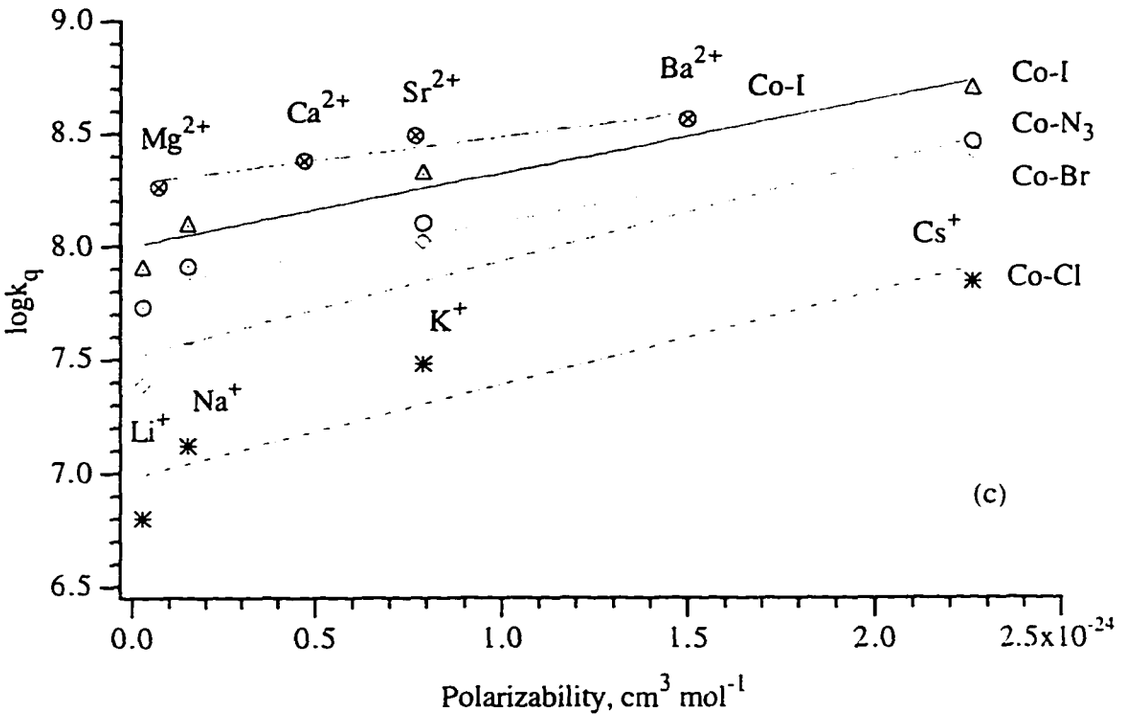
9.0
8.5
8.0
7.5
7.0
6.5
logk_q
0.0
0.5
1.0
1.5
2.0
2.5x10^-24
Polarizability, cm^3 mol^-1
Mg2+
Ca2+
Sr2+
Ba2+
Co-I
Co-I
Co-N3
Co-Br
Co-Cl
Cs+
K+
Na+
Li+
(c)

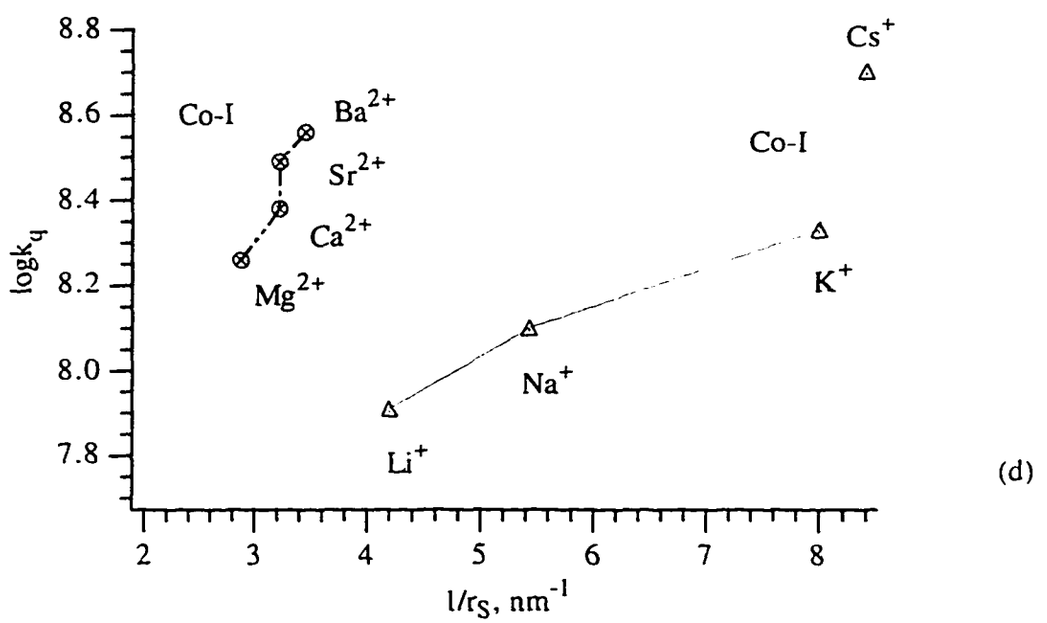
8.8
8.6
8.4
8.2
8.0
7.8
logk_q
2
3
4
5
6
7
8
l/r_S, nm^-1
Co-I
Ba2+
Sr2+
Ca2+
Mg2+
Co-I
Cs+
K+
Na+
Li+
(d)

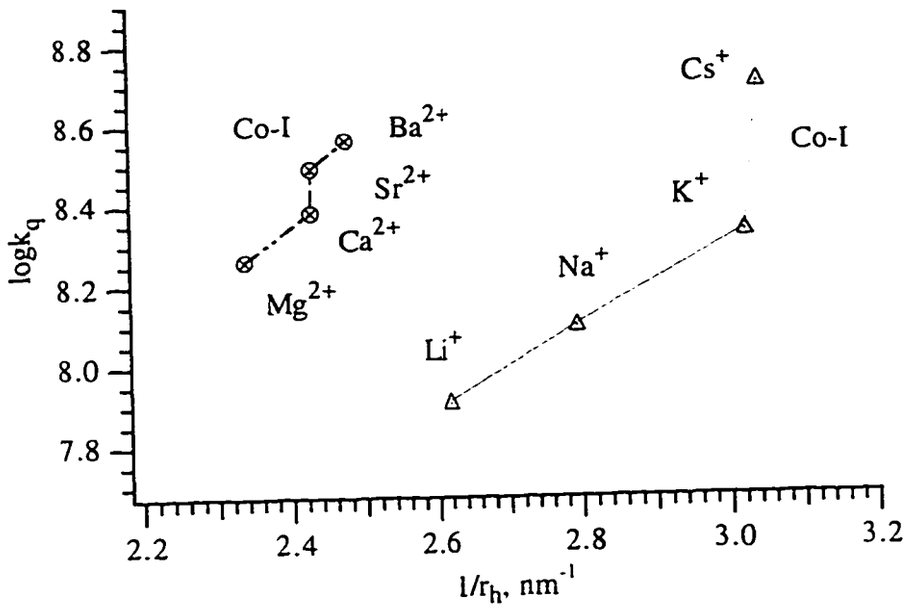

(e)

Figure 5.6 Specific cation effects on log k_q for $*[Pt_2(pop)_4]^{4-}$ / $[Co(CN)_5I]^{3-}$ in the presence of 0.50 M cation concentration of MCl or $M'Cl_2$ ($M = Li^+, Na^+, K^+, Cs^+$. $M' = Mg^{2+}, Ca^{2+}, Sr^{2+}, Ba^{2+}$) at 0.010 M $HClO_4$. Plot of $logk_q$ as a function of (a) crystal radii, r_C, (b) cation-water distance d_{M-O}, (c) polarizability α, (d) reciprocal of the Stokes radii, r_S, (f) reciprocal of the hydrated radii, r_h.
Markers, experimental. Straight lines in (a)-(c), fits to the experimental results.

For the alkyl ammonium cations, $R_nNH_{4-n}^+$, the situation is more complicated. The logarithm of the quenching rate constants increased in the sequence $NH_4^+ < MeNH_3^+ < Me_2NH_2^+ < Me_3NH^+$. Contrasting trends occurred when the size of alkyl group increased from methyl to ethyl or n-propyl. The rate constants then decreased with increasing size and polarizability, $EtNH_3^+ > Et_2NH_2^+ > Et_3NH^+$, and $MeNH_3^+ > EtNH_3^+ >$ n-$PrNH_3^+$, as shown in Figure 5.7.

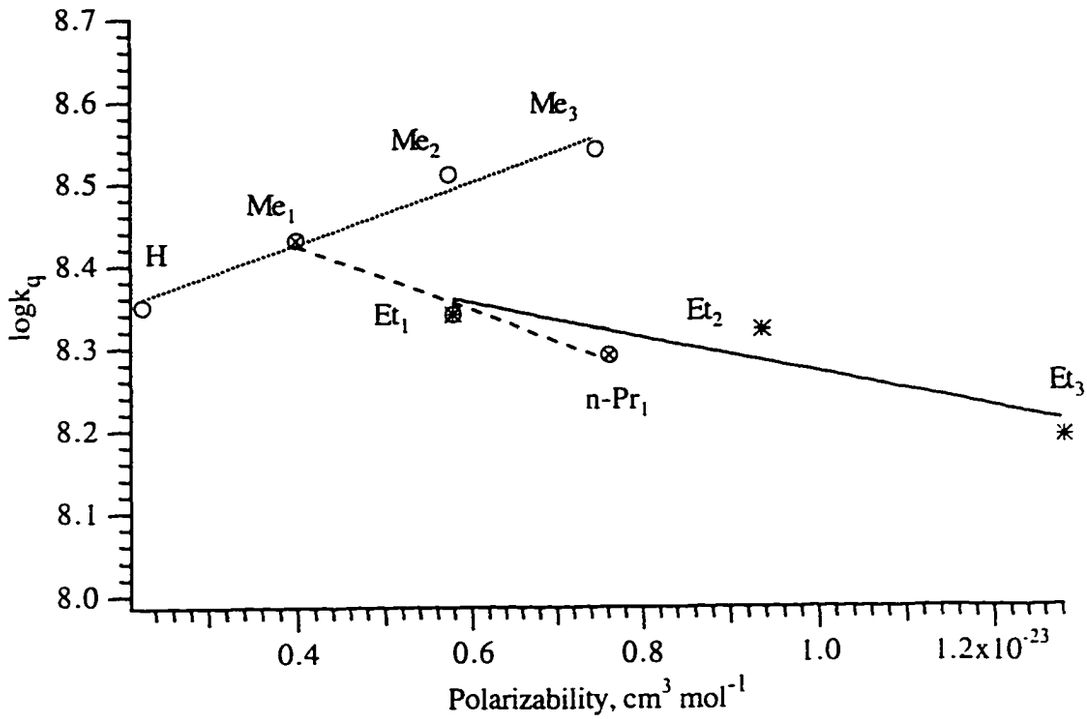

Figure 5.7 Specific cation effects on log k_q for $*[Pt_2(pop)_4]^{4-}$ / $[Co(CN)_5I]^{3-}$ in 0.50 M $R_nNH_{4-n}Cl$ (R = H, Me, Et, n-Pr, n = 0-3) / 0.010 M $HClO_4$ solutions. Markers, experimental points. Lines, linear fits to the data.

5.2.4 Quenching Products and Quantum Yields

5.2.4.1 Quenching Products

When a deaerated solution of $K_4[Pt_2(pop)_4]$, quencher $K_3[Co(CN)_5X]$ (X = Br or I) and 0.500 M KY/0.010 M $HClO_4$ (Y = Br or Cl) was irradiated at 370 nm with continuous degassing, the absorption bands of reactant $*[Pt_2(pop)_4]^{4-}$ and quencher $[Co(CN)_5X]^{3-}$ were bleached in a 1:2 molar ratio, accompanied by the development of new bands, which can be attributed to $[Pt_2(pop)_4X_2]^{4-}$ or $[Pt_2(pop)_4Y_2]^{4-}$ and possibly $[Pt_2(pop)_4XY]^{4-}$ (Figures 5.8-5.10). The reaction was terminated when the light source was removed, indicating neither thermal nor photocatalytic reactions contribute to what is a pure photochemical reaction.

When X = Y = Br, the absorption bands developed at 307 nm, 345 nm, and 395 nm, as shown in Figure 5.8. The photoproduct was identified as $[Pt_2(pop)_4Br_2]^{4-}$ by the following results. Firstly, the peak at 307 and the shoulder at 345 nm that developed, were consistent with the reported values for $[Pt_2(pop)_4Br_2]^{4-}$: λ_{max} (ε) = 305 nm (55400 $M^{-1}cm^{-1}$), 345 nm (11780 M^{-1} cm^{-1}),[168] and secondly, these absorbances had the reported ratio: experiment value, $\Delta A_{307}/\Delta A_{345} = 4.8 \pm 0.3$, compared to the literature value, $\varepsilon_{305}/\varepsilon_{345} = 4.7$. The apparent peak at 395 nm is not a product peak, but arises from convolution of the bleaching of the 369 nm $[Pt_2(pop)_4]^{4-}$ band and the tail of 345 nm absorption shoulder. This can be proved by comparing the ratio of A_{345}/A_{395} found in this experiment (0.61) with that calculated from published spectra (0.60).[169] Thirdly the amount of product formed based on the above analysis is equal to the amount of reactant $[Pt_2(pop)_4]^{4-}$ consumed, $(\Delta A/\varepsilon)_{Pt_2(pop)_4Br_2^{4-}} = (\Delta A/\varepsilon)_{Pt_2(pop)_4^{4-}}$, consistent with reaction (eq. 5.1). It can be concluded that $[Pt_2(pop)_4]^{4-}$ is quenched by $[Co(CN)_5Br]^{3-}$ to form the oxidation product, $[Pt_2(pop)_4Br_2]^{4-}$.

$$[Pt_2(pop)_4]^{4-} + 2[Co(CN)_5Br]^{3-} \xrightarrow[0.5\ M\ KBr]{h\nu} [Pt_2(pop)_4Br_2]^{4-} + Co(II)\ products \quad (5.1)$$

Interestingly, when 0.50 M KCl was used as the electrolyte instead of KBr, i.e. X = Br but Y = Cl, $*[Pt_2(pop)_4]^{4-}$ was quenched by $[Co(CN)_5Br]^{3-}$ to give a different product, $[Pt_2(pop)_4Cl_2]^{4-}$, not $[Pt_2(pop)_4Br_2]^{4-}$, as shown in Figure 5.9. The product can be easily indentified using the same method as above. New absorption bands at 283 nm and 338 nm are due to the formation of $[Pt_2(pop)_4Cl_2]^{4-}$, λ_{max} = 282 nm ($5x10^4$ L mol^{-1} cm^{-1}), 345 nm ($7x10^3$ L mol^{-1} cm^{-1}),[168] and $\Delta A_{283}/\Delta A_{338} = 5.7 \pm 0.3$, smaller than the published ε ratio, $\varepsilon_{282}/\varepsilon_{345} = 7$, but close to the reported absorbance ratio of 5.6.[169] The amount of $[Pt_2(pop)_4Cl_2]^{4-}$ formed is about equal to the amount of $[Pt_2(pop)_4]^{4-}$ consumed, $(\Delta A/\varepsilon)_{Pt_2(pop)_4Cl_2^{4-}} : (\Delta A/\varepsilon)_{Pt_2(pop)_4^{4-}} = 1.1 \pm 0.1$, as expected from equation 5.2.

$$[Pt_2(pop)_4]^{4-} + 2[Co(CN)_5Br]^{3-} \xrightarrow[0.5\ M\ KCl]{h\nu} [Pt_2(pop)_4Cl_2]^{4-} + Co(II)\ products \quad (5.2)$$

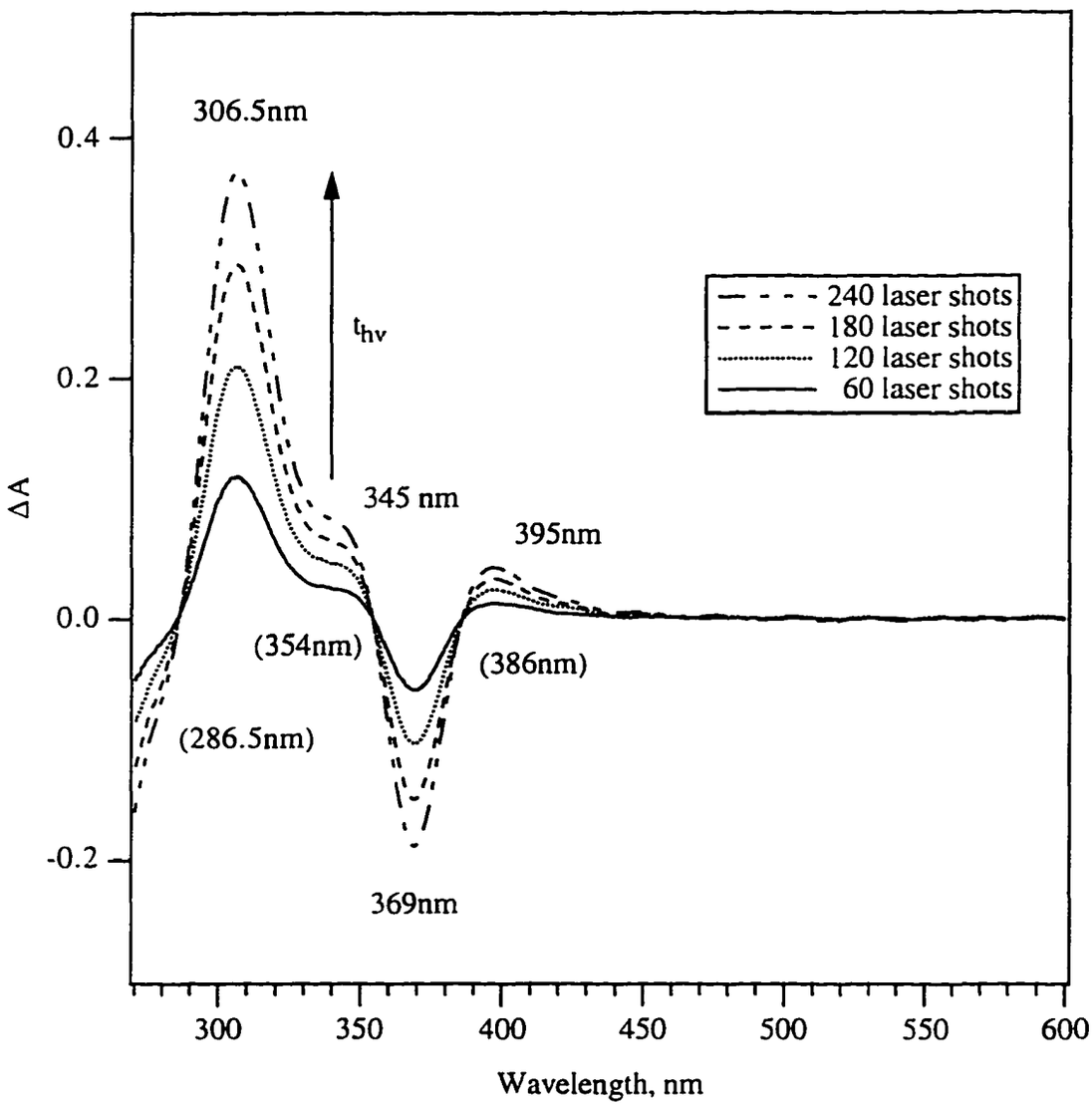

Figure 5.8 Absorbance change on reaction of $*[Pt_2(pop)_4]^{4-}$ with 1.1×10^{-3} M $[Co(CN)_5Br]^{3-}$ in 0.50 M KBr and 0.010 M $HClO_4$ aqueous solution. N_2 laser. Irradiation wavelength ($\lambda_{irrad.}$) = 370 nm.

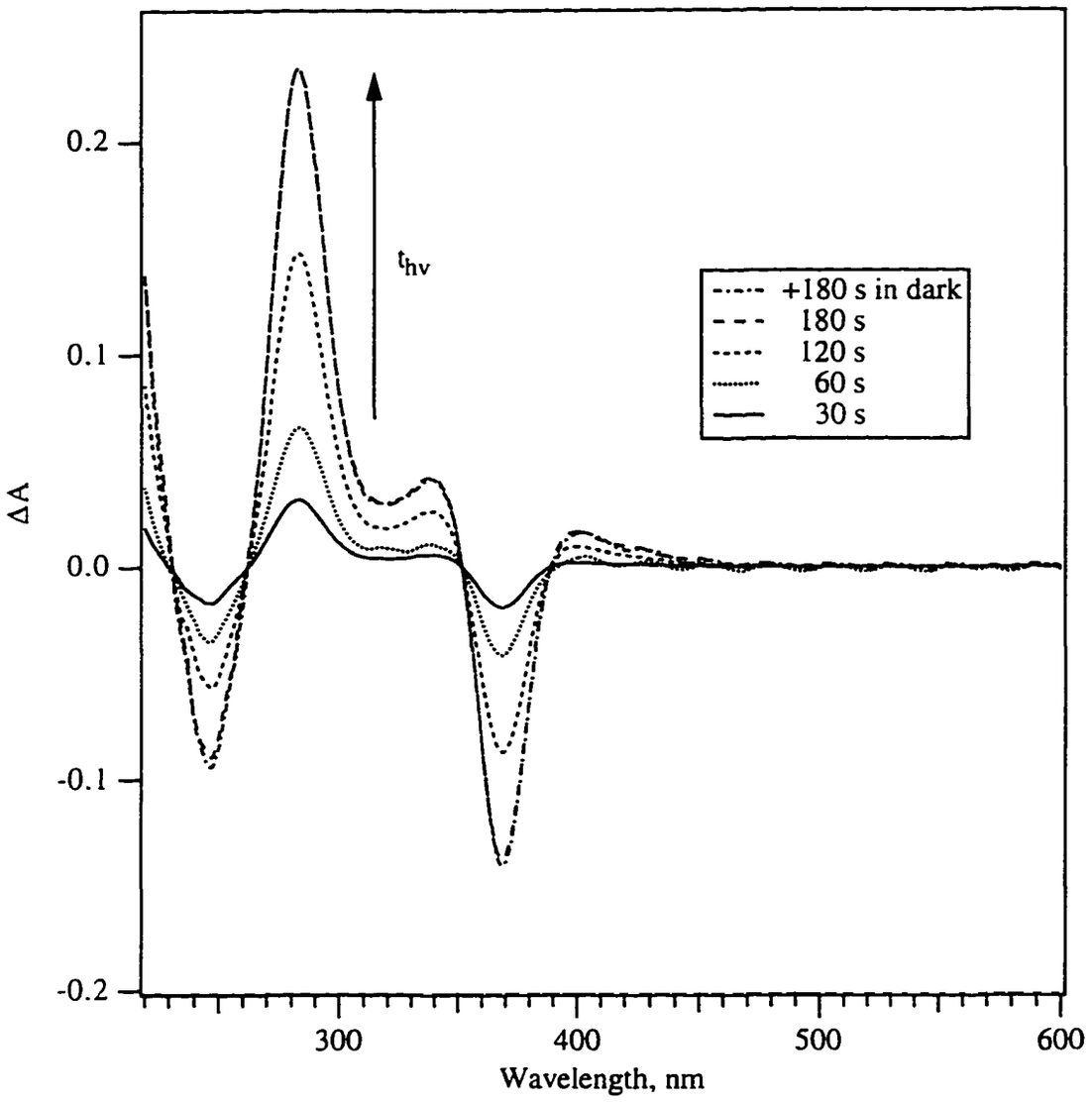

Figure 5.9 Absorbance change on reaction of $*[Pt_2(pop)_4]^{4-}$ with 1.6×10^{-4} M $[Co(CN)_5Br]^{3-}$ in 0.50 M KCl and 0.010 M $HClO_4$ aqueous solution. Hg lamp. $\lambda_{irrad.}$ = 370 nm. Irradiation time: 30 s, 60 s, 120 s, 180 s, and kept in dark for additional 180 s after the last irradiation.

Surprisingly, when $[Co(CN)_5I]^{3-}$ was used as a quencher instead of $[Co(CN)_5Br]^{3-}$ (X = I, Y = Cl), the main quenching product was found to be $[Pt_2(pop)_4I_2]^{4-}$ (as shown in Figure 5.10 and eq. 5.3), not $[Pt_2(pop)_4Cl_2]^{4-}$ as one would expect from the above experiment. New bands could be attributed to $[Pt_2(pop)_4I_2]^{4-}$ for the same reasons listed earlier. The main product peaks were found at 328 nm and 438 nm; literature for $[Pt_2(pop)_4I_2]^{4-}$, λ_{max} (ε) = 331 nm ($4x10^4$ M^{-1} cm^{-1}), 438 nm ($1.7x10^4$ M^{-1} cm^{-1}),[168] experiment absorbance ratio; A_{328}/A_{438} = 2.2, literature $\varepsilon_{331}/\varepsilon_{438}$ = 2.4, and $(\Delta A/\varepsilon)_{Pt_2(pop)_4I_2^{4-}} : (\Delta A/\varepsilon)_{Pt_2(pop)_4^{4-}} = 1.0 \pm 0.1$, consistent with reaction (5.3).

$$[Pt_2(pop)_4]^{4-} + 2[Co(CN)_5I]^{3-} \xrightarrow[0.5\ M\ KCl]{h\nu} [Pt_2(pop)_4I_2]^{4-} + Co(II)\ products \qquad (5.3)$$

It can be noticed from Figure 5.10 that the peaks generated were accompanied by a high energy shoulder, indicating the formation of a side product. The shoulders at 282 nm and 345 nm are as one would expect for a small contribution of $[Pt_2(pop)_4Cl_2]^{4-}$ (λ_{max} (ε) = 282 nm ($5x10^4$ M^{-1} cm^{-1}), 345 nm ($7x10^3$ M^{-1} cm^{-1})[168]). Another possible side product is $[Pt_2(pop)_4ClI]^{4-}$ (λ_{max} (ε) = 313 nm ($4.1x10^4$ M^{-1} cm^{-1}), 430 nm ($1.0x10^4$ M^{-1} cm^{-1})). These absorption bands are in between those of the $[Pt_2(pop)_4Cl_2]^{4-}$ and $[Pt_2(pop)_4I_2]^{4-}$ complexes and are likely to be buried under them.

Unfortunately, KI can not be used as bulk electrolyte like Cl^- or Br^- to see whether the product formed is $[Pt_2(pop)_4I_2]^{4-}$ or $[Pt_2(pop)_4X_2]^{4-}$ (X = Br, Cl) when quenchers $[Co(CN)_5X]^{3-}$ (X = Br, Cl) are used. It has been reported that I^- quenches $*[Pt_2(pop)_4]^{4-}$ in aqueous solution with a quenching rate constant log k_q = 5.7.[170]

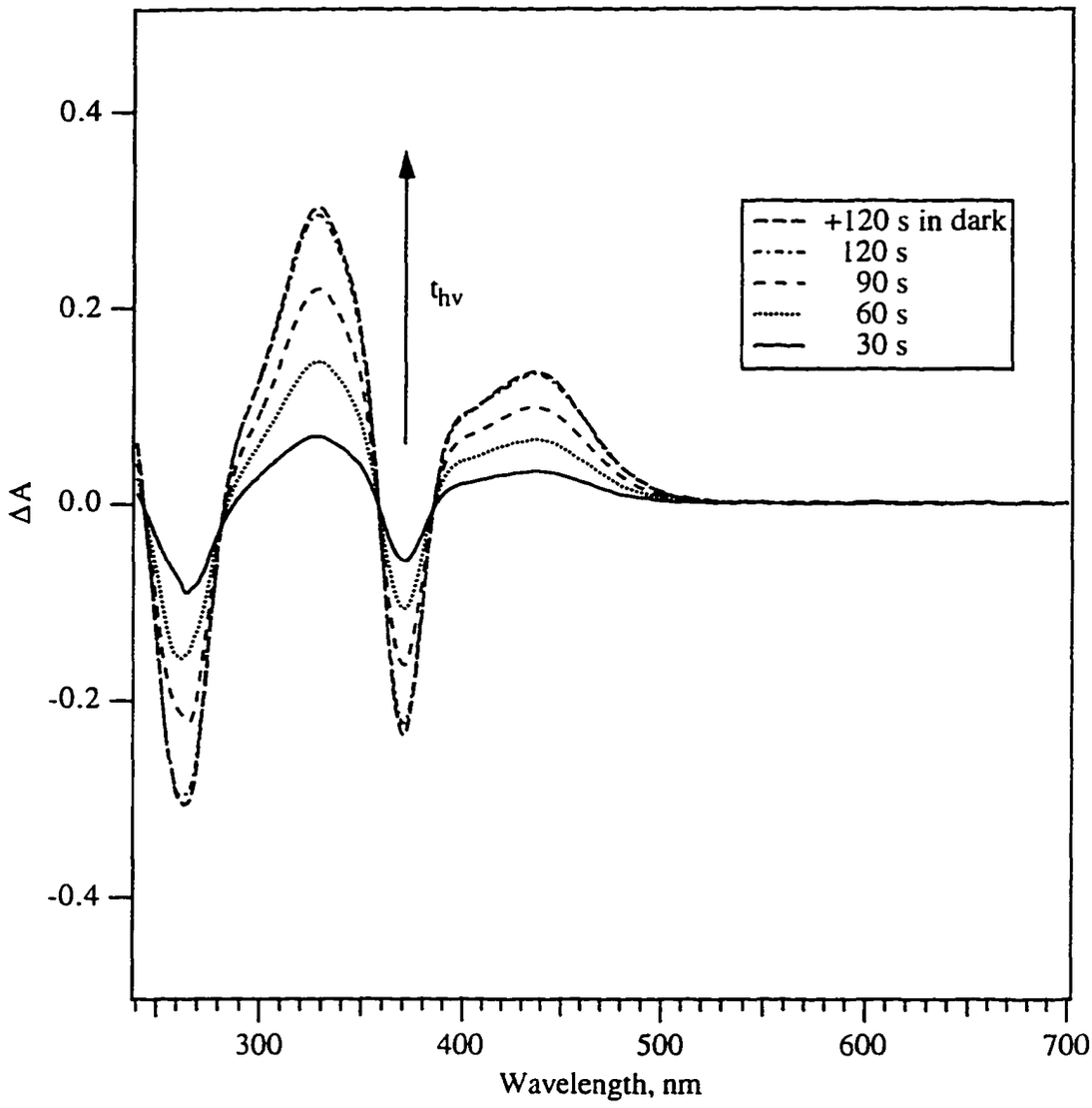

Figure 5.10 Absorbance change on reaction of $*[Pt_2(pop)_4]^{4-}$ with 1.7×10^{-4} M $[Co(CN)_5I]^{3-}$ in 0.50 M KCl and 0.010 M $HClO_4$ aqueous solution. Hg lamp. $\lambda_{irrad.}$ = 370 nm. Irradiation time: 30 s, 60 s, 90 s, 120 s, and kept in dark for additional 120 s after the last irradiation.

5.2.4.2 Quantum Yields and Quenching Efficiency

Consider the mechanistic scheme:

$$[Pt_2(pop)_4]^{4-}\ (^1A_{1g}) \xrightarrow{h\nu} *[Pt_2(pop)_4]^{4-}\ (^1A_{2u}) \xrightarrow{k_{isc}} *[Pt_2(pop)_4]^{4-}\ (^3A_{2u}) \qquad \text{Ø}_{isc} \qquad (5.4)$$

$$\left.\begin{array}{l} *Pt_2(pop)_4^{4-} + Co(CN)_5X^{3-} \underset{k_{-d}}{\overset{k_d}{\rightleftharpoons}} \{*Pt_2(pop)_4^{4-}, Co(CN)_5X^{3-}\} \\ \{*Pt_2(pop)_4^{4-}, Co(CN)_5X^{3-}\} \underset{k_{brxn}}{\overset{k_{rxn}}{\rightleftharpoons}} \text{Caged products} \end{array}\right\} \quad \eta_q \qquad (5.5)$$

$$\text{Caged products} \xrightarrow{k_{ce}} \text{Products} \qquad \eta_{ce} \qquad (5.6)$$

Assuming that no bulk recombination occurs, the quantum yield of product $\text{Ø}_{product}$ can be expressed as:

$$\text{Ø}_{product} = \text{Ø}_{isc}\,\eta_q\,\eta_{ce} \qquad (5.7)$$

where Ø_{isc} is the intersystem crossing quantum yield, η_q is the quenching efficiency, and η_{ce} is the cage escape efficiency.

The $\text{Ø}_{product}$ was found to be 0.027 ± 0.002 for the reaction between $*[Pt_2(pop)_4]^{4-}$ and $[Co(CN)_5Br]^{3-}$ in 0.50 M KCl/pH2 media, and 0.083 ± 0.02 for the reaction between $*[Pt_2(pop)_4]^{4-}$ and $[Co(CN)_5I]^{3-}$ in 0.50 M KCl/pH 2.

According to literature,[171] the main $[Pt_2(pop)_4]^{4-}$ absorption is $^1A_{1g} \longrightarrow {}^1A_{2u}$ which intersystem crosses to the corresponding triplet state $^3A_{2u}$ with a yield approaching unity, i.e. $\text{Ø}_{isc} = 1.0$.

$$\text{Since } \eta_q = \frac{k_q[Q]}{\sum k_i + k_q[Q]} = \frac{1/\tau - 1/\tau^0}{1/\tau} = 1 - \frac{\tau}{\tau^0} = \frac{k_q\tau^0[Q]}{1 + k_q\tau^0[Q]}, \quad (5.8)$$

$$\eta_{ce} = \frac{\Phi_{product}}{\Phi_{isc}\,\eta_q} = \Phi_{product}\,\frac{1 + k_q\tau^0[Q]}{k_q\tau^0[Q]} \quad (5.9)$$

The cage escape efficiency η_{ce} can thus be calculated from eq. 5.9 and was found to be 0.21 and 0.34 in $[Co(CN)_5Br]^{3-}$/KCl and $[Co(CN)_5I]^{3-}$/KCl media respectively.

5.3 Discussion

5.3.1 Salt Effects

5.3.1.1 Ionic Strength Effects

The value of log k_q in Table 5.4 clearly shows the substantial salt effect on the quenching of $*[Pt_2(pop)_4]^{4-}$ by the anion $[Co(CN)_5I]^{3-}$. The second-order rate constant increased from 5.2×10^7 to 4.1×10^8 M^{-1} s^{-1} (7.8 times increase) when the concentration of KCl salt was increased from 0.1 M to 0.8 M (8-fold increase).

As discussed in the Introduction, section 1.4.1, the rate constant for a bimolecular process can be calculated by eq. 1.42. The numerically integrated Debye-Eigen expressions were used to give estimates of the diffusional parameters k_d, k_{-d} and K_{eq}, as shown in Table 5.8. Clearly, the quenching of $*[Pt_2(pop)_4]^{4-}$ by $[Co(CN)_5X]^{3-}$ belongs to the "nearly diffusion controlled" regime because $k_t \approx k_{-d}$, and the experimental quenching rate constants k_q are substantially lower than the calculated k_d values, $k_q < k_d$ (Figure 5.5(a)). A best fit of the experimental data was generated using $k_t = 1.2\times10^9$ s^{-1}, and values of k_d and k_{-d} were calculated with the DE (Debye-Eigen) expressions. As shown in the Figure 5.5(a), numerically integrated DE expressions are found to give reliable

estimates of the diffusional paramenters for ionic strength values as high as 0.8 M KCl in the systems studied here. Similar observations have also been reported in the literature.[26,43,72] This is particularly noteworthy as Debye-Hückel theory makes several assumptions which are valid only in very dilute solutions (< 0.01 M).[45,172]

It should be pointed out that the calculated rate constant of the diffusive step k_d was obtained according to standard models originally developed for spherical reactants. For a non-spherical molecule, the radius was estimated using the equation $r = 0.5\ (d_x d_y d_z)^{1/3}$. This will be an adequate estimation if all the mutual orientations of the two reactants in the encounter complex correspond to the same reaction probability. In the system studied here, however, it is likely that the two reactants will need to approach each other in a special direction, such as the Co-X bond in line with the open coordination site (z-axis) of $*[Pt_2(pop)_4]^{4-}$. Under these conditions, r_Q has the same value, while the value of r_A is smaller, 0.33 nm instead of 0.43 nm. Applying this new value to the DE calculation results in a slightly smaller k_d and K_{eq} values, larger k_{-d} and k_t values, but an equally good best fit to the experimental result.

A good, if not better, linear fit can be obtained using the DHB (Debye-Hückel-Brønsted) expression (eq. 1.56) of $\log k_q$ versus $\mu^{1/2} / (1 + \beta a \mu^{1/2})$. The straight line (in Figure 5.5(a)) obtained from DHB fitting gave a slope of 11.6 ± 0.8, which is in good agreement with the product of the charges of the reacting species, (-4)x(-3) = 12. It seems that even the simplified DHB equation, which assumes that $\sigma_A = \sigma_Q = a = r_A + r_Q$ in the ionic strength function, is adequate enough for explaining the relationship between experimental rate constant k_q and ionic strength, and the slope of the straight line is close to the product of the charges of the reactants $Z_A Z_Q$.[173] In fact, in this case $r_A = 0.43 \approx r_Q = 0.47$, resulting in $\sigma_A = r_A + r_{K^+} \approx \sigma_Q$. Though the σ values are still smaller than the value $a = r_A + r_Q$, it was found that the rate constant is not sensitive to small changes in either σ or a. For example, a decrease in the r_A value from 0.43 nm to 0.33 nm results in a slightly

smaller slope of $Z_AZ_Q = 10 \pm 1$, which is still in reasonably good agreement with the expected value of $Z_AZ_Q = 12$. The DHB model is therefore valid for rationalizing the relationship between the rate constant and ionic strength. It should be noted though, that it has been reported the DHB expression may not be adequate for explaining the ionic strength dependence of other kinetic parameters such as cage escape yield, or for intra-molecular electron-transfer processes, as reported in the literature.[43,174]

The simpler Debye-Brønsted limiting equation (1.57) (DB), the expression most commonly applied in literature, fails to give a reasonable slope. As shown in Figure 5.5(b), the slope obtained by this fitting, 4.0 ± 0.2, is far smaller than the expected value of 12, though the line seems to fit the experimental points well. The error in the derived slope is due to the fact that both reactants are large complex anions. The closest approach between these two reactants is 9 Å, much larger than 3 Å, the value needed for the assumption of $\beta a = 1$ to be valid in the above Debye-Brønsted limiting equation. The above calculation indicates that it is important to choose the appropriate model to illustrate the relationship between the rate constants and the ionic strength when large molecules such as coordination complexes are involved in the reaction.

5.3.1.2 The Olson-Simonson Effect

Unfortunately, the electrolytes which can be used for testing the Olson-Simonson effect in this system are very limited in number. Many of the commonly used multivalent anions are either (i) strong conjugate bases of weak acids (e.g. PO_4^{3-}, CO_3^{2-}, $C_2O_4^{2-}$) which will be protonated in acidic media and change their charge type, (ii) complexes which have strong absorptions at the excitation wavelength (e.g. $[Cr(CN)_6]^{3-}$ complex), or (iii) strong oxidizing or reducing agents such as $S_2O_8^{2-}$ and $S_2O_3^{2-}$ which will react with excited state $*[Pt_2(pop)_4]^{4-}$.[158] Nevertheless, the results for those electrolytes used still

provided clear evidence that the Olson-Simonson effect is operating in this system. For the reaction between $*[Pt_2(pop)_4]^{4-}$ and $[Co(CN)_5I]^{3-}$, in the presence of 0.167 M $K_3[Co(CN)_6]$ / pH2 or 0.25 M K_2SO_4 / pH2 solution, the values of log k_q were found to be very close to that for KCl / pH2 and KNO_3 / pH2 at the same cation concentration, despite the very different values of the ionic strength (Table 5.5). As mentioned in section 1.4.2, the Olson-Simonson effect had been observed for ground state reactions between anions, and one example of excited state electron transfer between cations. With the addition of the excited state reaction between anions in this work, it seems evident that the effect is a rather general one. So far, only one exception has been reported; no trace of the Olson-Simonson effect was observed for the alkaline hydrolyses of potassium ethyl adipate and sebacate.[175]

It should be noted therefore, that when univalent ions are replaced with multivalent ions in the reactions between species with like charge, it is the concentration of the opposite charged ions rather than the ionic strength that should be used in the Debye-Hückel equations .[43]

5.3.1.3 Anion Effects

The anion effect on this system has also been investigated. As shown in Table 5.5, there is no anion effect when multivalent oxyanions or a complex anion were used. This, together with the observation that the reaction between $*[Pt_2(pop)_4]^{4-}$ and $[Co(CN)_5X]^{3-}$ is very slow in the absence of added cations, indicates that the cation plays an important role in the transition state of the reaction rather than just serving as an "inert" or "supporting" electrolyte, while the anion is not involved. This is probably the reason for the observation of the Olson-Simonson effect rather than the ionic strength effect.

Nucleophilic halide anions showed a special effect, though. The quenching rate constant was slightly affected by the addition of potassium salts of different halide anions; for example, the value of log k_q is 8.60 in 0.50 M KBr, which is larger than the value of 8.33 in 0.50 M KCl. This result is consistent with observations made by Che and co-workers who found that the reducing ability and oxidative quantum yield of $[Pt_2(pop)_4]^{4-}$ increased with the increasing nucleophilicity of halide anions in aerated aqueous solutions.[176] This effect can be explained in terms of nucleophilic attack on the unsaturated Pt center of the intermediate by the halide ions after the electron transfer step, as will be discussed later in section 5.3.2.

5.3.1.3 Specific Cation Effects

The cation effect on the quenching rate constant has been investigated, and it was found that the quenching rate constants decreased with the decrease of cation crystallographic radius; $Cs^+ > K^+ > Na^+ > Li^+$, and $Ba^{2+} > Sr^{2+} > Ca^{2+} > Mg^{2+}$ (Tables 5.6-5.7).

The attempt to use the Debye-Eigen equation to explain the cation effect failed. For example, according to a Debye-Eigen calculation, k_d for the reaction between $*[Pt_2(pop)_4]^{4-}$ and $[Co(CN)_5I]^{3-}$ will decrease about 8% with an increase in cation radius from Li^+ to Cs^+. This contradicts the experimental results, where a 6-fold increase in the quenching rate constant was observed on changing from Li^+ to Cs^+.

The results draw attention to some of the flaws of the Debye-Eigen treatment. It assumes that the solvent is unstructured and isotropic, and only considers purely electrostatic interactions between charged species, neglecting all other interactions including solvent-substrate interactions.[45] This is definitely a problem in aqueous solutions due to the variations of the solvent structure with electrolyte addition and the existence of other

interactions, such as H-bonding. It is therefore inadequate to use the Debye-Eigen equation to explain the specific salt effects on the rate constants.

Instead, the above specific cation effect on the quenching rate constants can be explained by the influence of added cations on the solvent structure. As discussed in the Introduction, section 1.4.3, the structure of water can be affected by the addition of electrolytes, becoming more or less structured compared to pure water. Within the alkali and alkali-earth series the structure making ability decreases with their "bare" ionic radii, i.e. the structure making ability of $Li^+ > Na^+ > K^+ > Cs^+$, and $Mg^{2+} > Ca^{2+} > Sr^{2+} > Ba^{2+}$. In a more structured aqueous solution the mobility of the reactant ions is lowered, which should lead to a decrease in the diffusion rate constant (k_d), and therefore a decrease in the quenching rate constant (k_q, eq. 1.42). As a consequence, smaller cations (such as Li^+ and Mg^{2+}) which give the largest proportion of structured water will result in the smaller quenching rate constants. That is, log k_q should decrease in the order: $Cs^+ > K^+ > Na^+ > Li^+$; and $Ba^{2+} > Sr^{2+} > Ca^{2+} > Mg^{2+}$, which is in agreement with the experimental results (Tables 5.6-5.7).

Such a large increase from Li^+ to Cs^+ (6 to 11 times for different quenchers) is unlikely to be solely due to the influence of electrolytes on the water structure and hence the diffusion rate constant k_d. It is reasonable also to require the involvement of the cation in the transition state. The linear correlations observed between the quenching rate constant log k_q and the cation polarizability (α),[163] cation crystal radii (r_C[124]), or cation-water distance ($d_{M\text{-}O}$[160]), Figure 5.6 (a)-(c), serve as evidence of such involvement, and this has also been suggested earlier in the literature[65,177] (see also section 1.4.3.5). Therefore, added cation not only changes the structure of the solvent, but is also involved in the transition state, assisting the reaction by forming a triangular or linear ion triplet with reactants (as discussed in section 1.4.3.5). The linear arrangement is expected to be more sensitive to the size or polarizability of the cation than the triangular arrangement.

Table 5.6 and Figure 5.6(a)-(c) show that the cation effect in all four complexes, $[Co(CN)_5Br]^{3-}$, $[Co(CN)_5Cl]^{3-}$, $[Co(CN)_5I]^{3-}$ and $[Co(CN)_5N_3]^{3-}$, is in the same direction. The complexes can be divided into two groups based on their different sensitivities to the polarizability and the size of the cations. Thus the quenching rate constant increased about 10 to 11 times from Li^+ to Cs^+ in the first group (i.e. $[Co(CN)_5Br]^{3-}$ and $[Co(CN)_5Cl]^{3-}$), while increasing only 5 to 6 times in the second group (i.e. $[Co(CN)_5I]^{3-}$ and $[Co(CN)_5N_3]^{3-}$). That is, the slopes in Figure 5.6(a)-(c) of the first group is 1.4 times larger than the second group whether plotted versus polarizability or the size of the cations. These results imply that the cation involvement in the transition state differs in the two groups. It is therefore reasonable to suggest that in the X = Br, Cl group the cation is in the center of a linear transition state, consistent with the larger effect of the polarizability of the cation on the rate constant. In the X = I, N_3 group the triangular ion triplet is likely to be involved due to the smaller effect of the polarizability of the cation on the quenching rate constant, and the significance of this triplet arrangement will be further discussed in section 5.3.2.

It is worth mentioning that the cation polarizability values obtained from different literature sources are not consistent. For example, only two sets of polarizability data for crystal alkaline or alkaline-earth metal ions were available and the values for a given ion differed as much as 40%.[161,163] This may result in some error and contribute to the scatter in Figure 5.6(a). In contrast, the crystal cation radii r_C (available from the CRC Handbook)[124] and cation-water distances d_{M-O} (available from a review article by Marcus)[160] are more reliable. Both set of parameters give reasonably good fits to the experimental data, as shown by the small chi square values χ^2 (defined as the sum of relative squared deviations of data points from best fit curve. It depends on the number of points), which range from 0.0002 to 0.0077 for r_C fitting and 0.0025 to 0.010 for d_{M-O}, smaller than that for the polarizability fittings (0.01 to 0.08) with the same number of data

points. The r_C and d_{M-O} fits are sufficiently good that one can venture to use them to estimate parameters. For the value d_{M-O} of the ammonium cation, Marcus only gave a range of 0.260 to 0.305 nm. Based on the $\log k_q$ values obtained in the NH_4^+ medium, the d_{M-O} value of NH_4^+ can be calculated from Figure 5.6(b) to be 0.27 ± 0.01 nm. As a confirmation of this procedure the calculation of r_C of NH_4^+ from Figure 5.6(c) results in a value of 0.13 nm, which is in good agreement with the literature value of 0.14 nm.[124] This procedure offers a new method for estimation of the parameters of cations which are hard to measure.

Poor correlations between $\log k_q$ and the reciprocal of the hydrated radii (r_h[164]), and Stokes radii (r_S[164,165]) of the cations were obtained, as can be seen from Figure 5.6(d)-(e). The reason may be follows. Since the formation of the precursor (or activated intermediate) would involve a more significant Coulombic barrier than the subsequent reaction step, extensive desolvation from the cation may be expected on interaction of the solvated cations with the anionic reactants. For example, a positive activation volume $\Delta V^{\neq}$ was reported for the reaction between $*[(Mo_6Cl_6)Cl_6]^{2-}$ and $[IrCl_6]^{2-}$ in a solution containing Na^+ cation,[73] and it was suggested that this positive $\Delta V^{\neq}$ resulted from significant desolvation brought about by the approach of the negatively charged reactants. It is therefore inappropriate to use the hydrated radii (or Stoke's radii) for the calculation and treatment of the rate constants. The correlation of the polarizability of the "bare" cation with rate constant indicates that the cation involved in the intermediate can not be the hydrated cation. Instead, a desolvation process before the formation of the activated complex is likely. In this case, the cation-water distance d_{M-O}, defined by Marcus as the distance between the center of a cation and that of the oxygen atom of the nearest water molecule,[160] or the radii for the "bare" ion r_C, should be better candidates for use in the measurement of the cation effect on the reaction, as has already been shown earlier in this section.

The semi-empirical method which was presented in section 1.4.3.1 can also be used to rationalize the alpha (α) sequence observed for the rate constants (i.e. rate increase in the order of $Li^+ < Na^+ < K^+ < Cs^+$; and $Mg^{2+} < Ca^{2+} < Sr^{2+} < Ba^{2+}$, see section 1.4.3.1 for notation). According to eq. 1.62, the rate constant between $*[Pt_2(pop)_4]^{4-}$ and $[Co(CN)_5X]^{3-}$ will be

$$\log k_q = \log k^0 + 2A\,F(\mu) + (B_{*Pt_2(pop)_4^{4-}} + B_{Co(CN)_5X^{3-}} - B_{\text{ion triplet}})[C_{\text{cation}}] \quad (5.10)$$

Both reactants are large anions which should show a strong beta (β) or decline sequence. The transition state is an ion triplet with an even larger size and well distributed charge, resulting in a very strong beta sequence. The β sequence from the ion triplet is very likely to overwhelm the β sequences brought about by the reactants. Contribution of these sequences results in a net overall α sequence, i.e. (β + β - very large β = α), which is in good agreement with the trends seen in the specific cation effect.

The effects of alkylammonium cations on the rate constants are quite different from those of simple inorganic cations. Figure 5.7 shows that the quenching rate constants for the alkyl ammonium cations increase with increasing number of methyl groups, i.e. $NH_4^+ < MeNH_3^+ < Me_2NH_2^+ < Me_3NH^+$. As discussed in section 1.4.3.4, the methylammonium series behave like a large simple inorganic cation such as Cs^+, so their effects on the rate constant can be explained in terms of their electrostrictive effect on water structure. The increasing size with number of methyl groups results in a decrease in charge-density of the cation and fewer structured water molecules, so an increase in the quenching rate constant is expected, $NH_4^+ < MeNH_3^+ < Me_2NH_2^+ < Me_3NH^+$, as is seen.

For alkylammoniums with larger alkyl groups, the effect on water structure is different. The quenching rate constant is not sensitive to the increasing number of the ethyl

groups, $EtNH_3^+ \geq Et_2NH_2^+ \geq Et_3NH^+$, which is due to the small structure making effects of ethylammonium ions (refer to section 1.4.3.4). The result that $MeNH_3^+ > EtNH_3^+ >$ $n\text{-}PrNH_3^+$ is also consistent with the increasing structure making ability with the larger size of the alkyl group, as discussed in section 1.4.3.4. Since the effect of alkylammoniums to the quenching rate constant is relatively small (maximum variation is 1.5 times, compared to 6 to 11 fold difference observed for alkaline and alkaline earth metal cations, Tables 5.6-5.7), it seems reasonable to associate them exclusively with changes in water structure and conclude that these alkylammoniums are not involved in the transition state.

5.3.2 Quenching Mechanism

5.3.2.1 Electron Transfer or Energy Transfer?

Results from Table 5.5 shows that $[Co(CN)_6]^{3-}$ had no quenching effect (in reality $k_q < 10^6\ M^{-1}\ s^{-1}$ based on the uncertainty of lifetime measurements, $\pm 0.1\mu s$) and can even be used as a background electrolyte for the study of salt effects. For other quenchers studied, the quenching rate constants decrease in the order $[Co(CN)_5I]^{3-} > [Co(CN)_5N_3]^{3-} > [Co(CN)_5Br]^{3-} > [Co(CN)_5Cl]^{3-}$ (Table 5.6). In addition, net oxidatively quenched platinum photoproducts were observed. For example, when $*[Pt_2(pop)_4]^{4-}$ was quenched by $[Co(CN)_5Br]^{3-}$ in a KBr or KCl medium, the photoproduct was identified as $[Pt_2(pop)_4Br_2]^{4-}$ or $[Pt_2(pop)_4Cl_2]^{4-}$ respectively (Figures 5.8-5.9). These products formed can be explained through a direct electron transfer pathway (ET) between $*[Pt_2(pop)_4]^{4-}$ and $[Co(CN)_5X]^{3-}$.

Electron transfer (ET): This mechanism involves electron transfer from excited state $*[Pt_2(pop)_4]^{4-}$ to $[Co^{III}(CN)_5Br]^{3-}$ to form a Co^{II}-fragment and the mixed valence species $[Pt^{II}Pt^{III}(pop)_4]^{3-}$ (first ET process). The large excess of nucleophile Y^- (Y = Br or Cl) in the medium can undergo nucleophilic attack at the coordinately unsaturated Pt^{III}

center, generating $[Pt^{II}Pt^{III}(pop)_4Y]^{4-}$. This intermediate can then react with a second mole of $[Co^{III}(CN)_5Br]^{3-}$ by a similar electron transfer sequence (second ET process), or undergo disproportionation[176] to give the final product $[Pt_2(pop)_4Cl_2]^{4-}$, as described in the following scheme, eqs. 5.11-5.16 (where X = Br, Y = Br, Cl, and ligands pop and CN are omitted for simplicity).

$$*Pt_2^{II,II} + X\text{-}Co \underset{k_{-d}}{\overset{k_d}{\rightleftharpoons}} \{*Pt_2^{II,II}, X\text{-}Co\} \tag{5.11}$$

$$\{*Pt_2^{II,II}, X\text{-}Co\} \overset{e^-}{\curvearrowright} \underset{k_{-ET}}{\overset{k_{ET}}{\rightleftharpoons}} \{Pt_2^{II,III}, Co^{II}\text{-fragment}\} \tag{5.12}$$

$$\{Pt_2^{II,III}, Co^{II}\text{-fragment}\} + Y^- \text{ (from bulk)} \xrightarrow{k_{Nu}} Pt_2^{II,III}Y + Co^{2+}(aq) + X^- \tag{5.13}$$

$$Pt_2^{II,III}Y + X\text{-}Co \xrightarrow{k_{Co}} Pt_2^{III,III}Y + Co^{II}\text{-fragment} + X^- \tag{5.14}$$

$$Pt_2^{III,III}Y + Y^- \text{ (from bulk)} \xrightarrow{k'_{Nu}} Pt_2^{III,III}Y_2 \tag{5.15}$$

or $$Pt_2^{II,III}Y + Pt_2^{II,III}Y \xrightarrow{k_{disp.}} Pt_2^{III,III}Y_2 + Pt_2^{II,II} \tag{5.16}$$

Scheme 5.1 Electron transfer followed by nucleophilic attack pathway of $*[Pt_2(pop)_4]^{4-}$ quenching by $[Co(CN)_5X]^{3-}$ in 0.5 M KY/pH2 media

Equations 5.14-5.15 and 5.16 are two competitive steps. If it is assumed that disproportionation can be neglected, the upper limit of the intermediate $Pt_2^{II,III}Y$ concentration can be obtained from a steady state treatment:

$$[Pt_2^{II,III}Y] = \frac{I_a \, \Phi_p}{k_{Co} \; [X\text{-}Co]} \qquad (5.17)$$

where I_a and Φ_p are the light absorbed by the $[Pt_2(pop)_4]^{4-}$ and the product ($[Pt_2(pop)_4Y_2]^{4-}$) quantum yield respectively, $[Pt_2^{II,III}Y]$ and [X-Co] are the concentrations of intermediate and quencher respectively.

For the reaction between $*[Pt_2(pop)_4]^{4-} + [Co(CN)_5Br]^{3-}$, $\Phi_p = 0.033$, and

$$I_a = \frac{I_0 \, f_a}{V} = \frac{(2.4 \times 10^{-9} \text{ mol s}^{-1}) \; (0.9)}{2.6 \times 10^{-3} \text{ L}} = 8.3 \times 10^{-7} \text{ M s}^{-1} \qquad (5.18)$$

where I_0 is the lamp intensity, f_a is the fraction of light absorbed by $[Pt_2(pop)_4]^{4-}$ complex, and V is the volume of the solution.

The value of k_{Co} is unknown, but can be estimated to be similar to the quenching rate constant k_q. This quenching process involves the reaction between energetic excited state $*[Pt_2(pop)_4]^{4-}$ and ground state quencher, while equation 5.14 involves the reaction between a reactive intermediate $Pt_2^{II,III}Y$ and the same quencher. For the sake of calculation the reactivity of the intermediate $Pt_2^{II,III}Y$ is assumed to be similar to the excited state $*[Pt_2(pop)_4]^{4-}$, i.e. $k_{Co} \approx k_q = 10^8 \text{ M}^{-1} \text{ s}^{-1}$. The upper limit of the intermediate concentration can thus be estimated to be:

$$[Pt_2^{II,III}Y] \leq \frac{(8.3 \times 10^{-7} \text{ M s}^{-1}) \; (0.033)}{(10^8 \text{ M}^{-1} \text{ s}^{-1}) \; (1.5 \times 10^{-4} \text{ M})} = 1.8 \times 10^{-12} \text{ M} \qquad (5.19)$$

The rate ratio of eq. 5.14 and 5.16, R, will then be:

$$R = \{k_{Co} \; [Pt_2^{II,III}Y] \; [Co\text{-}X]\} \; / \; \{k_{disp.} \; [Pt_2^{II,III}Y]^2\}$$

$$= \{k_{Co}\,[\text{Co-X}]\} / \{k_{disp.}\,[Pt_2^{II,III}Y]\}$$

$$\geq \frac{(10^8)\,(1.5\times10^{-4})}{k_{disp.}\,(1.8\times10^{-12})} = \frac{8\times10^{15}}{k_{disp.}} \qquad (5.20)$$

The calculation shows that even if $k_{disp.} = 10^{10}\ M^{-1}\ s^{-1}$ (the upper limit value for diffusion controlled rate constant), the ratio would be $R \geq 8\times10^5$. The large R value means the disproportionation is unlikely to compete efficiently with electron transfer to $[Co(CN)_5X]^{3-}$, and thus it is justified to neglect it. Even if k_{Co} is 2 to 3 magnitudes smaller than k_q, the R value is still about 10^3, and the conclusion of a small contribution of eq. 5.16 to the product is still justified.

In conclusion, $Pt_2^{III,III}Y_2$ is formed via two consecutive electron transfer processes (ET + ET), and the quencher and $*[Pt_2(pop)_4]^{4-}$ react in a 2:1 molar ratio, as would be expected from the stoichiometry for a redox reaction between $*[Pt_2(pop)_4]^{4-}$ and the quenchers from Scheme 5.1.

The electron transfer mechanism proposed above can also explain the quenching efficiency of different quenchers. The greater quenching efficiency of the $[Co(CN)_5X]^{3-}$ complexes compared to $[Co(CN)_6]^{3-}$ can be rationalized on the basis of reduction potentials of the excited state $*[Pt_2(pop)_4]^{4-}$ and quenchers. The excited state $*[Pt_2(pop)_4]^{4-}$ is a very strong reductant, $E^0([Pt_2(pop)_4]^{3-}/*[Pt_2(pop)_4]^{4-}) < -1$ V vs NHE,[148] or < -1.5 V vs SCE,[155] even better than $*[Ru(bpy)_3]^{2+}$, for which $E^0([Ru(bpy)_3]^{3+}/*[Ru(bpy)_3]^{2+}) =$ -0.88 vs NHE. Also the reducing ability of $*[Pt_2(pop)_4]^{4-}$ increases in the presence of halide anion.[178] The $E_{1/2}$ values of the $[Co(CN)_5X]^{3-}$ complexes obtained from the differential pulse polarography study (Table 5.3) show that they are all greater than the reduction potential of the $[Pt_2(pop)_4]^{3-}/*[Pt_2(pop)_4]^{4-}$ couple, except the unreactive, non-quenching hexacyano complex. The reduction potentials $E_{1/2}$ increase in the sequence $[Co(CN)_5Cl]^{3-}$, $[Co(CN)_5Br]^{3-}$, $[Co(CN)_5N_3]^{3-}$, and $[Co(CN)_5I]^{3-}$, indicating that $[Co(CN)_5I]^{3-}$ is a stronger oxidant than $[Co(CN)_5N_3]^{3-}$, $[Co(CN)_5Br]^{3-}$ or $[Co(CN)_5Cl]^{3-}$

. This correlates well with the observed trend of the quenching rate constant: $[Co(CN)_5I]^{3-}$ > $[Co(CN)_5N_3]^{3-}$ > $[Co(CN)_5Br]^{3-}$ > $[Co(CN)_5Cl]^{3-}$ >> $[Co(CN)_6]^{3-}$.

The above results clearly indicate that $*[Pt_2(pop)_4]^{4-}$ can be oxidatively quenched by the $[Co(CN)_5X]^{3-}$ ($X \neq CN$) in KY medium via a double electron transfer pathway to give final product of $[Pt_2(pop)_4Y_2]^{4-}$.

It was reported that the cage escape efficiency of $*[Pt_2(pop)_4]^{4-} + PVS^0 \longrightarrow PVS^- + [Pt_2(pop)_4]^{3-}$ is close to unity.[158] The smaller η_{ce} values obtained here (0.21 for $[Co(CN)_5Br]^{3-}$ in 0.5 M KCl/pH2 medium) indicate that

(i) the back electron transfer reaction from Co^{II}-fragment to $Pt^{II}Pt^{III}(pop)_4^{3-}$ is fast;

(ii) other parallel processes, such as energy transfer from $*[Pt_2(pop)_4]^{4-}$ to $[Co(CN)_5X]^{3-}$, may compete.

Due to the impossibility of observing the emission of $*[Co(CN)_5X]^{3-}$ in room temperature solutions, the second possibility can not be excluded. The question then arises: Could the product $[Pt_2(pop)_4Y_2]^{4-}$ be produced via energy transfer from $*[Pt_2(pop)_4]^{4-}$ to $[Co(CN)_5X]^{3-}$ (EN-T process), followed by electron transfer from excited state $*[Co(CN)_5X]^{3-}$ to $[Pt_2(pop)_4]^{4-}$ (ET process)?

Energy transfer (EN-T) pathway: From a thermodynamic point of view, for energy transfer to take place, the excited state energy of the quencher $[Co(CN)_5X]^{3-}$ should be lower than that of $*[Pt_2(pop)_4]^{4-}$.

The triplet energy (E_t) of $*[Pt_2(pop)_4]^{4-}$ $^3A_{2u}$ was estimated[149,155,158] from the crossing points of both the triplet absorption and emission bands to be 20.0 ± 0.8 kK. It was reported[158,179] that $*[Pt_2(pop)_4]^{4-}$ can be quenched via energy transfer to anthracene (E_t = 14.9 kK), $[Ru(bpy)_3]^{2+}$ (E_t = 16.9 kK), *trans*-stilbene (E_t = 17.5 kK), and 1.3-cyclohexadiene (E_t = 18.3 kK) with nearly diffusion controlled quenching rate constants. For quencher naphthalene (E_t = 21.2 kK), the quenching rate constant drops about 100

times with respect to quenchers having $E_t < 17.7$ kK. The rate constant was further dropped to less than 10^6 when the quencher is biphenyl, which has[158] $E_t = 23.0$ kK.

Though the energies of the lowest triplets of $[Co(CN)_5X]^{3-}$ (X = I, N_3, Br, Cl) are not available from the literature, and can not be measured directly because of the absence of the phosphorescence, useful information can still be obtained from the energy of the $[Co(CN)_6]^{3-}$ complex. The reactive excited state of $[Co(CN)_6]^{3-}$ is the lowest triplet $^3T_{1g}$.[180,181] The emission from $^3T_{1g}$ to ground state $^1A_{1g}$ has been observed by various authors and appears at 14 kK in solids at low temperature.[182-188] The luminescence of $[Co(CN)_6]^{3-}$ in solution is extremely weak at room temperature and not observable in aqueous solution. The lifetime of the $^3T_{1g}$ state was around 650 μs at 77 K,[185,189-191] and decreased dramatically with increasing temperature to about 2.6 ns at room temperature in H_2O (calculated by using a sampling technique and by deconvoluting the data).[192] Unfortunately the location of the absorption band of the $^1A_{1g} \longrightarrow {}^3T_{1g}$ transition is not trivial due to the extremely weak absorption, $\varepsilon \approx 0.3$-0.4 [181,184] for this spin-forbidden band. Mingardi and Porter reported the energy to be 18.5 kK,[182] but a higher energy located at around 24-27 kK was suggested after more studies.[183-185,187,190,193,194] It has been reported that $[Co(CN)_6]^{3-}$ can be sensitized by the excited state of biacetyl[180,195] which has the lowest excited state energy $E_t = 19.2$-19.7 kK.[101,196] Based on the energies of $^1A_{1g} \longrightarrow {}^3T_{1g}$ and $^3T_{1g} \longrightarrow {}^1A_{1g}$, and in combination with the energy transfer quenching studies, the energy of the 0-0 transition E_t of the lowest excited state, triplet $^3T_{1g}$ of $[Co(CN)_6]^{3-}$ has been suggested to be in the range of 18-20 kK.[173,185,189,190,193]

The fact that the excited state energy of biacetyl lies above the $[Co(CN)_6]^{3-}$, together with the observation that $[Co(CN)_6]^{3-}$ does not quench $*[Pt_2(pop)_4]^{4-}$, implies that the E_t lies in the order of biacetyl > $[Co(CN)_6]^{3-}$ > $[Pt_2(pop)_4]^{4-}$. Therefore biacetyl should not quench $*[Pt_2(pop)_4]^{4-}$ if the quenching mechanism involved is energy transfer. To confirm this, the quenching of $*[Pt_2(pop)_4]^{4-}$ by biacetyl was conducted in aqueous solution. Unfortunately, biacetyl did quench $*[Pt_2(pop)_4]^{4-}$ with the rate constate of k_q =

8.1×10^8 M^{-1} s^{-1}. The reasonable explanation is that biacetyl quenches $*[Pt_2(pop)_4]^{4-}$ via thermodynamically allowed electron transfer process ($E_{1/2}$ (biacetyl/biacetyl$^{-\cdot}$) = -1.03 V vs SCE,[101] greater than $E^0([Pt_2(pop)_4]^{3-}/*[Pt_2(pop)_4]^{4-}) < -1$ V vs NHE,[148] or < -1.5 V vs SCE[155]), rather than energy transfer. No net chemical reaction was observed during the $*[Pt_2(pop)_4]^{4-}$/biactyl interaction, which can be attributed to fast back electron transfer. This experiment was therefore inconclusive.

For the complexes $[Co(CN)_5X]^{3-}$, where X = I, N_3, Br, Cl, which are all weaker ligands than CN, the expectation is for lower E_t than $[Co(CN)_6]^{3-}$. Therefore, they may all be thermodynamically capable of quenching the excited state $*[Pt_2(pop)_4]^{4-}$ via an energy transfer process, giving $[Pt_2(pop)_4]^{4-}$ and excited state $*[Co(CN)_5X]^{3-}$.

After any such energy transfer process, however, the very short lifetime of the $*[Co(CN)_5X]^{3-}$ triplet would markedly reduce the probability of electron transfer interaction between the donor $[Pt_2(pop)_4]^{4-}$ and the acceptor $*[Co(CN)_5X]^{3-}$ to give a net chemical product during the donor lifetime. According to the energy gap law,[14] the triplet lifetime of $[Co(CN)_5X]^{3-}$ would be smaller than $[Co(CN)_6]^{3-}$ due to their lower E_t values. In fact, when $X \neq CN$, the O_h symmetry is broken, resulting in a further split of the triplet energies which leads to an even lower value of the lowest triplet excited state energy. This would further reduce the lifetime of the lowest excited state in the $[Co(CN)_5X]^{3-}$ complexes, i.e. τ ($[Co(CN)_5X]^{3-}$) < 2.6 ns. Therefore the energy transfer process followed by electron transfer from $[Pt_2(pop)_4]^{4-}$ to excited state $*[Co(CN)_5X]^{3-}$ is > (9.5 μs / 2.6 ns) $\approx$ 4000 times less favored than the direct electron transfer from the excited state $*[Pt_2(pop)_4]^{4-}$ to $[Co(CN)_5X]^{3-}$. The contribution of this convoluted pathway to product formation can thus be excluded.

5.3.2.2 Electron Transfer or Atom Transfer?

It is clear from the previous discussion that the excited state $*[Pt_2(pop)_4]^{4-}$ can be oxidatively quenched by $[Co(CN)_5X]^{3-}$ (X = Br) in the presence of KY (Y = Br, Cl) via the double electron transfer pathway (ET + ET) to give the final product $[Pt_2(pop)_4Y_2]^{4-}$. Surprisingly, for the reaction between $*[Pt_2(pop)_4]^{4-}$ and $Co^{III}(CN)_5I^{3-}$ in a KCl medium, the main product observed is $[Pt_2(pop)_4I_2]^{4-}$, not $[Pt_2(pop)_4Cl_2]^{4-}$ as one would expect from the ET + ET mechanism. An alternative pathway involving direct atom transfer of halide from $[Co(CN)_5X]^{3-}$ to $*[Pt_2(pop)_4]^{4-}$ (AT + AT) is thus suggested.

Atom transfer (AT): This mechanism involves I atom transfer from $[Co(CN)_5I]^{3-}$ to form $Pt^{II}Pt^{III}(pop)_4I^{4-}$ (first AT process), followed by a second atom transfer to the $Pt^{II}Pt^{III}(pop)_4I^{4-}$ intermediate from a second mole of $[Co(CN)_5I]^{3-}$ complex to give final product $Pt_2^{III}(pop)_4I_2^{4-}$ (second AT process), as described in the following (AT + AT) scheme, eqs. 5.21-5.23 (where X = I and Y = Cl).

$$\{*\overset{X\cdot}{\frown}Pt_2^{II,II}, X\text{-}Co\} \underset{k_{-AT}}{\overset{k_{AT}}{\rightleftharpoons}} \{Pt_2^{II,III}X, Co^{II}\text{-fragment}\} \quad (5.21)$$

$$\{Pt_2^{II,III}X, Co^{II}\text{-fragment}\} \xrightarrow{k_{ce}} Pt_2^{II,III}X + Co^{2+}(aq) \quad (5.22)$$

$$Pt_2^{II,III}X + Co\text{-}X \xrightarrow{k'_{AT}} Pt_2^{III,III}X_2 + Co^{2+}(aq) \quad (5.23)$$

Scheme 5.2 Direct atom transfer pathway of $*[Pt_2(pop)_4]^{4-}$ quenching by $[Co(CN)_5X]^{3-}$ in 0.5 M KY/pH2 media

Could the formation of $[Pt_2(pop)_4I_2]^{4-}$ product arise, however, from two consecutive ET steps (ET + ET), where in each case the halide ion comes from the caged Co^{II} fragment, i.e. iodide, not from the bulk medium, i.e. chloride (eqs. 5.24-5.25)?

$$Pt_2^{II,II} + Co\text{-}X \xrightarrow{k''_{ET}} \text{caged species} \xrightarrow{k''_{Nu}} Pt_2^{II,III}X + Co^{2+}(aq) \qquad (5.24)$$

$$Pt_2^{II,III}X + Co\text{-}X \xrightarrow{k'''_{ET}} \text{caged species} \xrightarrow{k'''_{Nu}} Pt_2^{III,III}X_2 + Co^{2+}(aq) \qquad (5.25)$$

The probability of this can be assessed as follows.

Though the ratio of bulk nucleophilicity of I^- and Br^- to Cl^- is about 100:1 and 7.8:1 respectively,[197] the concentration of quencher $[[Co(CN)_5X]^{3-}$ is 10^{-5} less than the $[Cl^-]$ in the medium. Assume that the number of Cl^- ions found in the reaction cage is n_{Cl^-}, and the radius of the cage is r_{cage}. The actual r_{cage} is not known, but can be estimated by taking the sum of the radii of $[Pt_2(pop)_4]^{4-}$ and $[Co(CN)_5X]^{3-}$, and the diameter of K^+, i.e. $r_{cage} = r_{Pt} + 2\, r_{K^+} + r_{Co\text{-}X} = 1.7$ nm. The experimental results from Figure 5.9 ($[Pt_2(pop)_4Cl_2]^{4-}$: $[Pt_2(pop)_4Br_2]^{4-} > 90\%$) combined with the above nucleophilicity ratios suggests that n_{Cl^-} has to be > 70, while Figure 5.10 ($[Pt_2(pop)_4I_2]^{4-}$: $[Pt_2(pop)_4Cl_2]^{4-} \geq 90\%$) suggests that n_{Cl^-} has to be ≤ 11, thus giving inconsistent solutions. Also taking $n_{Cl^-} = 70$, the calculated cage radius needs to be 4 nm, which is much larger than the r_{cage} assumed above, 1.7 nm. In addition, the above calculation is based on the assumption that K^+ cation and Cl^- anion have equal opportunities to reside in the cage. In reality K^+ should predominant in the cage with anion reactants. Adding this effect into the calculation would result in an even larger cage size (r > 4 nm) to obtain $n_{Cl^-} = 70$, which furthur deviates from the r_{cage} assumed above. Therefore the contribution of ET + ET processes to the product $[Pt_2(pop)_4X_2]^{4-}$ seems unlikely. In other words, product $[Pt_2(pop)_4X_2]^{4-}$ most likely comes from two consecutive atom transfer processes (AT + AT).

The minor products found in the reaction of $*[Pt_2(pop)_4]^{4-} + [Co(CN)_5X]^{3-}$ could be explained by two consecutive electron transfer processes (ET + ET) to give $[Pt_2(pop)_4Cl_2]^{4-}$, as described in scheme 5.2, or by atom transfer followed by electron

transfer (AT + ET, eqs. 5.26-28) (or *vice versa*, ET + AT, eqs. 5.29-31) to give $[Pt_2(pop)_4ClI]^{4-}$.

$$Pt_2^{II,II} + Co\text{-}X \xrightarrow{k''''_{AT}} Pt_2^{II,III}X + Co^{II}\text{-fragment} \quad (5.26)$$

$$Pt_2^{II,III}X + Co\text{-}X \xrightarrow{k''''_{ET}} Pt_2^{III}X + Co^{II}\text{-fragment} \quad (5.27)$$

$$Pt_2^{III}X + Y^- \text{ (from bulk)} \xrightarrow{k''''_{Nu}} Pt_2^{III}XY \quad (5.28)$$

$$Pt_2^{II,II} + Co\text{-}X \xrightarrow{k''''_{ET}} Pt_2^{II,III} + Co^{II}\text{-fragment} \quad (5.29)$$

$$Pt_2^{II,III} + Y^- \text{ (from bulk)} \xrightarrow{k''''_{Nu}} Pt_2^{II,III}Y \quad (5.30)$$

$$Pt_2^{II,III}Y + Co\text{-}X \xrightarrow{k''''_{AT}} Pt_2^{III}XY + Co^{II}\text{-fragment} \quad (5.31)$$

Could it be possible that the side products $[Pt_2(pop)_4Cl_2]^{4-}$ and $[Pt_2(pop)_4ClI]^{4-}$ were formed from the reaction of $[Pt_2(pop)_4I_2]^{4-}$ with Cl^- from the bulk? It has been reported from the literature[168] that the thermal substitution of $[Pt_2(pop)_4I_2]^{4-}$ by Cl^- is extremely slow, no replacement even after 3 days, which is much longer than the reaction time of several minutes here. The thermal exchange process, eq. 5.32, can thus be excluded. The substitution could be enhanced by light, but the reported quantum yields are very small (10^{-4} - 10^{-5}).[168] Calculation based on a simple theory[136,137] with 15% conversion of $[Pt_2(pop)_4]^{4-}$ and paramenters such as $\Phi([Pt_2(pop)_4]^{4-}) = 0.11$, $\varepsilon_{370}([Pt_2(pop)_4]^{4-}) = 3.5 \times 10^4\ M^{-1}\ cm^{-1}$, and $\Phi([Pt_2(pop)_4I_2]^{4-}) = 10^{-4}$ - 10^{-5}, $\varepsilon_{370}([Pt_2(pop)_4I_2]^{4-}) = 1.6 \times 10^4\ M^{-1}\ cm^{-1}$ estimated from the literature,[168,169] shows that

the fraction of secondary photolysis is only $4x10^{-5}$ - $4x10^{-6}$, so that the possibility of photoexchange, eq. 5.33, can also be ruled out .

$$Pt_2^{III,III}I_2 + Cl^- \xrightarrow[kT]{k_{sub.}} Pt_2^{III}ClI \text{ (or } Pt_2^{III}Cl_2) + I^- \text{ (or 2 } I^-) \qquad (5.32)$$

$$Pt_2^{III,III}I_2 + Cl^- \xrightarrow[h\nu]{k'_{sub.}} Pt_2^{III}ClI \text{ (or } Pt_2^{III}Cl_2) + I^- \text{ (or 2 } I^-) \qquad (5.33)$$

Therefore, product $[Pt_2(pop)_4I_2]^{4-}$ must be formed via AT + AT processes exclusively, $[Pt_2(pop)_4Cl_2]^{4-}$ via ET + ET, and $[Pt_2(pop)_4ClI]^{4-}$ via the combination of the two, AT / ET in either order (i.e. AT + ET or ET + AT).

In conclusion, when $[Co(CN)_5I]^{3-}$ was used as quencher, both the atom transfer pathway (the dominant pathway giving the major product $[Pt_2(pop)_4I_2]^{4-}$) and the electron transfer pathway (the minor pathway giving the side product(s) $[Pt_2(pop)_4Cl_2]^{4-}$ and/or $[Pt_2(pop)_4ClI]^{4-}$) operate. In contrast, only the electron transfer pathway operates when the quencher used is $[Co(CN)_5Br]^{3-}$. The greater ability to undergo atom transfer for $[Co(CN)_5I]^{3-}$ complex compared to its analogues $[Co(CN)_5Br]^{3-}$ or $[Co(CN)_5Cl]^{3-}$ can be attributed to the following reasons:

(i) The excited state $*[Pt_2(pop)_4]^{4-}$ has a strong affinity for the "soft" iodo ligand as reported in the literature.[198]

(ii) The stability of the mixed valence intermediate $Pt_2^{II,III}X$ increases with increasing nucleophilicity of X ($Cl^- < Br^- < I^-$).[176]

(iii) From a thermodynamic point of view, the bond strength or bond dissociation energy at 298 K, D^0_{298}, for Co-Cl, Co-Br, and Co-I are 389, 331, and 285 kJ/mol respectively,[124] indicating that the Co-I bond is much weaker than Co-Br or Co-Cl, so $[Co(CN)_5I]^{3-}$ can more easily undergo atom transfer than the bromo or chloro analogues.

The results observed here suggest that the ability of $*[Pt_2(pop)_4]^{4-}$ to undergo AT increases in the sequence $[Co(CN)_5Cl]^{3-} < [Co(CN)_5Br]^{3-} < [Co(CN)_5I]^{3-}$ (= $[Co(CN)_5N_3]^{3-}$?), which is consistent with literature findings that its atom transfer rates from alkyl halides increase in the order RCl < RBr < RI.[199]

Notice that the difference of $E_{1/2}$ values among the quenchers is very small (0.05 V), but the rate constant differs about 10-fold among different quenchers (Table 5.6), which correlates more closely with bond energy of Co-X. This also suggests that atom transfer is involved in the system.

In addition, it is obvious that back atom transfer will be less facile than back electron transfer, resulting in a higher cage escape efficiency for the atom transfer pathway than the electron transfer, which again is in good agreement with what is observed here. The cage escape efficiency, 0.34, in the $[Co(CN)_5I]^{3-}/Cl^-$ system is about 1.6 times higher than that in the $[Co(CN)_5Br]^{3-}/Cl^-$ system (0.21).

As discussed in section 1.4.3.5, the cation is involved in the transition state via an ion triplet. In order for atom transfer to take place it is clear that cation can not be in between the two reactants. Therefore it is necessary for the cation to be off center, as in a triangular ion triplet. In contrast, for electron transfer the linear arrangement would be more favorable if cation is involved in conducting the transfer of electron (Figure 5.11). As has already been pointed out in section 5.3.1.3, for quencher $[Co(CN)_5I]^{3-}$, the slope of $\log k_q$ versus polarizability or size of the cation is 1.4 times smaller than for $[Co(CN)_5Br]^{3-}$ (Figure 5.6(a)-(c)), which is consistent with the conclusion that atom transfer (involving a triangular ion triplet) is less sensitive to the size and polarizability of the cations than electron transfer (linear arrangement). In addition, $[Co(CN)_5N_3]^{3-}$ showed similar quenching behavior to $[Co(CN)_5I]^{3-}$, and $[Co(CN)_5Cl]^{3-}$ similar behavior to $[Co(CN)_5Br]^{3-}$. It is reasonable that quenchers in the same group would take the same

pathway to quench excited state $*[Pt_2(pop)_4]^{4-}$. In other words, in 0.5 M MCl/pH2 media $[Co(CN)_5Br]^{3-}$ and $[Co(CN)_5Cl]^{3-}$ quench excited state $*[Pt_2(pop)_4]^{4-}$ through the electron transfer pathway, while both atom transfer (major) and electron transfer (minor) pathways operate when the quencher is $[Co(CN)_5I]^{3-}$ or $[Co(CN)_5N_3]^{3-}$.

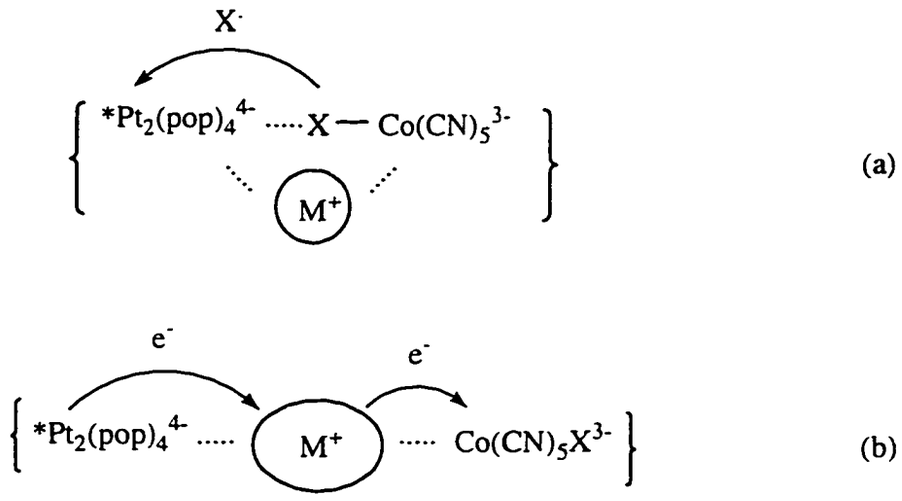

Figure 5.11 Cation involvement in (a) atom transfer, and (b) electron transfer processes.

5.4 Conclusions

(i) The emission of excited state $*[Pt_2(pop)_4]^{4-}$ is quenched by the complexes $[Co(CN)_5X]^{3-}$ (where X = N_3, I, Br, Cl, but not CN) but only in the presence of electrolytes such as the chloride salts MCl, M'Cl_2, or $R_nNH_{4-n}Cl$ (where M, M' and R represent alkaline, alkaline earth metals, and alkyl respectively with n = 0 - 3). The second-order quenching rate constants are in the range 10^7 to 10^9 L mol^{-1} s^{-1} at 0.5 M cation concentration, and these constants decrease along the complex series; $[Co(CN)_5I]^{3-}$ > $[Co(CN)_5N_3]^{3-}$ > $[Co(CN)_5Br]^{3-}$ > $[Co(CN)_5Cl]^{3-}$.

(ii) The quenching efficiency of the cobalt complexes increases with electrolyte concentration. The Debye-Eigen equation and the simplified DHB equation can be used to explain the relationship between the quenching rate constant and ionic strength in the monovalent electrolyte (KCl)solution.

(iii) In the reaction between excited state $*[Pt_2(pop)_4]^{4-}$ and quencher $[Co(CN)_5I]^{3-}$ with multivalent electrolyte solutions the quenching rate constants were governed by the cation concentration, not the ionic strength. That is the Olson-Simonson effect.

(iv) Specific cation effects are observed such that the quenching rate constants in presence of $Li^+ < Na^+ < K^+ < Cs^+$; $Mg^{2+} < Ca^{2+} < Sr^{2+} < Ba^{2+}$; $NH_4^+ < MeNH_3^+ < Me_2NH_2^+ < Me_3NH^+$; $Et_3NH^+ \leq Et_2NH_2^+ \leq EtNH_3^+$; and $n\text{-}PrNH_3^+ < EtNH_3^+ < MeNH_3^+$. The accelerating effect of the cations can be attributed to the changes of water structure due to the electrostricted or hydrophobic interaction between cations and water molecules. For the series of alkaline and alkaline earth metal cations, $\log k_q$ was found to be linear when plotted against either the crystal ionic radii r_C, the cation-water distance $d_{M\text{-}O}$, or the polarizability (α) of the cations, which can be related to the involvement of cation in the transition state of the reaction.

(v) When the quencher is $[Co(CN)_5I]^{3-}$, quenching occurs by atom transfer (dominant) and electron transfer (minor). For $[Co(CN)_5Br]^{3-}$ as quencher, only electron transfer is observed. Based on the sensitivity of the quenching rate constants to the cation effects it is suggested that quencher $[Co(CN)_5N_3]^{3-}$ behaves similarly to $[Co(CN)_5I]^{3-}$, while $[Co(CN)_5Cl]^{3-}$ resembles $[Co(CN)_5Br]^{3-}$.

5.5 Final Remarks

This work presents the first extensive systematic study of kinetic salt effects, including the ionic strength effect, the Olson-Simonson effect, and the specific cation effect, on reactions involving excited state coordination complexes. The linear dependence

of the quenching rate constant on the cation size provides a new method of obtaining the parameters of cations which may be hard to measure otherwise.

The study also presents the first example of $*[Pt_2(pop)_4]^{4-}$ abstracting a halide atom directly from a coordination complex. This observation provides new insight into the deactivation of excited state complexes and further illustrates the rich photochemistry of the $[Pt_2(pop)_4]^{4-}$ complex. In future work, product analysis for the reaction between $*[Pt_2(pop)_4]^{4-}$ and quencher $[Co(CN)_5N_3]^{3-}$ is needed to confirm the atom transfer mechanism implied in this study. The cationic complexes such as $[Co(NH_3)_5X]^{2+}$ (X = halides) can also be used as quenchers to further investigate the possibility of the atom transfer process on reactions between opposite charged complexes.

It would be interesting to compare the kinetic salt effect on the systems involving excited state and ground state coordination cations with the results reported in this Chapter. The cobalt(III)am(m)ine complexes synthesized provide a series of complexes which offer charges ranging from zero to 3+: $Co(tacn)(NCS)_3$, *cis/trans*-$[Co(NCS)_2(NH_3)_4]^+$ or $[Co(NCS)_2(en)_2]^+$, $[Co(NH_3)_5(NCS)]^{2+}$, and $[Co(NH_3)_6]^{3+}$, which can be used to quench the excited state of $*[Ru(bpy)_3]^{2+}$ and can be used for systematic studies of salt effects including specific anion catalysis as well as the charge and ligand effect of the quencher on the quenching mechanism.

REFERENCES

(1) Balzani, V.; Moggi, L. *Coord. Chem. Rev.* **1990**, *97*, 313.

(2) Sykora, J.; Sima, J. *Coord. Chem. Rev.* **1990**, *107*, 1.

(3) Neumann-Spallart, M.; Kalyanasundram, K.; Grätzel, C.; Grätzel, M. *Helv. Chim. Acta* **1980**, *63*, 1111.

(4) Wrighton, M. S. *J. Chem. Educ.* **1983**, *60*, 877.

(5) Whitten, D. G. *J. Chem. Educ.* **1983**, *60*, 867.

(6) Balzani, V.; Bolletta, F.; Ciano, M.; Maestri. *J. Chem. Educ.* **1983**, *60*, 447.

(7) Juris, A.; Balzani, V.; Barigelletti, F.; Campagna, S.; Belser, P.; Zelewsky, A. V. *Coord. Chem. Rev.* **1988**, *84*, 85.

(8) Balzani, V.; Bolletta, F.; Gandolfi, M. T.; Maestri, M. *Top. Curr. Chem.* **1978**, *75*, 1.

(9) Kutal, C. *J. Chem. Educ.* **1983**, *60*, 882.

(10) Kalyanasundaram, K. *Coord. Chem. Rev.* **1982**, *46*, 159.

(11) Hennig, H.; Rehorek, D.; Archer, R. D. *Coord. Chem. Rev.* **1985**, *61*, 1.

(12) Dickson, M. K.; Pettee, S. K.; Roundhill, D. M. *Anal. Chem.* **1981**, *53*, 2159.

(13) Balzani, V.; Carassiti, V. *Photochemistry of Coordination Compounds*; Academic Press: London, New York, 1970.

(14) Gilbert, A.; Baggott, J.; Wagner, P. J. *Essentials of Molecular Photochemistry*; CRC Press: Boca Raton, Ann Arbor, Boston, London, 1991.

(15) Lever, A. B. P. *Inorganic Electronic Spectroscopy*, 2nd ed.; Elsevier: New York, 1984.

(16) Balzani, V.; Moggi, L.; Manfrin, M. F.; Bolletta, F. *Coord. Chem. Rev.* **1975**, *15*, 321.

(17) Scandola, F.; Balzani, V. *J. Chem. Educ.* **1983**, *60*, 814.

(18) Porter, G. B. "Kinetics of photophysical processes"; In *Concepts of Inorganic Photochemistry*; Adamson, A. W., Fleischauer, P. D., Eds.; John Wiley & Sons, Inc.: New York, London, Sydney, Toronto, 1975; p 37.

(19) Evans, D. H.; O'Connell, K. M.; Peterson, R. A.; Kelly, M. J. *J. Chem. Educ.* **1983**, *60*, 290.

(20) Smith, D. C.; Gray, H. B. *Coord. Chem. Rev.* **1990**, *100*, 169.

(21) Bolletta, F.; Juris, A.; Maestri, M.; Sandrini, D. *Inorg. Chim. Acta* **1980**, *44*, L175.

(22) Laurence, G. S.; Balzani, V. *Inorg. Chem.* **1974**, *13*, 2976.

(23) Henbest, K.; Douglas, P.; Garley, M. S.; Mills, A. *J. Photochem. Photobiol. A:Chem.* **1994**, *80*, 299.

(24) Horváth, A.; Bakó, Z.; Papp, S.; Keszel, C. *J. Photochem. Photobiol. A:Chem.* **1990**, *52*, 271.

(25) Sandrini, D.; Gandolfi, M. T.; Maestri, M.; Bolletta. F.; Balzani, V. *Inorg. Chem.* **1984**, *23*, 3017.

(26) Chiorboli, C.; Scandola, F.; Kisch, H. *J. Phys. Chem.* **1986**, *90*, 2211.

(27) Che, C.-M.; Lee, W.-M.; Cho, K.-C.; Harvey, P. D.; Gray, H. B. *J. Phys. Chem.* **1989**, *93*, 3095.

(28) Endicott, J. F. "Charge-Transfer Photochemistry"; In *Concepts of Inorganic Photochemistry*; Adamson, A. W., Fleischauer, P. D., Eds.; John Wiley & Sons, Inc.: New York, London, Sydney, Toronto, 1975; p 81.

(29) Cotton, F. A. *Chemical Applications of Group Theory*, 3rd ed.; A Wiley-Interscience Publication: New York, Chichester, Brisbane, Toronto, Singapore, 1990.

(30) Zinato, E. "Substitutional Photochemistry of First-Row Transition Elements"; In *Concepts of Inorganic Photochemistry*; Adamson, A. W., Fleischauser, P. D., Eds.; John Wiley & Sons, Inc.: New York, London, Sydney, Toronto, 1975; p 143.

(31) Endicott, J. F.; Hoffman, M. Z. *J. Am. Chem. Soc.* **1965**, *85*, 3348.

(32) Adamson, A. W.; Sporer, A. H. *J. Am. Chem. Soc.* **1958**, *80*, 3865.

(33) Endicott, J. F.; Ferraudi, G. J.; Barber, J. R. *J. Phys. Chem.* **1975**, *79*, 630.

(34) Orhanovic, M.; Sutin, N. *Inorg. Chem.* **1977**, *16*, 550.

(35) Balzani, V.; Ballardini, R.; Sabbatini, N.; Moggi, L. *Inorg. Chem.* **1968**, *7*, 1398.

(36) Scandola, F.; Bartocci, C.; Scandola, M. A. *J. Am. Chem. Soc.* **1973**, *95*, 7898.

(37) Scandola, F.; Bartocci, C.; Scandola, M. A. *J. Phys. Chem.* **1974**, *78*, 572.

(38) Vogler, A.; Kunklly, H. *Inorg. Chim. Acta* **1975**, *14*, 247.

(39) Fleischauer, P. D.; Adamson, A. W.; Sartori, G. *Progr. Inorg. Chem.* **1972**, *17*, 1.

(40) Hug, G. L. *Optical Spectra of Nonmetallic Inorganic Transient Species in Aqueous Solution*; U.S. Goverment Printing Office: Washington, 1981; Vol. 69.

(41). Kirk, A. D.; Langford, C. H.; Sharma, D. K. *Inorg. Chem.* **1989**, *28*, 974.

(42) Langford, C. H.; Malkhasian, A. Y. S.; Sharma, D. K. *J. Am. Chem. Soc.* **1984**, *106*, 2727.

(43) Chiorboli, C.; Indelli, M. T.; Scandola, M. A. R.; Scandola, F. *J. Phys. Chem.* **1988**, *92*, 156.

(44) Fuoss, R. M. *J. Am. Chem. Soc.* **1958**, *80*, 5059.

(45) Rexwinkel, R. B.; Meskers, S. C. J.; Dekkers, H. P. J. M.; Riehl, J. P. *J. Phys. Chem.* **1992**, *96*, 5725.

(46) Livingston, R. S. *J. Am. Chem. Soc.* **1926**, *48*, 53.

(47) Pethybridge, A. D.; Prue, J. E. *Progr. Inorg. Chem.* **1972**, *17*, 327.

(48) Olson, A. R.; Simonson, T. R. *J. Chem. Phys.* **1949**, *17*, 1167.

(49) Ferranti, F.; Indelli, A. *J. Chem. Soc. Faraday Trans. 1* **1989**, *85*, 2241.

(50) Ferranti, F. *J. Chem. Soc. (A)* **1970**, 134.

(51) Kershaw, M. R.; Prue, J. E. *Trans. Faraday Soc.* **1967**, *63*, 1198.

(52) Basu, M. K.; Das, M. N. *J. Chem. Soc. (A)* **1968**, 2182.

(53) Zamboni, R.; Giacomelli, A.; Malatesta, F.; Indelli, A. *J. Phys. Chem.* **1976**, *80*, 1418.

(54) Indelli, A.; Nolan, G.; Amis, E. S. *J. Am. Chem. Soc.* **1960**, *82*, 3237.

(55) Campion, R. J.; Deck, C. F.; King, P.; Wahl, A. C. *Inorg. Chem.* **1967**, *6*, 672.

(56) Fava, A.; Bresadola, S. *J. Am. Chem. Soc.* **1955**, *77*, 5792.

(57) Scandola, M. A. R.; Scandola, F.; Indelli, A. *J. Chem. Soc. Faraday Trans. 1.* **1985**, *81*, 2967.

(58) McKay, H. A. C. *J. Inorg. Nucl. Chem.* **1964**, *26*, 1767.

(59) Shporer, M.; Ron, G.; Loewenstein, A.; Navon, G. *Inorg. Chem.* **1965**, *4*, 361.

(60) Spiccia, L.; Swaddle, T. W. *Inorg. Chem.* **1987**, *26*, 2265.

(61) Indelli, A.; Bartocci, V.; Ferranti, F.; Lucarelli, M. G. *J. Chem. Phys.* **1966**, *44*, 2069.

(62) Indelli, A.; Amis, E. S. *J. Am. Chem. Soc.* **1960**, *82*, 332.

(63) Dennis, C. R.; Leipoldt, J. G.; Basson, S. S.; Wyk, A. J. V. *Inorg. Chem.* **1986**, *25*, 1268.

(64) Jain, D. V. S.; Nandel, F. S. *J. Chem. Soc. Dalton Trans.* **1977**, 949.

(65) Dennis, C. R.; Basson, S. S.; Leipoldt, J. G. *Polyhedron* **1983**, *2*, 1357.

(66) Rasmussen, P. G.; Brubaker, C. H. *Inorg. Chem.* **1964**, *3*, 977.

(67) Leipoldt, J. G.; Bok, L. D. C.; Wyk, A. J. V.; Dennis, C. R. *J. Inorg. Nucl. Chem.* **1977**, *39*, 2019.

(68) Braga, T. G.; Wahl, A. C. *J. Phys. Chem.* **1985**, *89*, 5822.

(69) Stalnaker, N. D.; Solenberger, J. C.; Wahl, A. C. *J. Phys. Chem.* **1977**, *81*, 601.

(70) Basolo, F.; Pearson, R. G. "Oxidation-Reduction Reactions"; In *Mechanism of Inorganic Reactions*; 2nd ed.; John Wiley and Sons, Inc.: New York, London, Sydney, 1967; p 454.

(71) Gaines, G. L. *J. Phys. Chem.* **1979**, *83*, 3088.

(72) Greiner, G.; Pasquini, P.; Weiland, R.; Orthwein, H.; Rau, H. *J. Photochem. Photobiol. A:Chem.* **1990**, *51*, 179.

(73) Tanaka, H. K.; Sasaki, Y.; Saito, K. *Inorg. Chim. Acta* **1993**, *210*, 63.

(74) Yamaguchi, T.; Sasaki, Y. *Inorg. Chem.* **1990**, *29*, 493.

(75) Frank, H. S. *Proc. Roy. Soc. Lond. A* **1958**, *247*, 481.

(76) Frank, H. S.; Wen, W.-Y. *Discuss. Faraday Soc.* **1957**, *24*, 133.

(77) Ralston, J.; Healy, T. W. *J. Colloid. Interface Sci.* **1973**, *42*, 629.

(78) Eigen, M. *Discuss. Faraday Soc.* **1957**, *24*, 25.

(79) Némethy, G.; Scheraga, H. A. *J. Chem. Phys.* **1962**, *36*, 3382.

(80) Némethy, G.; Scheraga, H. A. *J. Chem. Phys.* **1962**, *36*, 3401.

(81) Samoilov, O. Y. *Discuss. Faraday Soc.* **1957**, *24*, 141.

(82) Mathieson, J. G.; Curthoys, G. *Aust. J. Chem.* **1975**, *28*, 975.

(83) Frank, H. S.; Evans, M. W. *J. Phys. Chem.* **1945**, *13*, 507.

(84) Young, T. F.; Wu, Y. C.; Krawetz, A. A. *Discuss. Faraday Soc.* **1957**, *24*, 37.

(85) Ashford, N. F.; Blandamer, M. J.; Burgess, J.; Laycock, D.; Waters, M.; Wellings, P.; Woodhead, R.; Mekhail, F. M. *J. Chem. Soc. Dalton Trans.* **1979**, 869.

(86) Millero, F. J. "The Partial Molal Volumes of Electrolytes in Aqueous Solutions"; In *Water and Aqueous Solutions*; Wiley: New York, 1972; p 519.

(87) Blandamer, M. J. *Adv. Phys. Org. Chem.* **1977**, *14*, 203.

(88) Sarma, T. S.; Ahluwalia, J. C. *Chem. Soc. Rev.* **1973**, *2*, 203.

(89) Fraser, R. T. M. *J. Am. Chem. Soc.* **1961**, *83*, 4920.

(90) Halpern, J.; Orgel, L. E. *Discuss. Faraday Soc.* **1960**, *29*, 32.

(91) Hughes, R. G.; Endicott, J. F.; Hoffman, M. Z.; House, D. A. *J. Chem. Educ.* **1969**, *46*, 440.

(92) Wegner, E. E.; Adamson, A. W. *J. Am. Chem. Soc.* **1966**, *88*, 394.

(93) Perrin, D. D. *Ionisation Constants of Inorganic Acids and Bases in Aqueous solution*, 2nd ed.; Pergamon Press: Oxford, New York, Toronto, Sydney, Paris, Frankfurt, 1982.

(94) Kirk, A. D.; Hewavitharana, A. K. *Anal. Chem.* **1988**, *60*, 797.

(95) Kirk, A. D.; Riske, W.; Lyon, D. K.; Rapko, B.; Finke, R. G. *Inorg. Chem.* **1989**, *28*, 792.

(96) Hibbert, D. B.; James, A. M. *Dictionary of Electrochemistry*, 2nd ed.; The Macmillan Press Ltd.: London, 1984.

(97) Hatchard, C. G.; Parker, C. A. *Proc. Roy. Soc. (London) A* **1956**, *235*, 518.

(98) Parker, C. A. "Measurement of Light by Chemical Methods"; In *Photoluminescence of Solutions*; Elsevier Publishing Co.: Amsterdam, London, New York, 1968; p 208.

(99) Demas, J. N.; Bowman, W. D.; Zalewski, E. F.; Velapoldi, R. A. *J. Phys. Chem.* **1981**, *85*, 2766.

(100) Kirk, A. D.; Namasivayam, C. *Anal. Chem.* **1983**, *55*, 2428.

(101) Murov, S. L.; Carmichael, I.; Hug, G. L. *Handbook of Photochemistry*, 2nd ed.; Marcel Dekker, Inc.: New York, Basel, Hong Kong, 1993.

(102) Demas, J. N. *Excited State Lifetime Measurements*; Academic Press: New York, London, Paris, San Diego, San Francisco, São Paulo, Sydney, Tokyo, Toronto, 1983.

(103) Kneeland, D. M. *Ph. D. Dissertation*, University of Victoria, 1991.

(104) Kanamori, K.; Kawai, K. *Bull. Chem. Soc. Jpn.* **1982**, *55*, 764.

(105) Angelici, R. J. "Carbonatotetraamminecobalt(III) nitrate, $[Co(NH_3)_4CO_3]NO_3$"; In *Synthesis and Technique in Inorganic Chemistry*; W. B. Saunders Co.: Toronto, 1969; p 16.

(106) Schlessinger, G.; Simmons, W.; Jabs, G.; Chamberlain, M. M. *Inorg. Synth.* **1960**, *6*, 173.

(107) Springborg, J.; Schäffer, C. E.; Wilson, M. L.; Wharton, J. M.; Hatfield, W. E. *Inorg. Synth.* **1978**, *18*, 75.

(108) Krishnamurthy, M. *J. Inorg. Nucl. Chem.* **1972**, *34*, 3915.

(109) Searle, G. H.; Geue, R. J. *Aust. J. Chem.* **1984**, *37*, 959.

(110) Barefield, E. K.; Wagner, F. *Inorg. Chem.* **1973**, *12*, 2435.

(111) Gmelin. "Azidosalze $[CoN_3A_5]X_2$"; In *Gmelins Handbuch Der Anorganischen Chemie*; Verlag Chemie Gmbh: Weinheim-Bergstr., 1964; Vol. Cobalt, System-Number 58, Part B; p 406.

(112) Fujita, J.; Shimura, Y. *Bull. Chem. Soc. Jpn.* **1963**, *36*, 1281.

(113) Abou-El-Wafa, M. H. M.; Burnett, M. G.; McCullagh, J. F. *J. Chem. Soc. Dalton.* **1986**, 2083.

(114) Flor, T.; Casabo, J. *Synth. React. Inorg. Met.-Org. Chem.* **1986**, *16*, 795.

(115) Alexander, K. A.; Bryan, S. A.; Dickson, M. K.; Hedden, D.; Roundhill, D. M.; Che, C.-M.; Butler, L. G.; Gray, H. B. *Inorg. Synth.* **1986**, *24*, 211.

(116) Buckingham, D. A.; Creaser, I. I.; Sargeson, A. M. *Inorg. Chem.* **1970**, *9*, 655.

(117) Neta, P.; Huie, R. E.; Ross, A. B. "Rate constants for reactions of the dithiocyanate radical ion in aqueous solution"; In *J. Phys. Chem. Ref. Data*; Lide, D. R., Ed.; American Chemistry Society: Washington, DC, 1988; Vol. 17; p 1167.

(118) Schuler, R. H.; Patterson, L. K.; Janata, E. *J. Phys. Chem.* **1980**, *84*, 2088.

(119) Caspari, G.; Hughes, R. G.; Endicott, J. F.; Hoffman, M. Z. *J. Am. Chem. Soc.* **1970**, *92*, 6801.

(120) Baxendale, J. H.; Bevan, P. L. T.; Scott, D. A. *Trans. Faraday Soc.* **1968**, *64*, 2389.

(121) Behar, D.; Bevan, P. L. T.; Scholes, G. *J. Phys. Chem.* **1972**, *76*, 1537.

(122) Schöneshöfer, M.; Beck, G.; Henglein, A. *Ber. Bunsenges. Phys. Chem.* **1970**, *74*, 1011.

(123) Nord, G. *Comments Inorg. Chem.* **1992**, *13*, 221.

(124) Weast, R. C.; Lide, D. R.; Astle, M. J.; Beyer, W. H. *CRC Handbook of Chemistry and Physics*, 70th ed.; CRC Press Inc.: Florida, 1990.

(125) Schöneshöfer, M. *Int. J. Radiat. Phys. Chem.* **1969**, *1*, 505.

(126) Schöneshöfer, M.; Henglein, A. *Ber. Bunsenges. Phys. Chem.* **1970**, *74*, 393.

(127) Schöneshöfer, M.; Henglein, A. *Ber. Bunsenges. Phys. Chem.* **1969**, *73*, 289.

(128) Beck, M. T. *Coord. Chem. Rev.* **1968**, *3*, 91.

(129) Jackson, W. G.; Hookey, C. N.; Randall, M. L.; Comba, P.; Sargeson, A. M. *Inorg. Chem.* **1984**, *23*, 2473.

(130) Tanaka, N.; Kobayashi, Y.; Kamada, M. *Bull. Chem. Soc. Jpn.* **1967**, *40*, 2839.

(131) Sillén, L. G.; Martell, A. E. *Part I: Inorganic Ligands. Part II: Organic Including Macromolecule Ligands*; Burlington House: London, 1971; Vol. 25.

(132) Gmelin. "trichloro-verbindung [$CoCl_3$dan]"; In *Gmelins Handbuch Der Anorganischen Chemie*; Verlag Chemie Gmbh: Weinheim-Bergstr., 1964; Vol. Cobalt, System-Number 58, Part B; p 596.

(133) Nakamoto, K. *Infrared and Raman Spectra of Inorganic and Coordination Compounds*, 4th ed.; John Wiley & Sons: New York, Chichester, Brisbane, Toronto, Singapore, 1986.

(134) Högfeldt, E. *Part A: Inorganic Ligands*, 1st ed.; Pergamon Press: Oxford, New York, Toronto, Sydney, Paris, Frankfurt, 1983; Vol. 21.

(135) Kirk, A. D.; Namasivayam, C. *Inorg. Chem.* **1988**, *27*, 1095.

(136) Wirth, G.; Linck, R. G. *J. Am. Chem. Soc.* **1973**, *95*, 5913.

(137) Wong, C. F. C.; Kirk, A. D. *Inorg. Chem.* **1976**, *15*, 1519.

(138) Adamson, A. W. *Faraday Discuss. Chem. Soc.* **1960**, *29*, 163.

(139) Magde, D.; McCusker, J.; Walda, K.; Hendrickson, D. R. "Subpicosecond photophysics of coordiantion compounds of iron(II) and cobalt(III)"; *XVIth International Conference on Photochemistry*, Vancouver, 1993; Abstracts, p 109.

(140) Kirk, A. D.; Kneeland, D. M. *Inorg. Chem.* **1989**, *28*, 4274.

(141) Kirk, A. D.; Kneeland, D. M. *Inorg. Chem.* **1995**, *34*, 1536.

(142) Haim, A.; Wilmarth, W. K. *J. Am. Chem. Soc.* **1961**, *83*, 509.

(143) Grassi, R.; Haim, A.; Wilmarth, W. K. *Inorg. Chem.* **1967**, *6*, 237.

(144) Miskowski, V. M.; Gray, H. B. *Inorg. Chem.* **1975**, *14*, 401.

(145) Wrighton, M.; Bredesen, D.; Hammond, G. S.; Gray, H. B. *J. Chem. Soc. Chem. Comm.* **1972**, 1018.

(146) Gutterman, D. F.; Gray, H. B. *J. Am. Chem. Soc.* **1971**, *93*, 3364.

(147) Zipp, A. P. *Coord. Chem. Rev.* **1988**, *84*, 47.

(148) Che, C.-M.; Butler, L. G.; Gray, H. B. *J. Am. Chem. Soc.* **1981**, *103*, 7796.

(149) Fordyce, W. A.; Brummer, J. G.; Crosby, G. A. *J. Am. Chem. Soc.* **1981**, *103*, 7061.

(150) Shimizu, Y.; Tanaka, Y.; Azumi, T. *J. Phys. Chem.* **1984**, *88*, 2423.

(151) Rice, S. F.; Gray, H. B. *J. Am. Chem. Soc.* **1983**, *105*, 4571.

(152) Hume, D. N.; Kolthoff, I. M. *J. Am. Chem. Soc.* **1949**, *71*, 867.

(153) Maki, N.; Fujita, J.; Tsuchida, R. *Nature* **1959**, *183*, 458.

(154) Kolthoff, I. M.; Khalafalla, S. E. "Effect on Polarograms of the Product Formed in the One-Electron Reduction of Hexaammine Cobalt(III) Ion (I)"; In *Modern Aspects of Polarography*; Kambara, T., Ed.; Plenum Press: New York, 1966.

(155) Heuer, W. B.; Totten, M. D.; Rodman, G. S.; Hebert, E. J.; Tracy, H. J.; Nagle, J. K. *J. Am. Chem. Soc.* **1984**, *106*, 1163.

(156) Fetterolf, M.; Friedman, A. E.; Yang, Y.-Y.; Offen, H.; Ford, P. C. *J. Phys. Chem.* **1988**, *92*, 3760.

(157) Roundhill, D. M.; Gray, H. B.; Che, C.-M. *Acc. Chem. Res.* **1989**, *22*, 55.

(158) Peterson, J. R.; Kalyanasundaram, K. *J. Phys. Chem.* **1985**, *89*, 2486.

(159) Kalsbeck, W. A.; Gingell, D. M.; Malinsky, J. E.; Thorp, H. H. *Inorg. Chem.* **1994**, *33*, 3313.

(160) Marcus, Y. *Chem. Rev.* **1988**, *88*, 1475.

(161) Rao, C. N. R.; George, M. V.; Mahanty, J.; Narsimhan, P. T. *A Handbook of Chemistry and Physics*, 2nd ed.; Van Nostrand Reinhold Company, London: New York, Toronto, Melbourne, 1970.

(162) Rosseinsky, D. R. *J. Am. Chem. Soc.* **1994**, *116*, 1063.

(163) Fowler, P. W.; Pyper, N. C. *Proc. R. Soc. Lond. A* **1985**, 377.

(164) Nightingale, E. R. *J. Phys. Chem.* **1959**, *63*, 1381.

(165) Robinson, R. A.; Stokes, R. H. *Electrolyte Solutions*; Butterworths Scientific Publications: London, 1955.

(166) Rieger, P. H. *Electrochemistry*; Prentice-Hall Inc.: New Jersey, 1987.

(167) Vansant, E. F. *Rec. Trav. Chim.* **1973**, *92*, 1355.

(168) Bryan, S. A.; Dickson, M. K.; Roundhill, D. M. *Inorg. Chem.* **1987**, *26*, 3878.

(169) Dickson, M. K. *Ph. D. Dissertation*, Washington State University, 1982.

(170) Roundhill, D. M.; Shen, Z.-P.; King, C.; Atherton, S. J. *J. Phys. Chem.* **1988**, *92*, 4088.

(171) Horváth, O.; Stevenson, K. L. *Charge Transfer Photochemistry of Coordination Compounds*; VCH Publishers, Inc.: New York, Weinham, Cambridge, 1993.

(172) Atkins, P. W. *Physical Chemistry*, 2nd ed.; W. H. Freeman and Company: San Francisco, 1982.

(173) Demas, J. N.; Addington, J. W. *J. Am. Chem. Soc.* **1976**, *98*, 5800.

(174) Chen, P.; Mecklenburg, S. L.; Duesing, R.; Meyer, T. J. *J. Phys. Chem.* **1993**, *97*, 6811.

(175) Indelli, A. *Trans. Faraday Soc.* **1963**, *59*, 1827.

(176) Che, C.-M.; Cho, K.-C.; Chan, W.-S.; Gray, H. B. *Inorg. Chem.* **1986**, *25*, 4906.

(177) Takagi, H.; Swaddle, T. W. *Inorg. Chem.* **1992**, *31*, 4669.

(178) Samuel, B. *Ph. D. Dissertation*, Washington State University, 1985.

(179) Roundhill, D. M.; Shen, Z.-P.; Atherton, S. J. *Inorg. Chem.* **1987**, *26*, 3833.

(180) Scandola, M. A.; Scandola, F. *J. Am. Chem. Soc.* **1972**, *94*, 1805.

(181) Nishazawa, M.; Ford, P. C. *Inorg. Chem.* **1981**, *20*, 294.

(182) Mingardi, M.; Porter, G. B. *J. Chem. Phys.* **1966**, *44*, 4354.

(183) Kirk, A. D.; Ludi, A.; Schläfer, H. L. *Ber. Bunsenges. Phys. Chem.* **1969**, *73*, 669.

(184) Kataoka, H. *Bull. Chem. Soc. Jpn.* **1973**, *46*, 2078.

(185) Wölpl, A.; Oelkrug, D. *Ber. Bunsenges. Phys. Chem.* **1975**, *79*, 394.

(186) Kirk, A. D.; Schlafer, H. L.; Ludi, A. *Can. J. Chem.* **1970**, *48*, 1065.

(187) Viaene, L.; D'Olieslager, J.; Ceulemans, A.; Vanquickenbourne, L. G. *J. Am. Chem. Soc.* **1979**, *101*, 1405.

(188) Mazur, U.; Hipps, K. W. *J. Phys. Chem.* **1980**, *84*, 194.

(189) Mazur, U.; Hipps, K. W. *J. Phys. Chem.* **1979**, *83*, 1884.

(190) Miskowski, V. M.; Gray, H. B.; Wilson, R. B.; Solomon, E. I. *Inorg. Chem.* **1979**, *18*, 1410.

(191) Hipps, K. W.; Crosby, G. A. *Inorg. Chem.* **1974**, *13*, 1543.

(192) Conti, C.; Castelli, F.; Forster, L. S. *J. Phys. Chem.* **1979**, *83*, 2371.

(193) Kida, S.; Fujita, J.; Nakamoto, K.; Tsuchida, R. *Bull. Chem. Soc. Jpn.* **1958**, *31*, 79.

(194) Vanquickenborne, L. G.; Hendrickx, M.; Postelmans, D.; Hyla-Kryspin, I.; Pierloot, K. *Inorg. Chem.* **1988**, *27*, 900.

(195) Porter, G. B. *J. Am. Chem. Soc.* **1969**, *91*, 3980.

(196) Vlcek, Jr. A.; Gray, H. B. *J. Am. Chem. Soc.* **1987**, *109*, 286.

(197) Roberts, J. D.; Caswrio, M. C. *Modern Organic Chemistry*; W. A. Benjamin, Inc.: New York, Amsterdam, 1967.

(198) Roundhill, D. M. *Photochemistry and Photophysics of Metal Complexes*; Plenum Press: New York, London, 1994.

(199) Creutz, C.; Song, J.-S.; Bullock, R. M. *Pure & Appl. Chem.* **1995**, *67*, 47.